



Large woody debris in river channels - hazard and dynamics

Dissertation

submitted to and approved by the

Department of Architecture, Civil Engineering and Environmental Sciences
University of Braunschweig – Institute of Technology

and the

Department of Civil and Environmental Engineering
University of Florence

in candidacy for the degree of a

Doktor-Ingenieur (Dr.-Ing.) /

**Dottore di Ricerca in Mitigation of Risk due to Natural Hazards on
Structures and Infrastructures^{*)}**

by

Alexandra Vergaro

Born 24 October 1970

from Firenze, Italy

Submitted on	20 March 2014
Oral examination on	05 May 2014
Professorial advisors	Prof. E. Caporali Prof. A. Dittrich

2014

^{*)} Either the German or the Italian form of the title may be used.

ACKNOWLEDGMENTS

The following study has been developed within the framework of the International Graduate College 'Mitigation of Risk due to Natural Hazards on Structures and Infrastructures'; carried out among the Dipartimento di Ingegneria Civile e Ambientale of University of Florence (Italy) and the Leichtweiß-Institut für Wasserbau of Technical University of Braunschweig (Germany).

A particular thanks to Prof. I. Becchi who has always accompanied me during my involvement with this topic, since my years at the University to my years at the Doctoral School, guiding me with his expertise, being constantly encouraging and stimulating for my research activity.

In the same manner I would like to thank Prof. E. Caporali who accepted the relay from my first advisor, and supported me in the hard work of concretisation of the whole activity.

Moreover, I would like to thank my German advisor Prof. A. Dittrich for his accurate review of the research work, the fruitful discussion and his valuable suggestions.

These results would have been impossible to achieve without the support of Dr. A. Crosato and Prof. W. Uijtewaai, who received me in their research group with cordiality and fruitful collaboration. A sincere thanks to them and to Mr. Sander, Mr. Ari and Mr. Jaap for their indispensable help and technical assistance during the experiments carried out at the Fluid Mechanics Laboratory of the Delft University of Technology.

My gratitude also to Prof. M. Rinaldi, F. Comiti and H. Piégay experts in geomorphology and LWD dynamics, who guided my first steps (many years ago) in this issue.

Furthermore, I have to thank Silvana and Petra for the precious help.

I am infinitely grateful to Antonio and Ettore for their effective contribution to this work with their patient, their support and their presence in every moment.

ABSTRACT

Large Woody Debris (LWD) are an integral component of the fluvial environment. They represent an environmental resource, but without doubt they represent also a risk factor for the amplification that could give to the destructive power of a flood event. While countless intervention in river channels, all over the world, have reintroduced wood in rivers with restoration and banks protection aims, in very recent time, during several flash flood events, LWD have had a great part in catastrophic consequences, point out the urgency of an adequate risk assessment procedure. At present, in fact, woody material dynamics in river channel is not systematically considered within the procedures for the elaboration of hazard maps: it results in loss of prediction accuracy and in underestimation of hazard impacts. The assessment inconsistency comes from the complexity of the question: several aspects in wood processes are not yet well known and the superposition of different physical phenomena results in conspicuous difficulty to predict critical scenarios.

The research activity is aimed to improve management skills for the assessment of the hydrologic risk associated to the presence of large woody debris in rivers. Improving knowledge about LWD dynamic processes and proposing effective tools for monitoring and mapping river catchments vulnerability have been the main objective of this thesis. In the development of the research program some aspects of wood dynamics have been deeply studied and the knowledge improved, utilizing critical review of the published works, field surveys and experimental investigations. LWD damaging potential has been analysed to support the identification of the exposed sites and the redaction of hazard maps, taking into account that a comprehensive procedure has to involve: a) Evaluation of wood availability in the river catchment; b) Identification of the critical cross sections; c) Prediction of hazard scenarios through the estimation of water discharge, wood recruitment and entrainment, wood transport and destination.

Particularly, survey sheets form for direct measurements has been implemented and tested in field to provide an investigation instruments for wood and river reach monitoring. The survey sheets are settled down to answer to several information requests involved in all the steps of a risk assessment procedure, as well as to provide useful indications for a better comprehension of the dynamics of wood in rivers.

Based on a critical analysis of the current state of the art, an improved theoretical mechanistic model of LWD entrainment has been proposed and tested with flume experiments, considering this feature a crucial aspect in wood dynamics, making the difference between the available material and the amount of wood that would be mobilized with high probability during a high flow. The proposed approach appears well performing, as it is able to provide a threshold parameter, showing relative small experimental scatter, and to discriminate between the entrainment modes (sliding,

rolling, floating). Moreover all the unknown parameters have been relate to the known undisturbed flow condition: this allows using hydraulic models, to obtain the undisturbed flow conditions near the single piece of wood or "log", which related to the developed survey sheets form, consents to predict the discharge causing local LWD incipient motion. While the probability of an event is normally known, such model allows estimating the probability and the amount of wood that would be mobilized, which represent one of the main, if not the more important starting point, for the construction of hazard scenarios.

Because of the simplifications made, further studies on wood entrainment in rivers are indeed needed.

ZUSAMMENFASSUNG

Großes Totholz sind ein natürlicher Teil von Fließgewässern. Sie repräsentieren einen Umweltschatz, aber auch einen Risikofaktor, denn die Zerstörungskraft im Falle von Überschwemmungen, wird dadurch gesteigert. Gegenwärtig werden die Auswirkungen von Holztrümmern in Flüssen bei der Entwicklung von Gefahrenzonenkarten nicht in Betracht gezogen, so wird die Risikoauswirkung unterschätzt. Die Unzuverlässigkeit der richtigen Einschätzungen kommt aus der Komplexität des Themas: die verschiedenen Eigenschaften von Holzprozessen sind nicht sehr bekannt und die Überlagerung verschiedener physikalischer Phänomene, macht es schwierig gefährliche Situationen vorauszusehen.

Das Ziel der Forschung ist die Verbesserung der hydrologischen Risikoeinschätzung, die mit Treibholz in Flüssen verbunden sind, die Verbesserung von Fachkenntnissen auf dem Gebiet des Treibholzes und effektive Vorschläge zur Überwachung und Vorausplanung die Verwundbarkeit von Flusseinzugsgebiet.

Bei kritischer Nachprüfung von publizierten Werken, gezielten Umfragen und experimentalen Forschungen, wurde das Schadenspotenzial von Treibholz analysiert um verwundbare Gebiete zu identifizieren und Gefahrenzonenkarten zu entwickeln. Insbesondere wurde ein Umfrageblatt für die direkte Massnahmenerfassung eingeführt und getestet, welches als Forschungsinstrument zur Überwachung von Holz und Flüssen dient.

Basierend auf einer gründlichen Analysierung des aktuellen Stands, wurde ein mechanistische Treibholzmodell „Entrainment“ vorgeschlagen und mit Rinnenexperimenten geprüft. "Entrainment" ist ein entscheidender Punkt im Holzdynamiken betrachtet.

Diese Methode kann Schwellparameter geben und die verschiedene „Entrainment“ Mechanismen (Rutschen, Rollbewegung und Auftriebskraft) analysieren.

TABLES OF CONTENTS

LIST OF FIGURES	V
LIST OF TABLES	X
SYMBOLS	XI
GLOSSARY	XIV
1 INTRODUCTION	1
1.1 PROBLEM STATEMENT AND STATE OF THE ART.....	1
1.2 AIM AND CONTRIBUTION OF THE RESEARCH	3
1.3 THESIS OUTLINE	4
2 LARGE WOODY DEBRIS IN RIVER CHANNELS	7
2.1 DEFINITIONS	7
2.2 DYNAMIC PROCESSES	8
2.2.1 <i>Production and recruitment</i>	8
2.2.2 <i>Entrainment and transport</i>	9
2.2.3 <i>Halt and deposition</i>	13
2.2.4 <i>Exit</i>	14
2.3 INTERACTIONS.....	14
2.3.1 <i>Hydraulic interaction</i>	14
2.3.2 <i>Morphologic interactions</i>	16
2.3.3 <i>Ecological interactions</i>	19
2.3.4 <i>Interaction with the anthropic environment</i>	19
3 LARGE WOODY DEBRIS HAZARD ANALYSIS	23
3.1 STATE OF THE ART	23
3.2 PROCEDURE FRAMEWORK FOR LARGE WOODY DEBRIS HAZARD ASSESSMENT.....	26
3.2.1 <i>Wood availability in river catchments</i>	26
3.2.2 <i>Critical sections</i>	27
3.2.2.1 Mean flow conditions.....	28
3.2.2.2 High flow conditions.....	30
3.2.2.3 Conclusions.....	33
3.2.3 <i>Critical scenarios</i>	33
3.3 CONCLUSIONS.....	35
4 MONITORING	37
4.1 SURVEY SHEETS FORM	37
4.1.1 <i>Framework</i>	37
4.1.1.1 Sheet 1: reach description	39
4.1.1.2 Sheet 2: sub-reach geomorphological characteristics	40
4.1.1.3 Sheet 3: LWD jam sheet	43
4.1.1.4 Sheet 4: large woody debris sheet.....	44
4.1.1.5 Sheet 5: interaction LWD, hydrodynamic and sediments	50
4.2 EXAMPLE.....	54

4.3	COMPARISON WITH REMOTE INVESTIGATIONS	58
4.4	CONCLUSIONS.....	62
5	LARGE WOODY DEBRIS ENTRAINMENT: GENERAL ASPECTS	65
5.1	INTRODUCTION	65
5.2	STATE OF THE ART	67
5.3	DISCUSSION	73
5.3.1	<i>Needs for research</i>	79
5.3.2	<i>Aim of research activities related to LWD entrainment</i>	79
6	LARGE WOODY DEBRIS ENTRAINMENT: PROPOSED APPROACH	81
6.1	THEORETICAL MODEL FOR THE NOVEL APPROACH	81
6.2	WEIGHT OF THE LOG	85
6.2.1	<i>Centre of gravity estimate</i>	89
6.3	DRAG FORCE ON PARTIALLY SUBMERGED LOG: ANALOGY TO THE FLOW AROUND A PIER.....	89
6.3.1	<i>Backwater prediction</i>	97
6.3.2	<i>Pitching Moment estimation</i>	101
6.3.2.1	Flow velocity profile	103
6.4	LIFT FORCE ON PARTIALLY SUBMERGED LOG: ANALOGY TO SHIP IN SHALLOW WATER.....	105
6.5	BUOYANCY FORCE	108
6.5.1	<i>Floatation centre determination</i>	110
6.6	INERTIA FORCES	113
6.7	ENTRAINMENT CRITERION	114
7	LARGE WOODY DEBRIS ENTRAINMENT: FLUME EXPERIMENTS	119
7.1	PRELIMINARY CONSIDERATIONS	120
7.1.1	<i>Similitude between model and prototype</i>	122
7.2	TEST DESCRIPTION	124
7.2.1	<i>Log settings</i>	125
7.2.2	<i>Flume setup</i>	127
7.3	RESULTS	131
7.3.1	<i>Preliminary experimental data analysis</i>	132
7.3.1.1	Water depth estimation.....	133
7.3.1.2	Log density variation.....	133
7.3.1.3	Flume characterization: undisturbed velocity profiles.....	134
7.3.1.4	Backwater prediction	140
7.3.2	<i>Analysis of the incipient motion condition during tests</i>	141
7.3.3	<i>Evaluation of the entrainment threshold: regression analysis</i>	148
7.4	CONCLUSIONS.....	158
8	SYNOPSIS.....	159
8.1	SURVEY METHODS.....	159
8.2	ENTRAINMENT CRITERION	161
8.3	CONCLUSIONS.....	163
9	BIBLIOGRAPHY	165
APPENDIX A.....		165
APPENDIX B.....		179

LIST OF FIGURES

FIGURE 2-1: TREE COMPONENTS.	8
FIGURE 2-2: CHARACTERIZATION OF THE WOODY DEBRIS AND SEDIMENTS FLOW PROCESSES AT REACH SCALE (MODIFIED FROM MONTGOMERY AND BUFFINGTON, 1993)	8
FIGURE 2-3: DISTRIBUTION OF LARGE WOODY DEBRIS IN CHANNEL OF DIFFERENT ORDER (FROM SALO AND CUNDY, 1987)	10
FIGURE 2-4: EXAMPLE OF LOG STABILITY PLOT (ABBE ET AL., 1997)	11
FIGURE 2-5: CLOGGED DEBRIS PARTIALLY BURIED. (VARA RIVER).....	11
FIGURE 2-6: UNCONGESTED TRANSPORT PLOTTED AT TWO DIFFERENT TIME STEP, FLOW DIRECTION FROM LEFT SIDE TO RIGHT SIDE (FROM BRAUDRICK AND GRANT, 2001).	12
FIGURE 2-7: SEMI-CONGESTED TRANSPORT PLOTTED AT TWO DIFFERENT TIME STEP, FLOW DIRECTION FROM LEFT SIDE TO RIGHT SIDE (FROM BRAUDRICK AND GRANT, 2001).	12
FIGURE 2-8: CONGESTED TRANSPORT PLOTTED AT TWO DIFFERENT TIME STEP, FLOW DIRECTION FROM LEFT SIDE TO RIGHT SIDE (FROM BRAUDRICK AND GRANT, 2001).	13
FIGURE 2-9: SCHEME OF THE FLOW FIELD AROUND AN IMMersed OBJECT (FROM JACKSON ET AL 2013).....	15
FIGURE 2-10: CHANNEL EVOLUTION IN PROXIMITY OF A DAM JAM: CHANNEL WIDENING AND AGGRADATION (FROM ABBE AND MONTGOMERY, 2003)......	17
FIGURE 2-11: FLOW FIELD AND SEDIMENTS DYNAMICS IN CORRESPONDENCE OF A BAR-APEX JAM (FROM JACKSON ET AL, 2013).....	18
FIGURE 2-12: CHANNEL EVOLUTION IN PROXIMITY OF A BAR-APEX JAM, WITH ISLAND FORMATION (FROM ABBE AND MONTGOMERY, 2003).	18
FIGURE 2-13: BED PROFILE OF THE THURRA AND CANN RIVERS (BROOKS ET AL., 2003).....	21
FIGURE 3-1: OVERVIEW OF THE RISK MANAGEMENT PROCESS (FROM PLIEFKE ET AL., 2007).	24
FIGURE 3-2: POTENTIAL HAZARD AND RISK SCENARIOS AT A CRITICAL LOCATION (FROM MAZZORANA AND FUCHS. 2010).	25
FIGURE 3-3: RECRUITMENTS ZONE AND MECHANISMS (ACCORDING TO MAZZORANA ET AL., 2009)	27
FIGURE 3-4: LWD FALLEN FROM ERODED BANK (CECINA RIVER).....	28
FIGURE 3-5: PLAN VIEW OF MEASURED NEAR-BED FLOW VELOCITIES IN CORRESPONDENCE OF A LWD WITH ROOTWAD, PARALLEL TO THE FLOW, DURING LOW FLOW CONDITION IN A NATURAL CHANNEL (ACCORDING TO ABBE AND MONTGOMERY 1996).	29
FIGURE 3-6: PROFILE OF MEASURED FLOW FIELD UPSTREAM THE LWD (ACCORDING TO ABBE AND MONTGOMERY 1996).	29
FIGURE 3-7: DEBRIS ACCUMULATION AT BRIDGE PIERS (SOUTH PLATTE RIVER, COLORADO).	30
FIGURE 3-8: CONGESTED FLOW (SAN ANTONIO RIVER TEXAS)	31
FIGURE 3-9: CHANNEL WIDENING IN PRESENCE OF DAM JAM (ABBE AND MONTGOMERY, 1996)	31
FIGURE 3-10: BRIDGE OBSTRUCTION AN FLOW DEVIATION (PASSIRIO RIVER, ALPS).	32
FIGURE 3-11: BRIDGE FAILURE (NY, USA).	32

LIST OF FIGURES

FIGURE 3-12: WOOD, SEDIMENT AND WATER FLUXES WITHIN A SYSTEM UNIT (MAZZORANA ET AL., 2011).....	34
FIGURE 4-1: FRAMEWORK FOR THE SHEET DRAWING UP.	38
FIGURE 4-2: JAM CLASSIFICATION ACCORDING TO ABBE AND MONTGOMERY (2003) AND WALLERSTEIN AND THORNE (2004), EXTRACT FROM SHEET 3.....	43
FIGURE 4-3: CODIFIED GRID TO SKETCH THE JAM POSITION IN THE CROSS SECTION.	44
FIGURE 4-4: GEOMETRICAL AND STRUCTURAL CHARACTERIZATION OF THE JAM, EXTRACT FROM SHEET 3.....	44
FIGURE 4-5: SAMPLES OF TREE TYPE (A) AND SHRUB TYPE (B).	45
FIGURE 4-6: SAMPLES OF LOG TYPE (A) AND CUT TYPE (B).....	47
FIGURE 4-7: GEOMETRICAL, STRUCTURAL AND PHYSICAL CHARACTERIZATION OF WOODY DEBRIS, EXTRACT FROM SHEET 4.	47
FIGURE 4-8: DEBRIS WITH BRANCH PORTIONS (BUTTS).	49
FIGURE 4-9: SAMPLES OF ADVENTITIOUS SPROUTS AFTER DEPOSITION.	49
FIGURE 4-10: JAM CAPTURED BY VEGETATION (PIAVE RIVER).....	52
FIGURE 4-11: LWD AND LOOSEN MATERIAL CAPTURED BY EDDIES DOWNSTREAM A TRANSVERSAL SILL, A ROOTWAD LAY DOWN THE STRUCTURE FOR THE REDUCED WATER DEPTH (ARNO RIVER).	52
FIGURE 4-12: LWD STRANDED (PIAVE RIVER).	53
FIGURE 4-13: SECTION CONTRACTION DUE TO AN IN-CHANNEL LWD (RIO CORDON, BELLUNO'S DOLOMITES).....	53
FIGURE 4-14: EFFECTS ON SCOUR AND DEPOSITION INDUCED BY A LWD (PIAVE RIVER).....	54
FIGURE 4-15: WITHDRAWAL OF A STEM SECTION.	55
FIGURE 4-16: DENSITY DISTRIBUTION (FROM LABORATORY ANALYSIS) FOR DIFFERENT CLASSES OF DECAY (EVALUATED IN FIELD): 1 INTACT, 2 SOLID, 3 POROUS, 4 DECAYED.	56
FIGURE 4-17: DENSITY DISTRIBUTION FOR DIFFERENT GEOMORPHOLOGICAL SURFACES: ACTIVE BAR, HIGH BAR, TRANSITION ZONE (BETWEEN ACTIVE AND HIGH BAR).....	56
FIGURE 4-18: DECAY CLASSES DISTRIBUTION ON THE ACTIVE BAR (AB) AND THE HIGH BAR (HB), ACCORDING TO THE FIELD OBSERVATIONS.....	57
FIGURE 4-19: DIAMETERS DISTRIBUTION OF ALLOCHTHONOUS (TRANSPORTED) DEBRIS DETECTED IN THE TWO SURVEYED RIVERS.....	57
FIGURE 4-20: LENGTHS DISTRIBUTION OF ALLOCHTHONOUS DEBRIS DETECTED IN THE TWO SURVEYED RIVERS.	58
FIGURE 4-21: RECTIFIED PHOTOGRAM SUPERIMPOSED ON THE REGIONAL CARTOGRAPHY (MAGRA RIVER).....	59
FIGURE 4-22: DEBRIS MEASURING ON PHOTOGRAM.	59
FIGURE 4-23: MORPHOLOGICAL SURFACES.....	60
FIGURE 4-24: LWD AND SURFACE DISTRIBUTION AS RECOGNIZABLE ON AERIAL IMAGERY.....	61
FIGURE 4-25: RELATIVE ERROR BETWEEN LWD DIAMETER, DIRECTLY MEASURED AND ESTIMATED ON PHOTOGRAM.....	62
FIGURE 4-26: RELATIVE ERROR BETWEEN LWD LENGTH, DIRECTLY MEASURED AND ESTIMATED ON PHOTOGRAM.....	62
FIGURE 4-27: SUPERIMPOSITION OF A HYPOTHETIC FLOW FIELD ON AERIAL IMAGERY.	63
FIGURE 5-1: DIMENSIONLESS PLOT OF FLOTATION THRESHOLDS FOR WOOD OF DIFFERENT PIECE DENSITIES AND DIAMETERS.....	66
FIGURE 5-2: BI-LOGARITHMIC PLOT OF FLOTATION THRESHOLD FOR WOOD OF DIFFERENT PIECE LENGTHS AND DIAMETERS (FROM ABBE ET AL. 1997).	67

FIGURE 5-3: A) CROSS-SECTIONAL VIEW OF PIECE LYING OBLIQUE TO FLOW; B) PIECE LYING PARALLEL TO FLOW (BRAUDRICK & GRANT, 2000).....	67
FIGURE 5-4: OBSERVED (HOLLOW SYMBOLS) AND PREDICTED (FILLED SYMBOLS) DEPTHS AND VELOCITIES AT ENTRAINMENT FOR PIECES IN LENGTH CLASS 1 AND DIAMETER CLASS 1 (A) AND 2 (B) WITHOUT ROOTWADS FROM BRAUDRICK (1998).	68
FIGURE 5-5: AN EXAMPLE OF THE RELATIONSHIP BETWEEN THE DIMENSIONLESS WATER DEPTH H^* AND THE DIMENSIONLESS FORCE Ψ FROM HAGA ET AL. (2002).	69
FIGURE 5-6: SKETCH OF INCIPIENT MOTION OF A SLIDING LOG (A) AND OF A ROLLING LOG (B) FROM BOCCHIOLA ET AL. (2006).	69
FIGURE 5-7: RELATIVE BUOYANCY Y_W^* AND THE ENTRAINMENT PARAMETER Y_R^* AGAINST X_S , R^* FROM BOCCHIOLA ET AL. (2006).	70
FIGURE 5-8: ESTIMATED REPRESENTATIVE DEPTH AGAINST D_W , D_{UP} AND D_{DOWN} , FROM BOCCHIOLA ET AL. (2006).	71
FIGURE 5-9: ENTRAINMENT PARAMETER PLOTTED VS. REYNOLDS NUMBER OF WATER FLOW, FROM CROSATO ET AL. (2011).	72
FIGURE 5-10: LONGITUDINAL WATER LEVEL PROFILES ALONG THE LOG SIDE AND THE FLUME SIDEWALL, FROM CROSATO ET AL. (2013).	73
FIGURE 5-11: TYPICAL EMERGING OBSTACLE (LIKE A BRIDGE PIER) IN SUB-CRITICAL FLOW.....	76
FIGURE 5-12: WAVE PATTERN ACROSS AN OBJECT IMMERSSED IN A FLOW (VAN MANEN & VAN OOSSANEN, 1988), AND THE DIVERGENT WAVES OBSERVED DURING THE FLUME EXPERIMENTS.	77
FIGURE 5-13: THE WATER SURFACE PROFILE DETERMINES THE SUBMERGED VOLUME AND THE BUOYANCY CENTRE.	78
FIGURE 5-14: ANALOGY BETWEEN FLOATING LOGS SHAPE (SHIELDS ET AL., 2004), AND HULL SHAPE.	78
FIGURE 6-1: SKETCH OF THE SYSTEM OF FORCES ACTING ON THE PARTIALLY SUBMERGED LOG.....	82
FIGURE 6-2: WATER ABSORPTION CURVES DURING SOAKING OF WOOD SAMPLES IN PLAIN WATER (KHAZAEI, 2008).	88
FIGURE 6-3: CUMULATIVE MASS VS. SQUARE ROOT OF TIME FOR A SOFTWOOD SAMPLE AND THE RELATIVE LINEAR REGRESSION CURVE (CANDANEDO & DEROME, 2005).	89
FIGURE 6-4: VARIATION OF DRAG COEFFICIENT WITH SLENDERNESS FOR CYLINDRICAL LOG WITH DIFFERENT SUBMERGENCE RATIO (SOURCE: GIPPEL ET AL., 1996).	90
FIGURE 6-5: RELATIONSHIP BETWEEN CD_{APP} AND BLOCKAGE RATIO B_R REFERRING TO HYGHELUND AND MANGA (2003).	92
FIGURE 6-6: VARIATION OF DRAG COEFFICIENT WITH ANGLE OF ORIENTATION FOR CYLINDRICAL LOG OF VARIOUS LENGTHS (L) AND DIAMETER (D). (SOURCE: GIPPEL ET AL., 1996).	92
FIGURE 6-7: WATER SURFACE MODIFICATION WITH OBSTACLE AND IDEALIZED SCHEME FOR THE APPLICATION OF THE MOMENTUM BALANCE (ADAPTED FROM CHABERNEAU AND HOLLEY, 2001).	93
FIGURE 6-8: CROSS SECTION LOCATION AT A BRIDGE (ADAPTED FROM BRUNNER, 2010).	95
FIGURE 6-9: BACKWATER IN CASE OF SUPERCRITICAL FLOW BETWEEN PIERS (FROM KASSEM SALAH EL-ALFY 2006)	99
FIGURE 6-10: THRESHOLD CONDITIONS FOR CHOKING IN SUBCRITICAL CHANNELS WITH ABRUPT CONTRACTIONS.	99
FIGURE 6-11: WATER SURFACE PROFILES FOR SUBCRITICAL FLOW THROUGH LATERAL CONSTRICTIONS UNDER CHOKING CONDITIONS, SHOWING THE EFFECTS OF DOWNSTREAM SUBMERGENCE (SOURCE: MOLINAS AND WU 2005).	100
FIGURE 6-12: PRESSURE COEFFICIENT DISTRIBUTION OF A CYLINDRICAL PIER SURFACE FROM TSUTSUI, 2008.....	102
FIGURE 6-13: SHIP SQUAT EFFECT.	106

LIST OF FIGURES

FIGURE 6-14: NAVIGATION IN DEEP WATER (1), NAVIGATION IN SHALLOW WATER (2)	106
FIGURE 6-15: SCHEMATIC ILLUSTRATION OF “SLOPE DRAG” ON A VESSEL MOVING UPSTREAM (FROM LANGBEIN 1962).	108
FIGURE 6-16: REFERENCE SKETCH FOR CALCULATING THE SUBMERGED AREA (FROM BRAUDRICK 1998)	109
FIGURE 6-17: WAVE SYSTEM SURROUNDING THE SHIP PROFILE (MODIFIED FROM BRIGHENTI ET AL., 2003).....	110
FIGURE 6-18: COMPARISON OF THE ANALYTICAL BOW-WAVE APPROXIMATION WITH EXPERIMENTAL MEASUREMENTS FOR A RECTANGULAR PLATE WITH FLARE ANGLES $\gamma = 0, 10, 15, 20$, AND INCIDENT ANGLE $\alpha = 10$ AND 20 (SOURCE DELHOMMENEAU ET AL., 2007).....	111
FIGURE 6-19: SKETCH PROPOSED FOR THE EVALUATION OF THE CENTRE OF BUOYANCY	112
FIGURE 6-20: TRENDS FOR ENTRAINMENT MODES AS A FUNCTION OF DISCHARGE.	115
FIGURE 6-21: SKETCH OF THE PROPOSED APPROACH FOR LWD ENTRAINMENT ASSESSMENT.	118
FIGURE 7-1: DESIGN SIZES FOR SMOOTHED SQUARE AND CIRCULAR LOG	126
FIGURE 7-2: FLUME SET UP FOR FIXED GRAVEL BED TRIALS.....	127
FIGURE 7-3: FLUME WATER SURFACE PROFILE FOR FREE FALL CONDITION.....	129
FIGURE 7-4: FLUME WATER LEVEL MAY BE REGULATED BY TAIL GATE ADJUSTMENT.....	130
FIGURE 7-5: SHARP CRESTED WEIR GEOMETRY.	131
FIGURE 7-6: MEASURED FLUME BED LEVEL AT DIFFERENT LOCATIONS.....	133
FIGURE 7-7: DENSITY VARIATION DURING DIFFERENT TRIALS.	134
FIGURE 7-8: WATER SURFACE PROFILE OBTAINED THE ONE-DIMENSIONAL STEADY FLOW EQUATION	135
FIGURE 7-9: COMPARISON BETWEEN MEASURED AND MODELLED WATER DEPTH FOR DIFFERENT WATER DISCHARGE AT 5.5 M FROM THE INLET. REFERRING TO THE WOODEN BED FLUME.	136
FIGURE 7-10: COMPARISON BETWEEN MEASURED AND MODELLED WATER DEPTH FOR DIFFERENT WATER DISCHARGE AT 7.0 M FROM THE INLET. REFERRING TO THE GRAVEL BED FLUME.....	136
FIGURE 7-11: FLUME MODELLED WITH HEC-RAS.	137
FIGURE 7-12: WATER PROFILE MODELLED WITH HEC-RAS FOR DIFFERENT DISCHARGES.	137
FIGURE 7-13: ACCELERATION OF THE FLOW PROVIDED BY THE SIMULATION.....	138
FIGURE 7-14: EXPERIMENTAL LOCATION FOR DIFFERENT TESTS.	138
FIGURE 7-15: MEASURED WATER DEPTH AT DIFFERENT DISCHARGES AND UNDISTURBED CONDITIONS; DIFFERENT LOCATIONS FOR EXPERIMENTAL TESTS ARE MARKED.	139
FIGURE 7-16: VELOCITY PROFILE AT THE ENTRAINMENT FOR EQUIVALENT DOWELS SHAPE AND ORIENTATION BUT DIFFERENT BED ROUGHNESS OR EXPERIMENTAL LOCATION.....	139
FIGURE 7-17: VELOCITY PROFILE AT THE ENTRAINMENT FOR EQUIVALENT DOWELS SHAPE AND ORIENTATION BUT DIFFERENT BED ROUGHNESS OR EXPERIMENTAL LOCATION (u^* IS THE FRICTION VELOCITY).	140
FIGURE 7-18: EXPERIMENTAL AND NUMERICAL WATER DEPTH DUE TO BACKWATER FOR DIFFERENT TESTS.....	141
FIGURE 7-19: FROUDE NUMBER AT THE ENTRAINMENT FOR DIFFERENT TESTS.....	142
FIGURE 7-20: REYNOLDS NUMBER AT THE ENTRAINMENT FOR DIFFERENT TESTS.	142
FIGURE 7-21: COMPARISON OF FROUDE NUMBERS AT THE ENTRAINMENT FOR DIFFERENT EXPERIMENTAL CONDITIONS.	143
FIGURE 7-22: DIFFERENT SURFACE WATER PROFILE FOR SHARP EDGED DOWELS AND FOR SMOOTHED EDGES DOWELS.	143

FIGURE 7-23: MEASURED THRESHOLD VALUES Ep^* OF THE ENTRAINMENTS PARAMETERS VS. THE REYNOLDS NUMBER Re	145
FIGURE 7-24: MEASURED THRESHOLD VALUES Ep^* OF THE ENTRAINMENTS PARAMETERS VS. THE FROUDE NUMBER Fr	146
FIGURE 7-25: MEASURED THRESHOLD VALUES Ep^* OF THE ENTRAINMENTS PARAMETERS VS. THE BLOCKAGE RATIO Br	147
FIGURE 7-26: MEASURED THRESHOLD VALUES Ep^* OF THE ENTRAINMENTS PARAMETERS VS. RELATIVE SUBMERGENCE $DW/DLOG$	147
FIGURE 7-27: MEASURED THRESHOLD VALUES Ep^* OF THE ENTRAINMENTS PARAMETERS VS. THE RELATIVE DENSITY RATIO ρ_{Log}/ρ_w	148
FIGURE 7-28: MEASURED THRESHOLD VALUES Ep^* OF THE ENTRAINMENTS PARAMETERS VS. THE RATIO DW/LEQ	153
FIGURE 7-29: VALUES OF THE ENTRAINMENT PARAMETERS Eps , Epr , Epb VS. THE RATIO DW/LEQ FOR SQUARE AND CIRCULAR LOGS ORIENTED AT 90° WITH RESPECT TO THE STREAM FLOW DIRECTION.....	156
FIGURE 8-1: AN EXAMPLE OF THE COLLECTED DATA AND THEIR ELABORATION.	160
FIGURE 8-2: MEASURED THRESHOLD VALUES OF THE PARAMETER Ep^* VS. THE RATIO H_w/L_{EQ}	162
FIGURE A - 1: SHEET 1: REACH DESCRIPTION.....	176
FIGURE A - 1: SHEET 1: REACH DESCRIPTION.....	176
FIGURE A - 2: SHEET 1: REACH DESCRIPTION.....	177
FIGURE A - 3: SHEET 2: SUB-REACH DESCRIPTION.....	178
FIGURE A - 4: SHEET 2: SUB-REACH DESCRIPTION.....	179
FIGURE A - 5: SHEET 3: JAM DESCRIPTION.....	180
FIGURE A - 6: SHEET 3: JAM DESCRIPTION.....	181
FIGURE A - 7: SHEET 4: KEY ELEMENT DESCRIPTION.....	182
FIGURE A - 8: SHEET 4: RACKED ELEMENT DESCRIPTION.....	183
FIGURE A - 9: SHEET 4: RACKED ELEMENT DESCRIPTION.....	184
FIGURE A - 10: SHEET 5: LWD AND SEDIMENTS INTERACTION.....	185
FIGURE A - 11: SURVEYED REGION IN PROXIMITY OF SECTION 2 OF THE UPPER REACH.....	186
FIGURE A - 12: TOPOGRAPHIC SURVEY OF SECTION 2.....	187

LIST OF TABLES

TABLE 4-1: SURVEY SHEET N.1	39
TABLE 4-2: SURVEY SHEET N.2.....	41
TABLE 4-3: SURVEY SHEET N.3.....	42
TABLE 4-4: SURVEY SHEET N.4.....	46
TABLE 4-5: SURVEY SHEET N. 5.....	51
TABLE 4-6: EXTRACT FROM THE RECORDED DATA.	55
TABLE 5-1: UNDISTURBED FLOW CONDITIONS, AND LOG PROPERTIES AT INCIPIENT MOTION, FROM CROSATO ET AL. (2011).....	72
TABLE 5-2: COMPARISON BETWEEN WEIGHT AND BUOYANCY FORCES AT ENTRAINMENT, CALCULATED USING EXPERIMENTAL DATA FROM BOCCHIOLA ET AL. (2006).....	75
TABLE 6-1: DENSITY OF SOME WOOD SPECIES*.....	85
TABLE 7-1: SCALE RELATIONSHIPS BASED ON FROUDE NUMBER SIMILITUDE, WITH $\rho_r=1$. FROM “HYDRAULIC MODELLING CONCEPT AND PRACTICE” ASCE MANUAL AND REPORTS ON ENGINEERING PRACTICE N. 97 (2000).....	123
TABLE 7-2: DESIGN LOG SIZE	126
TABLE 7-3: TYPICAL LOWLAND RIVERS BACKWATER LENGTHS.....	128
TABLE 7-4: EXAMPLE OF THE COLLECTED DATA FOR ONE TYPE OF TEST.	131
TABLE 7-5: MEASURED DATA AT THE ENTRAINMENT RELATED TO SQUARE SHAPED LOG, ORIENTED AT 90° WITH RESPECT TO THE FLOW, ON GRAVEL BED.	155
TABLE A - 1 : COLLECTED DATA IN PROXIMITY OF SECTION 2.....	187
TABLE A - 2: COLLECTED DATA IN PROXIMITY OF SECTION 2.	188
TABLE A - 3: PIONEER STANDING VEGETATION SURVEY IN THE HIGH BAR.	188

SYMBOLS

A_{sub}	[m ³]	Representative wetted cross section of the log
A_{wet}	[m ²]	Effective submerged area of the cross-section of the log
\vec{B}	[N, N]	Buoyancy force acting on the log $\vec{B} = \{B_x, B_y\}^T$
B_r	[1]	Blockage ratio provided by the log
$c(y)$	[m]	Wetted chord of log cross section
\vec{C}	[m, m]	Centre of instantaneous rotation $\vec{C} = \{x_C, y_C\}^T$
C_a, C_D^{app}	[1]	Apparent drag coefficient (C_D of a partially submerged object)
\vec{C}_B	[m, m]	Centre of buoyancy of the log $\vec{C}_B = \{x_{CB}, y_{CB}\}^T$
C_{Bk}	[1]	Blockage coefficient for squat
C_c	[1]	Contraction coefficient according Molinas (2005)
C_D	[1]	Drag coefficient of the bluff body in the flow
\vec{C}_G	[m, m]	Centre of gravity of the log $\vec{C}_G = \{x_{CG}, y_{CG}\}^T$
C_M	[1]	Inertia coefficient
C_o	[1]	Empirical coefficient for log orientation (Crosato et al. 2011)
C_r	[1]	Coefficient of representativeness $C_r = \frac{d_r}{d_w}$
C_w	[m]	Channel width
D_{50}	[m]	Medium value of the particle size distribution
d_{down}	[m]	Water depth just downstream of the log
D_{log}, d	[m]	Log diameter
d_r	[m]	Representative water depth
d_{up}	[m]	Water depth just upstream of the log
d_w, h	[m]	Undisturbed water depth
E^*	[1]	Entrainment parameter from Crosato et al. (2011)
E_p	[1]	Buoyancy parameter proposed $E_p = \frac{B_y}{\gamma_w A_{sub} L_{log}}$
E_p^b	[1]	Entrainment parameter relative to buoyancy mode
E_p^r	[1]	Entrainment parameter relative to rolling mode
E_p^s	[1]	Entrainment parameter relative to sliding mode
E_p^*	[1]	Threshold for the Entrainment parameter
f	[1]	Darcy Weisbach friction factor
F	[N]	Resulting hydrodynamic force acting on the log
F_D	[N]	Drag force acting on the log
F_I	[N]	Inertia force acting on the log
F_L	[N]	Lift force acting on the log
F_p	[N]	Pressure force in the stream direction
Fr_c	[1]	Critical Froude number of the undisturbed flow

SYMBOLS

Fr_w	[1]	Froude number of the undisturbed flow $Fr_w = \frac{U}{\sqrt{g \cdot d_w}}$
F_{squat}	[N]	Force due to the squat phenomenon
F_τ	[N]	Boundary shear force in the stream direction
g	[m/s ²]	Gravity acceleration
G_b	[1]	Basic specific gravity of wood $G_b = \frac{\rho_{kT}}{\rho_w}$
G_M	[1]	Specific gravity of wood at a given moisture
h^*	[1]	Dimensionless water depth: $h^* = \frac{d_w}{D_{log}}$
h_c^*	[1]	Threshold condition for floating according to Haga et al. (2002)
k	[m ⁻¹]	Wave number $k = 2\pi/\lambda$
k_{eT}	[1]	Energy loss coefficient for choking condition (Molinas 2005)
k_s	[m]	Effective roughness height
K_L	[1]	Correction factor for the contraction length (Molinas 2005)
K_s	[1]	Shape factor
K_{SG}	[m ^{1/3} s ⁻¹]	Strickler Glaucher coefficient
K_ϕ	[1]	Correction factor for the inlet angle (Molinas 2005)
L^*	[1]	Relative contraction length $L^* = L_{obs}/C_w$
L_b	[m]	Backwater length
L_c	[m]	Contraction reach length
L_e	[m]	Expansion reach length
L_{eq}	[m]	Length of obstruction in the stream-wise direction
L_{log}	[m]	Log length
L_{obs}	[m]	Average length of obstruction in the crosswise direction
M_c	[1]	Moisture content of wood $M_c = \frac{M_{water}}{M_{wood}}$
M_{eq}	[1]	Equilibrium moisture content of wood
M_{max}	[1]	Maximum moisture content of wood
M_{water}	[kg]	Mass of the water in wood
M_{wood}	[kg]	Mass of the oven-dry wood
n	[m ^{-1/3} s ¹]	Manning coefficient
O_r, σ	[1]	Opening ratio $O_r = 1 - B_r$
p	[N/m ²]	Static pressure of the flow
P	[1]	Velocity profile parameter
Q	[m ³ /s]	Flow rate
r	[1]	Residual ratio of energy between the expanded and contracted section
\vec{R}	[N]	Reaction of the riverbed acting on the log
Re_D	[1]	Reynolds number of a cylinder $Re_D = \frac{\rho_w \cdot U \cdot D}{\mu_w}$
Re_w	[1]	Reynolds number of the undisturbed flow $Re_w = \frac{\rho_w \cdot U \cdot d_w}{\mu_w}$
Re^*	[1]	Roughness Reynolds number $Re^* = \frac{u^* \cdot k_s}{\nu_w}$

R_H	[m]	Hydraulic radius	
S_b, S_o	[1]	Channel bed slope	$S_b = \tan(\alpha)$
T	[s]	Wave period	
u^*	[m/s]	Friction velocity	$u^* = \sqrt{\frac{\tau_b}{\rho_w}}$
U	[m/s]	Mean water velocity	
V_{log}	[m ³]	Volume of the log	
V_{wet}	[m ³]	Effective submerged volume of the log	
$w(x)$	[m]	Wave profile along the wetted surface of the log	
\vec{W}	[N]	Weight of the log	
x_L	[m]	Arm of the lift force respect to the origin of the coordinate system	
X_R^*	[1]	Drag to resistance forces ratio for rolling (Bocchiola et al. 2006)	
X_S^*	[1]	Drag to resistance forces ratio for sliding (Bocchiola et al. 2006)	
y	[m]	Local flow depth	
y_{bw}	[m]	Height of the bow wave above the mean free surface	
y_D	[m]	Arm of the drag force respect to the origin of the coordinate system	
y_o	[m]	Bed roughness length	
Y_r^*	[1]	Threshold condition for entrainment (Bocchiola et al. 2006)	
Y_w^*	[1]	Relative buoyancy	$Y_w = \frac{\rho_w \cdot d_w}{\rho_{log} \cdot D_{log}}$
α, s	[degree]	Channel bed slope angle	
γ_w	[N/m ³]	Specific weight of water	$\gamma_w = g \cdot \rho_w$
δ	[degree]	Rolling friction angle	
δ_{squat}	[m]	Maximum squat displacement	
Δy	[m]	Backwater rise	
θ	[m]	Piece angle with respect to flow	
κ	[1]	Von Karman constant	
λ	[m]	Wave length	
μ_{bed}	[1]	Friction coefficient between wood and bed	
μ_w	[Pa s]	Dynamic viscosity of water	
ν_w	[m ² /s]	Kinematic viscosity of water	$\nu_w = \mu_w / \rho_w$
ρ_{log}	[kg/m ³]	Log density	
ρ_{kT}	[kg/m ³]	Dry-fresh density of wood	
ρ_w	[kg/m ³]	Water density	
τ_b	[N/m ²]	Bed shear stress	
φ	[degree]	Inlet angle in the contraction zone (Molinas 2005)	
φ^*	[degree]	Relative inlet angle (Molinas 2005)	$\varphi^* = \varphi / 90^\circ$
Ψ	[1]	Dimensionless force according to Haga et al.	
τ_{0x}	[N/m ²]	Boundary shear stress in the flow direction	
ω	[s ⁻¹]	Radian frequency	$\omega = 2\pi / T$

GLOSSARY

Bank edge/ top debris	Unstable debris that have been deposited on the top of a bank.
Bank revetment	Unstable debris that revets a bank slope.
Bar apex jam/ head jam	Debris accumulation occurring at the upstream side of a bar (head) or originating a bar.
Bar top jam	Debris stranded on bars top easily remobilized.
Bench	A level shelf of land interrupting a declivity (with steep slopes above and below), at an intermediate level between high bars and terraces.
Bench jam	Accumulation with one or more key elements parallel or slightly angled to the flow, able to create hydraulically sheltered areas that encourage sediment and debris deposition
Bow	The front end of a ship
Canopy	The overhead branches and leaves of vegetation.
Dam jam	A type of debris jam that extends entirely across the channel as a result of the debris length being approximately equal to the channel width.
Debris	Floating or submerged material, such as logs, vegetation, or trash, transported by a stream.
Debris jam	Accumulation of transported or recruited debris material formed around large, whole trees that may be anchored to the bed or banks at one or both ends, in the stream system.
Debris flow jam	Jams resulting from the deposition of wood following debris flows initiated by shallow landslides
Deflector jam	A type of debris jam that redirects the flows to one or both of the banks. These types of jams usually occur when the channel width is slightly greater than the average tree height.
Draft/ Draught	The depth of a vessel's keel below the surface (especially when loaded)
Drift	Alternative term for "debris" that is floating in a river.
Flood jam	These jams are often mobile during large floods or dam-break events. They frequently deposit in the floodplain against standing trees or shrubs.
Flow deflection jam	See deflector jam.
Heartwood	The dense inner part of a tree trunk, yielding the hardest timber.
Hull	The main body of a ship or other vessel, including the bottom, sides, and deck but not the masts, superstructure, rigging, engines, and other fittings.
Keel	One of the main longitudinal beams (or plates) of the hull of a vessel; can extend vertically into the water to provide lateral stability
Large Woody Debris (LWD)	Type of debris consisting of trees, logs, and other organic matter with a length greater than 1.0 m and a diameter greater 0.1 m.
Log	A part of the trunk or a large branch of a tree that has fallen or been cut off.
Log rafts	Extensive floating accumulation.
Log step	Debris that span the channel with each end being held in place

	by boulders, bedrock, wood or sediment: sediment accumulates upstream of the log and water flows over the top creating a step in the channel profile.
Meander jam	These jams normally form on the outside bank at the downstream end of meander bends, primarily in large, low gradient alluvial channels. They are typically initiated by the deposition of two or more key members oriented as in bar apex jams. Wood that is floating downstream is racked against the rootwad, diverting flow toward the opposite bank. The racked wood and key pieces act to stabilize the stream bank and limit further lateral migration.
Parallel jam	A type of debris jam that is oriented parallel to the flow. These types of jams usually occur when the channel width is significantly greater than the maximum debris length.
Sapwood	The soft outer layers of recently formed wood between the heartwood and the bark, containing the functioning vascular tissue.
Sinkage	The movement of a ship to the bottom of the sea or some other body of water, because of damage or a collision.
Span accumulation	Debris accumulation that occur across an entire span of a bridge structure resulting from the size of the length of floating debris that exceeds the effective opening between piers.
Squat	Hydrodynamic phenomenon by which a vessel moving quickly through shallow water creates an area of lowered pressure that causes the ship to be closer to the seabed than would otherwise be expected.
Stern	The rear part of a boat
Underflow jam:	A type of debris jam that exists near the bank full level. These types of jams usually occur in small watersheds where the tree height is greater than the channel width.
Waterline	The line to which a vessel's hull is immersed when loaded in a specified way.

1 INTRODUCTION

1.1 PROBLEM STATEMENT AND STATE OF THE ART

Woody debris in river channels, are represented by wooden material coming from natural or anthropic fonts, which is displaced from its original collocation.

This material is an integral component of the fluvial environment like sediments and water discharge. Socio-economics changes, during the last decades, produced strong variations in land-use, this aspect combined with more recent strategies of management for forested and riparian areas, and climatic changes, have produced a relative abundance of Large Woody Debris (LWD) even in river reaches that have a long history of human alterations.

For the most, the presence and the effects of woody debris become evident when the flow conditions are critical, i.e. during and after flood events, because debris could amplify flood damages. In case of high flow, woody debris become floating material that may obstruct particular sections like bridge spans and culverts, causing backwater flooding and increasing the hydrodynamic loadings on structures. This material may impacts against structures and embankments, causing breaches and inundation; in addition, when water runs over the banks, floating debris represent a further issue of hazard for buildings and urban infrastructures. Even stable jams in the channel, reducing the flow section, may cause similar results. Even in ordinary discharge conditions, LWD interact with flow in dependence of their position in the hydraulic cross section, their dimensions and their orientation, producing accelerations, deviations of the stream flow and turbulences that may cause banks instability (Abbe and Montgomery, 2003). These are the reasons because of woody debris have been essentially perceived as a signal of risk exposure and environmental deterioration, so that they have been systematically removed from the river system for years.

Succeeding studies have shown that woody debris are a complex subject in river dynamics: if they could increase inundation risk and flood damages, on the other side they produce geomorphologic modifications in river channels which tend to increase river bed stability (Wallerstein and Thorne, 2004), moreover they cover a crucial role in the river ecosystem (Abbe and Montgomery, 1996). Many investigations have demonstrate that systematic removal of wood material in river channels is far to produce a reliable risk protection, while it results with evidence, in a detrimental action on river ecology and stability (Bisson et al., 2003; Shields and Cooper, 2000). At time, countless interventions in river channels, all over the world, have reintroduced wood in rivers with restoration and banks protection aims (Abbe et al., 1997, Shields et al., 2004). On the same time, during several flash flood events in very recent time

(i.e. November 2011 Cinqueterre, Liguria, Italy) LWD have had a great part in catastrophic consequences, pointing out the urgency of an adequate risk assessment procedure.

As for bed sediments, a management practice is required even for wood, with the aim to implement strategies allowing matching safety and morphologic and ecologic benefits.

The European Commission in the Flood Directive (Directive 2007/60/EC of the European Parliament and of the Council of 23 October 2007 on the assessment and management of flood risks. OJ L 288, 6.11.2007, P.27) underlines the requirement of “the better environmental option” in the redaction of Flood Risk Management Plans, considering nature protection and biodiversity policy strictly linked to flood risk protection: in this perspective a key role is recognized to large woody debris. Despite that, at present, woody material dynamics in river channel is not systematically considered within the procedures for the elaboration of hazard maps with a consequent loss of prediction accuracy and underestimation of hazard impacts (Mazzorana and Fuchs, 2009).

Most of all existing management plans indicate practices directed to guarantee recreational or commercial activities like fishing or shipping, etc. Risk reduction, if detectable, is just a secondary product of these practices. The rare guidelines closely related to risk due to large woody debris, are mainly focused on specific aspects i.e. like LWD transport and accumulation at bridges piers (hec09 Federal Highway Administration U.S.A, 2005; NCHRP REPORT 653, 2010, FHWA-HIF-12-003 HEC-18, 2012) or sometimes concern geographic and orographic situations (i.e. Design guideline for the reintroduction of wood into Australian streams, Australian Government, Land & Water, 2006) so far from the densely urbanized European regions which appear more exposed to the catastrophic consequences induced by LWD during flash flood events.

This deficit comes from the complexity of the question: several aspects in wood processes are not yet well known (Mazzorana et al., 2011) and the superposition of different physical phenomena results in conspicuous difficulty to predict critical scenarios (Mazzorana et al., 2009, 2011). At any rate many efforts were done in recent years to better understand processes and interactions involving woody debris; various the investigating methods adopted: field survey, remote sensing and monitoring, as well as mathematical and physical modelling.

A great part of the published investigations concern ecologic and geomorphologic interactions between LWD and rivers, while a limited number of flume experiments have been performed to study LWD entrainment (i.e. Braudrick and Grant, 2000; Bocchiola et al., 2006), transport and deposition conditions (Braudrick and Grant 2001; Haga et al., 2002; Betti et al., 2006). To better understand long-term impacts, field surveys have been mainly focused on relatively undisturbed forested catchments, while a limited number of studies have been conducted on engineered or urbanized reaches (Kail, 2003). These reaches (as the majority of European rivers), after centuries of human induced development, have recently recovered a small degree of

freedom by the increasing adoption of new management strategies that include the definition of a contiguous corridor where the river may migrate freely. Considering that these rivers usually cross urbanized areas and touch several hydraulic infrastructures, it is evident the necessity to study the effects of these recent managing strategies on fluvial environment.

1.2 AIM AND CONTRIBUTION OF THE RESEARCH

The present research has been directed to produce useful instruments and information for the development of a risk assessment procedure taking into account the presence and the dynamics of wood in rivers. Improving knowledge about LWD processes and proposing effective tools for monitoring and mapping river catchments vulnerability have been the main objectives of the work.

Without doubt a reliable risk assessment procedure for hydrologic hazards needs to deserve particular attention to the role of transported woody material during flash floods or debris flows.

A comprehensive procedure has to involve:

- Evaluation of wood availability in the river catchment by:
 - Vegetation evaluation (species, age, mortality...);
 - Valuation of hill slopes stability;
 - Valuation of the river banks stability;
 - Estimation of the in-channel material.

- Identification of the critical cross sections, resulting from:
 - Wood availability;
 - Wood stability;
 - Risk consequences.

- Prediction of hazard scenarios:
 - Estimation of water discharge;
 - Estimation of wood recruitment and entrainment;
 - Estimation of wood transport and destination.

Within the comprehensive procedure framework some aspects in each of the three main sections have been deeply studied and developed, utilizing critical literature review, field survey and experimental investigations.

A review of LWD damaging potential, based on literature material and direct observations in different river reaches, has been carried out to support the identification of the risk sources and of the exposed sites.

A survey sheets form for direct measurements has been implemented and tested in field in two Italian rivers. The sheets represent an investigation instrument for wood and river reach monitoring which answer to several information requests involved in different step of the risk assessment procedure (risk identification, hazard analysis, evaluation of the system vulnerability), as well as they provide useful indications for a better comprehension of dynamics of wood in rivers. Actually the proposed survey sheets are focused on the river morphology characterization and the in-channel wooden material evaluation, but their modular structure is suitable for integrations: extending, for example, the survey to the hill slopes or the standing vegetation state.

Among wood's dynamic processes, logs entrainment has been considered a crucial one, making the difference between the available material and the amount of wood that would be mobilized with high probability during a high flow.

For this reason, appraising the current state of the art, an improved theoretical mechanistic model has been proposed, combining knowledge from different disciplines, which takes into account more complexity of the flow field surrounding a partially submerged object lying on a flume bed. Under the new theoretical approach a threshold parameter is obtained and tested with flume experiments, to characterize the incipient motion condition that represent one of the essential starting points for the construction of hazard scenarios. Flow conditions typical of low land rivers have been taken into account for the experimental setting, being within these channel types that LWD has the greatest range of functions (e.g., Lisle and Kelsey, 1982; Keller et al., 1985; Montgomery et al., 1995).

Analysis of the experimental data, compared with those available in literature, has shown that water flow dynamics around the log, in contrast with the common idea (Braudrick and Grant, 2000), may have a stabilizing effect, even in case of low blockage ratio.

The proposed LWD entrainment approach could be integrated in a more general LWD management framework, arranging the data collected with the proposed survey sheets, flood hydrograph and a hydraulic model of the river, in order to predict the amount of wood that, with high probability, will be mobilized in a region during a particular event: this framework at a first stage could represent a basic approach to LWD risk assessment.

1.3 THESIS OUTLINE

The research work is presented in 6 chapters.

Chapter 2 provides an overview of large woody debris processes, their interaction with other fluvial and environmental components. Their positive and harmful functions are presented in this section.

Chapter 3 illustrates the matter of a comprehensive procedure for hydrologic risk assessment, presenting a framework for its elaboration, underlining the knowledge gaps. The following chapters contain the in-depth studies on particular aspects of the procedure with the original contribution.

In chapter 4 is illustrated the survey sheets form for direct measurements, developed to collect the necessary information to perform a predicting model and to monitoring river catchments under management; a filled in example is provided in Appendix A.

Chapter 5 is focused on entrainment of wooden objects in water flow: existing models are analysed and discussed and the needs for research are highlighted.

In chapter 6 a novel approach is proposed physically based on the stationary equilibrium of gravity, buoyancy, friction and hydrodynamic forces acting on the body partially submerged in a flow field: no any force has been neglected a priori and an original interpretation of some aspects of the problem has been adduced taking cues from different disciplines. A novel entrainment parameter has been then provided, able to discern between the different entrainment modes, allowing predicting even the type of incipient motion.

In chapter 7 the threshold value for the entrainment parameters has been experimentally derived from data coming from original tests and literature material with the method of regression analysis. The results are then exposed and discussed.

2 LARGE WOODY DEBRIS IN RIVER CHANNELS

Woody debris in river channels, are represented by wooden material coming from natural or anthropic fonts, which is displaced from its original collocation. This material is an integral component of the fluvial environment like sediments and water discharge and interacts with the others at all scale levels.

In hydrologic risk assessment the relevant debris are the large ones (defined by standardized dimensions) that produce the major impacts on river morphology, hydrodynamics and hazard.

2.1 DEFINITIONS

Wooden debris in literature are usually defined on the base of size, shape and dynamics. Generic woody debris (WD) are present in river channels as isolated elements or as accumulations, clusters that are commonly named *jam*. The relevant debris for the objective of this work are the large ones, named large woody debris (LWD) and characterized by the following dimensions: diameter ≥ 0.10 m, length ≥ 1 m. This material may be represented by complete plants or portions, and even waste material coming from human timber structures demolition (i.e. jetties or huts).

Jams are usually constituted by material of different sizes, all components are classified based on dimension and role in the cluster (Abbe & Montgomery, 1996):

- *Key members*: LWD which characteristics (size and plant structure) are likely to origin a cluster promoting other debris clogging;
- *Racked members*: LWD trapped in presence of cross section obstruction like key members, boulders, vegetation, etc., which do not have the capacity to originate a cluster;
- *Loose members*: organic matter (leaves, vegetation, and sticks) that increase the texture of the cluster, they do not influence the stability of the formation but increase sizeably the resistance to water flow.

Large woody debris may present different shape and size depending on the integrity of the different components of the original plant (Figure 2-1).

In riparian tree species is common to find multi-stemmed plants where two or more stems sprouts from a single rootwad. Reminding that woody debris are represented by wooden material displaced from its natural collocation, not necessarily dead, it is possible to found in rivers complete trees, with roots, stem, branches and also leaves, if the material is still living.

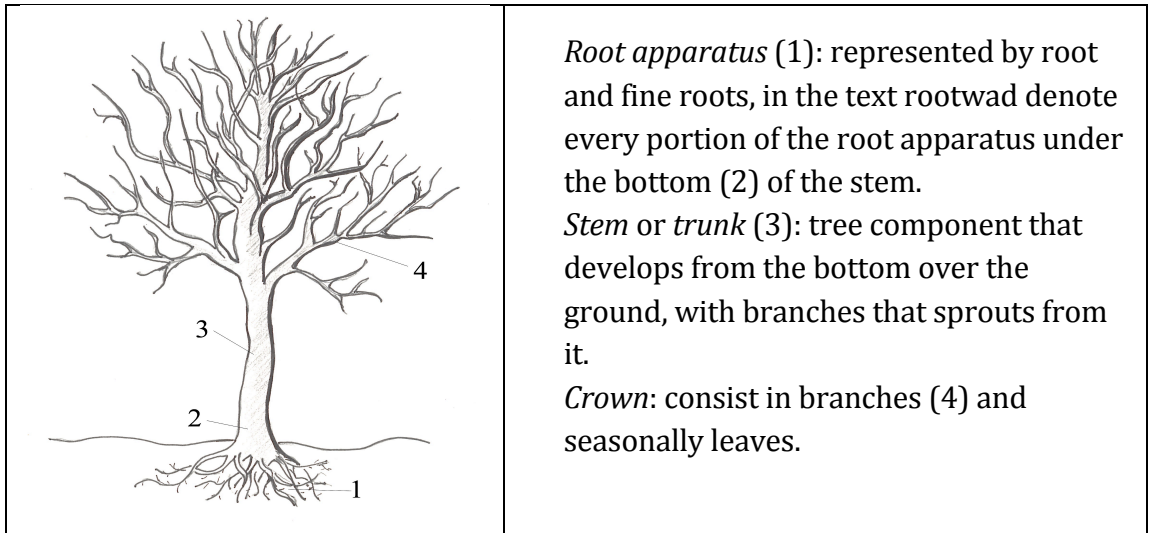


Figure 2-1: tree components.

2.2 DYNAMIC PROCESSES

In analogy to what happen for river sediments even for woody debris it is possible to identify different processes that regulate their dynamics at reach scale (Figure 2-2).

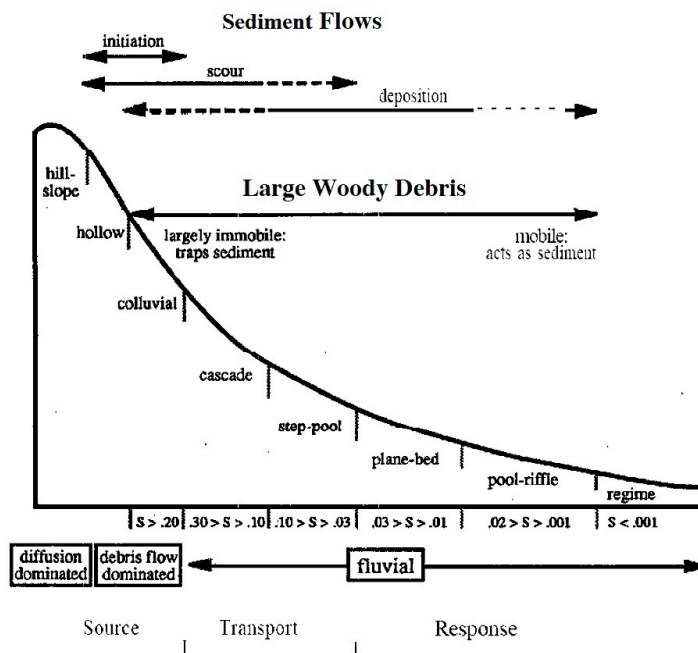


Figure 2-2: characterization of the woody debris and sediments flow processes at reach scale (modified from Montgomery and Buffington, 1993).

2.2.1 Production and recruitment

The riparian zone, the in channel vegetated islands and the hill slopes are the main source areas of vegetal material for the river channels. This material originates from

natural or man induced tree mortality, and demolition of artificial timber structures like huts or jetties.

Natural mortality is due to several causes, mainly biological processes and mechanical processes (Keller & Swanson, 1979). Biological processes like ageing, parasites, infections, pollution and natural standing trees competition, lead to plants or plant portion mortality. Dead plants may remain standing in their growth location for a long time before mechanical actions induce their definitive falling down. Mechanical processes, apart from harvesting practices and animals activities, consist mainly in increasing loadings or soil processes related to climatic, orographic and geologic condition of the watershed. Actions like wind-throw, snow loads and hydrodynamic loadings can produce breakages or definitive fall of plants; soil erosion, landslides and avalanches produce massive quantities of large woody debris. The same impact is induced from fires, which in particular produce wooden debris less dense and smooth shaped (without branches and rootwad).

Within a forested riparian area, the recruitment of wood to the stream channel is determined by tree height and distance to the stream (Robison & Beschta, 1990), while May and Gresswell (2003) point out that falling trees with a horizontal distance to the channel that exceeds their height can exert a destabilizing action on other trees (knock-on effect). Trees close to the stream and taller trees away from the stream have a greater chance of being recruited once they fall. Further trees may be recruited from the hill slopes with slow processes due to precipitation and weight, or rapid processes like landslide and avalanches that convey large volumes of standing and lying woody material. The rate of recruitment varies by vegetation development, management history, and physical factors such as soil compaction, soil stability, valley form, and channel morphology. Low order narrow channels, in forested regions, present a great availability of wood that intercept the stream channel without interact with it, then may remain stationary for long periods of time (greater than 200 years in some cases), but will become more mobile as they break down in size. In general wood loading varies with watershed extension, forest composition, due to the natural differences among tree species in growth height and proximity to water.

A small percentage of wood might be recruited by the re-exposure of ancient wood buried in floodplain sediments due to river course changes; to give an example, Wallerstein et al. (1997) and Wallerstein and Thorne (2004), examining degrading streams in northern Mississippi, observed a 7% on the total input of debris resulting from paleodebris (material introduced into the channel from old alluvial deposits containing preserved debris).

2.2.2 Entrainment and transport

Once recruited, directly (from riparian vegetation) or from hill slopes, woody debris may remain stably anchored at the input location or move toward due the stream flow action, depending on several features, mainly:

Debris sizes to channel sizes ratio: several field studies (Gurnell et al., 2000; Marcus et al., 2002; Abbe and Montgomery, 2006) confirm that in I and II order channels the debris that reach the channel are barely removed by the stream flow and may or not interact with it (sometimes they spans the entire channel width without contact with the water flow). The limiting factor to mobility, in this condition, is the transport capacity of the stream flow (Figure 2-3). In III and IV order channels, debris have the same size of the channel or less, and the flood discharges are able to mobilize e redistribute the debris along the river channel with a substantial equilibrium between recruitment and transport (Figure 2-4, Abbe et al., 1997).

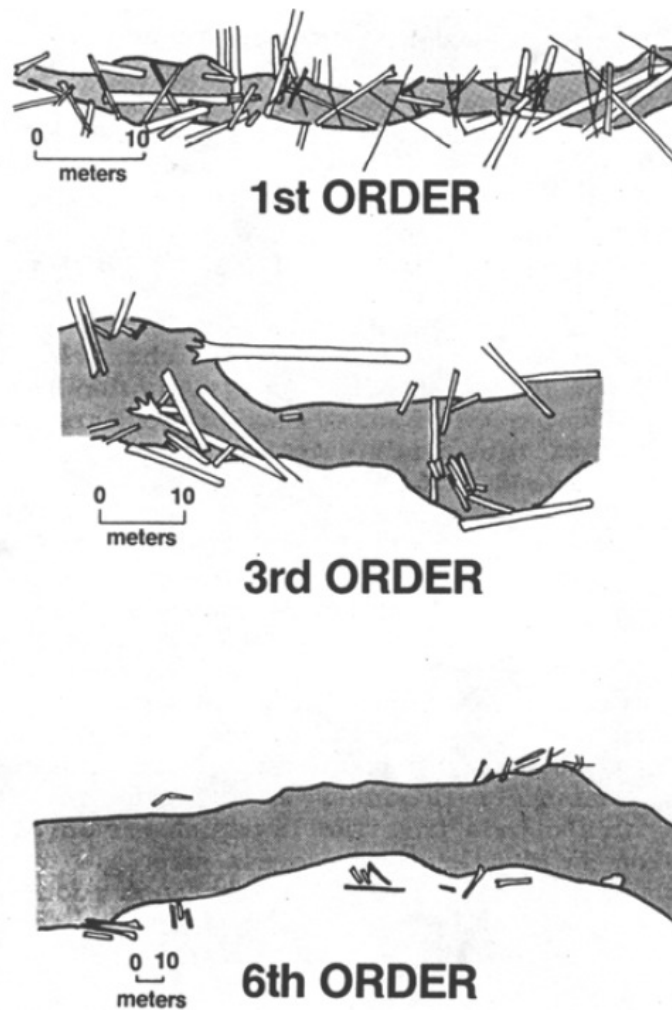


Figure 2-3: distribution of large woody debris in channel of different order (from Salo and Cundy, 1987).

In rivers with an order over VI, debris may be entrained even by ordinary discharge and are easily delivered far from the river main channel, deposited on banks and floodplain by the higher flows, or conveyed to the sea. In this situation the constraining factor to the abundance of woody debris within the channel is the recruitment. It is remarkable that this behaviour is opposite to the sediment behaviour (see Figure 2-2).

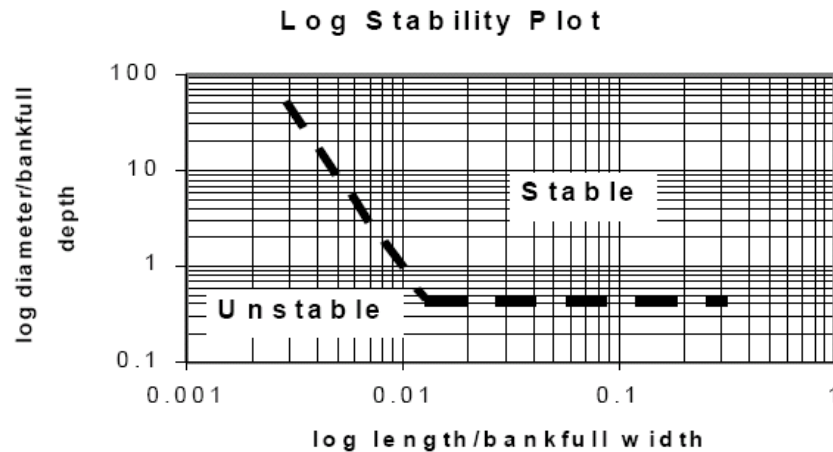


Figure 2-4: example of log stability plot (Abbe et al., 1997).

Interaction with bed sediments: large boulders inhibit debris movements and bed sediments may partially bury LWD (Figure 2-5), in a way that mobility is possible only in occurrence of high discharge and significant bed transport (debris might remain stable in this configuration for decades, influencing for a long time bed gradient).



Figure 2-5: Clogged debris partially buried. (Vara River).

Channel sinuosity increases woody debris stability and deposition.

For woody debris interacting with the stream flow, entrainment is mainly influenced by the following debris features:

- Dimensions;
- Density (which depend from tree species and debris history: low-density wood, such as spruce or western red cedar is more readily floated than higher-density wood such as Douglas fir; during the course of time,

waterlogging increases the density and stability of large wood in the channel);

- Shape: the presence of rootwad, branches, the complex structure of a plant contribute to its stability in particular in terms of interaction with bed sediments, bed forms and other woody debris.

In analogy with sediments incipient motion models, in very simplified conditions (cylindrical debris with a length size lesser than the channel width), it's possible to define the incipient motion condition based on the equilibrium balance between driving forces and resisting forces (Braudrick and Grant, 2000; Haga et al., 2002). Stream flow, water depth, water velocity, the material strength of the wood, the wood decay resistance and deformability of the bed influence both the resistive and driving forces. This topic will be widely discussed in chapter 5.

Entrainment may occurs with different modes mainly rolling, sliding, buoyancy, after, entrained woody debris become definitively floating objects that may be transported by the stream flow in different transport regimes depending on the magnitude of floating debris (density within a control volume). Braudrick and Grant (2001) with flume experiments with mobile bed and cylindrical dowels, observed three main types of transport:

Uncongested transport (Figure 2-6): the dowels cover less than 10 % of the flow free surface, contacts between single debris and interactions between debris and in-channel obstacles are infrequent, and dowels move independently.

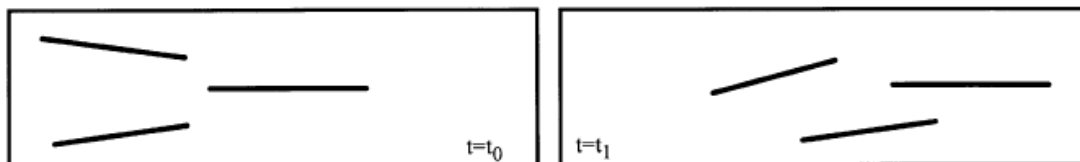


Figure 2-6: uncongested transport plotted at two different time step, flow direction from left side to right side (from Braudrick and Grant, 2001).

Semi-congested transport (Figure 2-7): intermediate situation where some dowels move like single pieces and others move as a group; pieces occupy a portion of the free surface ranging from 10% to 33%.

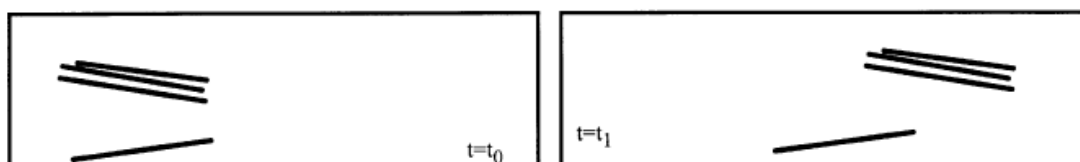


Figure 2-7: semi-congested transport plotted at two different time step, flow direction from left side to right side (from Braudrick and Grant, 2001).

Congested transport (Figure 2-8): pieces move as a unitary floating mass with frequent contacts and limited space for relative translations or rotations, only pieces at

the boundary of the group have a small degree of freedom, the dowels cover more than the 33% of the free surface.

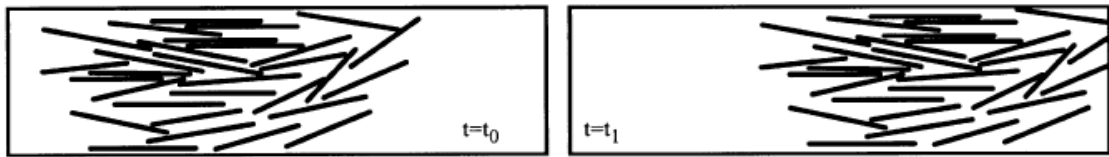


Figure 2-8: congested transport plotted at two different time step, flow direction from left side to right side (from Braudrick and Grant, 2001).

In the same experiments the authors observed that deposition on bars, resulting from the reduction of the water depth, is more frequent in case of uncongested or semi-congested transport.

Limited studies are dedicated to the evaluation of LWD travel distance when transported. In the above mentioned study, Braudrick and Grant (2001) hypothesize that the distance logs travel may be a function of the ratios of piece length and diameter to channel width, depth, and sinuosity but they didn't achieved sufficient confirmation to use such relation for a predictive model. Lyn et al. (2003) indicate that, in rivers, the delivery of debris to a given site "seems to occur in bursts, rather than continuously, even during a flow event of extended duration" and provide the following justification: "the debris is not generated in the vicinity of the site, and the bursts result from different travel times from different contributing areas." Furthermore they gain the conclusion that "the transport of debris occurs rather intermittently with long periods of comparative inactivity punctuated by short periods of intense activity, generally on the rising limb of the hydrograph."

2.2.3 Halt and deposition

When transported woody debris may be clogged by in channel obstacles, or within cross section with reduced water depth, etc.; if the flow magnitude is insufficient to entrain once more the debris, within the same event, the debris temporary arrested are deposited as single pieces or grouped formation. Obstacles may be represented by: boulders, vegetation, infrastructures, and jams.

Accumulation of large woody debris often occurs at specific points in a stream. The downstream end of a meander bend, the head of a side channel, the apex of a bar, pools, or other relatively low energy points often collect LWD that have been transported from upstream. In low gradient rivers and streams, channel width and sinuosity are key factors controlling the abundance and distribution of LWD accumulations (Nakamura & Swanson, 1994). Wide, unconstrained reaches bordered by floodplains and terraces retain abundant storage and depositional sites for transported logs. River reaches flowing through wide valleys, develop secondary channels at the base of terraces and along valley walls that trap wood mobilized during

large floods. The mouths of secondary channels may be significant LWD storage sites (Swanson and Lienkaemper, 1979; Nakamura and Swanson, 1994). Large accumulations are frequently the result of a key log that has been transported or fallen into the stream at a low energy point, became (or remained) stable in that location, it may collect additional debris that are transported from upstream. Depending on their structure and shape debris may be less or more prone to forming snags and acting as key members: i.e. like widely spreading or multiple-stemmed hardwoods other than nearly cylindrical conifers which are more readily transported and accumulated as racked members, enhancing the development of log-jams.

2.2.4 Exit

The natural run out of debris from the river channel occurs because of woody material deterioration as consequence of physical and biological processes. The firsts comprise all hits with in-channel features, the moulding action of bed sediments and water flow, and the alternation of wet and dry conditions that influences, with time, the texture and the porosity of the material. The seconds include parasites, moulds and funguses, the aquatic macro invertebrates that process the wood nutrients for the fluvial food chain.

Some woody debris cease to be suchlike because produce new roots where deposited, becoming stable as a standing alive plants.

Where river channels have the possibility to freely migrate in the floodplain, a rate of woody debris withdraws buried by sediments in abandoned paleo-channels; depending on the temporal scale assumed for the evaluation of the inflow and outflow rates they may be considered lost by the system while they may be exposed once again in successive lateral migration or incision phases.

Large amounts of wood leave the rivers conveyed to the sea.

2.3 INTERACTIONS

These functions vary between individual channels, depending on the size and morphology of the stream, which in turn depend on climate, watershed size, valley slope, geologic substrate, and relative inputs of water and sediments further than wood.

2.3.1 Hydraulic interaction

LWD in stream flow, moving or resting in stable configuration (as isolated pieces or jams), impact the hydraulic regime both in case of ordinary and higher water discharges.

Large woody debris, as any obstacle partially or totally immersed in a stream flow, alter the flow field (Figure 2-9) (Mutz, 2003; Jakson et al., 2013). Localized variations in velocity in proximity of LWD cause scour and deposition depending on the debris size, position and orientation within the channel, therefore modify also channel bed forms and banks. The combined effects of increased roughness caused by the wood, the bed forms, and the banks alterations, can increase upstream water surface elevation, reduce flow velocity, shear stress, and reach-average surface grain sizes (Montgomery et al., 2003).

Changes in hydraulic roughness may be translated into estimates of increases in water surface elevations for a range of flow events.

LWD debris act also as obstruction that produces, similarly, the above mentioned effects depending on the related blockage ratio. Several studies (Gippel, 1995; Gippel et al. 1996) confirm that till the width obstruction is less than 10% of the channel size there isn't a substantial increase in water elevation, due to the little effect in the total conveyance of the channel, while, at any rate, even small obstruction can cause local flow deflection and acceleration. Backwater risen become sizeable for a certain extent when the stream blockages is over than 50%; with flume experiments Young (1991) found out that a blockage ratio of 50% produces a 1% risen in base flow stage level, the same experiments revealed that blockage ratios higher than 80% are necessary to significantly increase flood levels. Furthermore the produced effects depend also by the density and spacing of debris (Ranga Raju et al. 1983; Shields and Gippel, 1995). The impact that multiple pieces of LWD have on flooding is determined by the distance separating each piece. If several pieces are located within two times the diameter of the next piece, there is no greater impact on water levels than one piece alone (Rutherford et al., 2002).

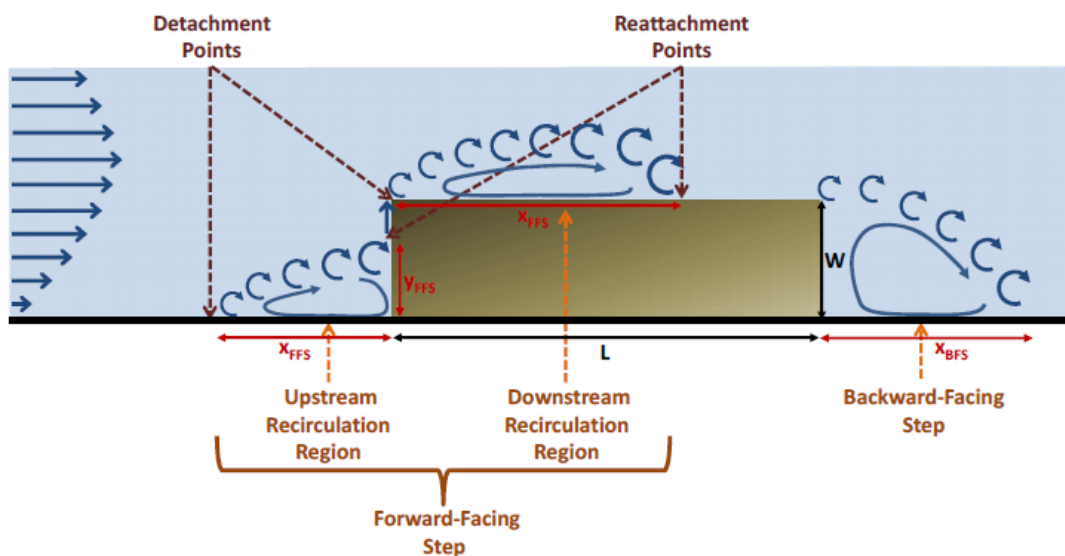


Figure 2-9: scheme of the flow field around an immersed object (from Jackson et al 2013).

Transported woody debris can clog narrow passages in the stream channel provoking contraction of the cross sections with the same results before mentioned.

In condition of congested transport the mass of floating debris creates banks of wooden material that tend to move downstream with a velocity that is different from the water surface velocity, the shear stress due to the wooden floating layer affected the stream velocity profile (Bocchiola et al., 2002).

2.3.2 Morphologic interactions

Large woody debris influence river geomorphology altering sediment transport and storage, channel dynamics and processes, and definitively channel morphology. These influences occur at multiple spatial scales within the riverine system, including the channel unit, the channel reach, the valley bottom, and the landscape depending on magnitude, size and distribution of woody debris and time of residence.

At the channel unit scale, LWD affect bed and bank erosion and influence the size and type of single pools, bars, and steps. Due to induced localized variation in flow velocity, scour and deposition take place depending on the debris size, position and orientation within the channel.

In case of a channel spanning log, immediately downstream, water velocity increases due to the flow being constricted. Upstream of a channel spanning log, velocity can decrease, creating sediment bars. Typically, erosion will occur directly downstream of LWD due to increased water velocity and scour (typical log-step configuration (Figure 2-5)). If debris occupies a large portion of the cross section it may lead to relevant variation of the channel slope.

LWD type, relative size, and orientation within the channel determine the specific influence of woody debris on velocity and habitat formation. In small streams, large woody debris often creates step pools configuration. In larger streams, LWD creates scour pools, and controls floodplain construction, island formation and side channel development. Channel width may be preserved by LWD acting as armour avoiding stream bank erosion. In contrast, channel widening may occur when LWD orientation causes flow to be directed to the bank side, resulting in bank erosion.

The magnitude of the blockage ratio related to a debris location and the permanence time interval, determine the scale of the morphologic influence. In some cases LWD may create dam jam of great impact (Abbe and Montgomery, 2003; Figure 2-10). The longevity of large debris in the stream environment is a significant variable in determining geomorphological influence. Old-growth conifers noted for their resistance to decomposition can persist in streambeds for hundreds of years, contributing to long-term stability. At the other extreme, some riparian species, although achieving a large size, decompose quickly unless continuously submerged, and so rarely has a lasting influence on the stream (Saldi-Caromile, Bates, Skidmore, Barenti, & Pineo, 2004).

Depending on the already mentioned LWD features (type, size, orientation, etc.) and on the hydraulic and morphologic characteristics of streams (i.e. flow regime, cross-section, sinuosity, sediment characteristic, and more) it is possible to observe a large variety of interactions and configurations that have been widely classified (Abbe and Montgomery, 2003; Wallerstein and Thorne, 2004). In this section just few examples have been proposed to synthesize the interaction mechanisms between sediments, woody debris and stream flow; a detailed description of all the possible configurations is not in the purpose of this work, in any case, a quite extensive inventory of LWD and LWD jam types is given in the glossary to support in the reading of the survey sheets form (refer to Chapter 4).

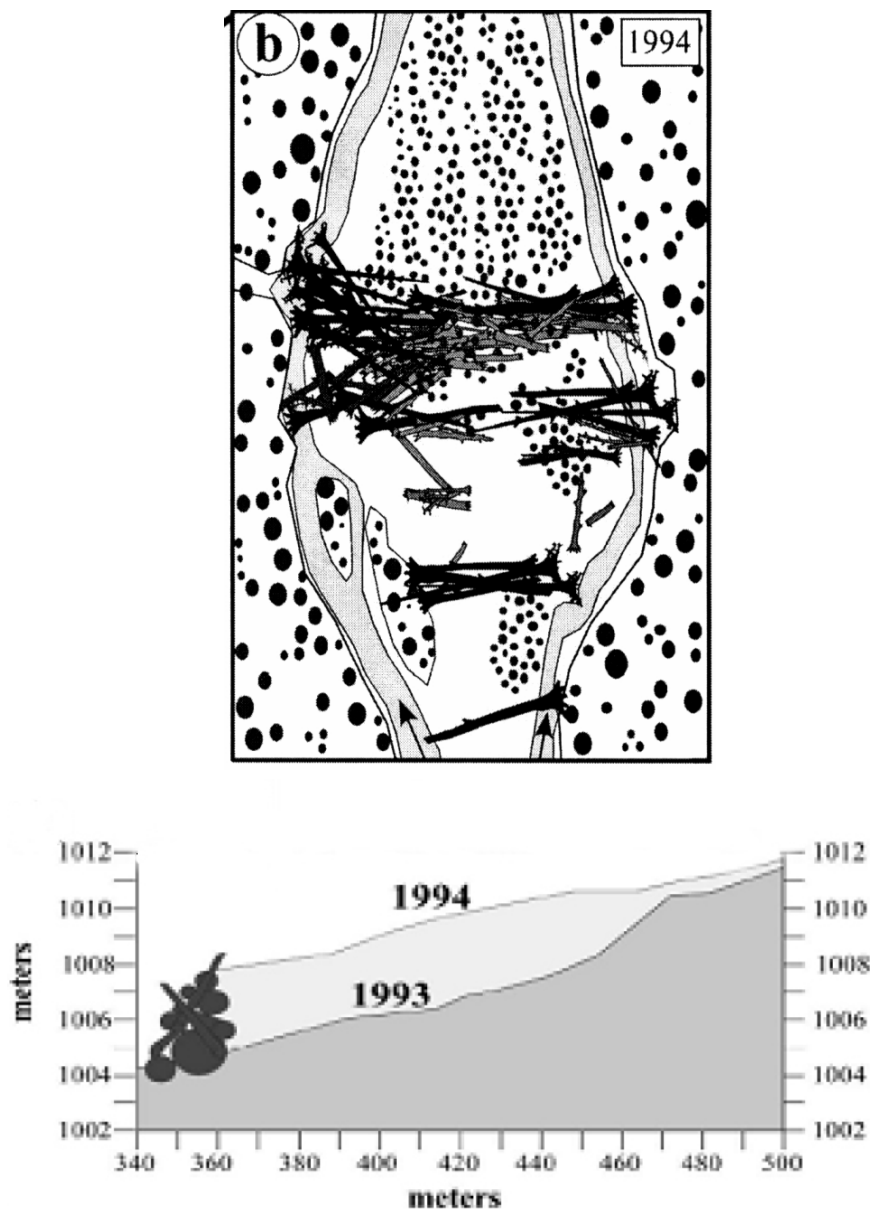


Figure 2-10: channel evolution in proximity of a dam jam: channel widening and aggradation (from Abbe and Montgomery, 2003).

LWD of significant dimension, with rootwad, acting as key element, tends to create bars as a result of the induced flow field (Figure 2-11), which may evolve in pioneer in-channel islands if the wooden material retains vegetation activity (Abbe and Montgomery, 2003; Figure 2-12).

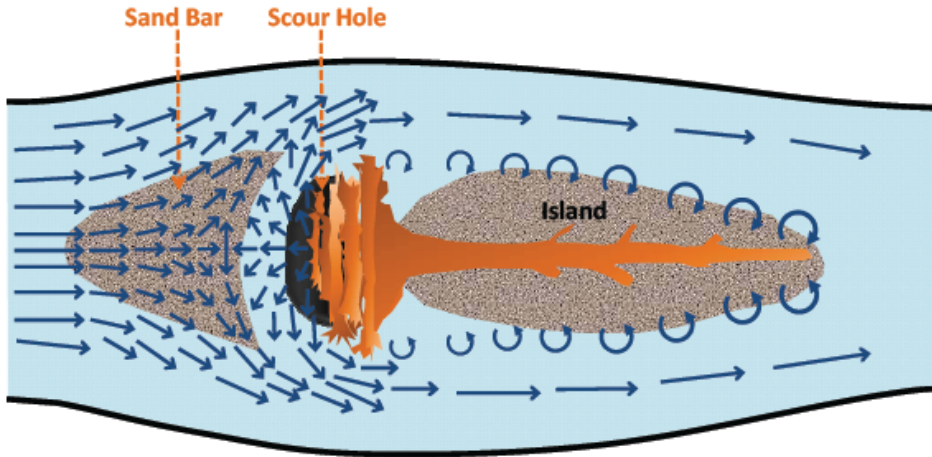


Figure 2-11: flow field and sediments dynamics in correspondence of a bar-apex jam (from Jackson et al, 2013).

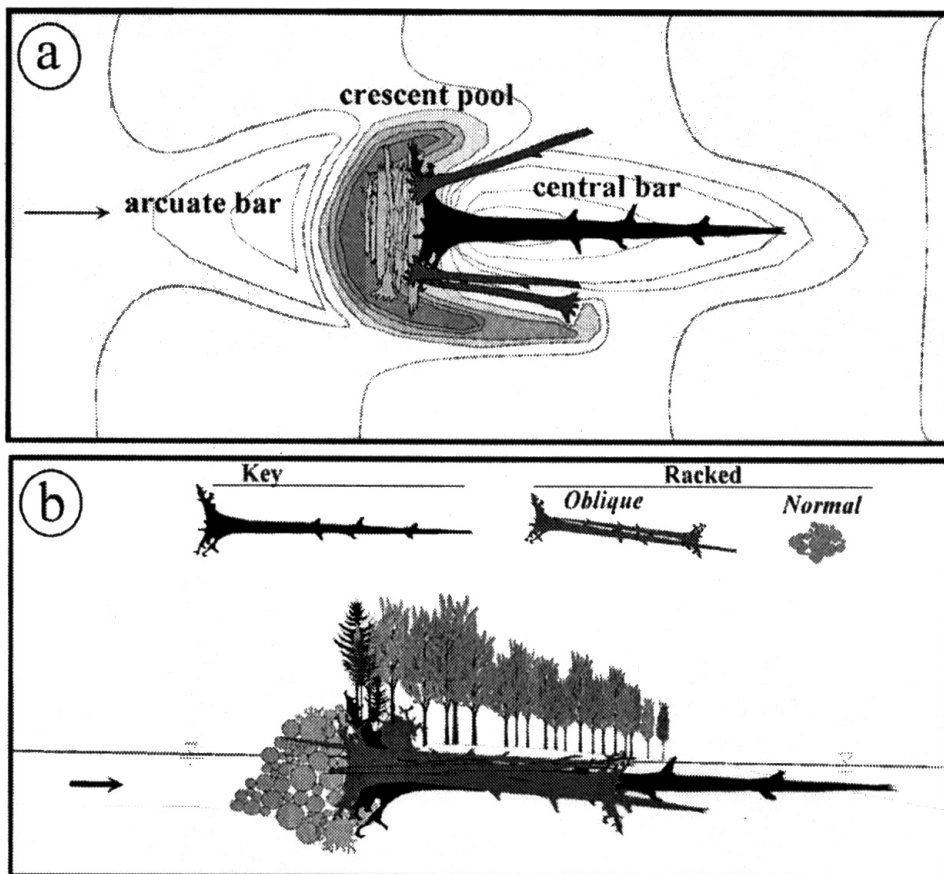


Figure 2-12: channel evolution in proximity of a bar-apex jam, with island formation (from Abbe and Montgomery, 2003).

LWD are then capable to extensively influence river channels width and shape, increasing the frequency of bend cut-offs and channel branching (Remich, 2002). Furthermore they can exert a large control on the overall sediment balance of the stream system resulting in significant impacts on the landscape scale.

2.3.3 Ecological interactions

As a consequence of the interactions previously described on flow velocity and water depths (pools), LWD provide essential habitats for aquatic organism by providing refuge for fish and invertebrates during periods of high and low flow conditions. During high flow, woody debris breaks up the current, creating eddies and areas of decreased flow. In low flow periods, pools created by LWD often are the last to dry up and provide habitat for aquatic organisms to retreat until the stream returns to a higher flow cycle. The biota impacted by the presence of wood ranging from microscopic bacteria, fungi and algae, to macro-invertebrates and fish encompassing all levels of the food chains.

LWD have also an important role in the basic levels of the food chain as they release nutrients in stream water and retain organic matter such as leaves, vegetation, and sticks that are being transported from the watershed through the stream. The retained material is processed by macro-invertebrates into a form that can be used as a food resource and incorporated into the food chain. If retention do not occur, the nutrients and energy in the organic debris are transported downstream.

The water recirculation, drops and eddies induced by LWD promote the water oxygenation with a positive effect on its quality.

The presence of large woody debris and jams increases the connectivity between channel and riparian zone. Lateral connection promotes floodplain and riparian habitats like side channels, off channel ponds and wetlands, etc.; these habitats represent ideal locations for feeding, reproduction and refuge for invertebrates, fish, amphibians, reptiles, birds, and mammals.

2.3.4 Interaction with the anthropic environment

Through centuries of civilizations humans have altered riverine environments. Firsts advanced cultures took advantage from the natural dynamics of rivers to develop themselves; next, human efforts have always been directed to mould the natural environment to correspond to communities' necessities.

With time the stream corridors have been altered directly through channelization, banks armouring, stream cleaning, and levees construction, among others, or indirectly through land use activities within the watershed. In particular wood have been largely exploited for centuries as building material and fuel, and the riparian zones have been deforested to give place to crops and urban settlements reducing sources of recruitment; debris have been removed from river channels to enhance

navigability and later, with the urbanization expansion, to protect in-channel infrastructures.

Channel geometry and wood loadings in the temperate zone are definitively altered by human activities and the characteristics of wood transport may be more closely associated with human practices than with channel size. The volume of wood in human-dominated rivers is often too small to have the same effects on either hydraulic or geomorphic variables as in stream or pristine rivers (Piégay, 2003). Hence the above mentioned effects of wood on river morphology are nowadays noticeable mainly in wild undisturbed catchments.

A noteworthy example is given by the Australian rivers that remained undisturbed till the Europeans colonization in the 19th century. A research conducted by Brooks et al (2003) in Australia, compares two adjacent rivers in East Gippsland, Victoria, the Cann River and the Thurra River. The floodplain of the first one have been intensely urbanized since the 1860s, while the floodplain of the second one remains relatively undisturbed. The authors indicate the widespread clearance of the riparian zone and the removal of wood from the Cann River as the main difference between the two catchments. In Figure 2-13 the effect of the management practice on the longitudinal profile of the river beds is visible, furthermore comparing the contemporary Cann River with its paleo-channel and with the contemporary condition of Thurra River, the current Cann River shows:

- a wider channel width;
- deeper mean depth;
- greater bankfull discharge and velocity;
- greater stream power;
- larger median grain size;
- greater likelihood of bank failure;
- no stable riffle-pool sequences;
- greater lateral migration;

underlining the shaping and stabilizing effects of wood in rivers.

Without doubt is too simplistic reduce to wood management the impact of urbanization in a river valley: excluding mining activities, the reduction of drainage surface is a significant impact that influences flow and sediment transport regimes. As a consequence is not possible to distinguish unequivocally the relative significance of increased flows and decreased LWD abundance in these evolution settings. Nevertheless acknowledging the interrelationship between LWD loss and more pervasive watershed changes, it is possible to make some judgments about the consequences of that loss by observing the immediate response of channels to LWD removal and by deduction from the observed roles of LWD in undisturbed channels. Consequently it is possible to conclude that those responses include a rapid increase in the rate of channel shifting, both horizontally (typically by widening) and vertically (typically by incision), rapid changes in the bed morphology depending on the type of

channel, and increasing in sediment discharge. If the LWD loss is a consequence of riparian clearing, several years are necessary to observe changes (as existing logs and jams deteriorate without concurrent replacement), while if LWD are actively removed from the channel the corresponding increase in sediment transport is more immediate and measurable within a single storm season (Bilby, 1984).

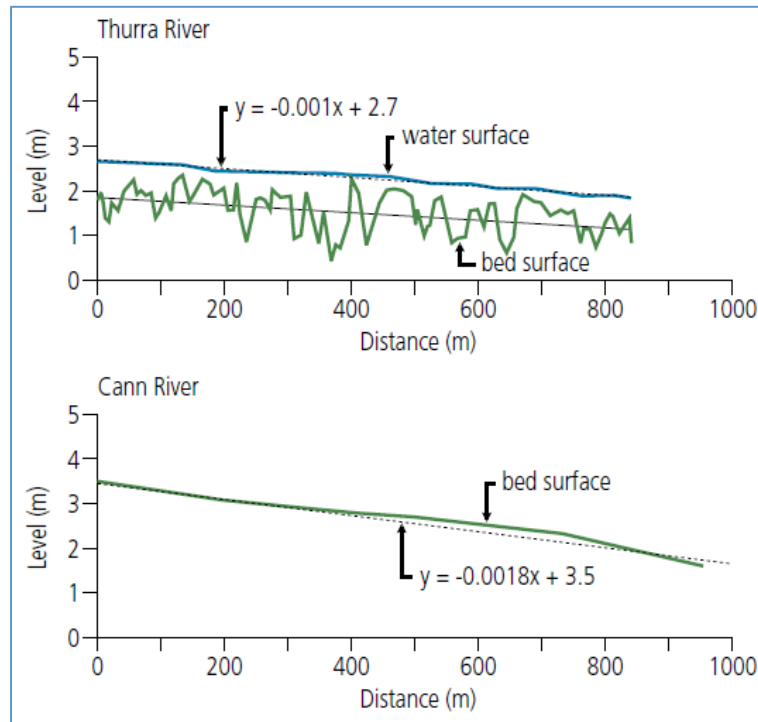


Figure 2-13: bed profile of the Thurra and Cann Rivers (Brooks et al., 2003).

What is clear is that natural processes of wood dynamics are far from being well understood, particularly in large rivers, because of the frequent high impact of human activities (Gurnell et al., 2002). In many European areas in last decades socio-economic changes have led to land use changes: the upper reaches of watersheds have been abandoned and the valley settlements have been expanded. Contemporaneously new management practices for riparian vegetation have been actuated. Comparing the present situation to the first decades of the 20th century, today, in riverine urbanized areas, we observe: an increased volume of wood in the river corridors, LWD of lower relative size due to the youth of riparian forest, increased transport capacity by the stream flow, due to increased runoff (as a result of reduced drainage and increased precipitation) and modified channel geometry. Therefore woody debris are usually perceived, and actually act, as a risk factor for riverine settlements.

Wood removal cannot be a management solution as it intervenes on just one component of the system, without achieving a consistent risk reduction because of its unpredictable effects on channel stability (we can only partly isolate the consequences of LWD loss in channels, because those consequences are amplified by other, concurrent changes as well), and with an inevitable deterioration of river habitats and

water quality. At the same time the mere replacement of lost LWD, with restoration aims, will not reverse all of the stream-channel changes, in large measure because only a fraction of the causal mechanisms is directly addressed by such an action (Booth et al., 1997).

3 LARGE WOODY DEBRIS HAZARD ANALYSIS

LWD removal has been for long time the common practice for wood risk reduction, until that several studies have demonstrate that loss of LWD alters channel form and processes, inducing greater sediment fluxes, more rapid bank erosion and incision, and loss of heterogeneity in bed morphology, with a global deterioration of water quality and biodiversity, and without a recognizable reduction in flood consequences (Shields and Cooper 2000; Bisson et al., 2003; see section 2.3.4). This awareness leads a great part of environmental agencies, all over the world, to reintroduce wood in rivers also if the effectiveness of this practice has still to be thoroughly demonstrated (doubts exist even that simple reintroduction of LWD will fully restores the lost functions of human altered streams, Booth et al., 1997).

At the same time the dramatic impacts of wood during extreme events point out the urgency of risk assessment methods capable to take into account all the risk factors and sources that may superimpose their effects.

3.1 STATE OF THE ART

Management practices which deals with LWD all over the world are principally focused on rivers requalification instead of risk reduction (i.e. Design guideline for the reintroduction of wood into Australian streams, Australian Government, Land & Water, 2006), few guidelines are directed to the reduction of the harmful impacts due to LWD on specific structures like bridges, culverts (hec09 Federal Highway Administration U.S.A, 2005; NCHRP REPORT 653, 2010) or dams (i.e. hydroelectric power plants). Most of the existing reports of singular riverine counties or environmental bureaus dealing with LWD, refer a general deficit in coordination, unambiguousness, applicability and coherence among the generic guidelines, recommendations and directives indicated by the chief governments. Presently a structured procedure to take into account the wood effects in the assessment of hydro-geologic risk is still missing, moreover bearing in mind wood impact designing river crossing is not yet a common practice.

The European Commission in the Flood Directive (Directive 2007/60/EC of the European Parliament and of the Council of 23 October 2007 on the assessment and management of flood risks. OJ L 288, 6.11.2007, P.27), recognizing the recurrent devastating impacts of floods on European population, economic activities and environment, recommended to the Members States to prepare fully comprehensive flood hazard an flood risk maps for relevant areas by the year 2013.

In particular the European Directive emphasizes the requirement of “the better environmental option” in the redaction of Flood Risk Management Plans, considering

nature protection and biodiversity policy strictly linked to flood risk protection: in this perspective a key role is recognized to large woody debris for their dual nature as risk factor and multifunctional environmental resource.

It is also manifests that till woody debris dynamics in rivers will be disregarded flood maps will be extremely ineffective: for example an expected water level that may be considered safe for a river crossing, in presence of LWD may be not, this means that flood impacts would be substantially underestimated.

Assessing woody debris impacts, problems arise from the complexity of the question: several aspects in wood processes are not yet well known (Mazzorana et al, 2011) and the superposition of different physical phenomena results in conspicuous difficulty to predict critical scenarios (Mazzorana et al. 2009, 2011).

Referring Pliefke et al. (2007), the risk management framework, to gain a fitting approach to risk, comprises three main phases: risk identification, risk assessment and risk treatment (Figure 3-1). Focusing just on the firsts steps of the procedure it is possible to perceive the complexity of the issue.

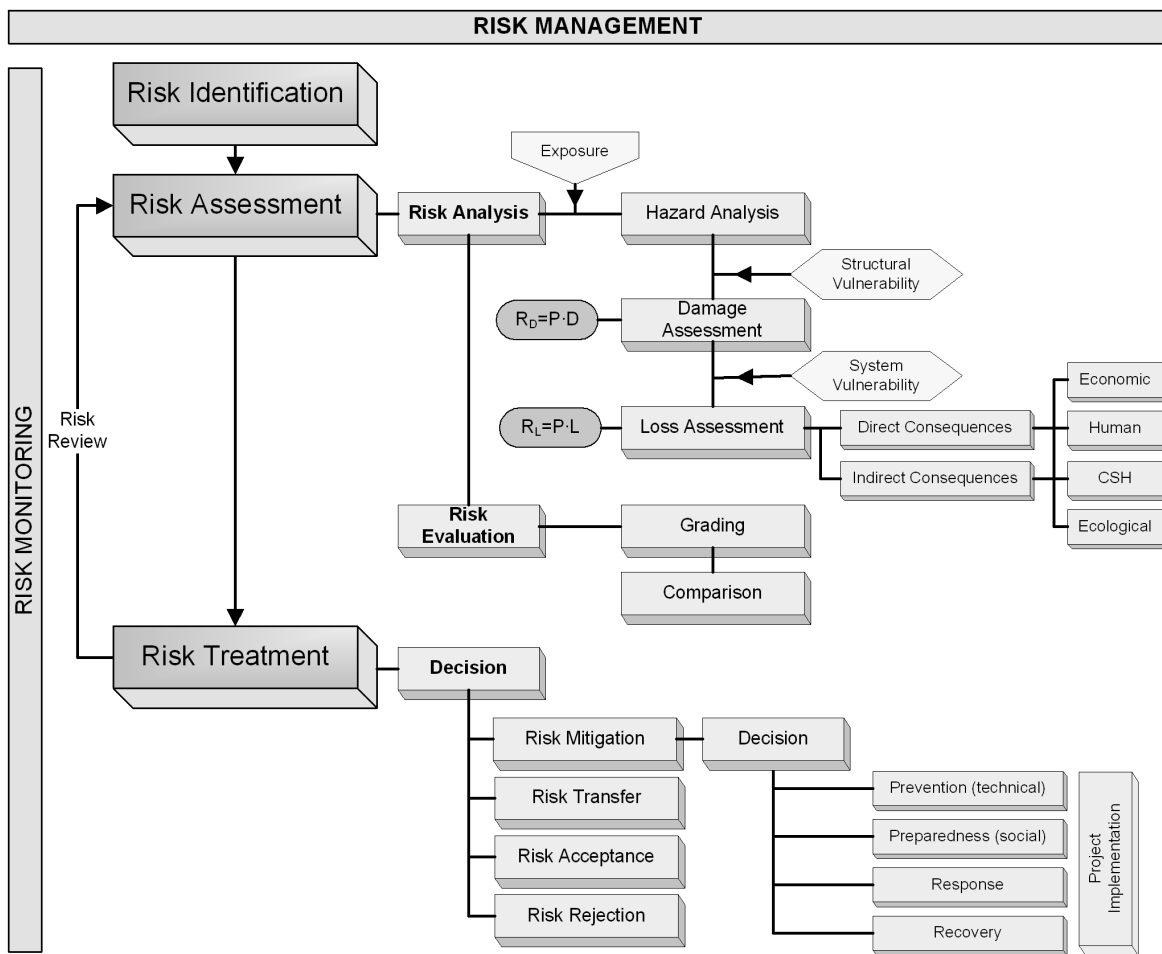


Figure 3-1: overview of the risk management process (from Pliefke et al., 2007).

The risk identification, that represents the first essential phase of the procedure, consists in defining the spatial domain of the analysis and identifying all risk sources

within the domain. Considering LWD, the spatial domain cannot be restricted to the exposed sites like in-channel structures or river neighbouring urban or industrial settlements, but has to be widened to the whole river catchment where the LWD supplying areas occur.

Next the first step of the risk assessment phase is the hazard analysis that consists in the identification and quantification of each hazard affecting the domain. The hazard is here represented by a multiple set of possibility: not only the amount of wood but also wood distribution inside the channel, wood relative size and orientation (with respect to the hydraulic cross section), and wood stability. Wood availability depends from various natural factors hydrogeological, forestry and climatic, whose magnitudes and frequencies have to be merged to quantify the global hazard.

Assessing damage, direct impacts on in-channel structures and infrastructures have to be considered, in this case the major consequence is the reduction or the complete loss of functionality of public utilities (roads, water supply, pipeline, etc.), furthermore all potential damages assessed for a flood occurrence may be transferred on LWD evaluation. Therefore the exposed elements are indeed the in-channel structures and every element, in river neighbourhood, that is reachable by a designed level in case of overbank (Figure 3-2).

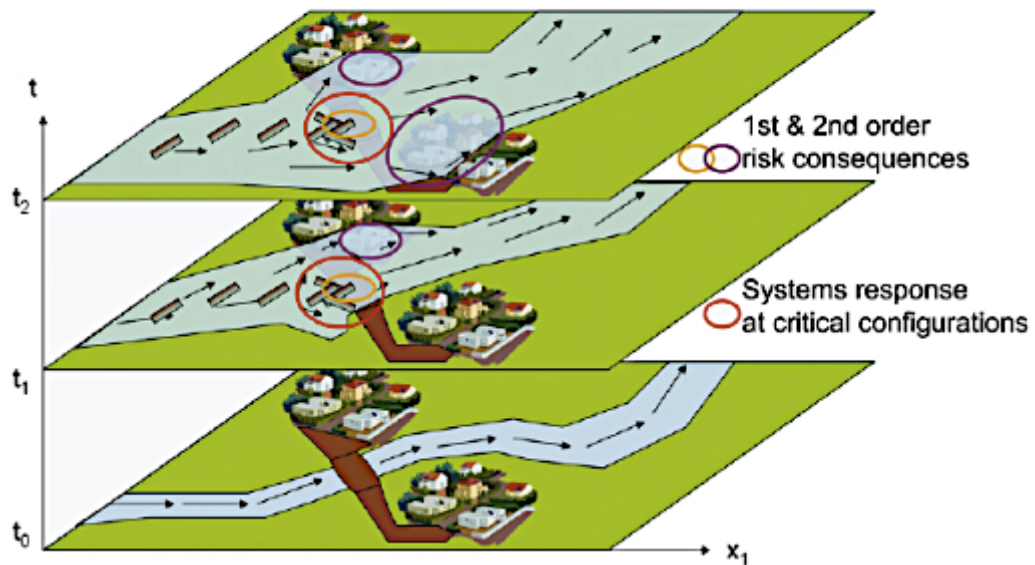


Figure 3-2: potential hazard and risk scenarios at a critical location (from Mazzorana and Fuchs, 2010).

The possibility to assess damages and losses (risk scenarios) and after that to complete the risk analysis process is strictly dependent from the possibility to predict hazard scenarios. Without the knowledge of the possible impact modes we cannot be able to define possible scenarios, but impact modes depend from wood dynamics that have still to be thoroughly stated.

3.2 PROCEDURE FRAMEWORK FOR LARGE WOODY DEBRIS HAZARD ASSESSMENT

To Mazzorana et al. (2011) is attributable the definition of the most comprehensive procedure to assess the hydrologic risk in presence of LWD.

A comprehensive procedure has to involve:

- Evaluation of *wood availability* in the river catchment by:
 - Vegetation evaluation (species, age, mortality...);
 - Valuation of hill slopes stability;
 - Valuation of the river banks stability;
 - Estimation of the in-channel material.
- Identification of the *critical cross sections*;
- Prediction of *hazard scenarios*:
 - Estimation of water discharge
 - Estimation of wood recruitment and entrainment;
 - Estimation of wood transport and destination.

While singular issues of the array may be undertaken, significant uncertainties on cause-effect relationships, on widespread system loadings and system response remain tough limits to the procedure applicability. Thus every contribution to the identification of the relevant impact factors and of the processes dynamics that determine possible system loadings during extreme events, and to the identification of the system response mechanisms, represents an enhancement in risk assessment skills.

In the following pages a wide overview of the main issues is given.

3.2.1 Wood availability in river catchments

The wood availability in the river catchment is given by the potential recruitment and the previously recruited in-channel material.

The periodic monitoring of the in-channel material is not sufficient to establish the temporal recruitment load if is not known the wood outflow rate (for transport or deterioration). Thus is necessary establishing all the possible sources (as stated in chapter 2) and all the possible recruitment areas.

Mechanical recruitment processes like landslides, avalanches, wind-throw, snow load, hydrodynamic loadings, animals, banks erosion and physical recruitment processes like natural mortality, parasites infection, pollution, have to be considered (Figure 3-3).

Hill slopes stability and banks stability are well studied processes that have to be merged with vegetation plots to establish potentially recruited volumes.

Mazzorana et al. (2009) propose a method for the identification of the recruitment areas exposed to hydrodynamic loadings (alluvial forests, lowland riparian forests and riverside woodlands) by the interpretation of aerial images, taking into account the

response of different vegetation and forest typologies to the hydraulic forces and impacts of flood processes. The proposed method assesses also the wood volumes and trunk position within the maximum extent of the flooded area.

The in-channel material can be determined with direct and remote monitoring techniques, in chapter 4, this topic will be widely discussed and a properly settled tool for direct surveys will be exposed.

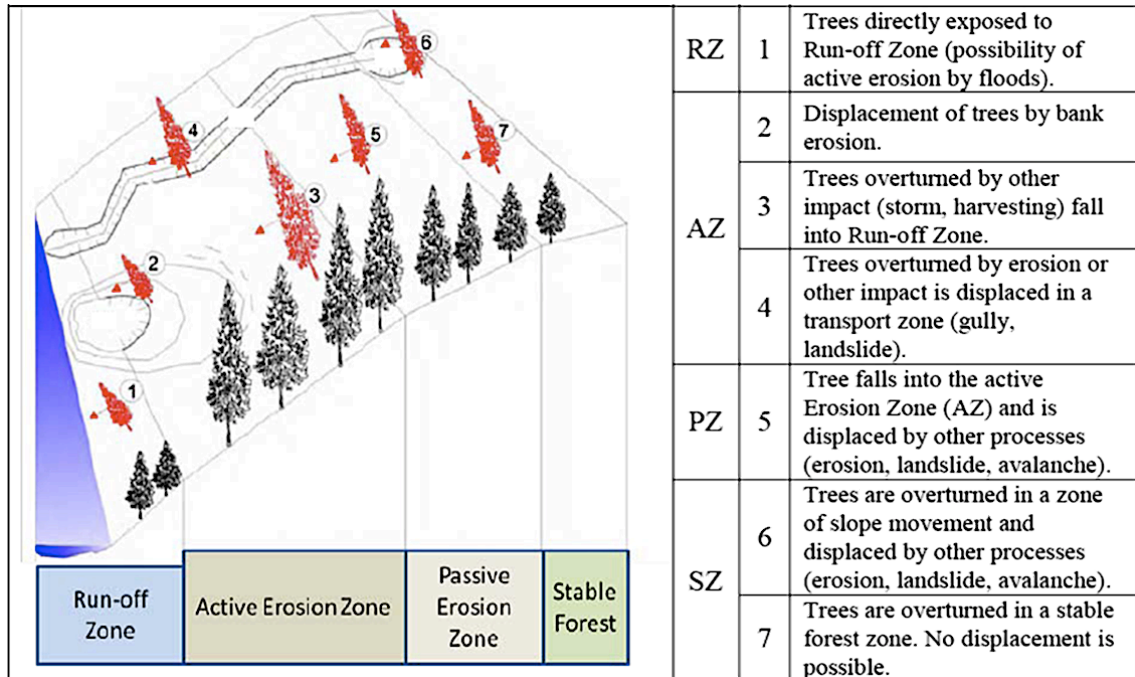


Figure 3-3: recruitments zone and mechanisms (according to Mazzorana et al., 2009).

3.2.2 Critical sections

The definition of critical sites along the river channel requires verifying some basic conditions (according to Mazzorana et al., 2011):

- Availability of recruited woody material in the upstream catchment;
- Occurrence of entrainment and transport processes that deliver part of the recruited volumes to the considered spatial domain supposed to be a critical location;
- Interaction phenomena of the transported woody material with the geometrical features of the critical configuration: woody material deposition and accumulation at specific geometrical elements and consequent potential effects (e.g. cross-sectional obstructions with consequent floodplain inundations) or contributes to increase loadings on structural components (e.g. bridge piers, bridge superstructure);
- Risk consequences: the above mentioned interactions determine an increase in risk exposure of vulnerable objects.

Stated in the previous section the point a), and postponing for the moment the point b) to the next section, let's focus on point c): a wider knowledge of the varieties of injuries that LWD may induce is here necessary to properly assess the critical configurations.

Actually a systematized classification of the potential damaging actions due to LWD is lacking, in this work a rational arrangement of possible actions will be exposed even if it cannot be considered an exhaustive categorisation.

In this context only mechanical or hydrodynamic detrimental actions due to LWD on structures, infrastructures and river channels natural features will be considered (without taking into account for navigation problems). Resulting from the analysis of literature material and from direct experience in field is determined that these actions may be different in dependence principally of *flow condition*, *stream order*, and *stability* or *instability* of the large woody debris.

3.2.2.1 Mean flow conditions

Stable woody debris in rivers can be a significant source of roughness and consequently influences flow at both the local and reach scale.

In mean flow circumstances we usually have stable woody debris. The principal effects in this configuration are:

- *Flow deflection;*
- *Turbulence.*

Flow deflection occurs when a stable LWD or a stable jam spans a portion of the channel width in contact with the stream flow (Figure 3-4), depending on debris size and orientation different effects may be observed. The relative size of the obstruction to the stream cross sectional area (blockage ratio) determines the intensity of the deflection and of the acceleration of the flow and the general resistance to it.



Figure 3-4: LWD fallen from eroded bank (Cecina River).

Several studies (Gippel, 1995; Gippel et al., 1996) confirm that till the width obstruction is less than 10% of the channel size there is not a substantial increase in flood risk, due to the little effect in the total conveyance of the channel, but even small obstruction can cause local flow deflection and acceleration. For orientation over 40° the stream flow (also in ordinary condition) may be redirected to the opposite bank, producing bank protection for one side and toe erosion to the other side. After a sufficient time interval it may produce banks failure, in any case it produces bank weakness.

A debris partially immersed in a flow field induces alterations on it as any obstacle does (i.e. bridge piers, boulders, etc.), the sudden redirection of the stream lines produces local vortices in the boundary layer along log sides and in the extent of the wake zone, as a consequence scour and deposition take place (Figure 3-5, Figure 3-6).

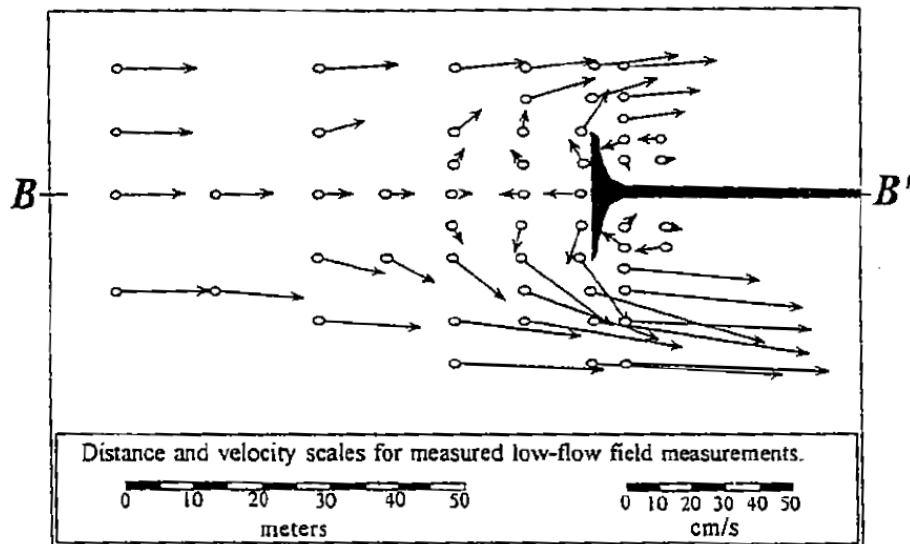


Figure 3-5: plan view of measured near-bed flow velocities in correspondence of a LWD with rootwad, parallel to the flow, during low flow condition in a natural channel (according to Abbe and Montgomery 1996).

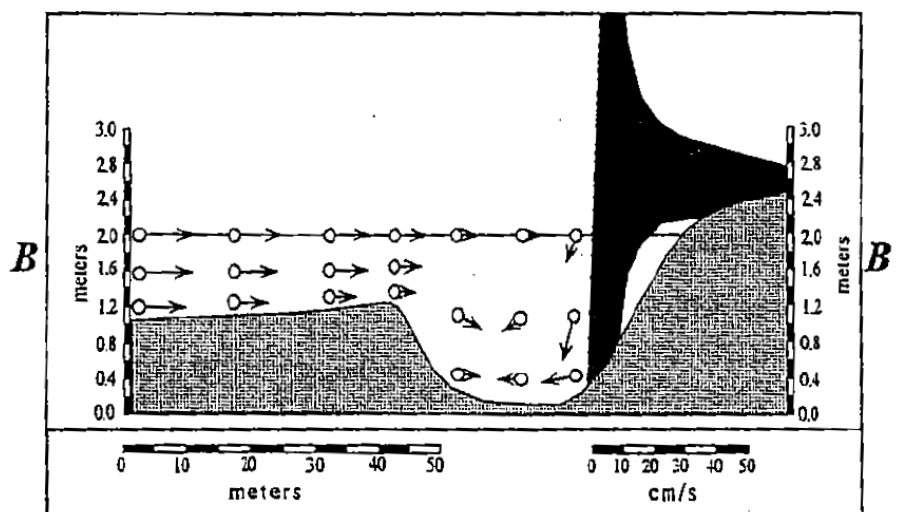


Figure 3-6: profile of measured flow field upstream the LWD (according to Abbe and Montgomery 1996).

Clearly, peak discharges give the main contribution to bed excavation but also ordinary discharges, in particular locations (like bridge piers or abutments, concrete dykes), may produce local effects contributing to the progressive exposure of the structure foundation (Figure 3-7).



Figure 3-7: debris accumulation at bridge piers (South Platte River, Colorado).

3.2.2.2 High flow conditions

In this situation debris may be stable or unstable then entrained and transported. Principal effects may be:

- *Flow deflection;*
- *Upstream rising;*
- *Flow deceleration;*
- *Woody debris dam formation and collapse;*
- *Hitting;*
- *Section blockage*

As previously mentioned the partial obstruction of the hydraulic cross section caused by LWD produces acceleration and deflection of the stream line that during peak flow may cause a significant banks erosion; in particular if banks are represented by not vegetated earth levees, breaches may occur with consequent runoff.

The presence of an in-stream obstacle produces also a backwater risen that may be sizeable for a certain extent only if the stream blockage is over than 50%, with flume experiments Young (1991) found out that a blockage ratio of 50% produces a 1% risen in base flow stage level, the same experiments revealed that blockage ratios higher than 80% are necessary to significantly increase flood levels. Furthermore the produced effects depend also by the concentration and spacing of debris (Ranga Raju et al., 1983; Shields and Gippel, 1995). The impact that multiple pieces of LWD have on flooding is determined by the distance separating each piece. If several pieces are

located within two times the diameter of the next piece, there is no greater impact on water levels than one piece alone (Rutherford et al, 2002).

In condition of congested transport (Figure 3-8) the mass of floating debris creates banks of wooden material that tend to move downstream with a velocity that is lower than the water flow velocity (often because of the presence of heavy debris like fresh material with branches and rootwad), the shear stress due to the wooden floating layer affects the velocity profile (Bocchiola et al, 2002) producing again backwater rising.



Figure 3-8: congested flow (San Antonio River Texas).

During extreme flow, debris dam may growth quickly as new formation in correspondence of in channel obstacles, or as consolidation of existing cluster, such obstructions of the cross section induce naturally backwater rising and channel widening as the water flow searches new routes to convey downstream (Figure 3-9). But the worst occurrence is the sudden collapse of these structures that produces downstream a peak flow of water, sediments and woody debris.

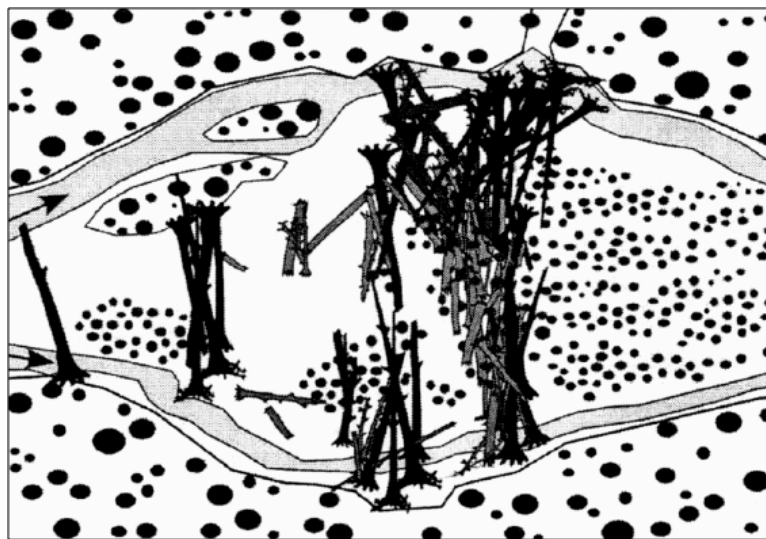


Figure 3-9: channel widening in presence of dam jam (Abbe and Montgomery, 1996).

The floating debris may hit all in-channel structures like bridge piers, abutments, water supply structures, dams, embankments causing breaches, and in case of overbank flow also buildings and other structures may be damaged. During the flash flood of Cinqueterre (Italy 2011), after the passage of the flood wave, many openings of buildings ground floors were found completely obstructed by floating LWD.

Section blockage is probably one of the most evident impact of LWD during extreme event (Figure 3-10), it may occurs in every narrow passage, in presence of in channel obstacles. As a consequence of the reduced flow discharge capacity of the section, back water rising occurs and the probability of overbank increases. If the obstacle is represented by a bridge the acceleration due to the restricted passage may produces elevated scour depth at pier toes or abutments. Furthermore the increasing pressure on the structure produced by water flow and woody debris may lead to the structure failure with loss in transport infrastructures (Figure 3-11).



Figure 3-10: bridge obstruction an flow deviation (Passirio River, Alps).



Figure 3-11: bridge failure (NY, USA).

3.2.2.3 Conclusions

Concluding, geometrical characteristics and physical characteristics (i.e. earthen banks) of a river cross section, and wood distribution and dimension contribute to the vulnerability of a location.

Considering the combination between channel size and morphology (stream order) and wood availability and relative size, in lowland streams (plane-bed and pool-riffle channels typically spanning a range of gradients between about 0.1% and 3%) LWD has the greatest range of functions (e.g., Lisle and Kelsey, 1982; Keller et al., 1985; Montgomery et al., 1996) (refer Figure 2-2).

Ignoring in this section LWD's ecological role, these functions include:

- Hydraulic roughness, which may increase by 50% or more through the disruption of flow imposed by a high concentration of LWD, logs, stumps, or debris jams;
- Sediment storage and pool formation;
- Bank erosion or protection as a result of flow deflection;
- Significant LWD transport because of the relative size between wood and the hydraulic cross section.

Keeping in mind that channels with these characteristics usually cross densely urbanized areas is reasonable to believe that lowland river catchments are the most exposed to risk.

Even if in Alpine and Apennine regions (typical mountainous watersheds) flash floods, characterized by debris flows or avalanches conveying downstream large amount of wood, show significant impacts (i.e. the events occurred at Cinqueterre in 2011 or in Switzerland in 2005).

3.2.3 Critical scenarios

To define possible hazard scenarios is necessary to effectively define system loading scenarios (i.e. flood with high LWD transport rates) and system response scenarios (i.e. bridge clogging or changes in flow pathways).

To reach the system loadings, defined the recruitment areas and the critical locations it is necessary to model the transport from the first to the second areas. According to Figure 3-12 for a segment of the river reach all the fluxes have to be determined and an entrainment model and a transport model have to be adopted.

Hydrodynamic models and sediment transport models are widely provided even if, when the flooding process is characterized by significant sediments load and woody debris transport, the predicted results may be less reliable.

The existing entrainment models are derived under simplified and limitative assumption and tested with a limited set of experimental data, in the next chapters the question of the entrainment dynamics will be deeply discussed and a novel criterion for the determination of a threshold condition will be proposed.

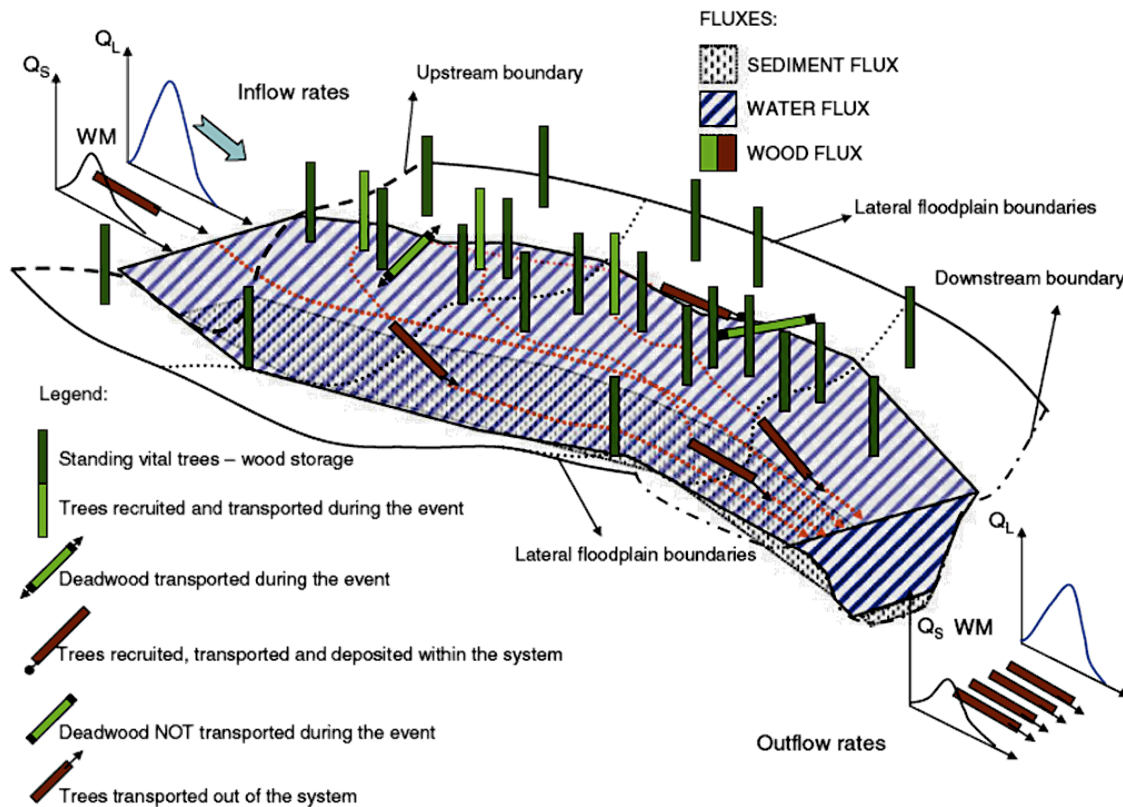


Figure 3-12: wood, sediment and water fluxes within a system unit (Mazzorana et al., 2011).

Determined the amount of wood that will be entrained with high probability by the flood discharge, several models may be adopted to estimate wood transport, in particular Mazzorana et al., propose a procedure that allow two approaches: one to estimate the main pathways of the wooden material and the possible deposition zones, and one to evaluate the interaction between the transported objects and in-channel obstacles such bridges.

The modelled configuration results in consequent flood levels and inundated areas and complex system response like failure of in-channel structures (natural or engineered) have to be taken into account.

Considered the elevated level of uncertainties, Mazzorana and Fuchs (2010) deal with the problem with a nested scenario approach: a scenario level structure is proposed, taking into account causes (system loading level) and effects (system response level) within a stream system, and next approached with a Formative Scenario Analysis (Scholz & Tietje, 2002) in combination with Fuzzy set theory that allows for making decisions in a fuzzy environment, which is made of fuzzy objectives, fuzzy constraints (imprecise and incomplete data), and fuzzy conclusions (subjective conclusions). The procedure results in qualitative and quantitative knowledge that can be integrated into scenario definition within the framework of natural hazard risk management.

3.3 CONCLUSIONS

The positive and negative effects of LWD in rivers have been for long time misunderstood. The existing management strategies are inadequate to deal with the issues matching safety and morphologic and ecological benefits.

Actually a structured procedure to take into account the wood effects in the assessment of hydro-geologic risk is still missing, in particular the risk identification and the hazard analysis present lacks of knowledge and implementation skills, system response mechanisms are only partly understood with consequent uncertainties in protection system functionality and mitigation efficacy.

Mazzorana et al in 2011 proposed a framework for a widespread analysis of the hazard impacts of wood in rivers. Within the proposed method some issues have been enhanced by the authors while some other have been assumed from literature.

The present work improves risk sources comprehension and introduces effective tools for monitoring and mapping river catchments vulnerability, focussing on the aspects less investigated in the cited work; in particular a suitable survey method to identify the catchment exposure detecting critical sections and wood availability, and to collect the necessary information for mapping woody debris distribution along the river channel is here proposed (chapter 4), and a novel criterion to derive an entrainment threshold condition is developed (chapter 5, 6 and 7).

Considered the complexity of the whole phenomenon, the superposition of several natural processes that results in significant uncertainties on cause-effect relationships, on widespread system loadings and system response, the possibility to apply the current methods of risk analyses for natural hazards, which are usually based on quantitative methods of impact assessment to a given environmental setting, results in simplifications that may be not able to effectively define the hazard scenarios.

Nevertheless a hydrodynamic model associated with an improved entrainment criterion may lead to the estimation of the volume of wood that will start to move with high probability, which is an essential starting point for the construction of hazard scenarios, and at first stage, i.e. defined an appropriated threshold level of acceptance for the entrained volume within the downstream limits of the considered domain, it may represent a basic approach to risk assessment on the base of which the employed agencies may define management strategies.

As a first result of this chapter the knowledge gaps in risk assessment have been identified and the impact overview, here carried out to recognize the critical sections, have indicated the requirements of the river catchments more impacted from large woody debris dynamic processes (section 3.2.2.3) on which directing the major investigative efforts.

4 MONITORING

Monitoring is a primary tool in environmental management: it allows to establish the existing condition necessary for planning management intervention and to check over the time system variability and response in absence or presence of interventions.

For wood monitoring in river channels direct and remote techniques are used. Remote monitoring, like high resolution aerial images and LiDAR (Light Detection And Ranging or Laser Radar), can give a global indication of the wooden material distribution, it's interaction with channel morphology pointing out trends and patterns at reach scale, while direct measures are essential for detailed surveys, to establish volume and characteristics of the material which are fundamental input for a predicting model.

4.1 SURVEY SHEETS FORM

The presented survey sheets form is principally intended for the collection of quantitative and qualitative data for the application of a predicting model but is generally conceived to collect useful information for a wider analysis of the behaviour of wood in river channels.

The exposed form is an advanced development of a template proposed by Betti et al (2006), adapted by the structure of the original survey sheet form for geomorphological characterization of river channels proposed by Thorne (1998).

The survey form is focused on the hydraulic and geomorphologic interactions between large woody debris and river. It is structured in two sections: one related to the river morphology characterization of the surveyed reach and the second one reserved to the woody debris characterization regarding spatial distribution, dimensions, physical properties (porosity, vitality, etc.) and interactions.

4.1.1 Framework

The integral form is arranged in 5 sections:

1. Reach description;
2. Sub-reach geomorphological characteristics;
3. LWD jam sheet;
4. LWD sheet;
5. LWD interactions.

The form is intended for jam formations and isolated elements: in the first case, following the sheets progression, after the global characterization occur the major elements, for the isolated debris there is just one element.

The complete report of a field survey is structured as in Figure 4-1: for any reach inspected a sheet 1 (Table 4-1) is draw up, next it is accompanied by a variable number of sheets 2 (Table 4-2) as the number of surveyed sub-reaches. For every sub-reach a variable number of sheets 3 (Table 4-3) will be draw up for every jam here detected. The number of filled in sheets 4 (Table 4-4) will be equal to number of LWD detected: some as key or racked debris in jam’s formations, some as isolated debris. Jams interactions with water flow and sediments will be valued globally considering the assemble as a single object, hence the amount of filled in sheet 5 (Table 4-5) will be equal to the number of jam plus the number of isolated elements found within the inspected region.

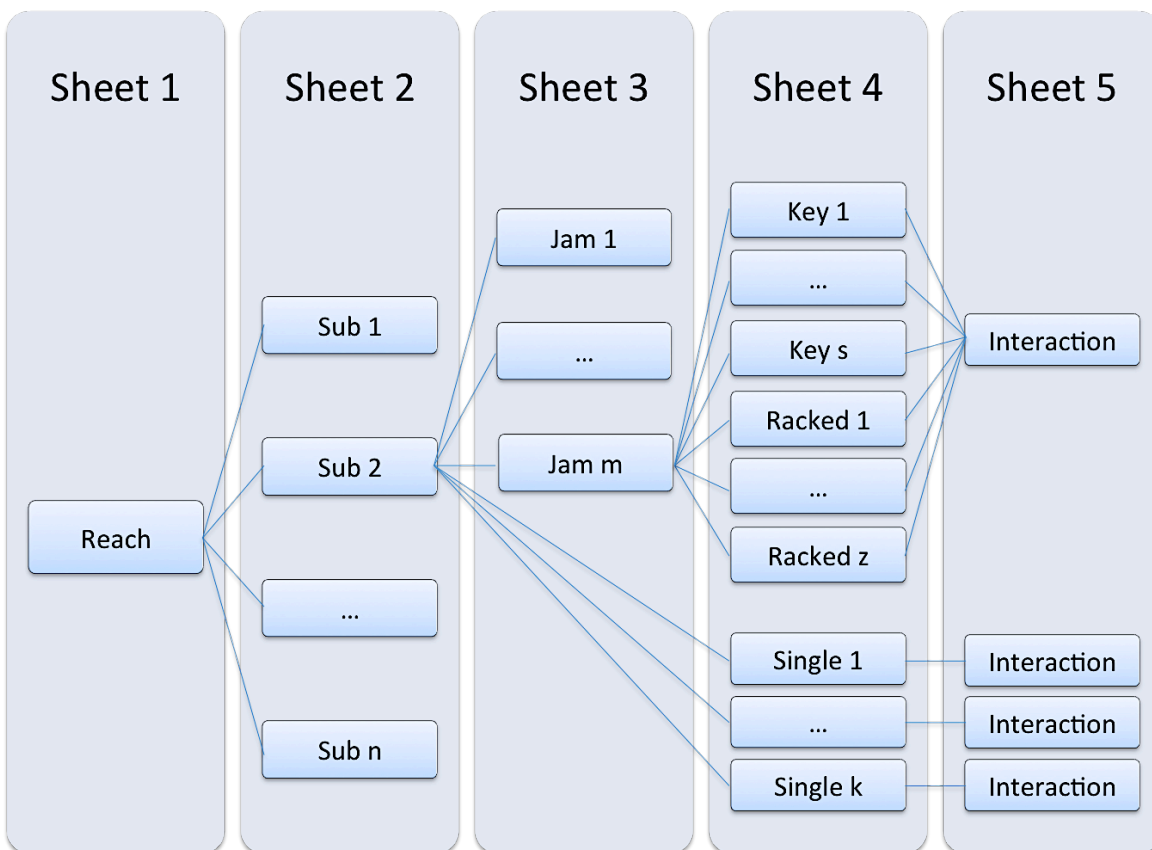


Figure 4-1: framework for the sheet drawing up.

Actually they are focused on the river morphology characterization and the in-channel wooden material evaluation but their modular structure is suitable for integrations: extending, for example, the survey to the hill slopes or the standing vegetation state.

In the following pages the sheets contents are explained in depth with regard to the wood material survey, while for the morphological characterization the references are Rinaldi and Surian (2003, 2004) and a filled in example is presented in Appendix A.

4.1.1.1 Sheet 1: reach description

During a field survey the inspected region has to be long around 20 times the bankfull width; it may be shorter but not under the size of a singular geomorphological unit of the river channel. Either extent has been chosen, the river channel has to present homogenous features inside the surveyed region in terms of: valley bottom morphology (width, orientation, incision rate), channel morphology and hydraulic characteristics.

Table 4-1: survey Sheet n.1

1. REACH DESCRIPTION	
General	
Date _____	Operators _____
River _____	Reach _____
Reach code _____	
GPS position _____	
Upstream end N _____	E _____
Downstream end N _____	E _____
General morphological characteristics	
Alluvial channel (large) <input type="checkbox"/>	Intermediate <input type="checkbox"/>
Channel morphology <input type="checkbox"/>	Confined (small) <input type="checkbox"/>
(alluvial or intermediate) R=straight, S=sinuuous, R-S BA=straight or sinuous with alternate bars	
M=meandering, W=wandering, CI=braided, A=anastomosing	
Bed configuration <input type="checkbox"/> R=cascade, SP=step pool, LP=plane bed, RP=riffle pool, DR=duneripple	
Reach sketch (length possibly of about 20 times channel width)	
<u>To report:</u> reach limits, subreaches (following sheets) limits, measured representative cross section	
Measurement of representative cross-section	
Mean channel slope	<input style="width: 50px; height: 15px;" type="text"/>
Water surface slope	<input style="width: 50px; height: 15px;" type="text"/>
Notes: it is preferable to measure a representative cross section and channel slope by a total station. In this case, the sheet is used to outline the measured cross section and to number the surveyed points and showing the geomorphic surfaces	

For the global description of the reach the river channel type has to be reported: alluvial channel, intermediate or confined (mountain creek) and the plan morphology (straight, sinuous, etc.). Aforementioned information are usually acquired from maps or aerial surveys and then carried out in a preliminary phase of the planned explorations, just little adjustments are necessary during the direct investigations.

The reach is named with an alphanumeric code (i.e. the first surveyed reach of the Magra River is named MR1), and every debris detected in that region will be correspondingly named with a code preceded by the reach code. In situ the general information concerning the current survey are noted: date, examiner, the GPS limits of the surveyed region.

If the survey purpose is a detailed picture of the river reach conditions, a full topographic measure of a representative cross section is required. The characteristic cross section must show all the typical features of the reach in terms of geomorphic surfaces: channels, active bars, high bars, intermediate surfaces, etc.. Such measures, more than providing the geometry of the channel, gives a rough indication of the frequency of submersion of the several surfaces. Positioning the detected jams or isolated LWD in the corresponding unit we may be able to make hypothesis on the water flow that generated the observed distribution of wood.

4.1.1.2 Sheet 2: sub-reach geomorphological characteristics

At the sub-reach scale it is possible to thoroughly recognize the morphologic and hydrodynamic conditions that regulate the presence of LWD in the river channel.

An appropriate choice of the sub-reach extension has to comprise a whole geomorphic unit (i.e. single bar, or a riffle unit or a pool unit, etc.), if no recent aerial imagery are available this selection has to be done in field considering the local conditions.

The goal of this section is not a comprehensive geomorphological analysis of the area but a pointed inspection of those characteristics that are considered relevant to understand wood processes in rivers. Therefore the collected information are functional for the bed sediments characterization and the surfaces characterization; a planimetric sketch of an area with a length of 1 to 3 times the channel width is suitable. Banks type, banks stability and banks active processes, like erosion or mass movement, are registered. Moreover standing vegetation and in-channel structures are checked for their relevance in wood recruitment and debris capture and deposition.

Table 4-2: survey Sheet n.2.

2. SUB-REACH GEOMORPHOLOGICAL CHARACTERISTICS				
Identification data				
Sub-reach code	_____			
GPS positions	_____			
Downstream end	N _____	E _____		
General morphological characteristics				
Bed configuration	<input type="checkbox"/> R=cascade, SP=step pool, LP=plane bed, RP=riffle pool, DR=duneripple			
Bed sediments	<input type="checkbox"/> A=clay, L=silt, S=sand, G=gravel, C=cobbles, M=boulders, R=bedrock			
Bars	<input type="checkbox"/> LA=lateral, LO=longitudinal, M=point, C=confluence, D=diagonal			
Surfaces	left	mid	right	
active channel	<input type="checkbox"/>	<input type="checkbox"/>	<input type="checkbox"/>	
chute channel	<input type="checkbox"/>	<input type="checkbox"/>	<input type="checkbox"/>	
bar (LA, LO, M, C, D)	<input type="checkbox"/>	<input type="checkbox"/>	<input type="checkbox"/>	
high bar	<input type="checkbox"/>	<input type="checkbox"/>	<input type="checkbox"/>	
pioneer islands	<input type="checkbox"/>	<input type="checkbox"/>	<input type="checkbox"/>	
established island	<input type="checkbox"/>	<input type="checkbox"/>	<input type="checkbox"/>	
berm/bench/shelf	<input type="checkbox"/>	<input type="checkbox"/>	<input type="checkbox"/>	
floodplain	<input type="checkbox"/>	<input type="checkbox"/>	<input type="checkbox"/>	
sec. channel (in floodplain)	<input type="checkbox"/>	<input type="checkbox"/>	<input type="checkbox"/>	
terrace	<input type="checkbox"/>	<input type="checkbox"/>	<input type="checkbox"/>	
hillslope	<input type="checkbox"/>	<input type="checkbox"/>	<input type="checkbox"/>	
Planform sketch (length possibly of about 1-3 times channel width)				
Cross section sketch				
<i>Note: show the geomorphic surfaces and vegetation</i>				
Bankfull channel size				
Width (m)	<input type="checkbox"/>	Measurement method (C=field, FA=aerial photos)	<input type="checkbox"/>	
Mean depth (m)	<input type="checkbox"/>			
Banks				
	left	right		
Type	<input type="checkbox"/>	<input type="checkbox"/>	NC=non cohesive, C=cohesive, CO=composite, S=layered	
Stability	<input type="checkbox"/>	<input type="checkbox"/>	S=stable, AR=retreating, AV=advancing	
Process	<input type="checkbox"/>	<input type="checkbox"/>	E=erosion, MM=mass movement	
Vegetation				
A=absent, E=grass/shrubs, AL=trees				
	left	mid	right	Main species
bank	<input type="checkbox"/>	<input type="checkbox"/>	<input type="checkbox"/>	_____
active bar	<input type="checkbox"/>	<input type="checkbox"/>	<input type="checkbox"/>	_____
high bar	<input type="checkbox"/>	<input type="checkbox"/>	<input type="checkbox"/>	_____
pioneer island	<input type="checkbox"/>	<input type="checkbox"/>	<input type="checkbox"/>	_____
established island	<input type="checkbox"/>	<input type="checkbox"/>	<input type="checkbox"/>	_____
berm/bench/shelf	<input type="checkbox"/>	<input type="checkbox"/>	<input type="checkbox"/>	_____
floodplain	<input type="checkbox"/>	<input type="checkbox"/>	<input type="checkbox"/>	_____
terrace	<input type="checkbox"/>	<input type="checkbox"/>	<input type="checkbox"/>	_____
hillslope	<input type="checkbox"/>	<input type="checkbox"/>	<input type="checkbox"/>	_____
In-channel structures				
Transversal structures	<input type="checkbox"/> P=bridge, T=weir, S=sill, C=check dam			
	left	right		
Bank protections	<input type="checkbox"/>	<input type="checkbox"/>	M=wall, G=gabion, P=groyne, IN=bioengineering	

Table 4-3: survey Sheet n.3.

3. LWD JAM SHEET		
Identification data		
Jam Code _____		
GPS Position N _____ E _____		
Classification		
Components		
in-situ/autochthonous <input type="checkbox"/>	combination <input type="checkbox"/>	transport/allochthonous <input type="checkbox"/>
Type		
bank input <input type="checkbox"/>	valley jam/debris dam <input type="checkbox"/>	debris flow jam <input type="checkbox"/>
log step <input type="checkbox"/>	flow deflection jam <input type="checkbox"/>	flood jam <input type="checkbox"/>
		bench jam <input type="checkbox"/>
		bar apex jam <input type="checkbox"/>
		bar top jam <input type="checkbox"/>
		meander jam <input type="checkbox"/>
		log rafts <input type="checkbox"/>
		bank edge/top <input type="checkbox"/>
		bank revetment <input type="checkbox"/>
Position		
Section	Bank	Plan view
thalweg (A1) <input type="checkbox"/>	bank toe <input type="checkbox"/>	point bar <input type="checkbox"/>
shallow (A2) <input type="checkbox"/>	anchored bank base <input type="checkbox"/>	lateral bar <input type="checkbox"/>
chute channel (A2, B1) <input type="checkbox"/>	anchored bank <input type="checkbox"/>	longitudinal bar <input type="checkbox"/>
active bar (B1) <input type="checkbox"/>	bank top <input type="checkbox"/>	outer meander bank <input type="checkbox"/>
high bar (B2) <input type="checkbox"/>	Vegetation	bridge <input type="checkbox"/>
berm/bench/shelf (B2) <input type="checkbox"/>	shrubs <input type="checkbox"/>	channel <input type="checkbox"/>
secondary channel (B2, C) <input type="checkbox"/>	pioneer veget (2-5 yrs) <input type="checkbox"/>	step <input type="checkbox"/>
pioneer island (B2, C) <input type="checkbox"/>	established veget (> 5 yrs) <input type="checkbox"/>	riffle <input type="checkbox"/>
established island (B2, C) <input type="checkbox"/>		pool <input type="checkbox"/>
floodplain (C) <input type="checkbox"/>		glide <input type="checkbox"/>
terrace (D) <input type="checkbox"/>		
Sketch of jam position		
	<div style="border: 1px solid black; width: 100%; height: 100%;"></div> <p style="text-align: center; font-size: small;">Planview sketch</p>	
Jam characteristics		
Jam size	Texture	Key elements
length (m) <input type="checkbox"/>	tight braided mesh <input type="checkbox"/>	number key elements <input type="checkbox"/>
width (m) <input type="checkbox"/>	loose braided mesh <input type="checkbox"/>	well visible <input type="checkbox"/>
height (m) <input type="checkbox"/>	tight parallel disposition <input type="checkbox"/>	partially visible <input type="checkbox"/>
number elements d>0.1 m <input type="checkbox"/>	loose parallel disposition <input type="checkbox"/>	presumable <input type="checkbox"/>
	no dominant disposition <input type="checkbox"/>	
	abundant fine debris <input type="checkbox"/>	
Jam sketch		
Point out key element(s), raked and relative identification code (LWDKn / LWDRn)		

4.1.1.3 Sheet 3: LWD jam sheet

The third sheet (Table 4-3) is focused on jam formations; every cluster of woody debris detected in the surveyed sub-reach, proceeding from the upstream limit to the downstream one, is named with a progressive code J_1, J_2, \dots, J_n and its GPS coordinates are registered.

First task is to establish the prevalent provenance of the components:

- *Autochthonous* elements: if the debris composing the jam didn't move away from the input site;
- *Allochthonous* elements: if they have been delivered to the survey location by the stream flow;
- *Combined* elements: if the jam presents both elements autochthonous and allochthonous.

Then the jams are recognized according to the classification proposed by Abbe and Montgomery (2003) and Wallerstein and Thorne (2004) Figure 4-2.

The definition of the main typologies here considered is reported in the Glossary fields.

Identification data			
Jam Code _____			
GPS Position	N _____	E _____	
Classification			
Components			
in-situ/autochthonous	<input type="checkbox"/>	combination	<input type="checkbox"/>
		transport/allochthonous	<input type="checkbox"/>
Type			
bank input	<input type="checkbox"/>	valley jam/debris dam	<input type="checkbox"/>
log step	<input type="checkbox"/>	flow deflection jam	<input type="checkbox"/>
		debris flow jam	<input type="checkbox"/>
		flood jam	<input type="checkbox"/>
		bench jam	<input type="checkbox"/>
		bar apex jam	<input type="checkbox"/>
		bar top jam	<input type="checkbox"/>
		meander jam	<input type="checkbox"/>
		log rafts	<input type="checkbox"/>
		bank edge/top	<input type="checkbox"/>
		bank revetment	<input type="checkbox"/>

Figure 4-2: jam classification according to abbe and Montgomery (2003) and Wallerstein and Thorne (2004), extract from sheet 3.

The jam formation is then sketched in a plan view and in a cross section view aided by a codified grid (Figure 4-3) that may make simpler the transcription of the information in a database.

In addition a jam sketch with the identification of the key elements and the racked elements with the corresponding code would be convenient at the end of sheet.

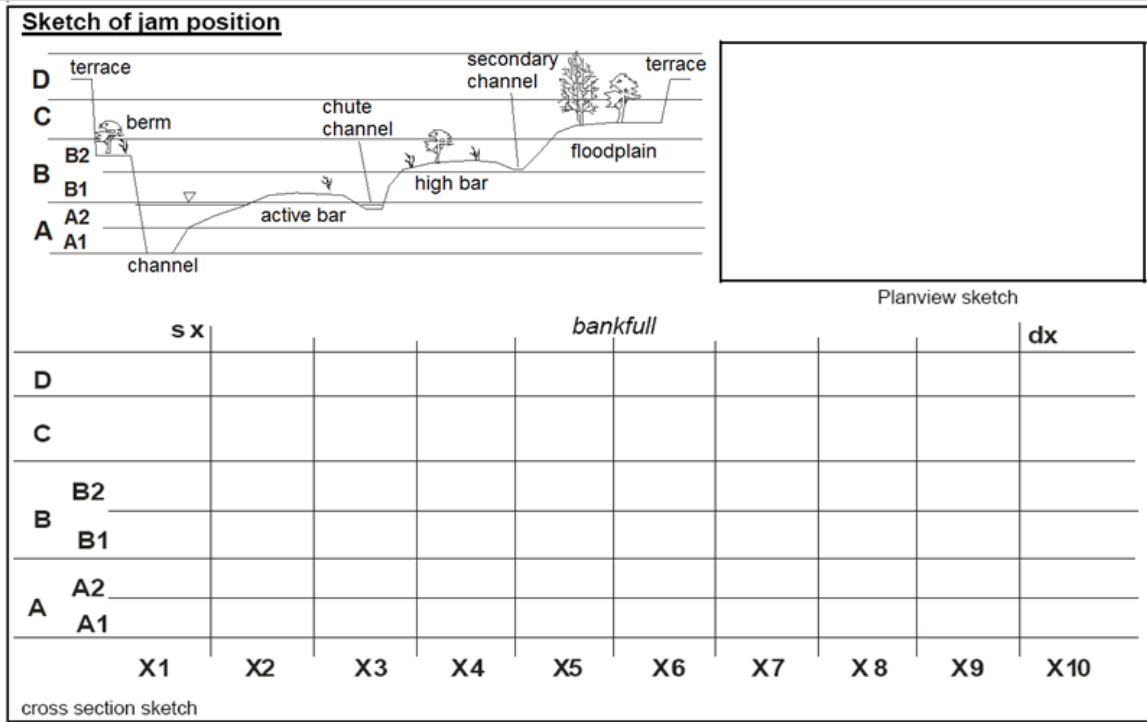


Figure 4-3: codified grid to sketch the jam position in the cross section.

The accumulation is measured approximating the shape of the ensemble to a parallelepiped then recording length, width and height. The number of the large elements and the number of those debris that can be recognize as key elements in the jam construction are reported. All these data, joint with an evaluation of the texture of the loosen material, permit to better estimate the aggregate volume of the group.

Jam characteristics		
Jam size	Texture	Key elements
length (m) <input type="text"/>	tight braided mesh <input type="text"/>	number key elements <input type="text"/>
width (m) <input type="text"/>	loose braided mesh <input type="text"/>	
height (m) <input type="text"/>	tight parallel disposition <input type="text"/>	well visible <input type="text"/>
number elements $d > 0.1$ m <input type="text"/>	loose parallel disposition <input type="text"/>	partially visible <input type="text"/>
	no dominant disposition <input type="text"/>	presumable <input type="text"/>
	abundant fine debris <input type="text"/>	

Figure 4-4: geometrical and structural characterization of the jam, extract from sheet 3.

4.1.1.4 Sheet 4: large woody debris sheet

The sheet 4 (Table 4-4) is settled for the complete description of the LWD located in the surveyed area. The same sheet is used for single elements, and elements grouped in a cluster: the code identify the nature of the large woody piece, for example

the code MR1_LWDS1 is attributed to the first single element (LWDS1) detected in the first reach surveyed in the Magra River (MR1); MR1_J1_LWDK1 e MR1_J1_LWDR1 indicate respectively the first key element (LWDK1) and the first racked element (LWDR1) constituting the first measured jam.

The objective of this sheet is to define the qualitative property of the LWD and its conditions; these information are fundamental to estimate wood density, nevertheless they may be useful to determine the interval of permanence in the river channel and consequently to deduct which flood event may be responsible of the object recruitment or delivering, and which one may be the supply area.

The type is attributed based on the arboreal structure (canopy) and on the native components preserved by the element:

- *Tree*: stays for a complete sample exhibiting roots, trunk and branches practically intact (Figure 4-5: a);
- *Shrub*: exhibits the same component of the tree type with a shrubby structure instead that tree-shaped (usually a main stem lacks), for some species it is the typical arboreal structure in other cases it may be a young plant of a tree species (Figure 4-5: b);
- *Log*: indicates a wooden object which has been moulded by the interaction with the stream flow, the bed sediments and all the obstacles encountered during transport (typically it is an allochthonous element but it may be also a residual of a fire), it may present traces of all components or not (Figure 4-6: a);
- *Cut*: indicates an harvesting residual (pre or post recruitment), the debris deposited on the lateral bars of the river channel are often cut and cropped to be used as combustible (Figure 4-6: b).



a)



b)

Figure 4-5: samples of tree type (a) and shrub type (b).

Table 4-4: survey Sheet n.4.

4. LARGE WOODY DEBRIS SHEET										
Identification data										
Type <input type="checkbox"/> K=key, R=racked, S=single Code _____ GPS Position N _____ E _____ (only in case of single debris, otherwise the Jam position is considered)										
Characteristics										
Type tree <input type="checkbox"/> shrub <input type="checkbox"/> log <input type="checkbox"/> harvest residual <input type="checkbox"/>			Branches no branches <input type="checkbox"/> only butts <input type="checkbox"/> some broken <input type="checkbox"/> all almost intact <input type="checkbox"/>			Roots Rootwad <input type="checkbox"/> Diameter (m) <input type="checkbox"/> Fine roots <input type="checkbox"/>				
Trunk decay intact (with bark) <input type="checkbox"/> no bark but solid <input type="checkbox"/> porous <input type="checkbox"/> highly decayed <input type="checkbox"/>			bark cover (%) leaves <input type="checkbox"/>			Origin natural mortality <input type="checkbox"/> bank erosion <input type="checkbox"/> landslide/debris flow <input type="checkbox"/> floated <input type="checkbox"/>				
Size diameter (m) <input type="checkbox"/> lenght (m) <input type="checkbox"/> tree/shrub: width (m) <input type="checkbox"/> lenght (m) <input type="checkbox"/> height (m) <input type="checkbox"/>										
Age and conditions										
Trunk age (years) <input type="checkbox"/> (when possible)					Present vegetative activity no activity <input type="checkbox"/> before deposition <input type="checkbox"/> after deposition (adventitious sprouting) <input type="checkbox"/> max age adventitious sprouts <input type="checkbox"/>					
Vitality strong <input type="checkbox"/> poor <input type="checkbox"/> dead <input type="checkbox"/>										
Position										
Section thalweg (A1) <input type="checkbox"/> shallow (A2) <input type="checkbox"/> chute channel (A2, B1) <input type="checkbox"/> active bar (B1) <input type="checkbox"/> high bar (B2) <input type="checkbox"/> berm/bench/shelf (B2) <input type="checkbox"/> secondary channel (B2, C) <input type="checkbox"/> pioneer island (B2, C) <input type="checkbox"/> established island (B2, C) <input type="checkbox"/> floodplain (C) <input type="checkbox"/>			Bank bank toe <input type="checkbox"/> anchored bank base <input type="checkbox"/> anchored bank <input type="checkbox"/> bank top <input type="checkbox"/>			Plan view point bar <input type="checkbox"/> lateral bar <input type="checkbox"/> longitudinal bar <input type="checkbox"/> outer meander bank <input type="checkbox"/> bridge <input type="checkbox"/> channel <input type="checkbox"/> step <input type="checkbox"/> riffle <input type="checkbox"/> pool <input type="checkbox"/> glide <input type="checkbox"/>				
Sketch of element position										
s x bankfull dx										
D										
C										
B2										
B1										
A2										
A1										
	X1	X2	X3	X4	X5	X6	X7	X8	X9	X10



a) b)

Figure 4-6: samples of log type (a) and cut type (b).

Presence and conditions of branches are reported, in particular with the term butt is intended a portion (few centimetres) of a branch next to the trunk (Figure 4-8). The rootwad if present is measured, the presence of fine roots denounces the origin of the debris: usually, mass failures of the banks produce complete plants with fine roots. The trunk decay, the percentage of bark cover and the presence of leaves are registered (Figure 4-7).

Characteristics			
Type	tree <input type="checkbox"/>	Branches	Roots
	shrub <input type="checkbox"/>	no branches <input type="checkbox"/>	Rootwad <input type="checkbox"/>
	log <input type="checkbox"/>	only butts <input type="checkbox"/>	Diameter (m) <input type="checkbox"/>
	harvest residual <input type="checkbox"/>	some broken <input type="checkbox"/>	Fine roots <input type="checkbox"/>
		all almost intact <input type="checkbox"/>	
Trunk decay		bark cover (%) <input type="checkbox"/>	Origin
intact (with bark) <input type="checkbox"/>		leaves <input type="checkbox"/>	natural mortality <input type="checkbox"/>
no bark but solid <input type="checkbox"/>			bank erosion <input type="checkbox"/>
porous <input type="checkbox"/>	species _____		landslide/debris flow <input type="checkbox"/>
highly decayed <input type="checkbox"/>			floated <input type="checkbox"/>
Size	diameter (m) <input type="checkbox"/>	length (m) <input type="checkbox"/>	height (m) <input type="checkbox"/>
tree/shrub:	width (m) <input type="checkbox"/>	length (m) <input type="checkbox"/>	
Age and conditions			
	Trunk age (years) <input type="checkbox"/> (when possible)	Present vegetative activity	no activity <input type="checkbox"/>
Vitality			before deposition <input type="checkbox"/>
strong <input type="checkbox"/>		after deposition (adventitious sprouting) <input type="checkbox"/>	
poor <input type="checkbox"/>		max age adventitious sprouts <input type="checkbox"/>	
dead <input type="checkbox"/>			

Figure 4-7: geometrical, structural and physical characterization of woody debris, extract from sheet 4.

These information are fundamental to produce an estimation of wood density: density depends essentially from wood species, wood portion, growth condition (diameter increase per year), water content and decay rate. To evaluate decay rate are commonly defined several decay classes that span a spectrum of stages from fresh

mortality to nearly complete decay. These classes are based on the physical appearance and structural integrity of individual dead wood element, at present there is not a standardized definition that means that the number of decay classes used varies from study to study. The settled form proposes four classes of decay (Figure 4-7):

1. *Intact*: freshly fallen material with residual vegetation activity or not;
2. *Solid*: dead material, sapwood and heartwood present a compact texture, bark cover could be pulled apart by hand;
3. *Porous*: wood sounds porous, fissures may be evident, bark if present is detached from sapwood;
4. *Highly decayed* or rotten: the material is fragile easily broken.

It is evident that in different climatic conditions same species can present different densities hence it should be preferable to create opportune database for singular river catchments (although correlation may be found with existing database, see subchapter 6.1.1). This means that samples should be taken in field for laboratory analysis, alternatively a better option could be using non-destructive field methods to measure wood density. Currently penetrometers are commonly used for measuring the density of standing trees: the penetrometer measures the depth into which a pre-loaded spring forces a pin in the wood. Decaying dead wood becomes softer starting from the surface layers (sapwood) extending to the core (heartwood) with the process progression, therefore measures of significantly decayed material are not consistent using common penetrometers. Mäkipää & Linkosalo (2011) comparing density measurements with penetrometer and laboratory analysis conclude that thicker measuring pins (standard pins are 2.5 mm thick) may be successfully used for quick density test in field (in a range of densities) using an appropriate linear regression to convert penetration measures to densities. Although the applicability is not currently extensible to more decomposed wood it seems to be an effective method to overcome subjective evaluations.

The several physical properties registered in this section may also be useful to give an idea of all actions undergone by the debris, an consequently, of the distance from the recruitment site; moreover they influence the debris tendency to be deposited or trapped in future situation of transport, and also the resistance that the debris may produce on the stream flow when stable.

The dimension of the LWD are taken:

- The diameter is measured at one third of the length starting from the foot of the trunk (it is rather than an equivalent diameter to approximate the debris to a cylinder as is usually done in dendrometric measurements);
- The length is the distance from the foot (where the rootwad is attached to the stem) to the top;

A shrub is approximated with a parallelepiped.



Figure 4-8: debris with branch portions (butts).

If it is possible, the age of the plant is determined by the annual growth rings counting; vitality and vegetation activity are evaluated marking if the activity is referable to a period preceding or succeeding the recruitment (the first case correspond to a recently recruited debris, the second case may correspond to a debris which is creating new roots after deposition). When the vegetation activity after deposition is consolidated, and new roots have stabilized the trunk, it cannot be considered a debris anymore (Figure 4-9).

The position and the sketch of the LWD are required only if it is a single debris.



a) sprouts of the current season



b) sprouts aged one year

Figure 4-9: samples of adventitious sprouts after deposition.

4.1.1.5 Sheet 5: interaction LWD, hydrodynamic and sediments

All the information that are thought to be relevant to understand the complex interaction between resting debris, bed sediments and water flow are collected in this section (Table 4-5).

The location is intended inside the sub-reach in exam, therefore left or right are not necessary referred to the left or right bank of the channel, but refer to the left or right side of the morphologic unit investigated.

The debris orientation is represented by the angle between the debris vector (directed from the bottom to the top of the trunk) and a stated direction that may be the geographic north or the flow direction (in case of braided channel morphology the low flow direction is observed in the closer channel). If the flood direction is undertaken it has to be supposed by field evidences. If the angle between the flow direction and the debris direction is comprised between -90° and 90° degree, the element is positioned with the rootwad in the upstream side and the top in the downstream side, this is a typical situation, as described in Chapter 2, vice versa if the angle is comprised between 90° and 270° . For jams the orientation is assumed equal to the orientation of the majority of the constituting elements.

The causes of deposition (only for allochthonous debris) are arranged in the following category:

- *Captured*: the LWD has been intercepted by obstacles inside the channel: boulders, vegetation (Figure 4-10), hydraulic infrastructures, wreckages, vortex (Figure 4-11), etc.;
- *Stranded*: the LWD has been deposited on a morphologic surface of the channel (usually an active bar, because on other surfaces the interaction with the vegetation is prevailing) as a consequence of the reduced water depth (for minor flood events or during the descending phase of flood flow) (Figure 4-12).

To assess the interaction of the LWD with the stream flow the following conditions are documented:

- magnitude of *submersion*;
- occurrence and magnitude of *underflows*: a single debris or a jam transversal to the flow may obstruct partially or entirely the hydraulic section inducing the flow to surmount or to underflow;
- the magnitude of the *flow deflection* and of the section *contraction* (Figure 4-13) induced by the LWD.

Table 4-5: survey Sheet n. 5.

5. INTERACTION LWD, HYDRODYNAMICS AND SEDIMENTS			
Location within the river corridor			
Left, right, mid <input type="checkbox"/>	Jam orientation	Rootwad orientation	Element orientation
	to the north (°) <input type="checkbox"/>	upstream <input type="checkbox"/>	to the north (°) <input type="checkbox"/>
	to low flow direction (°) <input type="checkbox"/>	downstream <input type="checkbox"/>	to low flow direction (°) <input type="checkbox"/>
	to flood direction (°) <input type="checkbox"/>	lateral (L/R) <input type="checkbox"/>	to flood direction (°) <input type="checkbox"/>
	inclination to horizontal (°) <input type="checkbox"/>		inclination to horizontal (°) <input type="checkbox"/>
Causes of deposition (for floated elements only)			
Captured	wreckage <input type="checkbox"/>	Stranded	
protruding clasts <input type="checkbox"/>		widening <input type="checkbox"/>	
banks <input type="checkbox"/>		shallowing <input type="checkbox"/>	
vegetation <input type="checkbox"/>			
anthropic structures <input type="checkbox"/>			
obstacle-surrounding <input type="checkbox"/>			
vortex <input type="checkbox"/>	Other _____		
Flow - LWD interaction			
completely submerged <input type="checkbox"/>	Sketch		
partially submerged <input type="checkbox"/>			
submersion head (cm) <input type="checkbox"/>			
submersion toe (cm) <input type="checkbox"/>			
underflow <input type="checkbox"/>			
underflow depth (cm) <input type="checkbox"/>			
flow deflection <input type="checkbox"/>			
contraction % <input type="checkbox"/>			
plunging jet <input type="checkbox"/>			
drop height (m) <input type="checkbox"/>			
Interaction LWD - sediments			
Local processes			
upstream	on the jam/element	downstream	
fill <input type="checkbox"/>	partially buried by sediment <input type="checkbox"/>	fill <input type="checkbox"/>	
scour <input type="checkbox"/>	totally buried by sediment <input type="checkbox"/>	scour <input type="checkbox"/>	
lateral deposition (L/R) <input type="checkbox"/>		lateral deposition (L/R) <input type="checkbox"/>	
lateral scour (L/R) <input type="checkbox"/>		lateral scour (L/R) <input type="checkbox"/>	
length (m) <input type="checkbox"/>		length (m) <input type="checkbox"/>	
width (m) <input type="checkbox"/>		width (m) <input type="checkbox"/>	
depth/height (m) <input type="checkbox"/>		depth/height (m) <input type="checkbox"/>	
Sediments			
upstream	on the key/jam	downstream	
clay <input type="checkbox"/>	clay <input type="checkbox"/>	clay <input type="checkbox"/>	
silt <input type="checkbox"/>	silt <input type="checkbox"/>	silt <input type="checkbox"/>	
sand <input type="checkbox"/>	sand <input type="checkbox"/>	sand <input type="checkbox"/>	
gravel <input type="checkbox"/>	gravel <input type="checkbox"/>	gravel <input type="checkbox"/>	
cobble <input type="checkbox"/>	cobble <input type="checkbox"/>	cobble <input type="checkbox"/>	
boulder <input type="checkbox"/>	boulder <input type="checkbox"/>	boulder <input type="checkbox"/>	
Notes and comments			



Figure 4-10: jam captured by vegetation (Piave River).



Figure 4-11: LWD and loosen material captured by eddies downstream a transversal sill, a rootwad lay down the structure for the reduced water depth (Arno River).



Figure 4-12: LWD stranded (Piave River).



Figure 4-13: section contraction due to an in-channel LWD (Rio Cordon, Belluno's Dolomites).



Figure 4-14: effects on scour and deposition induced by a LWD (Piave River).

The interaction with the bed sediments is evaluated in terms of local *scour* or *deposition* induced by the presence of the wooden object; in Figure 4-14 is noticeable the deposition of coarse sediments in the upstream side of the rootwad which is rounded by a scour zone due to the horse shoe vortex. Downward, along the lateral sides of the trunk it is possible to find finer sediments due to the wake effect. Inspecting a jam the global interaction is considered.

4.2 EXAMPLE

The proposed form has been tested in field, on some Italian rivers: in Appendix A a filled in example is presented, in this paragraph an example of the collected data is reported and some elaborations are presented.

The characteristics of the investigated reaches were different for size and channel slope (ranging from intermediate and alluvial channels) but in every case the channel morphology was among wandering and braided.

The essential equipment for field surveys consists in a metric tape, a dendrometric calliper and a handy GPS receiver, when is not necessary to measure a river section, in that case also a total station or at least an inclinometer is required. It has to be reminded that a handy GPS have a precision of 10 meters in determining the debris coordinates.

During a survey programme on the Magra River in Tuscany, additionally to the information settled in the sheets some stem sections were taken (Figure 4-15) to carry out some laboratory investigation to establish among others:

- density;
- porosity;
- age with C14 investigations;
- tree species, when the high decay of a debris impedes this interpretation.



Figure 4-15: withdrawal of a stem section.

In Table 4-6 an extract of the collected data is presented.

Table 4-6: extract from the recorded data.

ACTIVE BAR

SAMPLES	DIMENSION		GPS POSITION		ORIENTATION °N	ROOTWAD		SPECIES	TYPE	SPROUTS age	BARK COVER %	DECAY	VITALITY	LEAVES	FINE ROOTS
	L	D	N	E		L	D								
S1	21.2	0.29	4908395	573513	205	1.4	1.1	P	log	1yr	90	intact	strong	Y	Y
S1	22.5	0.28	"	"	"	"	"	"	"	"	"	"	"	"	"
S13	12.1	0.12	4909158	573554	295	0.8	1.2	P	log	/	100	intact	poor	Y	Y
S14	10.6	0.15	"	"	"	0.6	0.3	P	log	/	100	intact	poor	N	Y
S15	2.6	0.12	4908165	573545	20	/	/	NC	log	/	0	porous	dead	N	N
S16	6.3	0.11	4908161	573538	180	0.3	0.6	NC	log	<1yr	100	intact	strong	Y	NC
S17	19.7	0.17	4908146	573560	165	1.5	1.85	NC	log	<1yr	100	intact	strong	Y	Y
S17	"	"	"	"	"	"	"	"	"	"	"	"	"	"	"
S18	9.5	0.11	4908133	573569	140	1.5	0.9	S	log	/	100	intact	dead	N	N
S19	21.3	0.17	4908135	573594	237	1.4	0.7	P	log	1yr	100	intact	poor	N	Y
S20	10.7	0.21	"	"	"	1.2	0.65	P	cut	/	5	solid	dead	N	N
S21	12.8	0.18	4908124	573598	166	0.5	1.6	S(?)	log	/	30	solid	dead	N	N

HIGH BAR

SAMPLES	DIMENSION		GPS POSITION		ORIENTATION °N	ROOTWAD		SPECIES	TYPE	SPROUTS age	BARK COVER %	DECAY	VITALITY	LEAVES	FINE ROOTS
	L	D	N	E		L	D								
S3	19.5	0.4	4908318	573514	160	1.5	3.8	P	tree	/	60	solid	dead	N	Y
S4	16	0.14	4908303	573522	250	1.1	0.35	NC	log	/	40	solid	dead	N	Y
S5	8.4	0.18	"	"	180	/	/	NC	log	/	0	solid	dead	N	N
S6	11.8	0.19	"	"	184	0.9	0.45	S(?)	log	/	50	solid	dead	N	Y
S7	18.7	0.25	4908250	573581	170	1.5	1.2	P	log	/	40	solid	dead	N	Y
S8	4.4	0.15	4908237	573593	55	/	/	NC	cut	/	0	porous	dead	N	N
S9	1.4	0.13	4908254	573597	190	0.4	0.5	NC	log	/	0	porous	dead	N	N
S10	2.5	0.13	4908254	573603	220	/	/	A	log	/	10	solid	dead	N	N
S11	3.2	0.17	4908255	573608	NC	/	/	P	cut	/	50	solid	dead	N	N
S12	1.8	0.23	4908243	573611	70	/	/	NC	log	/	0	porous	dead	N	N
K1	5.1	0.31	4908292	573542	190	0.5	0.85	P(?)	cut	/	50	solid	dead	N	Y
K1	3.5	0.21	"	"	"	"	"	"	"	"	"	"	"	"	"
R1	7.2	0.2	"	"	"	1.7	0.5	P	log	/	50	solid	dead	N	Y
W8	16.7	0.15	4908276	570582	330	1.8	1.6	P	log	/	90	solid/porous	dead	N	Y
W9	14.2	0.16	"	"	NC	0.9	0.8	P	log	/	0	solid/porous	dead	N	Y

With the recorded information is possible to produce statics about debris characteristics in the studied reach: in particular the necessary information for a

predictive model of entrainment (as the one proposed in the next chapters) or transport are: size, density, initial position and orientation. But even other information concerning typical species and age gives general indications about size and weight.

In particular a fundamental parameter that is density, at present, in field may be only interpreted merging species and decay state. The comparison between the laboratory results and the field observation gives a good agreement between density and decay estimation (Figure 4-16, Figure 4-17, Figure 4-18).

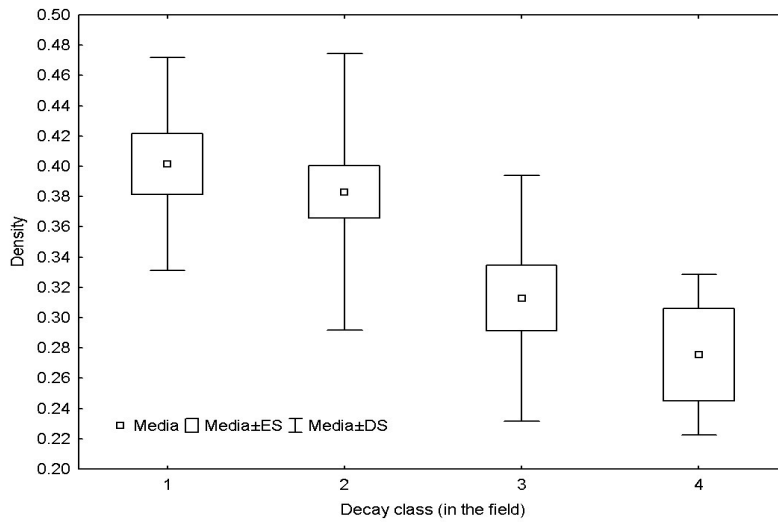


Figure 4-16: density distribution (from laboratory analysis) for different classes of decay (evaluated in field): 1 intact, 2 solid, 3 porous, 4 decayed.

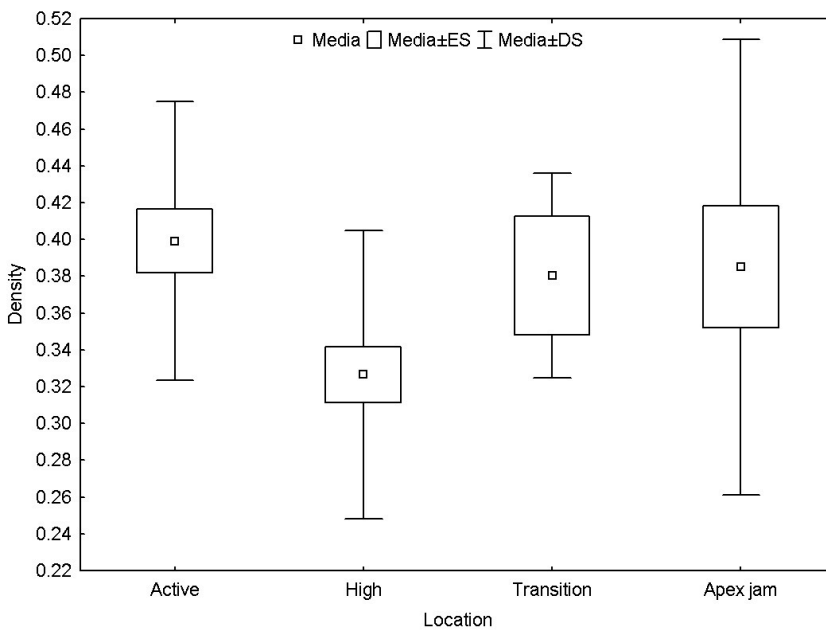


Figure 4-17: density distribution for different geomorphological surfaces: active bar, high bar, transition zone (between active and high bar).

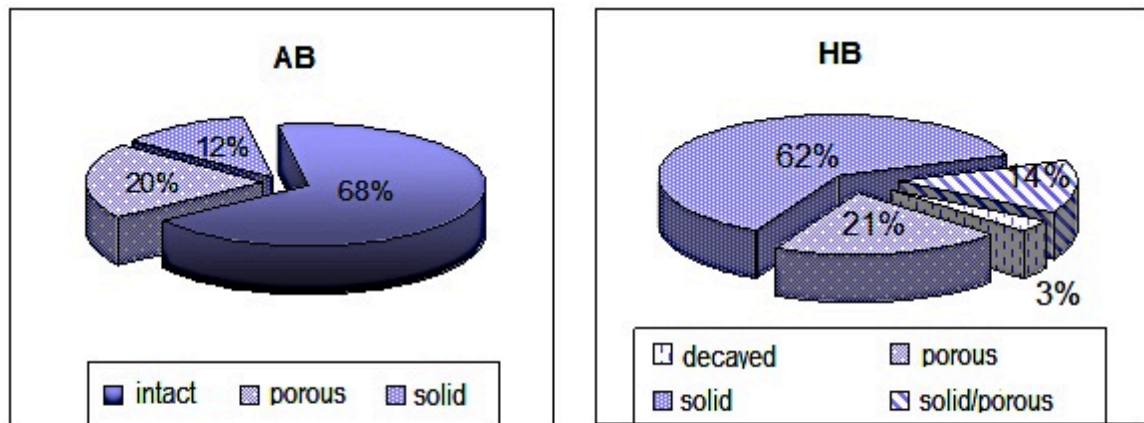


Figure 4-18: decay classes distribution on the active bar (AB) and the high bar (HB), according to the field observations.

An important operation of risk management is designing the riverine, in particular the in-channel and cross-channel infrastructures taking into account LWD loadings, in terms of active forces and of encumbrance. Direct surveys are fundamental to collect the necessary data to produce statics on volume and dimension of transported material for a river reach, through the inspection of the wooden material even as of the channel stability (lateral migration, banks processes, etc.), and then of the standing vegetation (NCHRP REPORT 653, 2010).

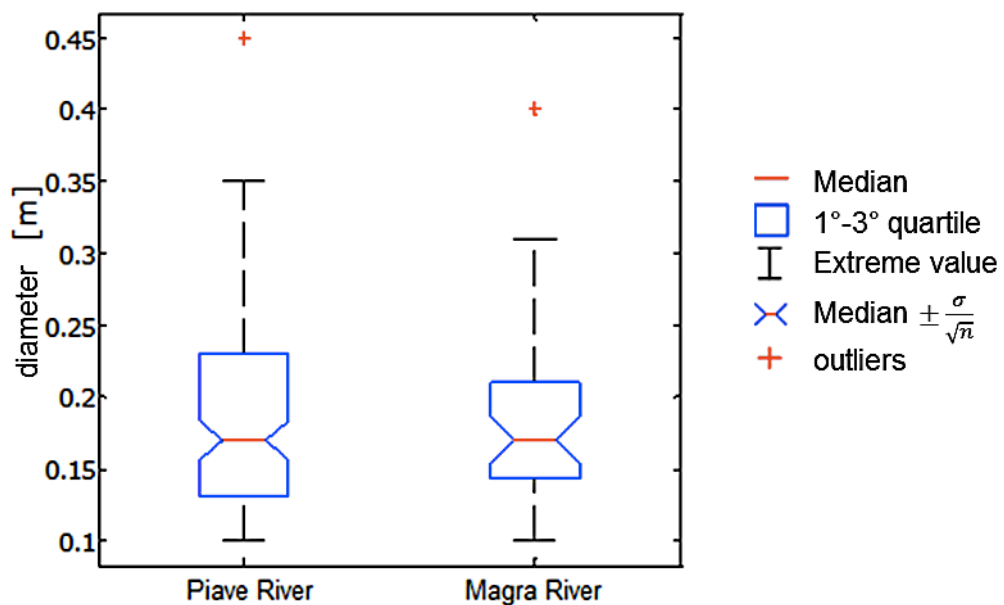


Figure 4-19: diameters distribution of allochthonous (transported) debris detected in the two surveyed rivers.

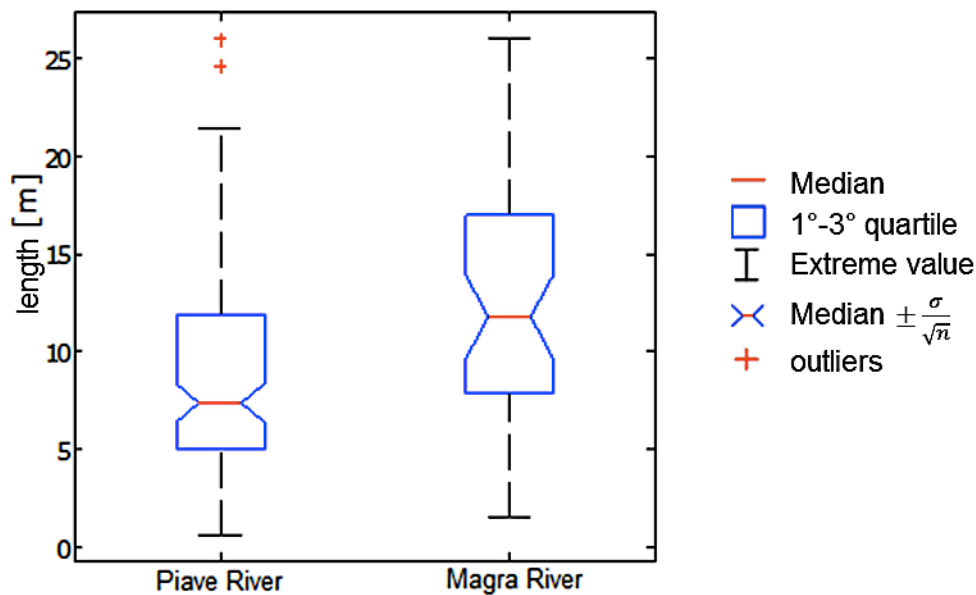


Figure 4-20: lengths distribution of allochthonous debris detected in the two surveyed rivers.

4.3 COMPARISON WITH REMOTE INVESTIGATIONS

Direct surveys have been compared with remote investigations performed using geo-referred high-resolution aerial imagery; the adoption of this methodology to explore wood patterns in a river catchment is quite recent (Labbe et al., 2005; Hughes et al., 2006). The technique consists in recognizing single debris or jams on a rectified image (Figure 4-21), and to measuring them with different methods depending on the software utilised (generally ArcGis, Figure 4-22).

The aerial imageries may have different resolution, for a reasonable investment of moneys in a river catchment investigation, the resolution usually do not overtake 10 cm per dot, which is the threshold size for LWD's diameter. A photogram with this characteristic usually embraces a surface of 282.5 ha.

The aerial imagery are captured in mean-low flow conditions to allow to distinguish the morphologic surfaces and the debris deposited during the preceding season; the appropriate period is usually the end of springs or the beginning of summer (in European latitudes), when the vegetation cover facilitates the identification of the surfaces and does not hide excessively the terrain. In this condition only debris lying in the channel or upon not much vegetated bars are visible; debris on banks, when visible because overhanging on the channel, may be counted even if not completely discernible, to give a rough idea of the global volume of wood.

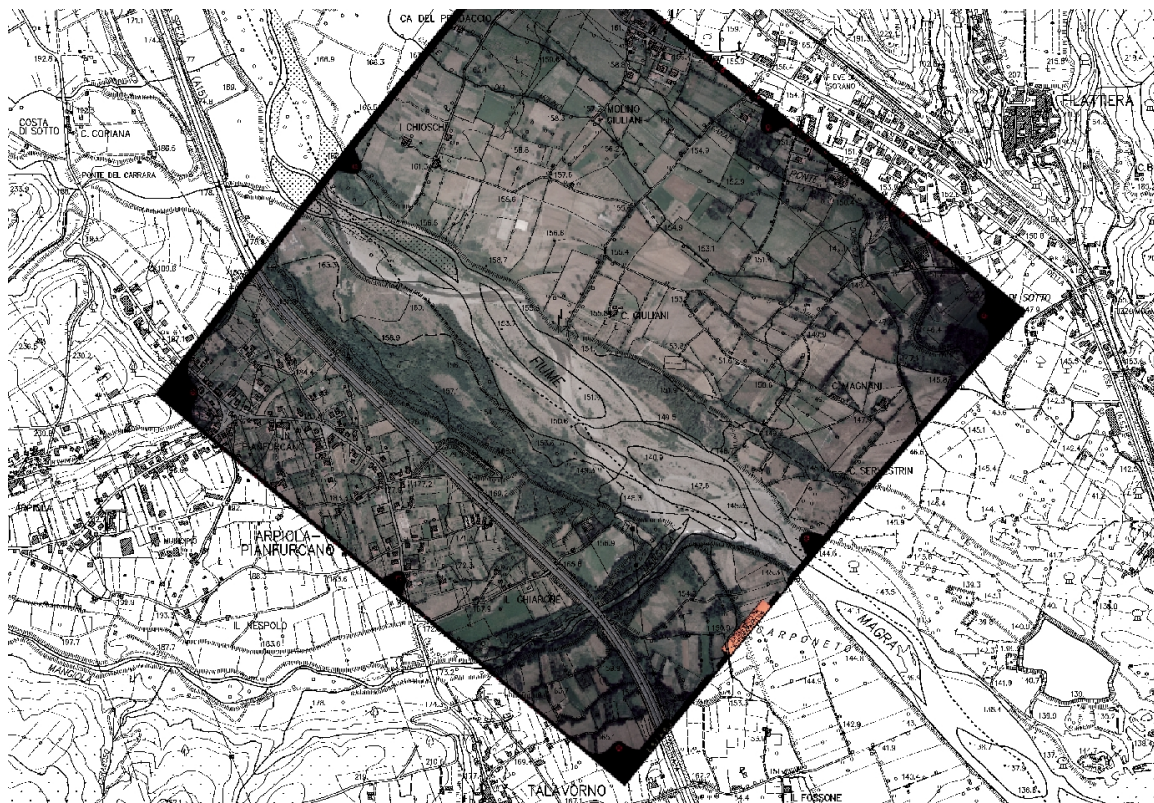


Figure 4-21: rectified photogram superimposed on the regional cartography (Magra River).



Figure 4-22: debris measuring on photogram.

On the rectified photogram is possible to ascertain:

- Distribution and extension of the identifiable morphologic surfaces (Figure 4-23);
- Spatial distribution, orientation, dimension and volume of LWD.

Because of the low water discharge the identification of the main channel require an interpretation of the images based on bed sediments characteristic (when visible on the picture) and on spatial distribution, similarly is done for secondary channels that are usually dry in this condition. Bars perimeters are discerned basing on sediments texture, colour (a darker shroud of an area may be interpreted as presence of silty sediments characteristic for high bars) and vegetation (sparse and smaller on the active bar). Intensely vegetated areas in contact with bars or channel are identified as islands.

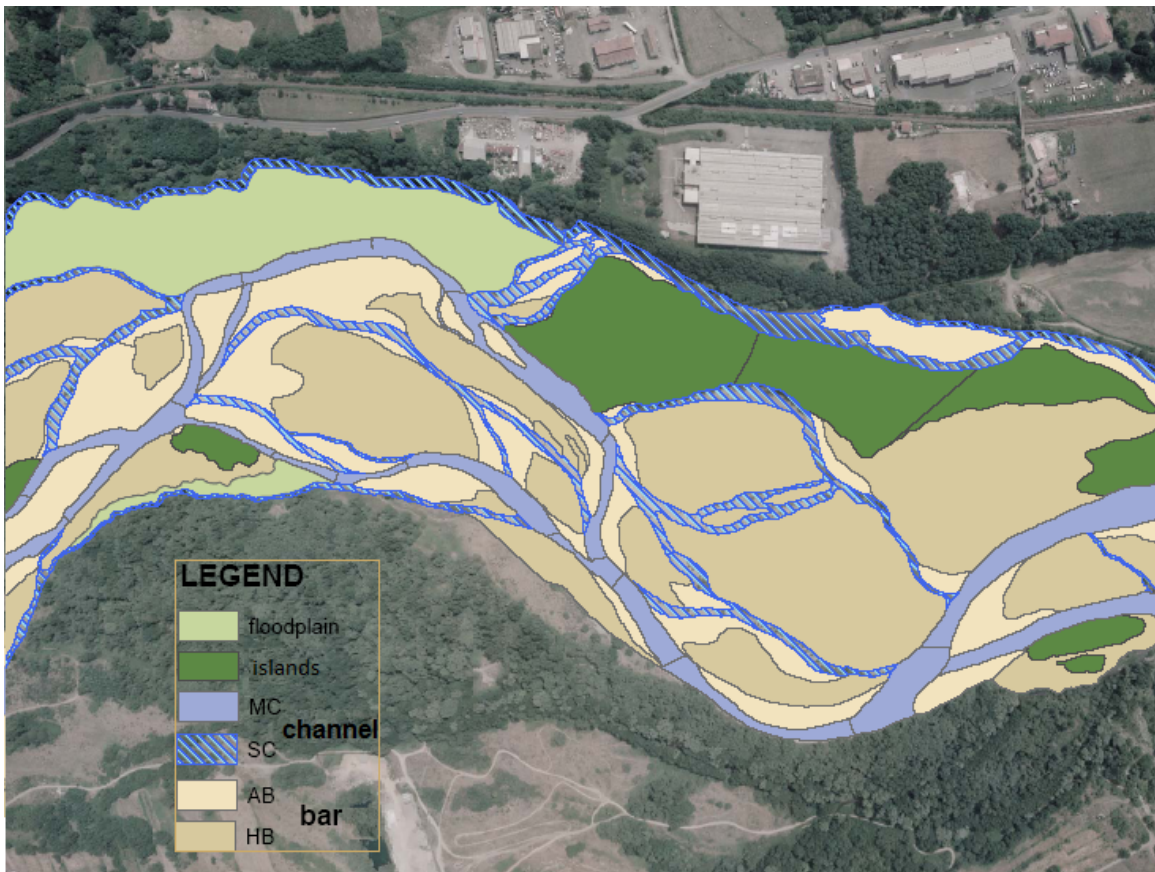


Figure 4-23: morphological surfaces.

For LWD analysis the agreement between the real distribution and the imagery interpretation is strongly influenced by the photogram resolution, it has to be marked that even the rectifying algorithm introduce an error that is estimable in the order of few centimetres. The algorithm perform an interpolation of the adjacent dots assigning them the prevailing colour, as a consequence some dimensions may be increased or decreased and contours may become less definite (Hughes et al, 2006). Another important factor is the time in the day when the flight take place, because of the shadows produced by the sunlight.

In Figure 4-24 the representation of wood distribution on the in-channel surfaces.

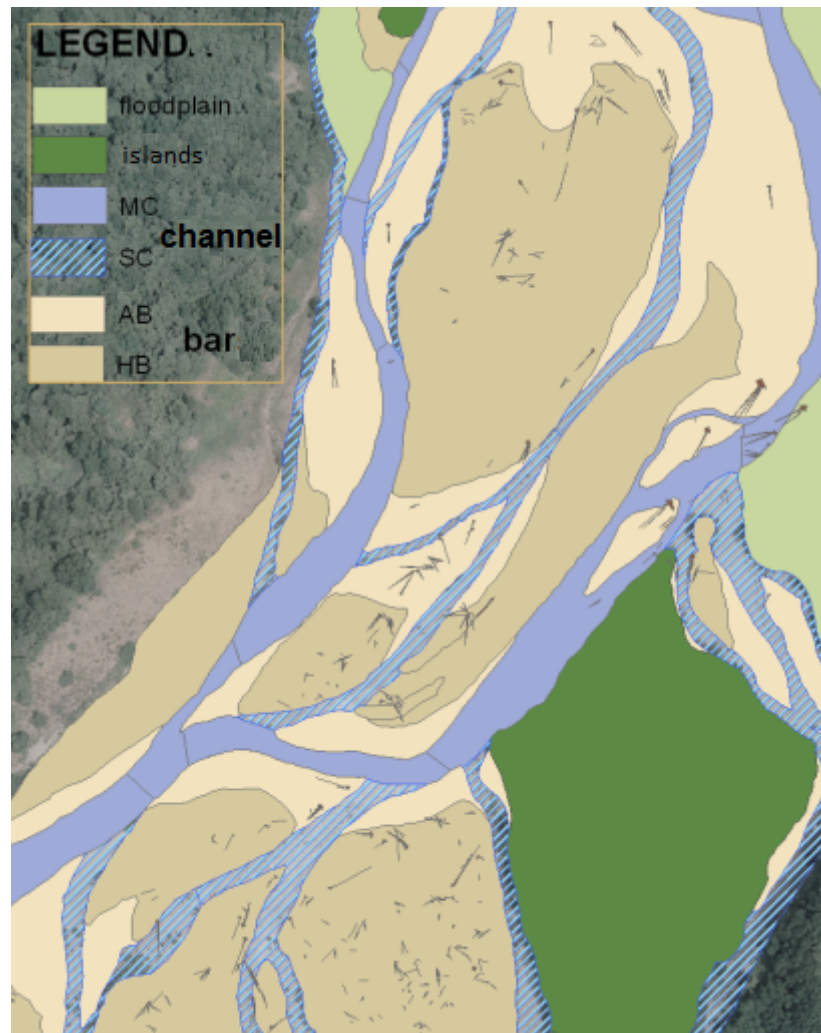


Figure 4-24: LWD and surface distribution as recognizable on aerial imagery.

Comparing the direct measurements with imagery interpretation the conclusions are essentially these:

- For diameters estimation the resolution is the main constraining factor: actually the size of LWD diameters has the same order of one or few dots, that is why it is frequent to overestimate their dimensions, in the diagram reported in Figure 4-25 is appreciable that with increasing size the relative error between direct measure and estimation decrease;
- For length estimation the overvalue of the dimension is more frequent (Figure 4-26) as a consequence of several occurrences: usually tree's stems become thinner at the top and then less discernible, sometimes the debris is considerably tilted and then its plan projection is measure instead of its complete extension, sometimes debris are buried and then not completely visible;
- Rootwad's margins are less sharp because of the presence of fine roots or intercepted loosen material, therefore they are not easily detectable.

Concluding rough errors are induced by the presence of vegetation and shadows.

Some limits of this method may be overtaken with the use of LIDAR surveys of the studied areas, this allow to produce digital elevation model (DEM) of the terrain and to better distinguish debris from the terrain surface and to estimate the height (and consequently the volume) of debris jam.

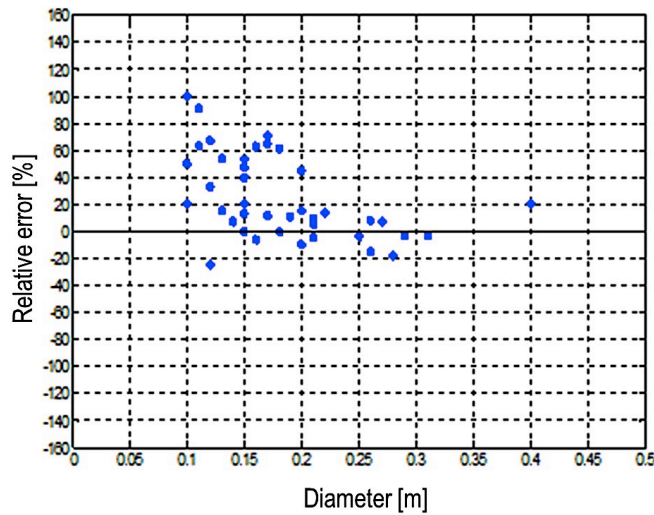


Figure 4-25: relative error between LWD diameter, directly measured and estimated on photogram.

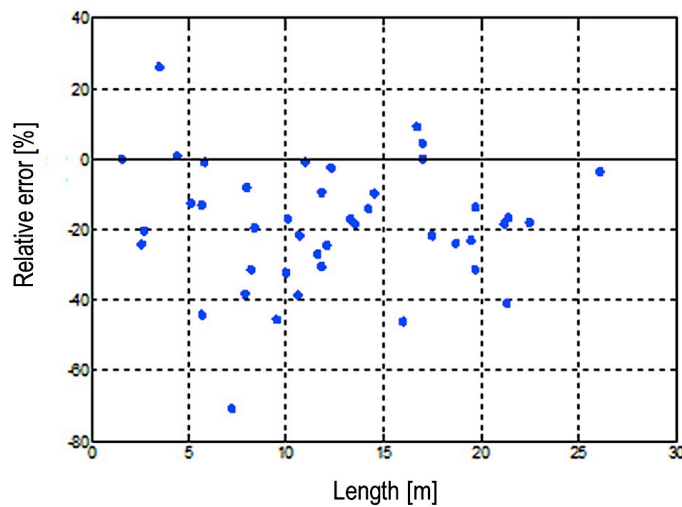


Figure 4-26: relative error between LWD length, directly measured and estimated on photogram.

4.4 CONCLUSIONS

The interpretation of aerial imagery presents indubitable advantages to monitoring wide areas or very large channels, this investigation method gives the possibility to have a global view of the river reach that is hardly accessible with a direct survey.

On the photograms it is possible to recognize patterns of the stream flow in different condition respect to the captured ones (for example in transitory levels from

low and high flow conditions), combining the boundaries of the geomorphologic surfaces and the debris distribution it is possible to suppose the flow field that may have produced the observed configuration (Figure 4-27). On the other side using aerial imagery is impossible to evaluate wood density that may be only deduct using statistics representative of the reach situation.

Furthermore the main limit of this method is related principally to the photograms resolution, to the standing vegetation hiding, and to the debris inclination respect to the terrain surface that lead to a global underestimation of wood volume in a surveyed region. What is more, it is absolutely a user dependent method as it depend from the subjective interpretation. Trained neural networks or imaginary elaboration algorithms may be useful to resolve this restrain.

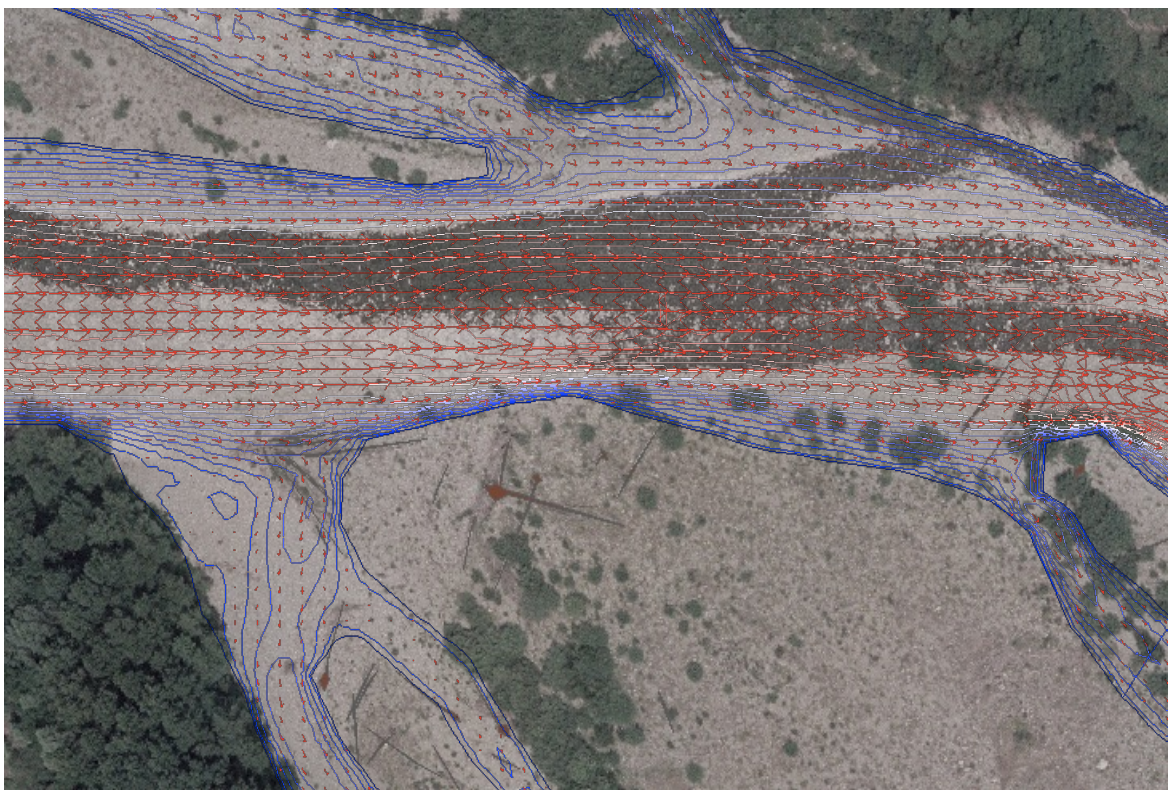


Figure 4-27: superimposition of a hypothetical flow field on aerial imagery.

For the redaction of management plans a deep understanding of the catchment condition is fundamental, and it cannot be achieved without a direct monitoring of a region. This requires economical efforts and time so that practical instrument as the survey sheets may facilitate and accelerate the operations. Furthermore when reduced to essential information and evaluations (i.e. like size and position, fresh or dated material, etc.) which do not require particular technical experience, the sheets are approachable, after a quick training, even by unprofessional users with basic instruments; which means that all the stakeholders in the river and riverine settlements protection (i.e. like fisheries associations, ecologist associations, civil protection volunteers, etc.) may be involved in monitoring operations.

Remote surveys may be useful for quick investigation after particular event to register the system response, and to identify critical areas that may require a direct survey. At present new techniques, like low-elevation high resolution imagery obtained using drone aircraft, seems to be promising to conduct frequent inspections with lower costs.

In a rational management strategy both methods, remote and direct, may be used agreeing the survey purposes.

5 LARGE WOODY DEBRIS ENTRAINMENT: GENERAL ASPECTS

Even though LWD entrainment is not the main topic of this thesis, it was considered crucial to spend effort in this field due to the major role that entrainment plays in the LWD risk assessment. Establishing the divergence between the total amount of wood in a river catchment and the quantity of material that may move with high probability during an high flow event is a primary step in the development of a management tool, leading the land agencies able to manage the environmental resources with an optimal balance between natural benefits and risk exposure.

A limited amount of literature is currently available to assess the stability of LWD, basically based on very simplified mechanistic models, that do not take into account whole interactions between wood, bed sediments and water flow. As a consequence the reliability of the proposed entrainment parameters is unsatisfactory.

In this chapter after an in depth analysis of the state of the art, the needs for research are presented, and the motivations that have aimed the experimental activities carried out at the Delft University of Technology are discussed.

5.1 INTRODUCTION

In rivers the debris propensity to move is strongly influenced by its geometric characteristics: size, shape, branches, rootwads and its density and decay ratio (refer to section 2.2.2), not less important are the geometric characteristics of the hydraulic section and the debris position in the section. The interaction among multiple pieces can play an important role for the incipient motion of LWD: stationary pieces can be entrained by the deviation of flow from other stationary pieces (Braudrick & Grant, 2000), while in other cases they can be blocked by other pieces or in-channel obstacles (boulders, vegetation). In a river channel since a LWD remain stable, it interacts with water flow and bed sediments, locally altering the hydraulic condition and the bed morphology. With a prolonged exposedness to water discharges insufficient to move the large woody debris, the local alterations of the flow conditions induce sediments redistribution and selection that in general tend to stabilize the wooden object, in these cases the entrainment mode of wood may be strictly connected with sediments mobility. Nevertheless, as for bed sediments, some basic mode may be recognized for the entrainment of single pieces of wood corresponding to sliding, rolling and buoyancy.

The flotation threshold for a rod-shaped log could be easily calculated considering the equilibrium between weight and buoyancy forces (Braudrick, 1998):

$$\cos^{-1}\left(1 - 2 \cdot \frac{d_w}{D_{log}}\right) - 2 \cdot \left(1 - 2 \cdot \frac{d_w}{D_{log}}\right) \sqrt{\frac{d_w}{D_{log}} - \left(\frac{d_w}{D_{log}}\right)^2} = \pi \cdot \frac{\rho_{log}}{\rho_w} \quad (5-1)$$

where D_{log} is the diameter of the log, ρ_{log} and ρ_w are the densities of wood and water, and d_w is the still water depth.

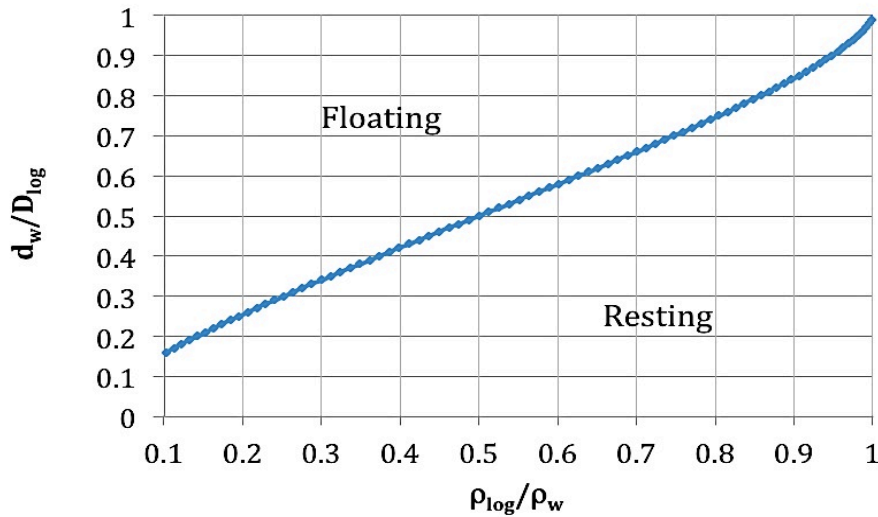


Figure 5-1: dimensionless plot of flotation thresholds for wood of different piece densities and diameters.

However according to Braudrick, LWD may move prior to flotation if the force of the water acting upon it is sufficient to overcome the frictional resistance of the log with the bed (Braudrick, 1998).

Despite the importance that many administrations all over the world recognize to LWD entrainment, a limited amount of literature is currently available for assessing the stability of LWD and the resulting fate and/or damages as a consequence of its mobility (Svoboda, Cuhaciyar, & Kimbrel, 2013). Nevertheless according Southerland (2010) the 40% of bend jam type structures becomes mobile after 5 years of monitoring, and the 60% of bend jam style LWD exposed to main channel flows becomes mobile.

In literature the incipient motion of single LWD is basically based on very simplified mechanistic models, that do not take into account whole interactions between wood, bed sediments and water flow. The derived incipient motion thresholds normally show a large scatter with experimental data, which make these parameters practically not really useful.

While mutual action between different wood pieces and interaction with bed sediments may be bypassed reducing the problem to the equilibrium of a cylindrical rigid body lying on a fixed planar bed, the modification of the flow field, induced by the presence of the object, and its effects on the forces acting on wood cannot be neglected, as highlighted in all the manuscripts found in literature.

5.2 STATE OF THE ART

The first study on stability of LWD in streams can be ascribed to Abbe et al. (1997). The authors demonstrate how log size and stream channel size and depth interact to influence LWD stability, proposing a qualitative log stability plot (Figure 5-2).

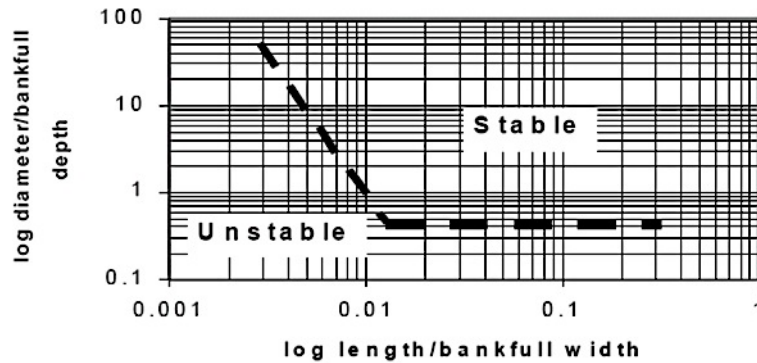


Figure 5-2: bi-logarithmic plot of flotation threshold for wood of different piece lengths and diameters (from Abbe et al. 1997).

Ishikawa (1989) conducted the first flume experiment on LWD dynamics, observing the movement of groups of logs through artificial constrictions and across alluvial fans. He measured the water depth for different bed slope gradients at which logs start to move, considering also logs at different orientation angle to the flow direction for a constant discharge of 0.3 l/s. He found that pieces orientation, respect to flow, altered the logs stability, with flow-parallel pieces being the most stable.

Braudrick & Grant (2000) assumed that the cylinder (approximating the log) moves initially by sliding, and then derived the water depth at the entrainment using the equilibrium equation for translation in the flow direction (Figure 5-3). Their mathematical model was obtained ignoring the lift force considered negligible due the partially submersion of the log, assuming the drag coefficient C_D from literature for the calculation of the drag force, and assuming a constant water depth d_w along the log sides for the calculation of the submerged volume and the wetted surface.

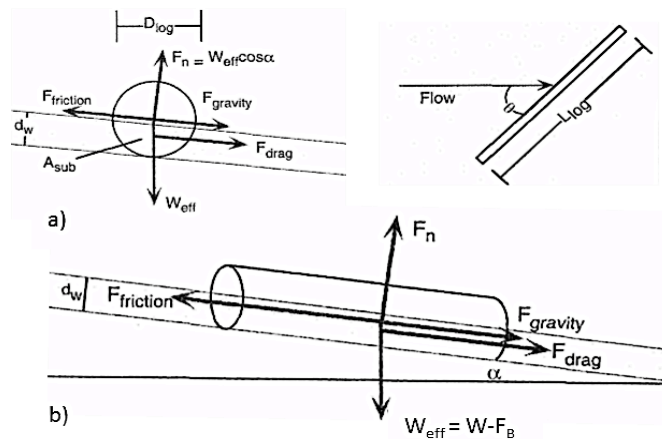


Figure 5-3: a) cross-sectional view of piece lying oblique to flow; b) piece lying parallel to flow (Braudrick & Grant, 2000).

According to the given scheme the entrainment condition may be expressed by the equilibrium between the resulting hydrodynamic force (F) and the resting force (R) in the stream direction, being:

$$F = \frac{U^2}{2} \rho_w C_D (L_{log} d_w \sin \theta + A_{sub} \cos \theta) \tag{5-2}$$

$$R = \left(g \rho_{log} L_{log} \frac{\pi D_{log}^2}{4} - g \rho L_{log} A_{sub} \right) (\mu_{bed} \cos \alpha - \sin \alpha) \tag{5-3}$$

where L_{log} is the length of the log, ρ_{log} and ρ_w are the densities of wood and water, A_{sub} is the submerged area of the log perpendicular to piece length, μ_{bed} is the friction coefficient between wood and bed, U is the mean water velocity, θ is the angle of the log relative to flow, α is the channel bed slope angle.

As a consequence the entrainment results in a function of four log characteristics, length, density, diameter and orientation, and three hydraulic characteristics, slope, water depth and velocity. The authors ran numerical simulations using the equilibrium equation to calculate the water depth at entrainment, using values coming from various previous works. Next tested the numerical model in a series of flume experiments considering three different initial orientations for the wooden cylinders. In Figure 5-4 are reported the comparison between the results of the experiments (hollow symbols) and the entrainment depth and velocity predicted by the model (filled symbols), considering two length classes (30 cm and 60 cm), and two diameter classes (2.54 cm and 3.81 cm).

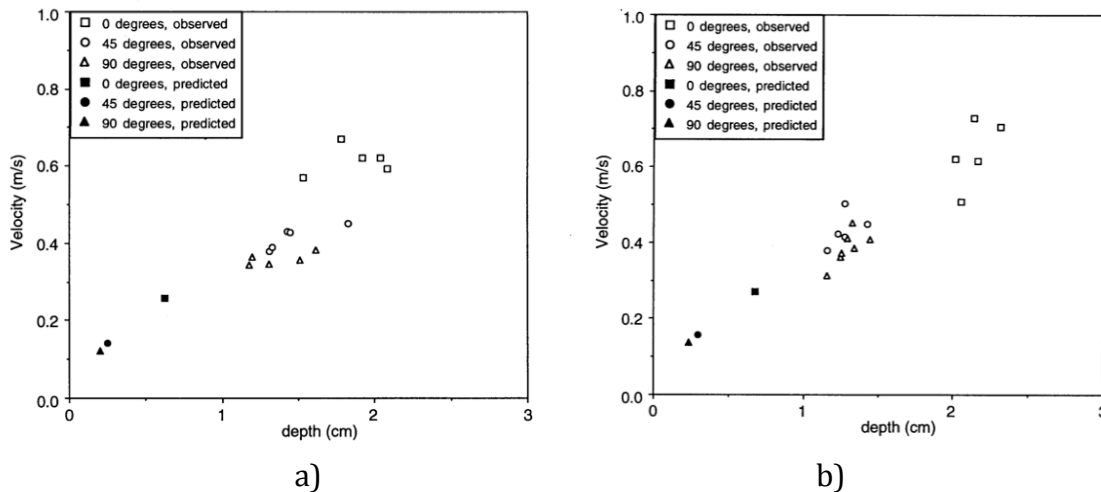


Figure 5-4: observed (hollow symbols) and predicted (filled symbols) depths and velocities at entrainment for pieces in length class 1 and diameter class 1 (a) and 2 (b) without rootwads from Braudrick (1998).

In conclusion they found that the proposed model, although formulated for sliding, did not predict adequately the entrainment of those object parallel to the flow that were most expected to move sliding, and recognized that the used drag coefficients were not appropriate for the experimental conditions.

Haga et al. (2002) maintained the physical model used by Braudrick and Grant just introducing two dimensionless parameters:

$$h^* = \frac{d_w}{D_{log}} \quad \text{dimensionless water depth} \quad (5-4)$$

$$\Psi = \frac{F}{R} \quad \text{dimensionless force} \quad (5-5)$$

Figure 5-5 shows an example of the relationship between Ψ and h^* . If the driving force F is smaller than the resisting force R , or $\Psi < 1$, the log remains stationary. If F is greater than R , or $\Psi > 1$, the log begins to move by sliding or rolling. To conclude if h^* is beyond the threshold for floating h_c^* it follows that $R = 0$ and $\Psi \rightarrow \infty$ and the log is transported by floating.

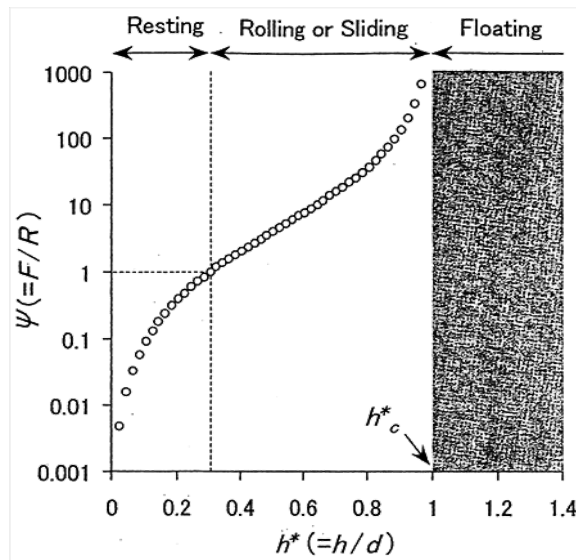


Figure 5-5: an example of the relationship between the dimensionless water depth h^* and the dimensionless force Ψ from Haga et al. (2002).

Bocchiola et al. (2006), based on their laboratory observations, proposed an extension of the model by Braudrick and Grant, allowing for a second entrainment mode for cylindrical logs lying on an immobile planar bed, depending on the initial orientation of the log. Hence they developed two equilibrium equations: for sliding and rolling. The lift force is still neglected in this model.

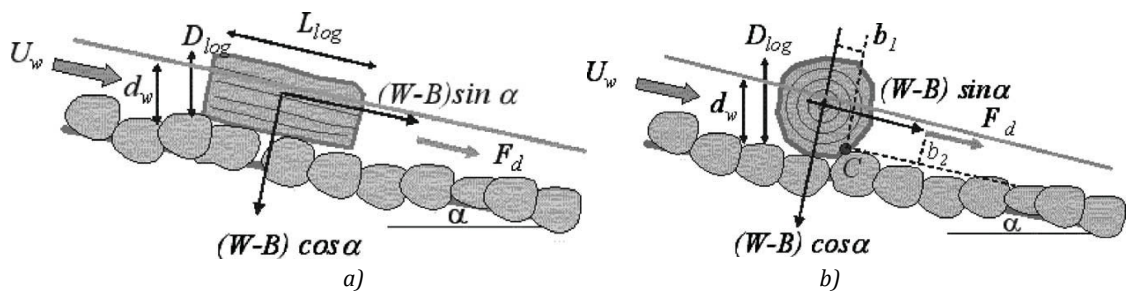


Figure 5-6: sketch of incipient motion of a sliding log (a) and of a rolling log (b) from Bocchiola et al. (2006).

Introducing the dimensionless parameter Y_w^* , Eq. 5-6, denoting the relative buoyancy, the threshold condition Y_r^* for incipient motion, Eq. 5-7, can be expressed for both sliding or rolling log at a given water depth d_w , as a function of the normalized ratio of the drag force and the resistance to motion $X_{S,R}^*$:

$$Y_w^* = \frac{\rho_w \cdot d_w}{\rho_{log} \cdot D_{log}} = \frac{\rho_w}{\rho_{log}} h^* \tag{5-6}$$

$$Y_r^* = \frac{1}{1 + C_D \cdot X_{S,R}^*} \tag{5-7}$$

where:

$$X_S^* = \frac{U^2}{2g L_{log} (\mu_{bed} \cos \alpha - \sin \alpha)} \quad \text{for sliding} \tag{5-8}$$

$$X_R^* = \frac{U^2}{2g D_{log} (\tan \delta \cos \alpha - \sin \alpha)} \quad \text{for rolling} \tag{5-9}$$

δ is the dry friction angle ($\tan \delta$ is the slope of the channel at which the log starts to rolling in dry condition).

According to the mechanistic model at the entrainment the relative buoyancy Y_w^* have to be equal to the threshold parameter Y_r^* .

$$Y_w^* = \frac{\rho_w \cdot d_w}{\rho_{log} \cdot D_{log}} = Y_r^* = \frac{1}{1 + C_D \cdot X_{S,R}^*} \tag{5-10}$$

Nevertheless laboratory experiments showed that this condition is not realized, as shown in Figure 5-7, in which the relative buoyancy Y_w^* at the entrainment is represented by the hollow square symbols, while lines represent the mathematical formulation stated by Eq. 5-7, considering different values for the apparent drag coefficient C_a .

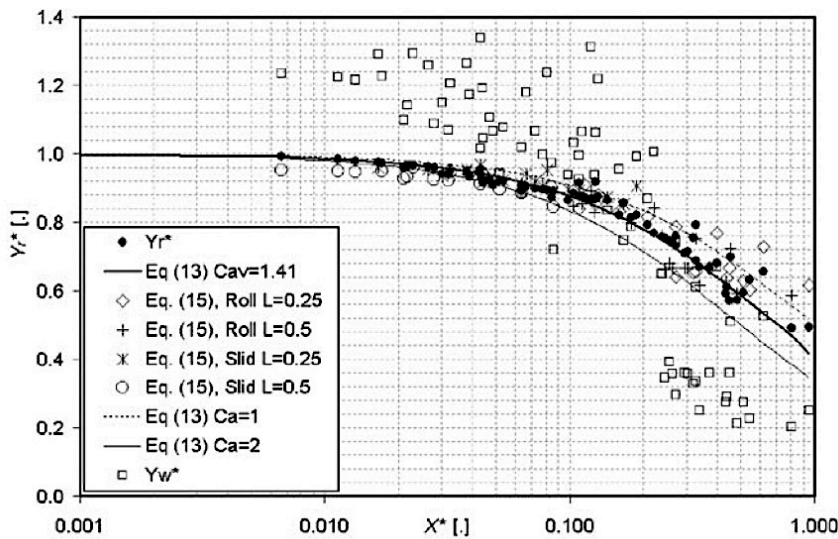


Figure 5-7: relative buoyancy Y_w^* and the entrainment parameter Y_r^* against $X_{S,R}^*$ from Bocchiola et al. (2006).

As recognized by the authors the entrainment condition stated by Eq. 5-10 hold if a proper value of drag coefficient C_D is taken, and the log is immersed in a water depth equivalent to that given by the undisturbed water depth. Nevertheless the presence of the log intensely modify the local water profile, suggesting the necessity to take into account this aspect in the force balance at incipient motion. Starting from the experimental results, they calculated a representative water depth d_r , defined as the water depth that satisfy the Eq. 5-10 at the incipient motion of the log: they established that d_r is not directly related with the undisturbed water depth d_w or the measured depths at 1 cm upstream d_{up} and 1 cm downstream the log position d_{down} , but introducing a coefficient of representativeness $C_r = d_r/d_w$, is possible to provide an empirical correlation between C_r and the relative buoyancy Y_w^* (Figure 5-8), showing a good coefficient of determination ($R^2 = 0.93$) for the cases investigated.

Finally the sensitivity analysis to drag coefficient and representative water depth showed that the modelling of wood entrainment is much more sensitive to the choice of the representative water depth than to the choice of the drag coefficient, at least for the considered cases of low submergence.

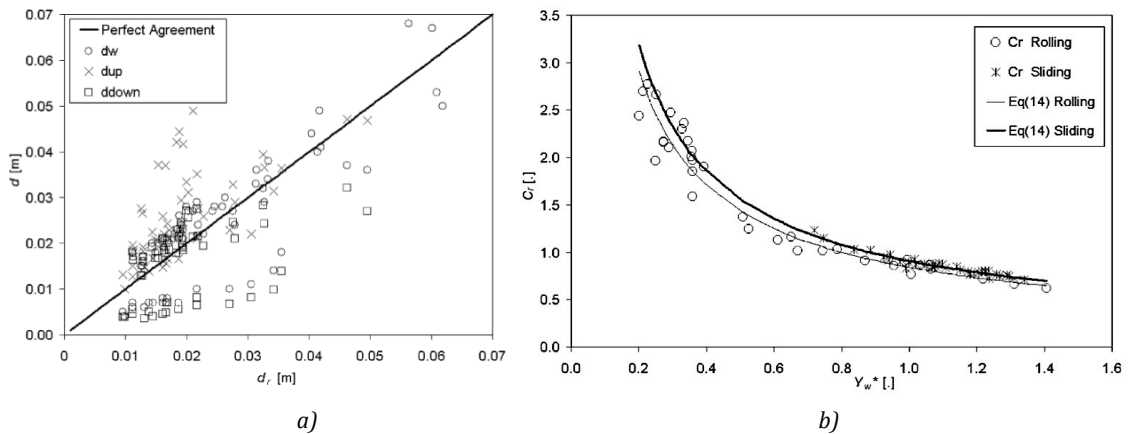


Figure 5-8: estimated representative depth against d_w , d_{up} and d_{down} , from Bocchiola et al. (2006).

Crosato et al. (2011) in a straight flume with fixed bed carried out some experiments using two different cross-sectional shapes, square and circular cylinder, and different initial orientation with respect to flow direction. The logs were relatively large with respect to the flume width so that their presence considerably affected the water flow, creating strong flow acceleration along their sides.

As Haga, the authors considered as entrainment parameter E^* the ratio between the drag force and the friction force acting on the log. Assuming many simplifications and integrating the laboratory experiments with other data available in literature, they proposed a semi-empirical expression for the entrainment threshold:

$$E^* = C_o \frac{U^2}{gD_{50} \left(\frac{\rho_w - \rho_{log}}{\rho_w} \right)} \left(\frac{d_w}{D_{log}} \right)^2 \quad (5-11)$$

where C_o is an empirical coefficient taking into account log orientation, D_{50} is the sediment size on the bed surface. Based on experimental results, the authors suggested using the following values: $C_o = 0.5$ for logs parallel to the flow direction; $C_o = 1$ for logs perpendicular to water flow direction.

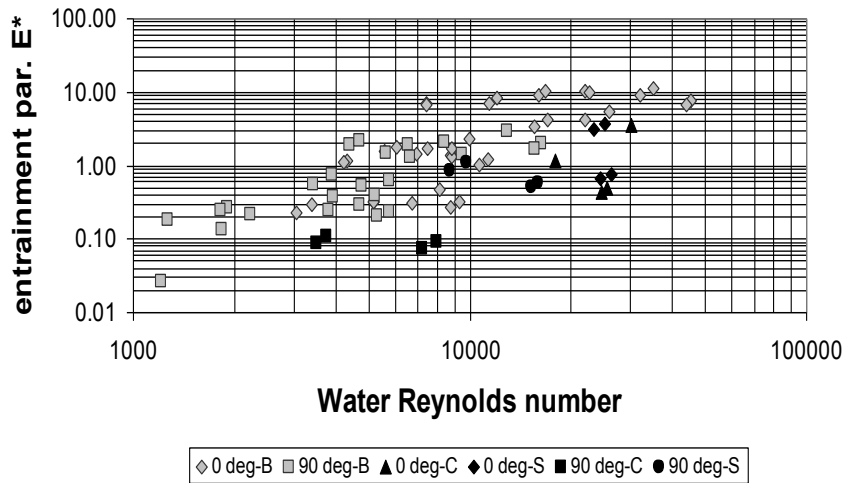


Figure 5-9: entrainment parameter plotted vs. Reynolds number of water flow, from Crosato et al. (2011).

Based on the experimental observations the authors recognized that the variation of the water depth experienced by the log along its sides parallel to flow cannot be neglected as it affects with opposite contribution each terms of the equilibrium equation. In particular the authors noticed that in most of the cases considered at initiation of motion the buoyant water depth (the water depth at which a log starts to float in still water) was smaller than the undisturbed water depth.

Table 5-1: undisturbed flow conditions, and log properties at incipient motion, from Crosato et al. (2011).

Log	Initial orientation (degrees)	Discharge (l/s)	undisturbed water depth (cm)	flow velocity ¹ (m/s)	Submerged volume ² (cm ³)	Average weight (g)	Log density (kg/m ³)	Buoyant water depth (cm)
Gravel bed								
Circular -dry	0	9.9	7.84	0.32	2324.79	1591.3	364.55	5.85
Circular -dry	90	2.9	4.62	0.16	1151.33	1591.3	364.55	5.85
Circular -wet	0	10.3	7.86	0.33	2332.23	1639.3	375.53	5.96
Circular -wet	90	3.2	4.44	0.18	1089.65	1639.3	375.53	5.96
Square -dry	0	9.8	8.32	0.29	2724.8	2014.2	462.39	6.05
Square -dry	90	6.4	6.62	0.24	2168.05	2014.2	462.39	6.05
Square -wet	0	10.6	8.27	0.32	2708.425	1973.3	453.00	5.93
Square -wet	90	6.1	5.62	0.27	1840.55	1973.3	453.00	5.93
Wooden bed								
Circular -dry	0	7.2	6.15	0.29	1697.80	1604.8	367.64	5.92
Circular -dry	90	1.4	3.35	0.10	733.37	1604.8	367.64	5.92
Circular -wet	0	12.1	8.35	0.36	2514.01	1796.9	411.65	6.48
Circular -wet	90	1.5	3.45	0.11	764.63	1823.2	417.67	6.52
Square -dry	0	9.4	6.47	0.36	2118.925	2016.2	462.84	6.06
Square -dry	90	3.5	4.67	0.19	1529.425	2016.2	462.84	6.06
Square -wet	0	10.1	6.63	0.38	2171.325	2068.2	474.78	6.22
Square -wet	90	3.9	4.21	0.23	1378.775	2068.2	474.78	6.22

This result was observed only for the logs oriented parallel to the flow (0 degree in Table 5-1) for both shapes (circular and square): at the entrainment only sliding of the log was observed, while floating occurred only after was covered some distance (Rajbhandari, 2010).

The variation of the water depth experienced by the log along its sides parallel to flow was investigated by Crosato et al. (2013). Measurements of the water level profiles around the logs and against the sidewalls of the flume (shown in Figure 5-10) indicate that the water flow near the logs strongly depends on longitudinal flow acceleration, curvature of the streamlines around the log and log shape.

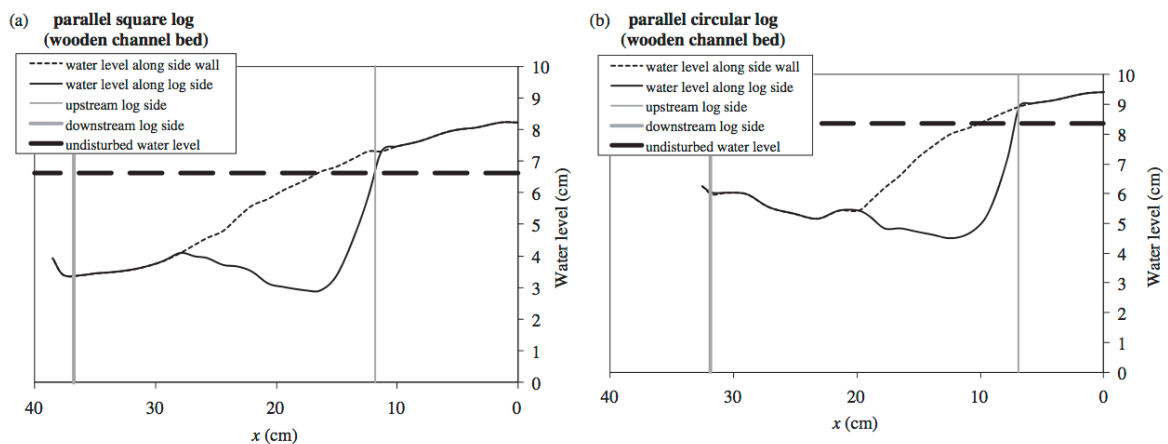


Figure 5-10: longitudinal water level profiles along the log side and the flume sidewall, from Crosato et al. (2013).

The authors attempted to establish an entrainment threshold value, using the same simplified equation, Eq. 5-10, provided by Bocchiola et al. (2006) without obtaining feasible results. The conclusion of their work is that is not possible to analyse the entrainment condition without taking into account local water acceleration and streamline curvature caused by the presence of the log, as well as the three-dimensional water flow around the logs.

5.3 DISCUSSION

The analysis of the state of the art has shown just a limited amount of literature currently available to assess the stability of LWD. Field studies related to large woody debris movements and the conditions for their entrainment, are very few, mainly because large wood movements are possible only during high discharge, in which circumstances field measurement are not sheltered (Braudrick et al., 2000). Moreover even physical experiments to observe the log entrainment are limited.

Since the former experimental studies (Braudrick & Grant, 2000; Haga et al., 2002) the theoretical approach to the entrainment condition for single log has been based on a simplified forces balance acting on a cylinder partially immersed in a uniform flow

field, lying on an immobile planar bed: the entrainment occurs when the overall driving force overcomes the reaction force.

The large scatter of experimental data (Figure 5-7, Figure 5-9), which characterizes all the models found in literature, suggests how the entrainment of LWD could not be assessed by simple entirely analytical approaches, as those proposed by Braudrick, or Haga, which consider only the incipient motion due to sliding, using a simplified mechanistic approach.

In order to reduce the scatter of data, Bocchiola et al. (2006), starting from the experimental evidence that the presence of the log locally modify the flow, introduced the concept of a representative water depth, defined as the uniform water depth that verify the equilibrium between the driving and reaction forces acting on the log, according to the mechanistic approach proposed by Braudrick et al. (2000). This parameter was back calculated by the experimental data, showing a good correlation with the relative buoyancy for the cases considered by the authors (Figure 5-8). Finally they showed how the proposed entrainment parameter is very sensitive to both drag coefficient and representative water depth, underlining how the right choice of the water depth is the main factor affecting the reliability of the model.

The principal lack of the semi-empirical approach proposed by Bocchiola et al. (2006) is that no physical insight of the representative water depth is provided. Even the established empirical correlation, seems to be too much simplistic: since this parameter has been introduced to take into account the local change in water depth due to the presence of the obstacle, it make sense to expect that it has to be related to the flow conditions around the obstacle and not simply to the relative buoyancy as proposed by the authors. Moreover, despite the entrainment model due to Bocchiola et al. considers also the initiation of motion due to rolling, it is not able to discern between different entrainment modes: the user have to know a priori how the log will be destabilized by the flow.

The importance of the variation of the water depth experienced by the log along its sides parallel to flow, is confirmed by the laboratory experiments carried out by Crosato et al. (2011 and 2013) that used relative large log with respect to the flume width. The water level measured along the sides of the log showed a great variation from the undisturbed water depth (refer to Figure 5-10), which could significantly alter the buoyancy force acting on the log. The importance, and the effect on the entrainment, of the water level profile along the logs is confirmed also by the analysis of the experimental data showed in Table 5-1: for all the logs positioned parallel to the flow, at initiation of motion the buoyant water depth (the water depth at which a log starts to float in still water) was smaller than the undisturbed water depth. The same result could be found considering the experimental data from Bocchiola et al. (2006), as shown in Table 5-2, in which the buoyancy forces acting at the initiation of motion have been calculated considering both the undisturbed water depth d_w and the representative water depth d_r proposed by the authors.

Table 5-2: comparison between weight and buoyancy forces at entrainment, calculated using experimental data from Bocchiola et al. (2006).

Run	Gravel bed (Sliding)										
	Llog	Dlog	ρ_{log}	dw	d _{up}	d _{down}	dr	Uw	Weight	Buoyancy with dw	Buoyancy with dr
	[m]	[m]	[kg m ⁻³]	[m]	[m]	[m]	[m]	[m s ⁻¹]	[N]	[N]	[N]
<i>Triplochiton</i>											
T1	0.25	0.028	470.0	0.017	0.019	0.017	0.013	0.201	0.713	0.963	0.689
T2	0.25	0.039	427.0	0.021	0.026	0.021	0.016	0.248	1.256	1.615	1.136
T3	0.25	0.050	426.0	0.027	0.031	0.026	0.020	0.302	2.060	2.663	1.806
T4	0.25	0.065	321.0	0.028	0.033	0.027	0.020	0.314	2.623	3.367	2.135
T5	0.50	0.028	462.0	0.016	0.018	0.016	0.013	0.192	1.404	1.795	1.381
T6	0.50	0.039	439.0	0.021	0.024	0.021	0.017	0.248	2.588	3.236	2.468
T7	0.50	0.050	391.0	0.024	0.030	0.025	0.019	0.281	3.788	4.598	3.378
T8	0.50	0.065	344.0	0.029	0.035	0.028	0.022	0.323	5.633	7.067	4.879
<i>Fagus</i>											
F1	0.25	0.027	707.0	0.022	-	-	0.018	0.254	0.993	1.225	0.994
F2	0.25	0.039	686.0	0.028	-	-	0.025	0.316	2.010	2.251	1.984
F3	0.25	0.050	705.0	0.036	-	-	0.031	0.433	3.395	3.712	3.136
F4	0.25	0.066	708.0	0.044	-	-	0.040	0.502	5.940	5.942	5.320
F5	0.25	0.099	692.0	0.068	-	-	0.056	0.669	13.064	13.824	11.013
F6	0.50	0.027	700.0	0.023	-	-	0.019	0.265	1.966	2.549	2.112
F7	0.50	0.039	699.0	0.030	-	-	0.026	0.334	4.096	4.837	4.150
F8	0.50	0.050	709.0	0.038	-	-	0.033	0.450	6.828	7.854	6.743
F9	0.50	0.066	694.0	0.049	-	-	0.042	0.533	11.646	13.359	11.268
F10	0.50	0.099	695.0	0.067	-	-	0.060	0.658	26.241	27.196	23.939

According to the mechanistic approach universally assumed, this implies that at the entrainment the buoyancy force acting on the log is higher than its weight, which makes no sense, as it means that equilibrium is not established in the vertical direction (normal to the flow). It has to be noticed that using the representative water depth as proposed by Bocchiola et al. (2006), the buoyancy force is always less or equal to the log weight, as required by the equilibrium condition, if no other vertical stabilizing hydrodynamic force is present (i.e. negative lift forces).

This behaviour could be ascribed to the disturbed water profile around the logs and its effect on the forces acting on wood, which is, unless waterlogged, typically less dense than water.

Buoyancy depends mainly on the difference between water and wood densities, but also on the wet volume of the log, according to the Archimedes' law. The density of wood depends upon the type of wood (species, heartwood versus sapwood) and the state of decay: in dry condition a fresh dead wood is denser than a dated dead wood but in wet condition the more advanced the decay the more easily water saturates the log, increasing the global density. The submerged part of the log depends on the water level along the log side, which is not easily estimable.

All the methods found in literature consider a constant water depth around the log, even if the experiments indicate a remarkable difference between water depth just upstream of the log d_{up} , and just downstream of the log d_{down} . The reason of this behaviour is well known, and it is related to local dynamical effects that cause the water surface in the vicinity of the obstacle to be disturbed: just upstream of the obstacle there is a local mound due to Bernoulli stagnation effects, while around the

sides of the obstacle the water level drops where the velocity is higher. The local effect quickly decays away from the obstacle but produces a change of the mean water level across the whole channel: just upstream the obstacle there is a backwater risen Δy , which slowly disappears upstream and which effect can extend for a long way, as shown in Figure 5-11.

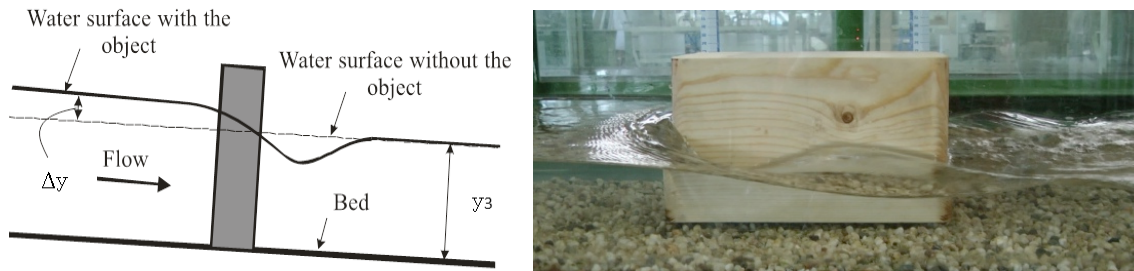


Figure 5-11: typical emerging obstacle (like a bridge pier) in sub-critical flow.

The flow near the obstacle is so complicated that for practical problems it is not feasible to accurately calculate the forces acting on it from fluid-mechanical principles. Moreover the empirical expression from conventional fluid mechanics for the drag on a submerged bluff body could not be truly applied to the present problem, because of free surface effects: the shape of the free surface immediately around the obstacle controls the resistance of the object to water flow.

A free surface flow over a partially submerged obstacle sets up waves emanating mainly from the front and backside of the object. The waves created consist mainly of divergent and transverse waves, well known in naval hydrodynamics, because an important part of the resistance to motion of a ship is due to the energy radiated by these waves (Van Manen & Van Oossanen, 1988). The divergent waves are observed as the wake of a ship with a series of diagonal or oblique crests moving outwardly from the point of disturbance. These waves were first studied by Kelvin, who found that regardless of the speed of the ship, they were always contained in the 19.5° (each side) symmetric wedge following the ship (Figure 5-12).

The divergent waves do not cause much resistance against the ships forward motion, while the transverse waves, which appear as troughs and crests along the length of a ship, constitute the major part of the wave-making resistance of a ship. This force acting on the partially submerged body has to be added to the viscous forces (the form and wake drag) in order to obtain the overall hydrodynamic force. This justifies the use of an apparent drag coefficient used by Bocchiola to distinguish it from that acting on a fully immersed cylinder into unconfined flow (Crowe et al., 2001), and the higher value adopted with respect to that assumed by Braudrick.

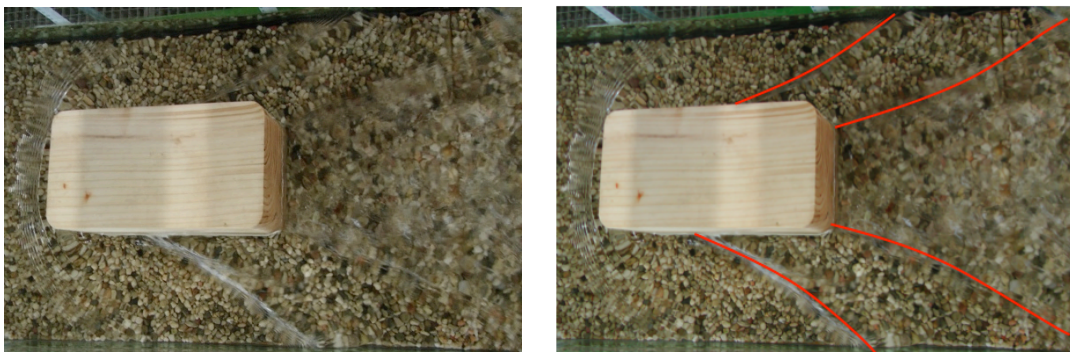
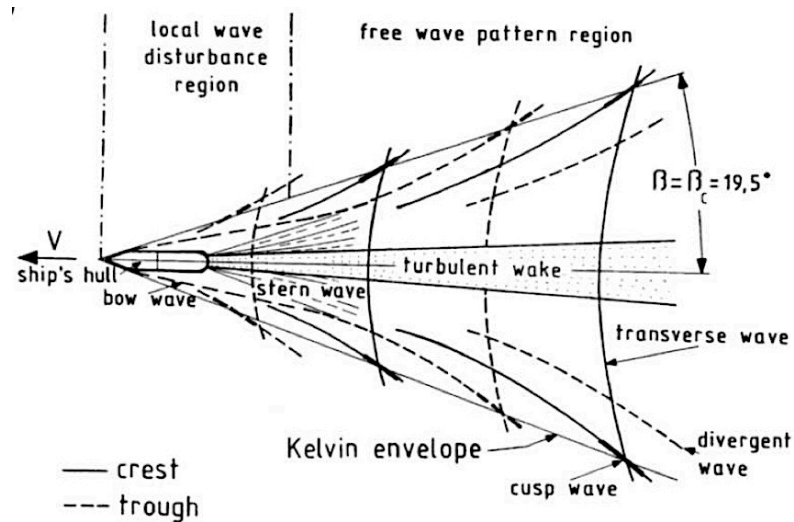


Figure 5-12: wave pattern across an object immersed in a flow (Van Manen & Van Oossanen, 1988), and the divergent waves observed during the flume experiments.

The system of wave produced by the partially immersed dowel has a wavelength that is an increasing function of the velocity of the flow: for a slow flow there may be several wave crests and troughs around the obstacle, although they might be barely perceptible; for a faster flow both the height and wavelength are larger. Hence, the water level at the rear of the body (the downstream side) will be an oscillatory function of velocity, and so is the net force.

The waves height along the surface of the obstacle modify also the centre of buoyancy, being the centroid of the displaced volume of fluid, according to the Archimedes' law: weight force, acting through its centre of gravity, and the upward buoyancy force may be not aligned (Figure 5-13), producing a rotational moment, that could affect the entrainment.

The problem appears to be complicated even by a "Bernoulli" effect: depending on the shape and orientation of the obstacle, the water velocity under the obstacle could be accelerated, because of the confined section among the channel bed and the log sides. This increase in velocity results in a higher drag comparable to this higher "effective" speed, and in addition to this, the accelerating water can pull the immersed object down (known as "sinkage" or "squat" in the context of ship engineering): the lift force, which in all the models found in literature was not taken into account, could be negative in this case.

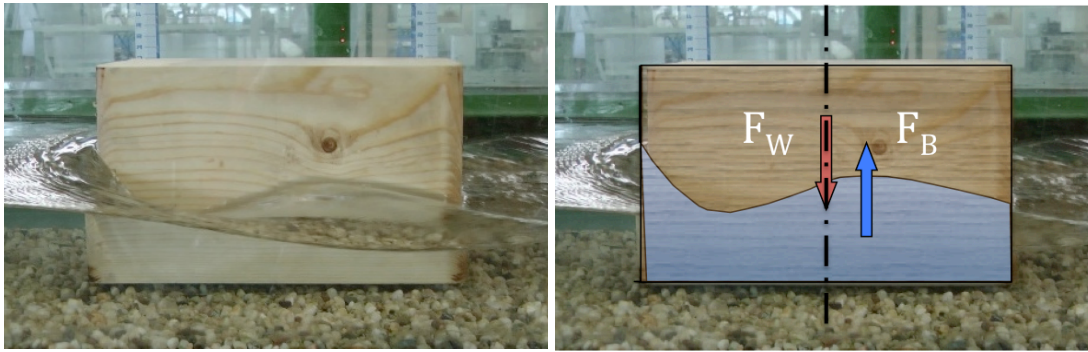


Figure 5-13: the water surface profile determines the submerged volume and the buoyancy centre.

The possibility of a negative lift force is known in several fields of the hydraulic engineering. For a submerged rectangular obstacle in turbulent flow over a bedrock surface, this condition could arise in the case of shallow flow, due to the standing wave above the block, induced by flow blocking (Carling et al., 2002). As stated by the authors, for a rectangular block, lift force can occur only for full submergence. For a cylindrical log parallel to the flow, instead, a negative lift force could result also in the case of partial submergence, as a consequence of the curvature of the wetted surface, in analogy with the squat phenomenon (Saunders, 1957), one of the most important problems related to shipping in shallow water (very shallow water can be taken to be 15% of the ship's waterline length or less).

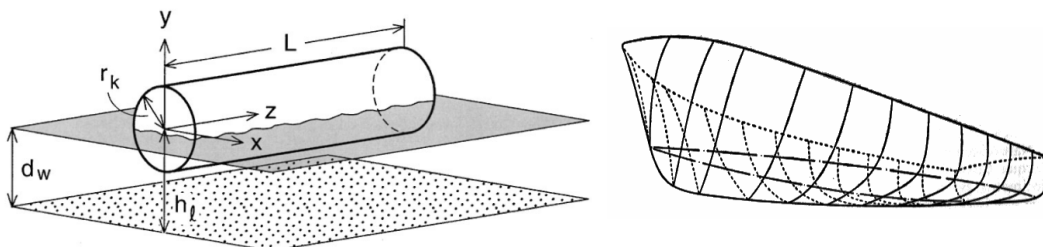


Figure 5-14: analogy between floating logs shape (Shields et al., 2004), and hull shape.

A vessel underway tends to lower the pressure field surrounding its hull. The motion induced in the water creates kinetic head at the expense of potential head, and the vessel is lower than when at rest. Moreover, variations in the distribution of the potential head over the hull are reflected in a so-called change in trim, usually a settling of the stern and a rise in the bow. Both effects, sinkage and a change in trim, sometimes collectively called squat, result in an increase in draft and a loss in bed clearance in shallow water. The squat is usually greater in shallow than in deep water because the decrease in bed clearance tends to increase the reduction in potential head, resulting in greater squat. Squat increases with speed.

These simple qualitative considerations suggest that for a LWD partially submerged the lift force probably is negative.

Considering the combined effects due to the previously described phenomena contributes to a more realistic description of the entrainment physics, and has a manifest effect in the key piece incipient movement.

5.3.1 Needs for research

The analysis of the state of the art has shown that much effort have to be spent in order to clearly understand the real physics behind the log entrainment, and that analytical approaches are too much simplistic to describe the complex phenomena that are related to LWD entrainment. The lack of field measurements and experimental data limits the understanding of the real physics behind the log entrainment, making the proposed entrainment parameters found in literature practically not really useful.

Analysis of data available in literature seems suggest that buoyancy force is the major responsible of the stability of LWD, as it directly affects the reaction force between log and riverbed, which is the only one contrasting the sliding of the LWD. Moreover the results of the experiment carried out by Crosato seem to indicate that the flow field around the log has a stabilizing effect on the log. This result is confirmed also by the analysis performed on the experimental measurement of Bocchiola, which produce a water depth at the entrainment higher than the buoyancy depth, representing the minimum depth of still water needed to float the log.

These considerations suggest that a reliable entrainment model have to take into account the water profile along the submerged log, altered by the standing wave produced by the dynamic effects related to the presence of the wood piece in the flow field, and to the backwater rise, as highlighted by Crosato et al. (2013).

Moreover studies related to the evaluation of local modified water profile around the submerged LWD are of great interests, because LWD also interacts with sediment transport and deposition and possibly with riverine species dynamics. Further research is also needed to explore the complex geometry of natural logs, including rootwads and branches, which extremely complicate the statement of entrainment equations.

5.3.2 Aim of research activities related to LWD entrainment

The general aim of the thesis is concerning LWD risk assessment. Due to the importance that entrainment have in the hazards related to the presence of LWD in river channel, it is desirable that a realistic entrainment model would be available for the administrations delegate to compile the risk management plans.

The theoretical approach developed, and the experiment carried out at the Delft University of Technology, have been sustained by the aim to provide a more realistic model for LWD entrainment, able to take into account all the lacks underlined in the previous sub-chapters, and to give an insight in the understanding of the physics behind this phenomenon.

Due to the analogy with other free-surface hydrodynamics studies well known in literature, an integrated approach is proposed, obtained adjusting to LWD entrainment the correlations found in other engineering fields, in order to: i) reduce the lack of field measurements and experimental data related to LWD entrainment, ii) reduce the need of flume experiments, and iii) indicate a way for further researches.

6 LARGE WOODY DEBRIS ENTRAINMENT: PROPOSED APPROACH

In this chapter a novel theoretical approach is presented, which makes use of several experimental correlations, rearranged from other engineering fields to the LWD entrainment. The present work differs from analyses reported in literature for a different arrangement of the already known terms, for the introduction of an entrainment parameter related to the standing wave around the log produced by the presence of the obstacle in the flow field, in analogy with wave formation in naval context, and because it takes into account the effects of blockage ratio and upstream backwater, due to the presence of the obstacle. Moreover, the lever arms of the hydrodynamic forces acting on the log, which could affect the rolling entrainment mode, and the location of the floatation centre, have been considered. All the parameters used to evaluate the proposed incipient motion threshold for incipient motion of individual logs, have been related to the undisturbed water conditions.

Experimental results, obtained with flume experiments carried out at the Fluid Mechanics Laboratory of Delft University of Technology, have been used to test the theoretical model and to derive an empirical correlation for the proposed threshold parameter. Also experimental data found in literature (Bocchiola et al, 2006; Crosato et al., 2011) have been utilised. Because an in depth analysis of the entrainment is out of the scope of this thesis, and a well-established threshold of LWD movement has not yet been quantified, the research was restricted to the simple case of individual logs. Straight and smooth logs of different cross-sectional shape were considered avoiding log-log interaction. Just log parallel or orthogonal to the flow were studied.

The outcome is a parameter suitable to characterize the incipient motion condition, which join under a unified approach the different entrainment modes associated with the initial position of a log along the river bed (i.e. parallel or perpendicular to flow direction), being able to discern between sliding, rolling and floating modes, and which shows a good correlation with experimental data. Moreover it could be used, together with the proposed survey sheets (refer to section 4), to provide a much reliable first order assessment for wood entrainment.

6.1 THEORETICAL MODEL FOR THE NOVEL APPROACH

The concerns about the impact of LWD on the local flow (section 5.3) justify the need to keep into account the modification of the local water profile (Crosato et al., 2013), affecting the force balance at incipient motion. This issue has been apparently neglected in the wood entrainment models so far developed, and recently simply considered with the introduction of a representative uniform water depth (Bocchiola

et al., 2006). A conceptual mechanistic model, based on the bi-dimensional stationary equilibrium of gravity, buoyancy, friction and hydrodynamic forces acting on a rigid body, has been thus developed and verified through the interpretation of scale flume model experiments. Classes of permissible rotations and translations have been formulated for large woody debris, thought as rigid bodies initially resting on rigid surfaces, then these were proposed as the criteria on which to base incipient translation and rotation analyses. The shape of the log is approximated as a cylinder. The presence of roots and branches has not been considered.

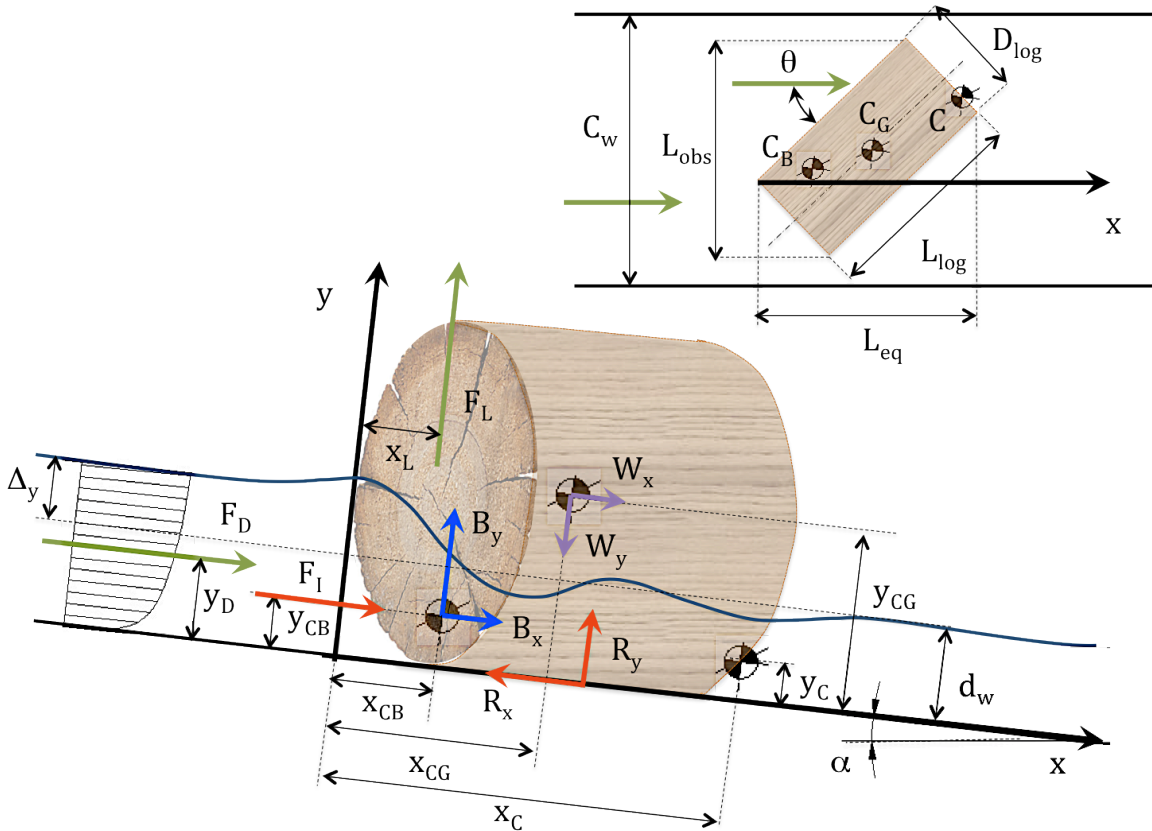


Figure 6-1: sketch of the system of forces acting on the partially submerged log.

A motionless log partially immersed in a time-varying stream flow of instantaneous undisturbed water depth d_w (in absence of the log), and channel width C_w , lying on an immobile planar bed (Figure 6-1), is exposed to the following system of forces (Alonso, 2004), widely described in the following sections:

- Gravity force (\vec{W}): the weight of the log due to the gravity acting in the vertical direction.
- Buoyancy force (\vec{B}): the upward force exerted by a fluid that opposes the weight of an immersed object, according to the Archimedes' law.
- Bed reaction (\vec{R}): the force exerted by the riverbed on the log in contact with it, characterized by the friction coefficient μ_{bed} between wood and bed.

- *Drag force* (F_D): the force acting in the flow field direction, resulting from the hydrodynamic distribution of pressure and shear stress along the wetted surface of the log.
- *Lift force* (F_L): the force acting normally to the flow field direction, resulting from the hydrodynamic distribution of pressure and shear stress along the wetted surface of the log.
- *Inertia force* (F_I): the apparent mass force due to the acceleration of the flow, assumed applied to the centre of floatation.

According to the mechanistic approach, possible modes for incipient motion are mainly translation (lifting or sliding) and rotation (pivoting). In this work “general” motion types arising by the combination of these two basic motion modes have not been considered. Permissible motions are therefore formulated in terms of the notation depicted in Figure 6-1, according to the Newton’s first law, considering the classical Coulomb friction model. According to the used notation:

- C_B is the centre of floatation.
- C is the centre of instantaneous rotation.
- C_G is the centre of gravity.
- y_D is the arm of the drag force with respect to the origin of the coordinate system.
- x_L is the arm of the lift force with respect to the origin of the coordinate system.

If we consider the absence of any obstacle for sliding ($y_c = 0$), the equilibrium to translation in flow direction (x axis) states that incipient motion of the log occurs when the sum of the component of gravity (W_x) and buoyancy (B_x) in the flow direction and the drag (F_D) and inertia (F_I) forces exerted by flow, overcome the friction force (R_x) on the bed proportional to the difference between the log weight and the sum of buoyancy (B_y) and lift (F_L) forces:

$$F_D + B_x + W_x + F_I \geq \mu_{bed}(W_y - F_L - B_y) \quad (6-1)$$

In case of the presence of an obstacle instead ($y_c \neq 0$), the sliding could not occur, and a possible initial motion mode might be log rolling. In this case the equilibrium equation has to be written considering the moment of the forces acting on the log with respect to the centre of instantaneous rotation C (see Figure 6-1). Thus the incipient motion occurs when:

$$\begin{aligned} F_D(y_D - y_C) + (B_x + F_I)(y_{CB} - y_C) + W_x(y_{CG} - y_C) + F_L(x_C - x_L) + \\ B_y(x_C - x_{CB}) \geq W_y(x_C - x_{CG}) \end{aligned} \quad (6-2)$$

In some cases the arm of the obstacle (x_c) is so great (for instance in case of very slender log parallel to the flow) that the only possible incipient motion could be the

simple buoyancy. In this case the equilibrium in y direction gives the condition for the initiation of motion:

$$F_L + B_y \geq W_y \quad (6-3)$$

After some simple substitutions it is possible to obtain the following expressions for the three incipient motion conditions:

a) Sliding Mode:

$$B_y \geq \frac{\mu_{bed} \cdot \cos(\alpha) - \sin(\alpha)}{\mu_{bed}} \cdot W - \frac{F_D + F_I + B_x}{\mu_{bed}} - F_L \quad (6-4)$$

b) Rolling Mode:

$$B_y \geq \frac{(x_C - x_{CG}) \cdot \cos(\alpha) - (y_{CG} - y_C) \cdot \sin(\alpha)}{(x_C - x_{CB})} \cdot W - \frac{(y_D - y_C)}{(x_C - x_{CB})} \cdot F_D - \frac{(x_C - x_L)}{(x_C - x_{CB})} \cdot F_D - \frac{(y_{CB} - y_C)}{(x_C - x_{CB})} \cdot (F_I + B_x) \quad (6-5)$$

c) Buoyancy mode:

$$B_y \geq W \cdot \cos(\alpha) - F_L \quad (6-6)$$

The problem has been therefore conducted to the calculation of three entrainment conditions, all related to the buoyancy force acting normal to the flow, which has been recognized as the main feature affecting the entrainment. The assessment of the proposed conditions requires that all the factors in Eqs. 6-4, 6-5 and 6-6 have to be determined. To achieve it, some hypotheses on the position of the floatation point, and the instantaneous centre of rotation are required, and the unknown forces W , B , F_D , F_I and F_L have to be quantified, and related to the flow condition. Commonly, from a hydraulic point of view, it is usually convenient to relate all the unknown parameters to the known downstream flow conditions, as the flow causing LWD entrainment is expected to be subcritical.

In the following paragraphs possible solutions to the estimate of the unknown parameters and problem uncertainties will be discussed and supported with experimental results. Differently from previous works the drag force has not been calculated assuming literature values for the C_D coefficient, but obtained using experimental correlations (usually adopted for bridges problems), the lift and inertia forces have not been neglected a priori, and the buoyancy force has not been assumed equivalent to the hydrostatic case.

6.2 WEIGHT OF THE LOG

The weight of the log is clearly related to the gravity acceleration g , and could be evaluated by the product between log density ρ_{log} and its volume, which for the entrainment assessment could be reasonably approximated by the volume of a cylinder with a cross section A_{log} and a length L_{log} :

$$W = g \cdot A_{log} \cdot L_{log} \cdot \rho_{log} \quad (6-7)$$

Despite the simplistic equation, the correct estimate of the real weight of the log is not straightforward, being affected by the correct estimate of the log density. Wood density, exclusive of water, varies greatly with type of wood (species, heartwood versus sapwood), growth conditions, part of the tree measured: the main stem generally has a higher wood density than branches. The density of most species falls between about 320 and 720 kg/m³, but the range of density actually extends from about 160 kg/m³ for balsa to more than 1200 kg/m³ for some other imported woods. In Table 6-1 are collected few quantitative information taken from a publicly available source.

Table 6-1: density of some wood species*.

World regions	Common name	Botanical name	Density (kg/m ³)		
			min	max	medium
Latin American	Balsa (Tropical America)	Ochroma	110	200	160
North America - Europe	Basswood	Tilia glabra or Tilia americanus	300	600	398
North America - Europe	Poplar, yellow	Liriodendron tulipifera	350	500	427
North America - Europe	Magnolia, cucumber	Magnolia acuminata	570	570	516
North America - Europe	Sycamore	Platanus occidentalis	400	600	539
North America - Europe	Maple, black	Acer nigrum	600	750	620
North America - Europe	Ash, white	Fraxinus americana	650	850	638
North America - Europe	Beech	Fagus grandifolia or americana	700	900	655
Africa	Oak, American Red	Quercus borealis	740	740	657
Asia - Oceania	Locust honey	Gleditsia triacanthos	650	700	666
Africa	Mahogany, African	Khaya ivorensis	500	850	668
Latin American	Oak, American White	Quercus alba	700	770	710
North America - Europe	Applewood or wild apple	Pyrus malus	650	850	745
North America - Europe	Boxwood/Buis	Buxus sempervirens	950	1200	1030
Latin American	Greenheart	Nectandra rodioei	1060	1230	1100
Latin American	Lignum Vitae	Guaiacum officinale or sanctum	1170	1330	1200

* data from: <http://www.worldagroforestry.org/sea/Products/AFDbases/WD/index.htm>

For dead and downed tree, the main sources of uncertainties are related to the moisture content (defined as the ratio between the weight of water in wood and that of the oven-dry wood) and the rate of decay, which greatly affects its density. A third factor, minerals and extractable substances, has a marked effect only on a limited number of species.

Wood decay is governed by numerous physical and biological factors, and occurs primarily by a loss of mass, reflected as decreasing wood density (Hartley, 1958). The

number of publications on this subject has rapidly grown in the last years, due to the important role that dead wood plays for the forest ecosystem, providing habitats and food sources, a store of carbon, nutrients, and water, as well as influencing geomorphic processes (Woodall et al., 2009). Moreover regional-scale inventories of dead wood are becoming more common: for example Forest Inventory and Analysis (FIA) program of the U.S. Forest Service conducts a national inventory of woody material including coarse woody detritus and dead downed trees (Northern Research Station).

Commonly the used approach is based on the definition of some decay classes that span a spectrum of decay from fresh mortality to nearly complete decay. Decay classes are largely qualitative, and are based on the physical appearance and structural integrity of individual dead wood pieces (Woudenberg et al., 2010). The number of decay classes used varies from study to study, and in general, decay classes developed by different authors are not consistent. Moreover, numerous studies have shown that density variation within each decay class is wide, with the range of wood density within a class varying from one site to another and the density distribution of classes greatly overlapping (Mäkinen et al., 2006; Rajala et al., 2010). Despite the great uncertainties, the values provided by some existing databases could be useful for a first assessment of the log density.

One of the more extensive database is that proposed by Harmon et al. (2008), which uses the common system for the Pacific Northwest based on five decay classes (Sollins, 1982). Starting on this classification, Harmon et al. (2008) developed a set of density reduction factors, defined as the ratio between the decayed density (current mass/fresh volume) of a piece of dead wood compared to its initial density (Miles & Smith, 2009), including estimates of uncertainty, based on a thorough literature review and unpublished data. The proposed database, available on line (Forest Service Department of Agriculture), which considers more than 250 species, could be used for a rough estimate of the density of the sampled LWD (refer to chapter 4.1.1.4) in case of lack of better information.

The main source of uncertainties in the evaluation of wood density is related to its moisture content M_c , defined as the ratio between the mass of water in wood M_{water} , and the mass of the oven-dry piece of wood M_{wood} :

$$M_c = \frac{M_{water}}{M_{wood}} \quad (6-8)$$

Actually wood is a heterogeneous, hygroscopic, anisotropic fibrous material: liquid water (free water) or water vapour can exist in cell lumens and cavities, and can be held chemically (bound water) within cell walls. Green wood is often defined as freshly sawn wood in which the cell walls are completely saturated with water.

The moisture content is a function of relative humidity and temperature of the surrounding air. To reduce confusion introduced by the variable of moisture content, the density of wood usually is calculated on the oven-dry weight and the volume at some specified moisture content. Commonly used bases are oven-dry weight and

volume at: (i) green, (ii) oven-dry, and (iii) 12% moisture content. Oven-dry weight and green volume are often used in databases to characterize density of species, which is referred to a basic specific gravity G_b , defined as the dry-fresh density of wood ρ_{kT} relative to the density of water at 4.4°C (1000 kg/m³). It has to be noticed that volume of fresh wood is greater than the volume as dry because of the swelling phenomenon. So the dry density of wood is always greater than its dry-fresh density ρ_{kT} .

Moisture content is strictly related to the relative humidity h and temperature of the surrounding air. The equilibrium moisture content M_{eq} could be calculated for practical purpose by the empirical equations proposed by Simpson (1973), which could be applied to wood of many species.

$$M_{eq} = \frac{18}{W_o} \cdot \left[\frac{Kh}{1 - Kh} + \frac{K_1Kh + 2K_1K_2K^2h^2}{1 + K_1Kh + K_1K_2K^2h^2} \right] \quad (6-9)$$

where, for temperature T in Celsius:

$$W_o = 349 + 1.29T + 0.0135T^2 \quad (6-10)$$

$$K = 0.805 + 0.000736T - 0.00000273T^2 \quad (6-11)$$

$$K_1 = 6.27 - 0.00938T - 0.000303T^2 \quad (6-12)$$

$$K_2 = 1.91 + 0.0407T - 0.000293T^2 \quad (6-13)$$

Conceptually, the moisture content at which only the cell walls are completely saturated (all bound water) but no water exists in cell lumens is called the fibre saturation point: the specific gravity of wood based on oven-dry weight does not change at moisture content values above the approximate fibre saturation point because the volume does not change. The fibre saturation point of wood averages about 30% moisture content, but in individual species and individual pieces of wood it can vary by several percentage points from this value.

The density values of the log at a given moisture M_c can be evaluated by (Simpson & TenWolde, 1999):

$$\rho_{log} = 1000 \cdot G_M \cdot (1 + M_c) \quad (6-14)$$

where G_M is the specific gravity based on volume at moisture content M_c , which could be calculated by:

$$G_M = \begin{cases} \frac{G_b}{1 - 0.265 \cdot G_b \cdot \left(\frac{0.3 - M_c}{0.3}\right)} & \text{for } M_c < 0.3 \\ G_b & \text{for } M_c \geq 0.3 \end{cases} \quad (6-15)$$

Eq. 6-15 adjusts for average shrinkage and swelling that occurs below 30% moisture content and affects the volume of wood.

Maximum moisture content for any basic specific gravity can be calculated from:

$$M_{max} = 100 \cdot \frac{(1.54 - G_b)}{1.54 \cdot G_b} \quad (6-16)$$

Contact with liquid water can induce rapid changes in the moisture content of wood, in contrast to the slow changes that occur due to water vapour sorption. Absorption of liquid water may continue until the maximum moisture content is reached. The mechanism of water absorption is called capillary action or wicking.

The rate of liquid water absorption in wood depends on several factors, mainly by the species of wood. The water-absorption patterns of the three wood genotypes are presented in Figure 6-2, showing the characteristic moisture absorption behaviour of wood: the wood samples exhibited an initial high rate of moisture sorption followed by slower absorption in the later stages, the relaxation phase (Kumar & Flynn, 2006). Moreover the rate of absorption is most rapid in the longitudinal direction (that is, when the transverse section or end grain is exposed to water).

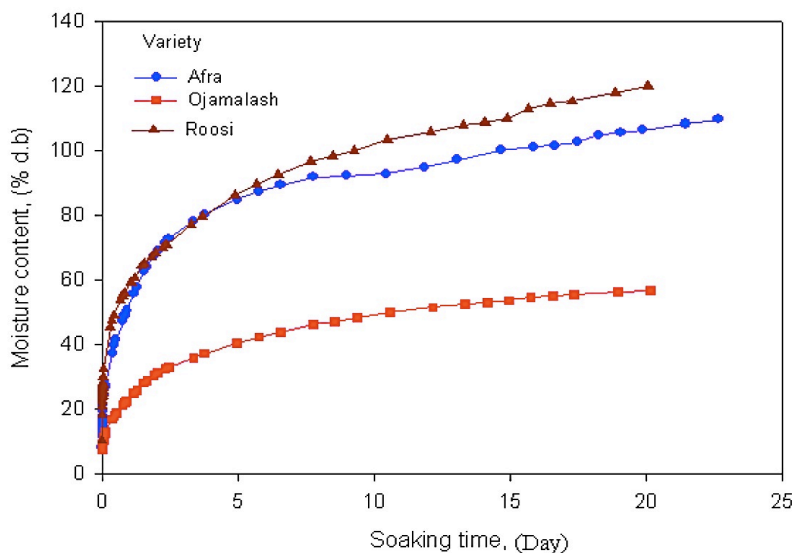


Figure 6-2: water absorption curves during soaking of wood samples in plain water (Khazaei, 2008).

The time evolution of the mass of water absorbed per unit area of specimen surface m_{water} is usually modelled by the following equation (Krus & Künzel, 1993), normally providing a good agreement with experimental data:

$$m_{water} = A_w \cdot \sqrt{t} \quad (6-17)$$

Measured values of the water absorption coefficient A_w for softwoods are in the range 10–16 g m⁻² s^{-1/2} in the longitudinal direction and 1.0–7.0 g m⁻² s^{-1/2} in the transverse directions (Kumaran, 1999). These values could be used in a first attempt to evaluate the time requested to reach the maximum moisture content.

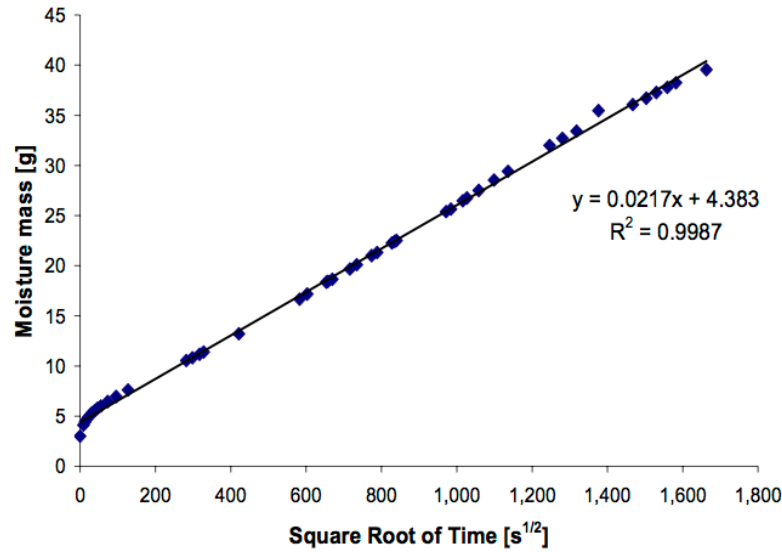


Figure 6-3: cumulative mass vs. square root of time for a softwood sample and the relative linear regression curve (Candanedo & Derome, 2005).

6.2.1 Centre of gravity estimate

Wood is an anisotropic fibrous tissue with a moisture content that could be different throughout its volume. Despite this inhomogeneity could affect the position of its mass centre this aspect could be reasonably neglected, assuming the mass centre of the log corresponding to the barycentre of the cylinder approximating the log volume.

6.3 DRAG FORCE ON PARTIALLY SUBMERGED LOG: ANALOGY TO THE FLOW AROUND A PIER

In fluid dynamics, drag force commonly refers to the resultant of the forces acting opposite to the relative motion of any object moving with respect to the surrounding fluid. For the considered cases (see Figure 6-1) the steady state stream-wise force component acting on submerged bodies (drag force F_D) can be expressed as:

$$F_D = \frac{U^2}{2} \rho_w C_D \cdot (A_{sub} \cos \theta + d_w L_{log} \sin \theta) \quad (6-18)$$

where C_D is the drag coefficient, ρ_w is the fluid density, $A_{sub} \cos \theta + d_w L_{log} \sin \theta$ is the projected area of the submerged part of the body onto a plane perpendicular to the flow direction, and U is the mean flow velocity. In this work the undisturbed flow conditions immediately downstream of the obstacle are used to evaluate A_{sub} and U , as the flow causing LWD entrainment is expected to be subcritical.

As stated in all the works found in literature related to the study of incipient motion of LWD, the use of a correct value of the drag coefficient C_D is necessary to obtain reliable entrainment predictions. The dimensionless drag coefficient C_D depends on body geometry and dimensionless parameters describing the dynamical behaviour of the flow around the obstacle.

In an open channel, the drag force acting on deeply submerged bodies is the sum of two effects:

- The *skin friction*, which is due to the shear stress on the surface of the object;
- The *wake resistance*, which is due to the pressure difference between the upstream and the downstream surface of the object, usually noted as a *form drag* component.

In case of deeply submerged cylinders of varying slenderness L_{log}/D_{log} the drag coefficient is solely dependent on the cylinder Reynolds number Re_D , and decrease with decreasing slenderness and orientation θ (Prandtl & Tietjens, 1934; Rouse, 1961), while in case of flow with free surface effects, the drag coefficient can be greater as a consequence of additional induced drag created by the interaction between the wake behind the object, the water surface and the roughness of the streambed (Hygelund & Manga, 2003). The drag increase observed at lower submergence values could be attributed to wave drag (Wallerstein et al., 2002): the standing surface waves modify the pressure distribution on the log, so that wave drag can be regarded as an added form of resistance (Shields & Gippel, 1995). In these cases the wake resistance may be further ascribed to two components:

- *Form drag*, which is due to the difference between the higher pressure on the upstream side of the body (where the flow impacts and where the depth is greater) and the lower pressure in the wake or separation zone on the downstream side of the obstacle;
- *Wave drag*, which is due to the force required to form the standing surface waves around the obstacle.

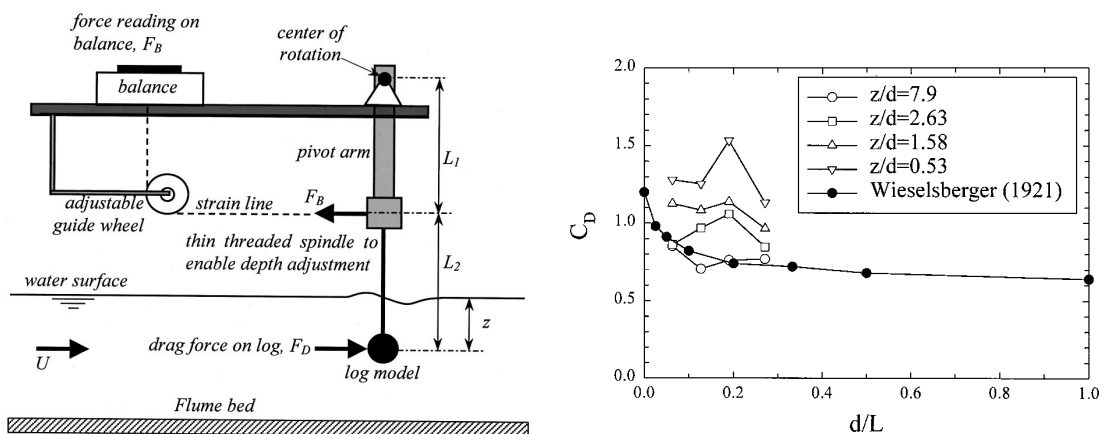


Figure 6-4: variation of drag coefficient with slenderness for cylindrical log with different submergence ratio (Source: Gippel et al., 1996).

To obtain a reliable prediction, other dimensionless parameters have to be considered. For a single smooth faced object in free surface flow, the drag coefficient can be expressed in terms of a functional equation (Carling et al., 2002), as provided by dimensional analysis of the main variables affecting the flow:

$$C_D = f \left(Re_w, Fr_w, \frac{d_w}{D_{log}}, \frac{D_{log}}{L_{log}}, B_r, P, K_s \right) \quad (6-19)$$

where the shape factor K_s has been added in order to consider object different from a simple cube, while the velocity profile parameter P accounts for non-logarithmic profiles effects, which could arise, for example, in case of shallow water. Other than selecting an appropriate reference level in the flow depth for the mean velocity U , the effect of non-logarithmic velocity profile usually can be neglected (Flammer et al., 1970). Re_w and Fr_w are respectively the Reynolds number and Froude number of the undisturbed flow, B_r is the blockage ratio of the LWD, D_{log}/L_{log} is the aspect ratio of the submerged log, and d_w/D_{log} is the submergence ratio.

The blockage ratio (B_r) is defined as the ratio between the projected area of the log normal to the main flow direction and the channel cross-sectional area. Referring to Figure 6-1, it is possible to evaluate the blockage ratio as:

$$B_r = \frac{A_{sub} \cdot \cos(\theta) + L_{log} \cdot d_w \cdot \sin(\theta)}{C_w d_w} \quad (6-20)$$

where C_w is the width of the channel. In case of a cylindrical log, B_r will be a function of d_w because A_{sub} changes with the instantaneous water depth.

In literature is usual to indicate the increment of C_D , due to wave drag, using an apparent drag coefficient C_D^{app} , in order to distinguish it from the classical values for the case of circular cylinders in infinitely large volumes of fluid, such as those that can be found in most fluid mechanics texts (Batchelor, 1967). Shields and Gippel (1995) provided a formula to calculate the variation of the drag coefficient depending on Br .

$$C_D^{app} \sim \frac{C_D}{(1 - B_r)^2} \quad (6-21)$$

C_D is the drag coefficient for the cylinder in an infinitely large volume of fluid, and for $10^3 < Re < 10^5$, C_D has been experimentally determined to be approximately between 1.0 and 1.2 (Batchelor, 1967). However the measured data showed a large scatter from the provided formula, similar, for low blockage, to the data presented by Hygelund and Manga (2003), which indeed for a range of Br from 0.3 to 0.7 did not found any significant correlation between C_D^{app} and B_r (Figure 6-5).

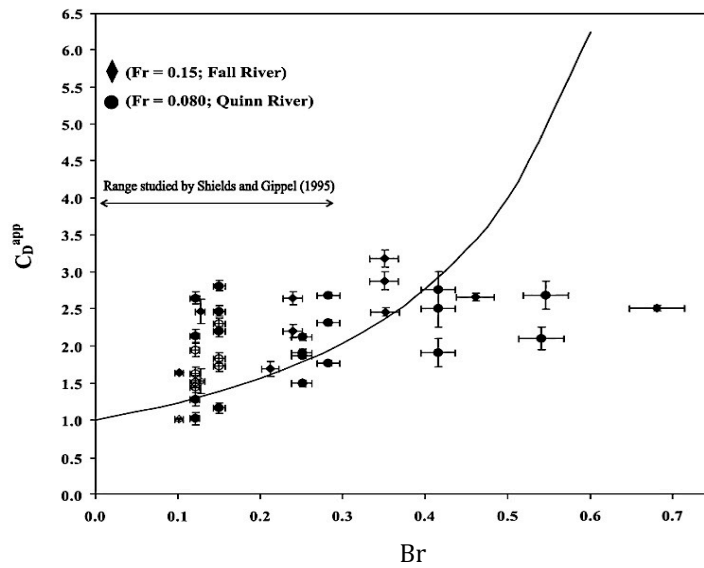


Figure 6-5: relationship between C_D^{app} and blockage ratio Br referring to Hyghelund and Manga (2003).

Drag coefficient appears to be less influenced by the slenderness ratio of the log L/d , where L is the log length and d the log diameter (Gippel et al., 1996), much more by the orientation to the flow direction.

The reduction of the drag coefficient for low angle of orientation could partly explaining the experimental evidence that LWD are normally not randomly oriented to the flow direction (Gippel et al., 1996), preferring the low values (between 0° and 35°): it is probable that debris are rotated by the flow in most lowland rivers.

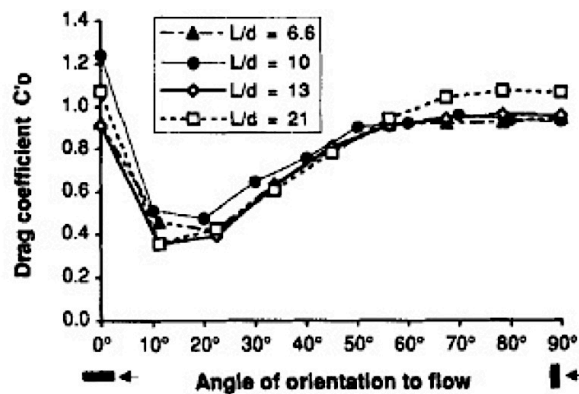


Figure 6-6: Variation of drag coefficient with angle of orientation for cylindrical log of various lengths (L) and diameter (d). (Source: Gippel et al., 1996).

Exact determination of wave drag for a cylinder is not straightforward because it requires separating the three main component of the drag force. Naval architects have developed elaborate combinations of model basin tests and boundary-layer models to evaluate the wave drag of ships and submerged vehicles (Weinblum et al., 1950; Wigley, 1953), which are not easily applicable to the considered setting.

The overall drag force, incorporating all the physical processes on the object, can be indeed simply measured experimentally considering the momentum loss in a flow.

When water in a river or canal flow past an obstacle such as a bridge pier, piles, woody debris, the water level could be different upstream and downstream of the obstacle. The water level rise Δy , caused by the presence of bridge piers is indicated as backwater.

Many researchers have used the concept of a momentum balance to analyse the backwater effects due to objects in an open channel flow. They have obtained relationships to account for the resistance of objects in terms of a drag coefficient as a way to calculating the resulting backwater effect (Ranga Raju et al., 1983; Shields & Gippel, 1995; Fenton, 2003). Comparing all the investigations it results that there are almost no energy losses at the front face of an obstacle, but because of the sudden local deviation of the flow, as the water flows downstream, interacting flows and turbulent flow processes cause energy losses for some distance. These losses are distributed and are difficult to measure or calculate, as they take place in boundary layers, shear layers, separation zones, vortices, and subsequent turbulent decay in the wake. For this reason the problem can be quantified more easily using momentum than energy as the underlying principle. Hence a relationship between the drag force acting on the obstacle and the magnitude of backwater Δy could be established applying a theoretical approach based on the momentum equation (Charbeneau & Holley, 2001). It is necessary to introduce two sections where momentum will be evaluated (Figure 6-7). Section 1 is at a short distance upstream of the obstacle, just behind the local stagnation mound, where the free surface is sensibly horizontal across the channel (start of the contraction zone). Section 3 is further downstream, where the effects of the obstacle, in the form of a region of velocity defect in the cross section, have already dissipated (end of the expansion zone).

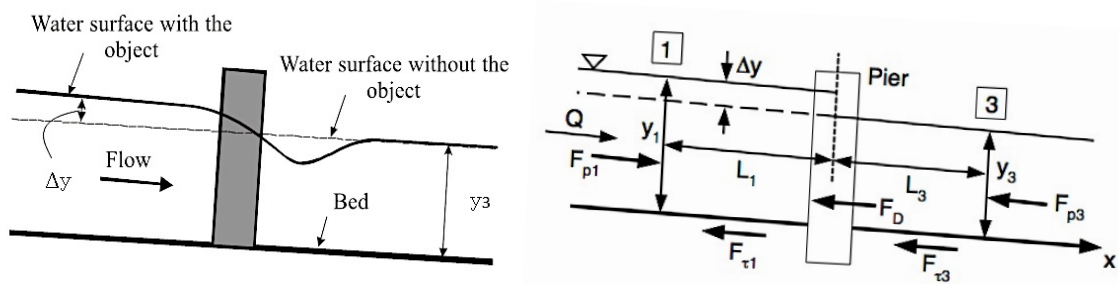


Figure 6-7: water surface modification with obstacle and idealized scheme for the application of the momentum balance (adapted from Chaberneau and Holley, 2001).

Referring to a uniform flow, the one-dimensional momentum equation for the control volume (from cross section 1 to 3) in the x direction (Figure 6-7) gives:

$$F_{p1} - F_{p3} - F_{\tau 1} - F_{\tau 3} + W_{x1} + W_{x3} - F_D = \rho_w Q(U_3 - U_1) \quad (6-22)$$

where F_p is the pressure force, F_τ the boundary shear force, W_x is the component in the flow direction of the weight of water, F_D the drag force, Q the flow rate and U_x the mean flow velocity in the cross section x, and ρ_w is the density of the water.

For a rectangular channel of width C_w , the net pressure force could be evaluated considering a hydrostatic pressure distribution at the inlet and outlet section of the control volume:

$$F_p = F_{p1} - F_{p3} = \gamma_w \frac{y_1}{2} C_w - \gamma_w \frac{y_3}{2} C_w = \gamma_w y_3^2 C_w \left[\frac{\Delta y}{y_3} + \frac{1}{2} \left(\frac{\Delta y}{y_3} \right)^2 \right] \quad (6-23)$$

In which the backwater $\Delta y = y_1 - y_3$ has been introduced.

The boundary upstream and downstream shear stress could be evaluated as:

$$\tau_{0x} = \frac{f}{8} \rho_w U_x^2 \quad (6-24)$$

where f is the Darcy-Weisbach friction factor.

In order to evaluate the total shear force acting on the control volume, some simplifying hypotheses have to be set: a first attempt could be neglect the friction force acting on the obstacle, assuming the log smoother than the river channel. Under this hypothesis, considering just the wetted perimeter of the river channel inside the control volume, the total shear stress reduces to:

$$F_\tau = F_{\tau1} + F_{\tau3} = \frac{f}{8} \rho_w U_x^2 C_w (L_1 + L_3) \Phi_\tau \quad (6-25)$$

$$\Phi_\tau = \left(\frac{1}{1 + \frac{\Delta y}{y_3}} \right)^2 \left[1 + 2 \frac{y_3}{C_w} \left(1 + \frac{\Delta y}{y_3} \right) \right] \frac{L_1}{L_1 + L_3} + \left(1 + 2 \frac{y_3}{C_w} \right) \frac{L_3}{L_1 + L_3} \quad (6-26)$$

Assuming constant water depths upstream and downstream (Figure 6-7) the weight of water in stream wise direction becomes:

$$W_x = W_{x1} + W_{x3} = \gamma_w y_3 C_w S_b \left[\left(1 + \frac{\Delta y}{y_3} \right) L_1 + L_3 \right] \quad (6-27)$$

where $S_b = \tan(\alpha)$ is the channel bed slope for the idealized representation (Figure 6-7), and γ_w is the specific weight of water.

All the equations showed can be combined to give the relationship between the drag force and the backwater:

$$F_D = \gamma_w y_3^2 C_w \left[\frac{\Delta y}{y_3} + \frac{1}{2} \left(\frac{\Delta y}{y_3} \right)^2 \right] - \frac{f}{8} \rho_w U_x^2 C_w (L_1 + L_3) \Phi_\tau + \gamma_w y_3 C_w S_b \left[\left(1 + \frac{\Delta y}{y_3} \right) L_1 + L_3 \right] - \rho_w U_x^2 y_3 C_w \left(\frac{\frac{\Delta y}{y_3}}{1 + \frac{\Delta y}{y_3}} \right) \quad (6-28)$$

Considering the expression of the drag force, Eq. 6-18, it is possible to obtain the quantitative relationship between the drag coefficient and the backwater rise:

$$C_D = \frac{1}{O_r F_{r3}^2} \left[2 \frac{\Delta y}{y_3} + \left(\frac{\Delta y}{y_3} \right)^2 \right] - \frac{f}{16} \frac{L}{y_3} \frac{\Phi_\tau}{O_r} + \frac{2}{O_r F_{r3}^2} \frac{L}{y_3} S_b \left[\left(1 + \frac{\Delta y}{y_3} \right) \frac{L_1}{L} + \frac{L_3}{L} \right] - \frac{2}{O_r} \left(\frac{\frac{\Delta y}{y_3}}{1 + \frac{\Delta y}{y_3}} \right) \quad (6-29)$$

in which F_{r3} represent the Froude number at the cross section 3 and O_r is the opening ratio, simply related to the blockage ratio by the following relation:

$$O_r = 1 - B_r \quad (6-30)$$

For very low gradients, like the typical ones of low land rivers, considering a short distance between the two cross sections, so that friction force could be considered negligible, Eq. 6-29 becomes:

$$C_D = \frac{1}{O_r F_{r3}^2} \left[2 \frac{\Delta y}{y_3} + \left(\frac{\Delta y}{y_3} \right)^2 \right] - \frac{2}{O_r} \left(\frac{\frac{\Delta y}{y_3}}{1 + \frac{\Delta y}{y_3}} \right) \quad (6-31)$$

An estimate of the effective distances L_1 and L_3 , could be obtained considering the typical values of the contraction and expansion reach lengths for bridge piers, respectively L_c and L_e (Brunner, 2010), as the presence of the resting log in the channel has conceptually the same effect on the flow. These distances will vary depending upon the degree of constriction, the shape of the constriction, the magnitude of the flow, and the velocity of the flow.

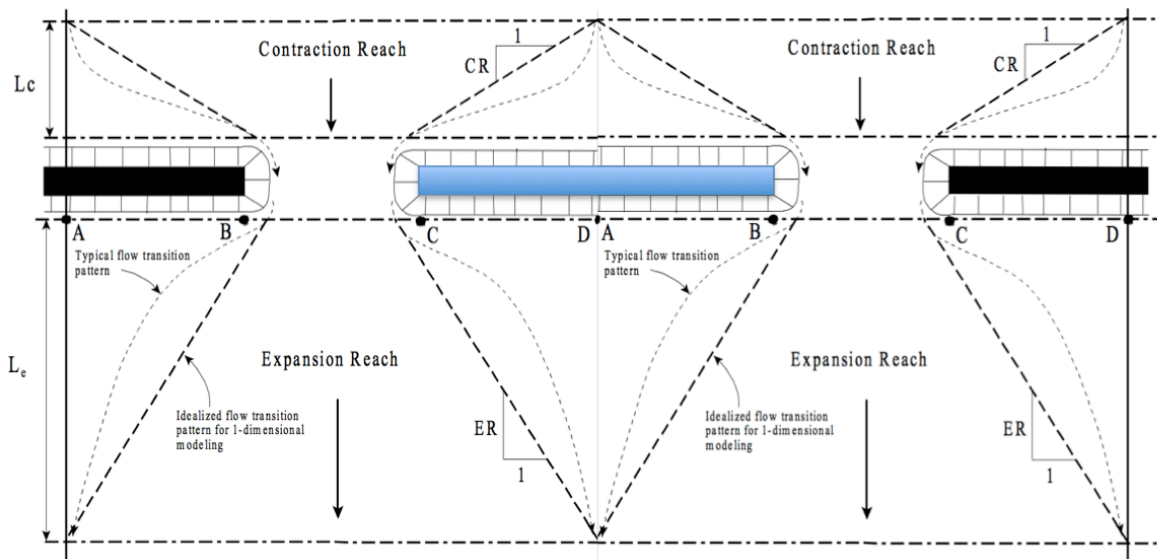


Figure 6-8: cross section location at a bridge (adapted from Brunner, 2010).

According to the Hydrologic Engineering Center of the US Army Corps of Engineers, the traditional 4:1 rule of thumb for the expansion ratio (ER) leads to a consistent over prediction of the energy losses in the expansion reach: in most cases expansion ratio belongs between 1:1 and 2:1. Referring to Figure 6-7 the expansion ratio could be obtained from the following equation (rearranged to the considered case from Brunner 2010):

$$ER = 2 \cdot \frac{L_e}{L_{obs}} = 0.489 + 0.608 \cdot \left(\frac{Fr_2}{Fr_3} \right) \quad (6-32)$$

being: L_{obs} the length of obstruction caused by the log in the crosswise direction, Fr_2 and Fr_3 the Froude numbers respectively at section 2 (the most constricted section) and at section 3 (downstream of the obstruction). Taking into account the cylindrical shape of the log, the average length of obstruction caused by the log could be evaluated according to the following equation (refer to Figure 6-7):

$$L_{obs} = \frac{A_{sub}}{d_w} \cdot \cos(\theta) + L_{log} \cdot \sin(\theta) \quad (6-33)$$

For the contraction ratio CR instead the following equation could be used (rearranged to the case considered from Hunt and Brunner, 1995):

$$CR = 2 \cdot \frac{L_c}{L_{obs}} = 2.07 - 0.33 \cdot \left(\frac{Fr_2}{Fr_3} \right) \quad (6-34)$$

Known L_e and L_c it is easy to obtain L_1 and analogously L_3 .

$$L_1 = L_c + 0.5 \cdot L_{eq} \quad (6-35)$$

$$L_3 = L_e + 0.5 \cdot L_{eq} \quad (6-36)$$

in which L_{eq} is the length of the obstacle in the stream-wise direction:

$$L_{eq} = \frac{A_{sub}}{d_w} \cdot \sin(\theta) + L_{log} \cdot \cos(\theta) \quad (6-37)$$

In conclusion it is possible to correlate the drag force acting on the obstacle to the increase of the water level in the channel, due to the presence of the obstacle, knowing the downstream flow conditions, which in case of subcritical flow correspond to the undisturbed flow conditions, and the geometry of the object. This is a significant result because it is possible to obtain a reliable value of the C_D using experimental relationship relating backwater to the geometry of the obstacle.

In the next section are reported the main studies related specifically to backwater prediction for bridge piers, which could be adapted to LWD entrainment.

6.3.1 Backwater prediction

The amount of the water level increase upstream of an obstruction depends mainly upon its geometric shape, its position in the stream, the quantity of flow, and the percentage of channel contraction. Due to its importance, the interaction between bridge piers and channel flow has been investigated in the past. Bridge piers and partially submerged resting logs could be considered similar in terms of their hydraulic behaviour, so that the backwater effect due to a bridge pier may be used to calculate the backwater effect of a submerged LWD.

For subcritical flow Flammer and al. (1970) have shown that the opening ratio must exceed 20 to prevent flow blocking between obstacle and sidewall, affecting the backwater curve and hence the drag coefficient. So considering the typical dimensions of LWD, typically over the meter, it seems reasonable taking into account the backwater effect for entrainment assessment. Referring to more detailed literature the analysis of the state of the art related to the backwater correlations, in this chapter are summarized the principal correlations that could be used to predict the backwater rise due to the presence of the LWD in the stream flow.

In 1934 Yarnell conducted a large number of tests, obtaining the most widely used empirical relationship for calculating the increase in the water level due to bridge piers:

$$\frac{\Delta y}{y_3} = K_s \cdot (K_s + 5 \cdot Fr_3^2 - 0.6) \cdot (B_r + 15 \cdot B_r^4) \cdot Fr_3^2 \quad (6-38)$$

where Δy is the backwater generated by the bridge pier, y_3 is the original (i.e., undisturbed) local flow depth, Fr_3 is the corresponding Froude number at section 3, at the downstream side of piers (Figure 6-7), B_r is the blockage ratio of the flow, and K_s is a shape coefficient reflecting the pier shape ($K_s = 1.25$ in case of square nose and tail piers).

Operating the same flow classification used in case of bridge piers, for large woody debris entrainment, the flow can be divided into two classes:

- Class A Low flow: the water flow through the bridge is completely subcritical;
- Class B Low flow: the flow is choked within the LWD obstructing channel and an hydraulic jump takes place downstream;

The above equation is applicable for class A flow with: rectangular and trapezoidal section, blockage ratio between 0.117 and 0.5, skew angle θ less than 10 degrees, and pier length-width ratio 4:1. Yarnell stated that the backwater (Δy) increases by 5% and 10% for the ratios 7:1 and 13:1, respectively.

Despite there was a wide scatter in the results, Yarnell's equation has found wide acceptance, probably for the large number of experiments that were performed: he

obtained his empirical relationship, which is still used in open channel flow packages such as HEC-RAS, on the basis of 2600 experiments of various pier shapes.

Outside of the range of applicability some other relationship could be applied: for ratio of pier length to pier width ranging between 5:1 and 30:1 it is possible to use the relationship found by Kassem Salah El-Alfy (2009) for rectangular pier, which could be applied in case of blockage ratio between 0.1 and 0.58 and Froude numbers between 0.2 and 0.62:

$$\frac{\Delta y}{y_3} = 0.256 - 0.367 \cdot O_r + 0.389 \cdot Fr_3 \quad (6-39)$$

This relationship, obtained by a regression of experimental data, could be applied for Froude ranging between 0.2 and 0.62 and slenderness ratio between 5:1 and 30:1. For these reasons it seems to be more appropriate for LWD in lowland rivers.

For class B low flow, other relationships are necessary: contracting flows beyond a certain limit results in a phenomenon called choking. Under choking conditions, flows pass through critical depths in the contracted channel reach (section 2).

Two different choked flows could take place in subcritical channels. In the first case, the water surface profile passes through only the critical depth of the contraction; whereas in the second case it passes through both the critical depth of the contraction and the critical depth of the non-contracted downstream channel. Both types of flow are subjected to the same analysis since in both cases the flow passes through critical depth. Downstream from the contraction, the water surface returns to normal flow provided that a long reach of uniform channel exists.

As stated by Henderson (1966) the limiting value of the blockage ratio Br for distinguishing between class A (unchoked flow) and class B (choked flow) was used by Yarnell (1934) employing the energy principle, according to the following assumptions $E_1 = E_2$ and $M_2 = M_3$. Under these hypotheses when the value of Froude number at section 2 equals unity ($Fr_2 = 1$), the flow at section 2 is critical and the corresponding value of Froude number at section 3 (Fr_{3c}) could be evaluated by:

$$B_r^2 = \frac{27 \cdot r^3 \cdot Fr_{3c}^2}{(2 + Fr_{3c}^2)^3} \quad (6-40)$$

in which r is the residual ratio of energy between sections 2 and 3 ($r \approx 0.9-1.0$). When the downstream value of Froude number under normal flow conditions, Fr_3 , is less than the critical value of Froude number Fr_{3c} , then the flow between piers is subcritical (class-A or un-choked flow), and vice versa, when the downstream value of Froude number under normal conditions, Fr_3 , is greater than the critical value of Froude number Fr_{3c} the flow in the contracted region is supercritical (class-B or choked flow). In this case experimental data seems to indicate that the backwater rise is not affected by the opening ratio, depending mainly from the ratio Fr_3/Fr_{3c} as shown in Figure 6-9: a new relationship have to be considered in order to evaluate the

backwater rise. Literature review suggests to use the approach proposed by Molinas and Wu (2001).

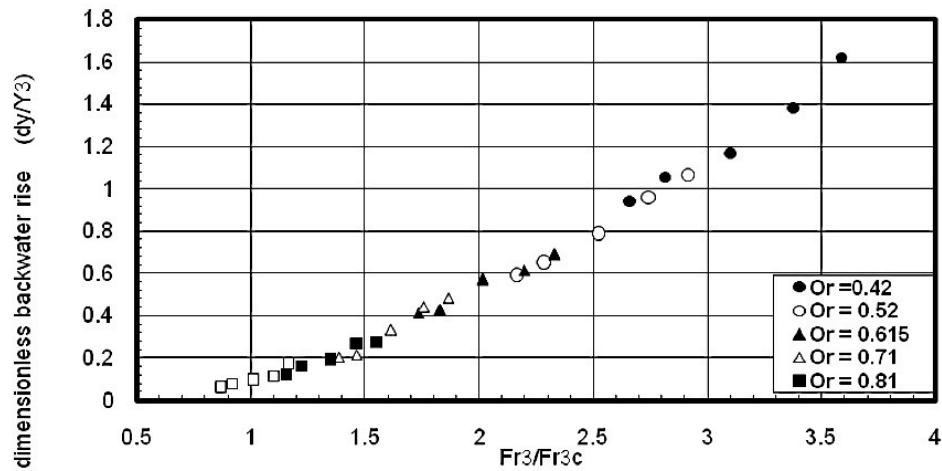


Figure 6-9: backwater in case of supercritical flow between piers (from Kassem Salah El-Alfy 2006).

Head losses through contractions are smaller than the corresponding losses through expansions (Chow, 1959; Henderson, 1966) and in most cases can be neglected. However, for choked flows head losses through contractions are significant and not negligible. Yarnell’s equation, which neglects energy losses, fails to predict limited opening ratios: the relationship between the upstream Froude number (F_1), and the opening ratio σ (O_r) under threshold choking conditions for abrupt contractions is shown in Figure 6-10.

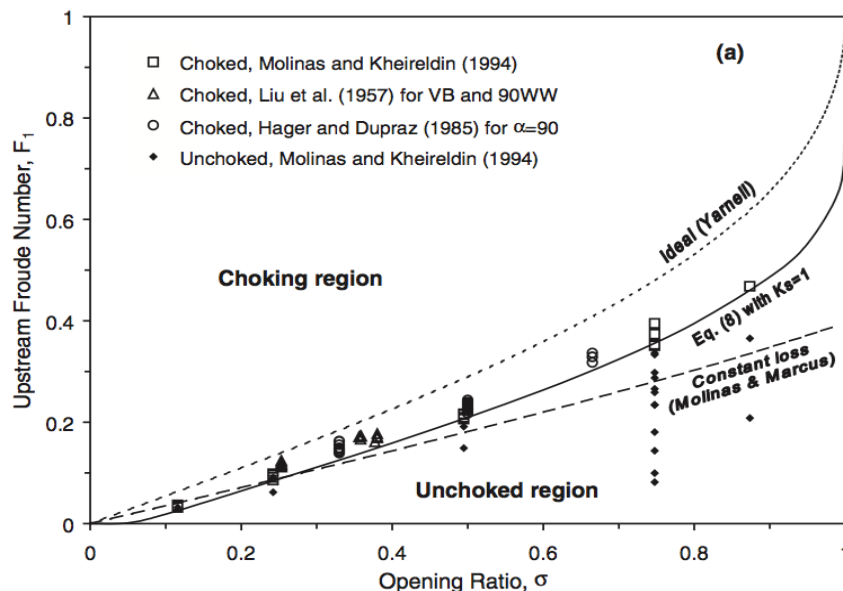


Figure 6-10: threshold conditions for choking in subcritical channels with abrupt contractions (from Molinas et Wu 2005)

Moreover under choking conditions the upstream flow is independent of downstream conditions. Therefore is not appropriate relating the backwater at

section 1 to quantities evaluated at section 3: according Molinas et al. (2005) the threshold conditions for choking can be derived from the following equation:

$$O_r = \left(\frac{3 + k_{eT}}{C_c^{\frac{2}{3}}} \right)^{\frac{3}{2}} \frac{Fr_1}{(2 + Fr_1^2)^{\frac{3}{2}}} \quad (6-41)$$

in which O_r is the opening ratio, k_{eT} is the energy loss coefficient for threshold choking conditions and C_c is the contraction coefficient that takes into account the contraction of the flow due to the separation (in first approximation it could be considered close to the unity), as shown in Figure 6-11.

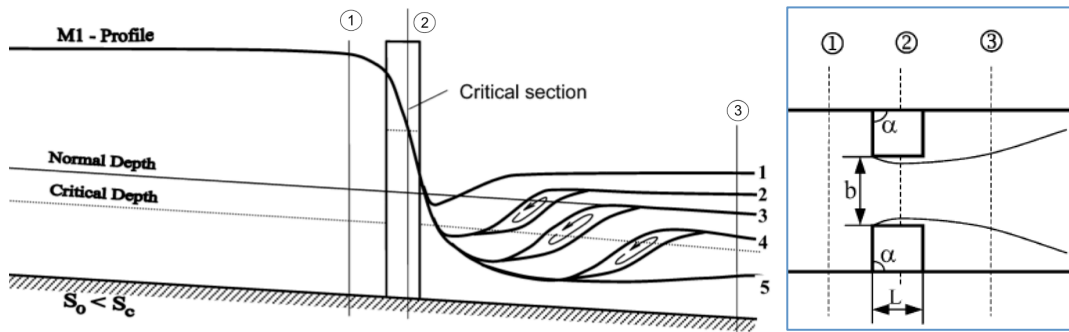


Figure 6-11: water surface profiles for subcritical flow through lateral constrictions under choking conditions, showing the effects of downstream submergence (source: Molinas and Wu 2005).

The energy loss coefficient k_{eT} could be obtained considering the following formula obtained from a nonlinear regression analysis of the experimental data of Molinas:

$$k_{eT} = 0.432(K_L + K_\varphi) \cdot K_S \cdot (1 + O_r)^{0.25} \cdot \exp\left(\frac{0.18}{O_r}\right) \quad (6-42)$$

in which K , K_L , and K_φ are coefficients accounting for the effects of the encroachment shape, length L_{obs} of the contraction zone, and inlet angle φ (defined as the angle between the mean stream and the flow driving surface), on the energy loss coefficient. Theoretical values for these coefficients are unachievable due to their complexity, so they were determined by Molinas, using experimental data.

$$K_L = 0.625 \cdot (1 - e^{-L^*}) \quad (6-43)$$

$$K_\varphi = (\varphi^*)^{0.87} \quad (6-44)$$

where $\varphi^* = \varphi/90^\circ$ is the relative inlet angle and $L^* = L_{obs}/C_w$ is the contraction length relative to the channel width C_w , $K_S = 1.0$ for sharp corner and $K_S = 0.4$ for rounded corner conditions. For other encroachment structure shapes K_S should vary between 0.40 and 1.0 depending on the severity of the corner.

Molinas showed that the general discharge equation for choked flows through a lateral contraction in subcritical flow could be expressed by the following relationships:

$$Fr_1^* = C_d^* \cdot O_r \quad (6-45)$$

$$Fr_1^* = \frac{Fr_1}{(2 + Fr_1^2)^{3/2}} \quad (6-46)$$

$$C_d^* = \frac{C_c}{(3 + k_{eT})^{3/2}} \quad (6-47)$$

Therefore the proposed discharge equation can be used to predict the water depth upstream of contractions (Q given, y_1 unknown). In this case L^* , φ^* and K_S are determined first from the given channel and contraction geometry. Then, K_L , K_φ and k_{eT} are computed using Eqs. 6-42, 6-43 and 6-44 respectively. Next, C_d^* is computed using Eq. 6-47, from which Fr_1^* is calculated according to Eq. 6-45. Finally Fr_1 is solved from Eq. 6-46, and the upstream depth for the given discharge is obtained from the definition of Fr_1 . For a rectangular section, indicating with C_w the width of the channel, the water depth upstream of the obstacle can be thus evaluated according to:

$$y_1 = \sqrt[3]{\frac{Q^2}{g \cdot C_w^2 \cdot Fr_1^2}} \quad (6-48)$$

6.3.2 Pitching Moment estimation

As stated in chapter 6.3, the drag force acting on a partially submerged obstacle consists of three main components: skin friction, form drag and wave drag. In order to obtain a rough estimation of the pitching moment due to the drag force, some simplifying hypotheses have to be contemplated. Commonly a good approximation could be considering the skin friction negligible. Moreover in first approximation it might be supposed that the contribution of the wave drag does not change too much the lever arm of the overall drag force, which becomes, in this way, a function of the pressure upstream and downstream of the obstacle, which is strongly correlated to backwater, and to the velocity profile of the oncoming stream. In other terms, in first analysis, it is considered that the form drag and the wave drag have different magnitude, but the same line of action. This is a strong hypothesis that has to be investigated more in depth, but this issue is out of the aim of the thesis.

The lever arm of the drag force could be roughly estimated considering the pressure distribution along the vertical direction, in the front and rear part of the obstacle, that could be evaluated considering a stagnation condition on the two surfaces. Figure 6-12 presents the pressure coefficient distribution measured along the

centreline of a cylindrical pier (Tsutsui, 2008). The inside and outside from the outline of the pier indicate negative and positive pressure areas, respectively. The upper and lower side from the ground and the scour level indicate negative and positive pressure areas, respectively.

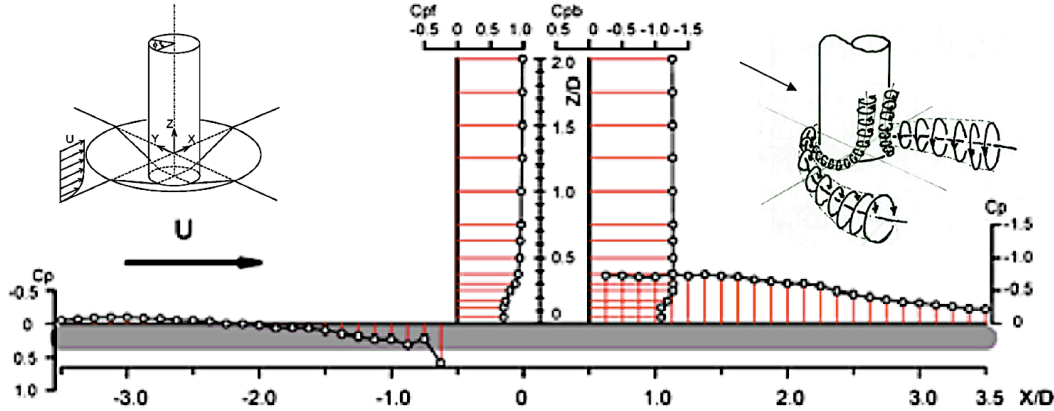


Figure 6-12: pressure coefficient distribution of a cylindrical pier surface from Tsutsui, 2008.

This supports that the hypothesis of a stagnation pressure on the front and rear surface of the log can be realistic, for the two orientations considered ($\theta = 0^\circ$ and 90°):

$$p_o = p + \frac{\rho u^2}{2} \tag{6-49}$$

Referring to Figure 6-1 it is possible to calculate the lever arm of the drag force. Neglecting the dynamic component of the forces acting downstream, due to the separation, and considering a stagnation condition, supposing that flow does not alter significantly the hydrostatic pressure distribution over the entire submerged frontal surface:

$$y_D = \frac{1}{F_D} \int_0^{d_{up}} \left[\gamma_w (d_{up} - z) + \rho_w \frac{u(y)^2}{2} \right] c(y, D_{log}) \cdot y \cdot dy - \frac{1}{F_D} \int_0^{d_{down}} \gamma_w (d_{down} - y) \cdot c(y, D_{log}) \cdot y \cdot dy \tag{6-50}$$

where F_D is the drag force calculated by the backwater estimation, d_{up} and d_{down} are the water depth respectively just upstream and downstream of the obstacle, γ_w is the specific weight of water, ρ_w the density of water, $u(y)$ is the velocity profile, and $c(y, D_{log})$ is the function that represent the width of the obstacle, varying with y .

$$c(y, D_{log}) = \begin{cases} B & \text{for square sections} \\ 2 \cdot \sqrt{D_{log} \cdot y - y^2} & \text{for cilindric sections} \end{cases} \tag{6-51}$$

Considering that the goal is to obtain just an estimate of the lever arm of the drag force, the following simplification is justified: d_{up} and d_{down} could be considered near to y_1 and y_3 (refer to Figure 6-7). For orientation of the log different from 0 or 90° (not considered in this thesis), the hypothesis of a stagnation condition over the entire submerged frontal surface could be not acceptable.

6.3.2.1 Flow velocity profile

In order to obtain a reliable value of the lever arm of the drag force, a realistic flow velocity distribution has to be established. This could not be a simple task considering that the rough bottom surfaces existing in rivers may affect the development of the log-shaped velocity profile, especially in case of shallow flows.

It is well established, both experimentally and from dimensional arguments (Nezu & Rodi, 1986) that the flow velocity distribution is well represented by:

$$\frac{u}{u^*} = \frac{1}{\kappa} \cdot \ln\left(\frac{y}{y_o}\right) \quad (6-52)$$

where u is the time averaged flow velocity at a distance y above the bed, y_o the bed roughness length (distance above the bed where the flow velocity goes to zero), κ the von Karman's constant (approximately 0.41 for clear water), and u^* is the friction velocity, defined as:

$$u^* = \sqrt{\frac{\tau_b}{\rho_w}} \quad (6-53)$$

Where ρ_w the water density and τ_b is the bed shear stress that for steady uniform flow could be expressed as:

$$\tau_b = \rho_w g d_w S_o \quad (6-54)$$

where S_o is the bed slope.

The value of y_o depends on the flow regime. For hydraulically smooth flows, turbulence will be drastically suppressed in an extremely thin layer near the boundary. In this region a linear velocity profile holds (O' Connor, 1995), while for hydraulically rough flows no viscous sub-layer will exist, because the roughness elements will protrude through such layer.

If k_s is the effective roughness height, flow regimen could be obtained considering the Roughness Reynolds number Re^*

$$Re^* = \frac{u^* \cdot k_s}{\nu_w} \quad (6-55)$$

- for $Re^* < 3$ the flow is hydraulically smooth and $y_o = \nu_w / (9u^*)$
- for $Re^* > 70$ the flow is hydraulically rough and $y_o = k_s / 30$

According to Nezu e Nakagawa (1993) the “law of the wall” strictly applies only in a relative thin layer ($y/d_w < 0.2$) near the bed, but it is commonly used as a reasonable approximation throughout most the flow. It is by no means exact considering that wake effects near the free surface can be important (Lyn, 1991). Integrating the flow velocity distribution it is possible to obtain the depth-averaged velocity U :

$$U = \frac{1}{d_w} \int_{y_o}^{d_w} u(y) \cdot dy \quad (6-56)$$

in which the lower limit of integration is not zero to avoid the singularity of the logarithmic law at $y = 0$;

The channel roughness is normally available in terms of the dimensionless manning’s coefficient, which could be related to the roughness height according to the relation:

$$n = \frac{k_s^{\frac{1}{6}}}{8.1 \cdot \sqrt{g}} \quad (6-57)$$

Extensive tables of Manning’s n values for different channel characteristics are given in Chow (1959) and Yen (1991). As previously stated this equation could only be applied to uniform hydraulically rough, fully turbulent flow. For flows with fixed-bed (skin or grain) like in many laboratory experiments, the equivalent roughness height could be obtained starting from the work of Nikuradse (1933), which permit to obtain the dimensionless Darcy-Weisbach friction coefficient f for a pipe with diameter D as a function of the flow Reynolds number Re , and the relative roughness k_s/D .

$$Re^* = \frac{U \cdot D}{\nu_w} \quad (6-58)$$

Brownlie (1981) re-examined the Nikuradse’s data and provided a diagram that could be used for sidewall correction. For open channel flow the pipe diameter have to be replaced by $4R_H$ (hydraulic radius).

In a study of flow resistance associated with rip-rapped surfaces, Maynord (1991) reviewed a number of formulations commonly used to estimate the Darcy-Weisbach friction coefficient and found a power-law equation that could be used for most riprap (i.e. fixed-bed) problems in very wide open-channel flows:

$$\sqrt{\frac{8}{f}} = 6.89 \cdot \left(\frac{d_w}{D_{50}} \right)^{1/6} \quad (6-59)$$

which applies in the range $2.2 < d_w/D_{50} < 23$.

The Darcy-Weisbach friction coefficient and Manning's roughness are related by:

$$\sqrt{\frac{8}{f}} = \frac{d_w^{1/6}}{n \cdot \sqrt{g}} = \frac{U}{\sqrt{g \cdot d_w \cdot S_o}} \quad (6-60)$$

The logarithmic profile approach is often used to describe the mean velocity distribution in boundary layer flows (Monin & Yaglom, 1971). However, in the lower layers of shallow flows over rough surfaces found in rivers, bottom roughness may affect the development of the log-shaped velocity profile. Nikora and Smart (1997) found deviations from the log-law flow in the roughness layer that is a 3D inner layer of the flow in gravel-bed rivers.

In such flows, a velocity inflection has been observed, resulting in so-called s-shaped profiles (Marchand et al., 1984; Baiamonte et al., 1995). In most cases, these deviations are due to the wake effect resulting from the presence of bed forms, gravel clusters or large-scale roughness elements that deform the mean velocity profile as observed by Nelson et al. (1993) and Buffin-Bélanger and Roy (1998). Therefore their occurrence is local, and could be neglected in the context of this work.

6.4 LIFT FORCE ON PARTIALLY SUBMERGED LOG: ANALOGY TO SHIP IN SHALLOW WATER

In order to obtain a reliable value of the Lift force acting on a partially submerged log, some aspects have to be taken into account. Even in this case the references have to be pursued in the naval field. Actually, most naval architects are aware of the wave resistance hump, which occurs on surface vessels in very shallow water (Shields et al., 2004). In this condition, surface vessels have a large local maximum in the wave resistance curve at a Froude depth number (based on the ship's waterline length) of 1.0. Moreover shallow water deeply affects the lift forces.

In the naval context one of the most important problems related to shipping in shallow water is the ship squat, which produces a bodily sinking of a vessel, reducing the under-keel clearance. Vertical squat is not extra draught due to shallow water effects; it is due to water flow being restricted under the ship's hull, according to Bernoulli's Law, depending on the hull shape.

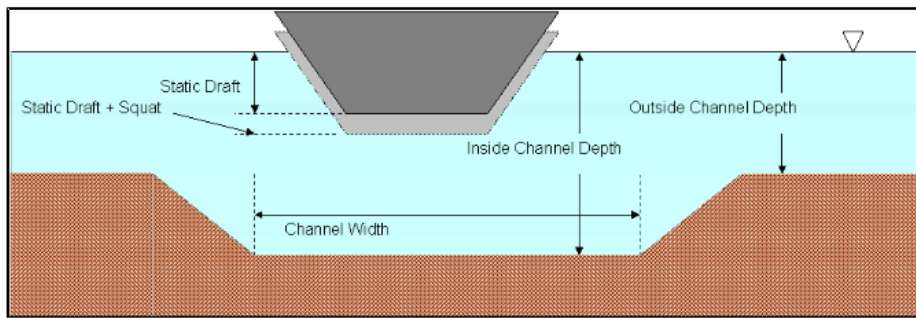


Figure 6-13: ship squat effect.

This phenomenon is produced when water, which should normally flow under the hull, encounters resistance due to the close proximity of the hull to the seabed (Figure 6-14). This causes the water to move faster, creating a low-pressure area with lowered water level surface. As the ship is generally not symmetrical about its half-length and because of the viscous effects of water, the changes in pressure are not identical for the fore and aft parts of the hull. This causes the ship to trim forward or astern depending on the hull shape. Thus, the magnitude of squat depends on the hull shape, the side and under-keel clearance and the speed through the water (Figure 5-14).

From a hydrodynamic point of view, this phenomenon could be described in terms of a negative lift force, acting on the body. In the same manner we could aspect this force acting on cylindrical log resting in a stream flow, producing a probably negative lift for a LWD partially submerged.

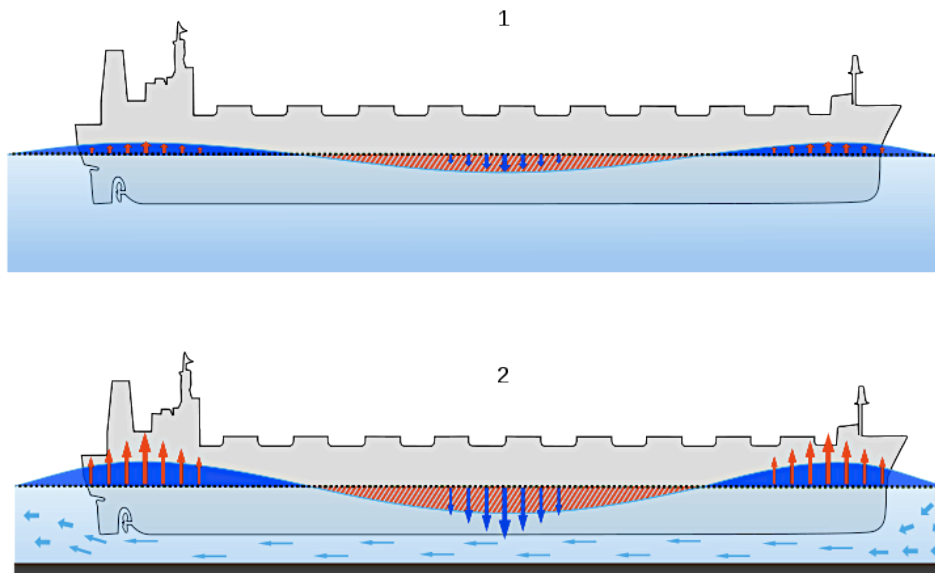


Figure 6-14: navigation in deep water (1), navigation in shallow water (2).

Several formulas could be found in literature, relating the squat displacement of the bow, or of the stern, to the hull types block coefficient, the speed of the vessel, etc. The

theoretical methods (Tuck & Taylor, 1970) generally require detailed information about the geometry of the hull. The empirical methods (Eryuzlu & Hausser, 1978) are normally based on data from model tests or full-size ships and use the leading hull parameters, the speed of the ship, and the principal geographical data. The following dimensionless ratios are widely considered: Froude number (based on the undisturbed water depth), water depth/draft, ship length/water depth. Despite the different formulas, squat varies directly with breadth (doubling breadth doubles squat), by the square of speed (doubling speed quadruples squat), and can be doubled depending on the blockage ratio.

The method proposed by Barrass (1979) has been considered reasonably adaptable to the present context. According Barrass the maximum squat could be calculate with the following equation (S.I units):

$$\delta_{squat} = \frac{C_B \cdot Br^{0.81} \cdot U^{2.08}}{20} \quad (6-61)$$

Where C_B is the blockage coefficient, depending on the shape of the hull, Br is the blockage ratio, defined as the ratio between the submerged cross section area of the ship, and the wetted cross section area of the channel, and U the vessel's speed in knots (1 knots = 0.5144 m/s).

Eq. 6-61 could be used to a rough estimate of the lift coefficient. Considering that the sinking of the vessel has to be balanced by the buoyancy force, it is possible to estimate the force acting on the log (assuming floatation at the undisturbed water depth d_w), considering the volume of water displaced by the squat phenomenon, according to the Archimedes' law:

$$F_{squat} = \gamma_w \cdot \delta_{squat} \cdot c(d_w) \cdot L_{log} \quad (6-62)$$

where γ_w is the specific weight of water, L_{log} is the length of the log, and $c(y)$ is the function that represent the width of the obstacle, varying with y according to the Eq. 6-51, evaluated at the undisturbed water depth d_w .

As a first approximation this force could be considered the lift force acting on the log. Definitely:

$$F_L = -\gamma_w \cdot \frac{C_{Bk} \cdot Br^{0.81} \cdot \left(\frac{U}{0.5144}\right)^{2.08}}{20} \cdot c(d_w) \cdot L_{log} \quad (6-63)$$

For a circular log it is reasonable to consider the blockage coefficient typical of the finer hulls ($C_{Bk} = 0.6$), while for a rectangular log lift could be neglected ($C_{Bk} = 0$).

Obviously the proposed approach is just a very simplistic estimate of the lift force, which could be used just in case no other information would be available.

6.5 BUOYANCY FORCE

According to the Archimedes' law: "any object, wholly or partially immersed in a fluid, is buoyed up by a force equal to the weight of the fluid displaced by the object". This principle is truly applicable in case of still water, under the assumption of a hydrostatic pressure distribution. Moreover it has to be mentioned that for a floating body in a uniform river flow, the buoyant force, acting along the line through the centre of buoyancy C_B and the centre of gravity C_G , is deflected by the slope angle (S in Figure 6-15), producing a force in the stream direction, known in the context of river channel navigability as "Slope Drag" (Langbein, 1962).

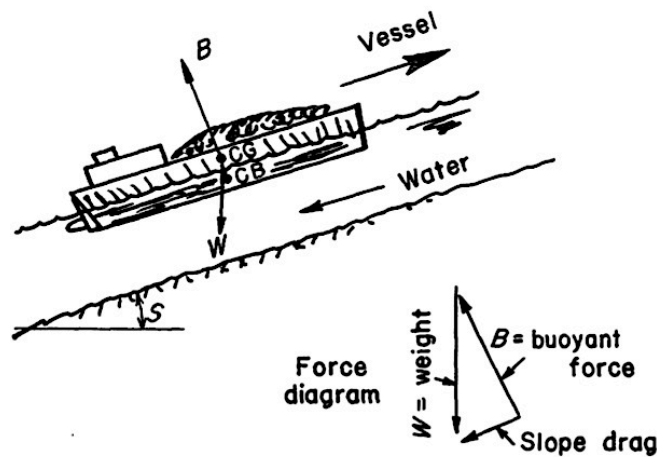


Figure 6-15: schematic illustration of "slope drag" on a vessel moving upstream (from Langbein 1962).

Referring to the coordinate system shown in Figure 6-1, let $p = p(x, y, z)$ the general pressure distribution in proximity of the log. The buoyancy force \vec{B} could be expressed, as a consequence of Gauss theorem, as:

$$\vec{B} = - \int_{\partial V_{wet}} (p(x, y, z) \cdot \vec{n}) \cdot dV = - \int_{V_{wet}} \left(\frac{\partial p}{\partial x} \cdot \vec{i} + \frac{\partial p}{\partial y} \cdot \vec{j} + \frac{\partial p}{\partial z} \cdot \vec{k} \right) \cdot dV \quad (6-64)$$

where ∂V_{wet} represent the frontier of the effective wetted volume, and \vec{n} is the outward normal.

Eq. 6-64 leads to the Archimedes' law in case of still horizontal water, with a hydrostatic pressure distribution. The application of the hydrostatic law to the pressure distribution of steady flow in the cross section of a channel is valid only for parallel flow, such as uniform flow, and for practical purposes the hydrostatic law of pressure distribution is also applicable to gradually varied flow as an approximation (Chow, 1959). For highly concave or convex curvilinear flow, the pressure distribution over the section may noticeably deviates from hydrostatic such that the Archimedes' law became invalid. Despite some researchers have tried to experimentally evaluate correction coefficients in order to take into account the variability of pressure distribution along the flow (Hassan, 2004), it is really difficult to apply these

correlations in the present context, because of the high distortion of the water depth along the lateral sides of the log (Figure 5-13) due to the standing wave (Figure 5-12). In conclusion it is not so simple to correctly evaluate the buoyancy force acting on a log partially submerged, even in case of a uniform undisturbed flow. Nevertheless, as stated in section 5.3.1, this force seems to be the major responsible of the stability of LWD. In order to overcome these problems has been introduced a dimensionless parameter E_p defined as the ratio between the effective buoyancy force, and that due to Archimedes' law in case of still water at the undisturbed depth d_w

$$E_p = \frac{B_y}{\gamma_w A_{sub} L_{log}} \quad (6-65)$$

This parameter is equal to the ratio between the effective submerged volume of the log V_{wet} and the volume submerged in case of still water at the undisturbed depth d_w in case of a hydrostatic pressure distribution as results from Eq. 6-64:

$$E_p = \frac{\gamma_w V_{wet}}{\gamma_w A_{sub} L_{log}} = \frac{V_{wet}}{A_{sub} L_{log}} \quad (6-66)$$

Due to the stated concerns, this parameter could be only experimentally evaluated, while the submerged cross-area of the log A_{sub} is easily evaluable, being a function just of water depth and shape of the log (Figure 6-16).

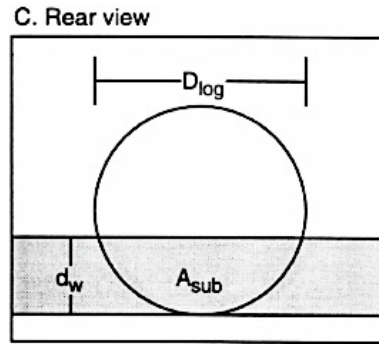


Figure 6-16: reference sketch for calculating the submerged area (from Braudrick 1998).

For cylindrical log A_{sub} could be calculated by the piece diameter D_{log} , according to the following equation:

$$A_{sub} = \left(\cos^{-1} \left(1 - \frac{2 \cdot d_w}{D_{log}} \right) - \sin \left(\cos^{-1} \left(1 - \frac{2 \cdot d_w}{D_{log}} \right) \right) \right) \cdot \frac{D_{log}^2}{8} \quad (6-67)$$

The component of the buoyancy force in the flow direction (B_x in Figure 6-1) has to be neglected in case of experimentally evaluated drag coefficient, as it is implicitly considered in its definition.

6.5.1 Floatation centre determination

The floatation centre determination is basically related to the wave profile generating on the lateral surface of the partially submerged obstacle, which affects the wetted volume. The waves height along the surface of the obstacle modify the centre of buoyancy, being the centroid of the displaced volume of fluid: weight force, acting through its centre of gravity, and the upward buoyancy force may be not aligned (Figure 6-1), producing a rotational moment.

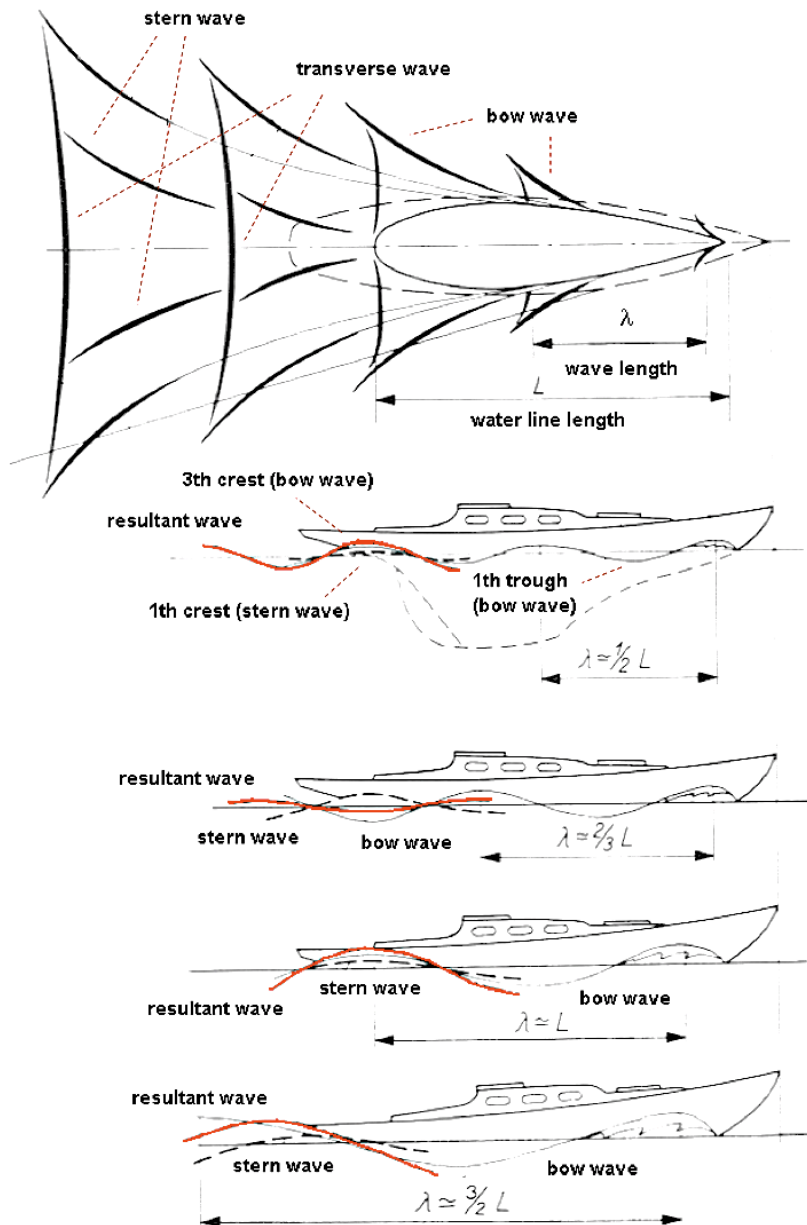


Figure 6-17: wave system surrounding the ship profile (modified from Brighenti et al., 2003).

The prediction of the height, the wavelength and the shape of the produced wave is not an easy task, well known in the ship context as it is directly related to the resistance of the ship (Havelock, 1908, 1934, and 1951)

Some simple expressions could be found in literature, based on elementary fundamental theoretical considerations, and experimental data, relating the wave characteristics to the draft-based Froude number.

A parabolic wave profile seems to be in fairly good agreement with experimental measurements for the front of the bow waves, i.e. between the leading edge of the bow and the crest of the bow wave, while for the zone between the wave crest and the ship stem a sinusoid with a wave length $\lambda = 2\pi U^2/2$ could be considered (Delhommeau et al., 2007).

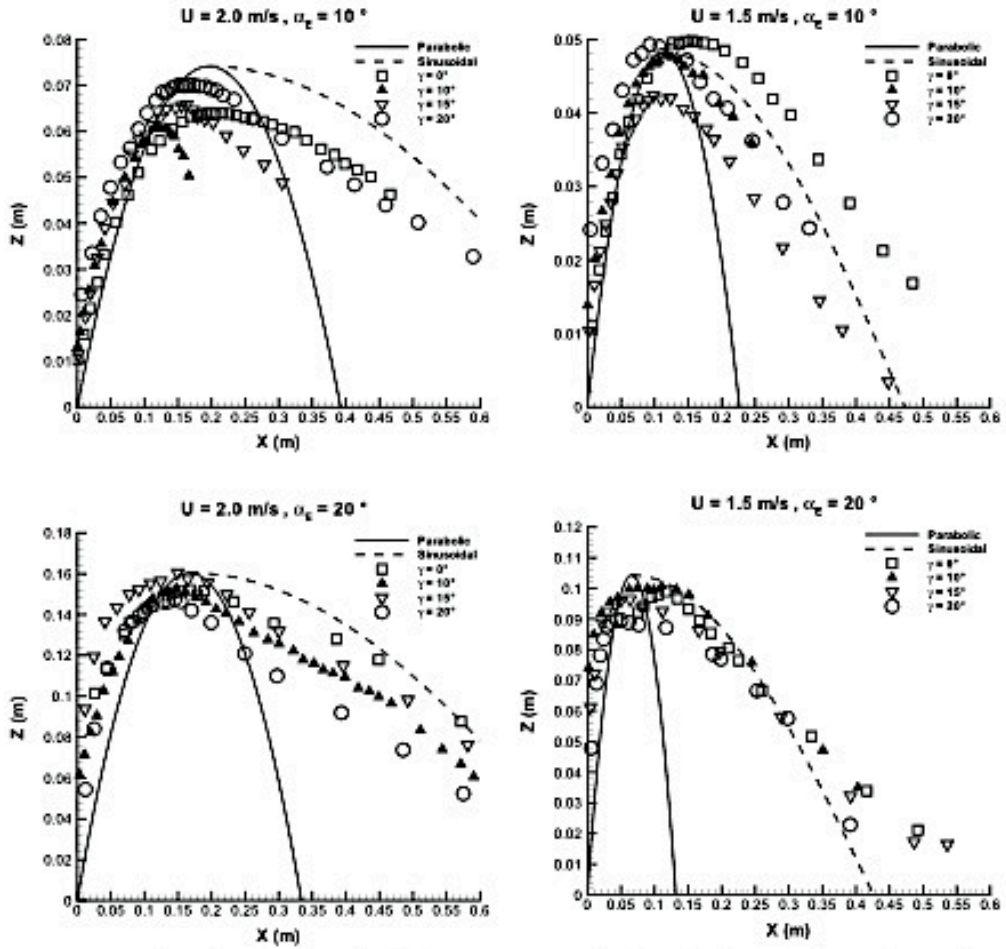


Figure 6-18: comparison of the analytical bow-wave approximation with experimental measurements for a rectangular plate with flare angles $\gamma = 0, 10, 15, 20$, and incident angle $\alpha = 10$ and 20 (source Delhommeau et al., 2007).

Delhommeau et al. (2007) give simply analytical expressions for the height and the shape of the bow wave, which could be applied to evaluate the position of the centre of buoyancy. According Delhommeau et al. the height of the bow wave, y_{bw} , above the mean free surface, is given by:

$$\frac{y_{bw}g}{U^2} = \frac{2.2}{1 + Fr} \cdot \frac{\tan(\alpha_E)}{\cos(\alpha_E)} \tag{6-68}$$

where U is the ship speed, Fr the Froude number related to the draft of the ship’s hull, and α_E the waterline entrance angle.

For applying these results to the LWD entrainment, some approximations are necessary: the position of the wave crest could be considered at the leading edge of the log (perhaps the mathematical position stated by the author, could be used for oriented log) and it is possible to consider the draft equal to the undisturbed water depth. Moreover an estimate of the wavelength has to be provided. According to Fenton (1990) for long wave (or shallow water) the following dispersion relation could be used:

$$k d_w = \frac{\omega \sqrt{\frac{d_w}{g}}}{1 - \frac{1}{6} \omega^2 \frac{d_w}{g}} \tag{6-69}$$

in which $k = 2\pi/\lambda$ is the wavenumber, and $\omega = 2\pi/T$ is the radian frequency, being T the period. Under this hypothesis the wave profile could be obtained equalizing the wave speed and the mean flow velocity:

$$\lambda = 2\pi \sqrt{\frac{U^2 d_w}{6 g (1 - Fr)}} \tag{6-70}$$

$$w(x) = y_{bw} \cos\left(\frac{2\pi}{\lambda} x\right) \tag{6-71}$$

According to the assumptions made for the evaluation of the contraction length (refer to chapter 6.3), it is possible to consider as a first approximation an entrance angle of 45°. Knowing the wave profile $w(x)$ it is possible to obtain a rough estimate of the wetted volume V_{wet} , and the centre of buoyancy, defined as the centroid of this volume, considering the superposition of the wave profile with a linear decrease of the water depth along the lateral surface of the log, due to the backwater, according to the following scheme:

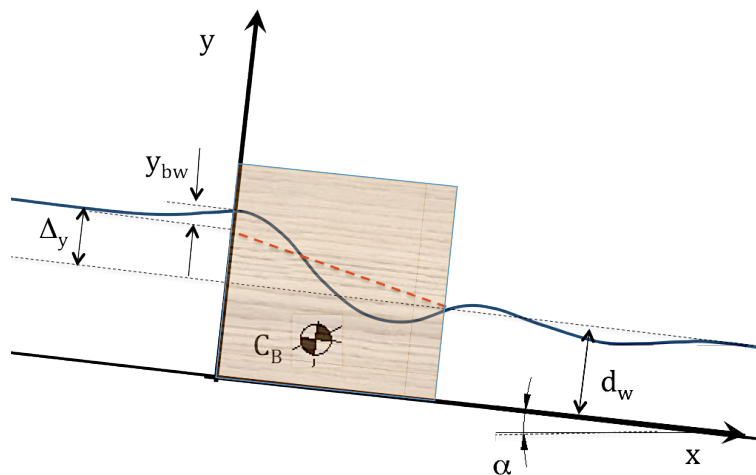


Figure 6-19: Sketch proposed for the evaluation of the centre of buoyancy.

Accordingly the water depth $y(x)$ along the log become:

$$y(x) = d_w + \Delta y - \frac{\Delta y}{L_{eq}} x + y_{bw} \cos \left(\sqrt{\frac{6 g (1 - Fr)}{U^2 d_w}} x \right) \quad (6-72)$$

This allows evaluating the centre of buoyancy as the ratio between the first moments of the wetted area and the extension of the wetted surface. For example the formula for the evaluation of y_{CB} is:

$$y_{CB} = \frac{S_x}{A} = \frac{\int_0^{L_{eq}} dx \int_0^{y(x)} y \cdot dy}{\int_0^{L_{eq}} dx \int_0^{y(x)} dy} \quad (6-73)$$

6.6 INERTIA FORCES

An accurate entrainment analysis of in stream LWD, requires to take into account for the unsteady nature of stream flows, typical of upland tributary. Obviously the complexity and infinity variety of possible unsteady flow motions may suggest limiting the analysis to the steady flow conditions, due to the difficult to obtain reliable inertial coefficient, affected by the fluctuations related to the shedding vortex (Sarpkaya & Garrison, 1963). According to Alonso (2004) however, for quasi-constant flow accelerations of about 0.001 m/s^2 for roughly an hour (quite common for example in ephemeral streams of northern Mississippi), the evolution undergone by the inertial coefficient is short enough that could be approximated by its steady state asymptotic value. The same conclusions could be applied to the drag and lift coefficients, given that both have the same vertical origin. This allows considering the more interesting case, from the risk assessment point of view, of a log partially submerged in the path of a stream flood wave, considering the inertia forces acting on the submerged log.

The inertia force is the force that occurs due to movement of mass and is proportional to the acceleration of displaced mass.

$$F_I = C_M \rho_w V_{wet} \dot{U} \quad (6-74)$$

Where C_M is the inertia coefficient and V_{wet} is the wetted volume of the log, which could be evaluated according to the procedure stated in chapter 0, or simplistically considering the log volume wetted by the undisturbed water depth ($V_{wet} = A_{sub} L_{log}$).

The inertia coefficient is a correction factor that accounts for the force that must be applied to accelerate the mass of water displaced by the log. As a first attempt, the inertia coefficient could be fixed at $C_M = 2.0$, basing on the values reported by Wright and Yamamoto (1979) for cylinders near plane walls, even because, as stated by Alonso, the inertia of single logs is not a significant factor, for actual stream flood event.

6.7 ENTRAINMENT CRITERION

Considering the difficulties in estimating a representative wave profile $w(x)$, the buoyancy force related to the submerged volume of the log V_{sub} , hence strongly affected by backwater and the water free surface profile near the log, remains the main uncertainty that have to be addressed.

As stated in paragraph 6.5 the real buoyancy force acting on the log could be related to a nominal value according to the Eq. 6-65, in which all the uncertainties related to the flow around the log have been summarized in the dimensionless parameter E_p .

The incipient motion conditions defined in section 6.1, Eqs. 6-4, 6-5 and 6-6 could be thus rearranged considering the expression of the buoyancy force provided by Eq. 6-65, the definition of the drag force, Eq. 6-18, and the weight of the log, Eq. 6-7.

After some manipulations it is possible to obtain the following equations:

a) Sliding mode:

$$E_p \geq \frac{\rho_{Log} A_{Log}}{\rho_w A_{sub}} \left(\cos \alpha - \frac{\sin \alpha}{\mu_{bed}} \right) - \frac{F_D + F_I + \mu_{bed} F_L}{\mu_{bed} g \rho_w A_{sub} L_{log}} \quad (6-75)$$

b) Rolling mode:

$$E_p \geq \frac{\rho_{Log} A_{Log}}{\rho_w A_{sub}} \cdot \left[\frac{(x_C - x_{CG}) \cdot \cos \alpha - (y_{CG} - y_C) \cdot \sin \alpha}{(x_C - x_{CB})} \right] - \frac{1}{g \rho_w A_{sub} L_{log}} \left[F_D \frac{(y_D - y_C)}{(x_C - x_{CB})} + F_I \frac{(y_{CB} - y_C)}{(x_C - x_{CB})} + F_L \frac{(x_C - x_L)}{(x_C - x_{CB})} \right] \quad (6-76)$$

c) Buoyancy mode:

$$E_p \geq \frac{\rho_{Log} A_{Log}}{\rho_w A_{sub}} - \frac{F_L}{g \rho_w A_{sub} L_{log}} \quad (6-77)$$

These three equations state that incipient motion of log is not allowed until the right hand side is greater than the parameter E_p , which represents the same physical quantity for all the entrainment modes considered, being just related to the shape of the resting log and the local flow conditions (refer to section 6.5), independently from equilibrium concerns. As a consequence, it is possible to join under a unified approach sliding, rolling and buoyancy modes, obtaining a more general expression, that allows to verify the incipient motion condition and the relative mode at the same time.

The value of the parameter E_p at the entrainment could not be assessed a priori, but could be experimentally evaluated. Actually for each undisturbed water depth (or analogously for each discharge) it is possible to calculate the right hand side of the previous equations, starting from the relationships proposed in the aforementioned

paragraphs, all related to the undisturbed flow: at the incipient motion these equal the value of the parameter E_p . If we indicate with E_p^s , E_p^r and E_p^b the entrainment parameters respectively related to the sliding, rolling and buoyancy mode:

$$E_p^s = \frac{\rho_{Log} A_{Log}}{\rho_w A_{Sub}} \left(\cos \alpha - \frac{\sin \alpha}{\mu_{bed}} \right) - \frac{F_D + F_I + \mu_{bed} F_L}{\mu_{bed} g \rho_w A_{Sub} L_{Log}} \quad (6-78)$$

$$E_p^r = \frac{\rho_{Log} A_{Log}}{\rho_w A_{Sub}} \cdot \left[\frac{(x_C - x_{CG}) \cdot \cos \alpha - (y_{CG} - y_C) \cdot \sin \alpha}{(x_C - x_{CB})} \right] - \frac{1}{g \rho_w A_{Sub} L_{Log}} \left[F_D \frac{(y_D - y_C)}{(x_C - x_{CB})} + F_I \frac{(y_{CB} - y_C)}{(x_C - x_{CB})} + F_L \frac{(x_C - x_L)}{(x_C - x_{CB})} \right] \quad (6-79)$$

$$E_p^b = \frac{\rho_{Log} A_{Log}}{\rho_w A_{Sub}} - \frac{F_L}{g \rho_w A_{Sub} L_{Log}} \quad (6-80)$$

the incipient motion of the log will be then established when:

$$\min\{E_p^s, E_p^r, E_p^b\} \leq E_p^* \quad (6-81)$$

being E_p^* the threshold value obtained by experiments.

For a given log the entrainment parameters could be therefore evaluated as a function of the local water depth, or, if the rating curve is known, as a function of the water discharge (Figure 6-20).

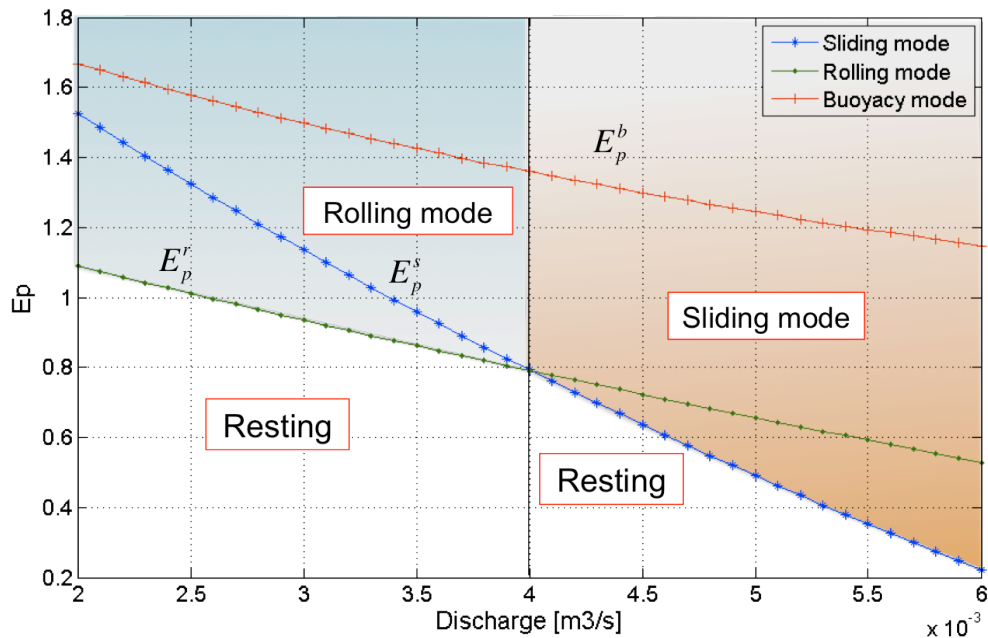


Figure 6-20: trends for entrainment modes as a function of discharge.

For the log considered in Figure 6-20, according to the entrainment condition stated by Eq. 6-81, the incipient motion should be by rolling for the lowest discharge

(less than 0.004 m³/s), and by sliding otherwise. The discharge able to displace the logs instead, should be established by the threshold value E_p^* .

LWD entrainment has been therefore reduced to the feasible calculation of three entrainment conditions, and to the evaluation of a threshold value for the parameter E_p , which has to be experimentally evaluated.

Substituting the expressions of the forces acting on the log, described in the previous chapters, it is possible to obtain the following general expressions of the entrainment parameters:

$$E_p^s = \frac{\rho_{Log} A_{Log}}{\rho_w A_{Sub}} \left(\cos \alpha - \frac{\sin \alpha}{\mu_{bed}} \right) - \frac{C_M \dot{U}}{g \mu_{bed}} - \frac{C_D U^2}{2g \mu_{bed}} \left(\frac{\cos \theta}{L_{log}} + \frac{d_w \sin \theta}{A_{Sub}} \right) + \frac{C_{Bk} \cdot c(d_w) \cdot Br^{0.81}}{20A_{Sub}} \left(\frac{U}{0.5144} \right)^{2.08} \quad (6-82)$$

$$E_p^b = \frac{\rho_{Log} A_{Log}}{\rho_w A_{Sub}} + \frac{C_{Bk} \cdot c(d_w) \cdot Br^{0.81}}{20A_{Sub}} \left(\frac{U}{0.5144} \right)^{2.08} \quad (6-83)$$

$$E_p^r = \frac{\rho_{Log} A_{Log}}{\rho_w A_{Sub}} \cdot \left[\frac{(x_C - x_{CG}) \cdot \cos \alpha - (y_{CG} - y_C) \cdot \sin \alpha}{(x_C - x_{CB})} \right] - \frac{C_D U^2}{2g \mu_{bed}} \left(\frac{\cos \theta}{L_{log}} + \frac{d_w \sin \theta}{A_{Sub}} \right) \frac{(y_D - y_C)}{(x_C - x_{CB})} - \frac{C_M \dot{U}}{g \mu_{bed}} \cdot \frac{(y_{CB} - y_C)}{(x_C - x_{CB})} + \frac{C_{Bk} \cdot c(d_w) \cdot Br^{0.81}}{20A_{Sub}} \left(\frac{U}{0.5144} \right)^{2.08} \frac{(x_C - x_L)}{(x_C - x_{CB})} \quad (6-84)$$

For the LWD entrainment assessment these expressions could be further simplified considering the following assumptions:

- LWD has the greatest range of functions (refer to section 3.2.2.3) within lowland channel types, characterized by low gradient. This allows neglecting the effects due to bed slope ($\sin \alpha \sim 0$).
- Analysis of LWD orientation distribution shows how LWD are mainly aligned to the mean flow. Moreover the drag force normally reaches its maximum value for $\theta = 0^\circ$, and $\theta = 90^\circ$. This allows considering just these two values.
- For square shaped logs the lift force could be neglected.

It is interesting to notice that under these hypotheses the entrainment condition could be bring back to a formulation similar to that proposed by Bocchiola et al. (2006). For example, for a square shaped log, aligned to a uniform flow ($\dot{U} = 0, \theta = 0$), the entrainment condition for sliding become:

$$E_p^s = \frac{\rho_{Log} D_{Log}}{\rho_w d_w} \left(\cos \alpha - \frac{\sin \alpha}{\mu_{bed}} \right) - \frac{C_D U^2}{2g \mu_{bed} L_{log}} = E_p^* \quad (6-85)$$

which could be rewritten as:

$$\frac{\rho_{Log} D_{Log}}{\rho_w d_w} = \frac{\mu_{bed} E_p^*}{\mu_{bed} \cos \alpha - \sin \alpha} + \frac{C_D U^2}{2g L_{log} (\mu_{bed} \cos \alpha - \sin \alpha)} \quad (6-86)$$

or analogously, according to the Bocchiola notation:

$$Y_w^* = \frac{1}{K \cdot E_p^* + C_D \cdot X_S^*} \quad (6-87)$$

in which K is a constant related to the bed slope and its roughness, and E_p^* plays a role similar to the coefficient of representativeness C_r (refer to section 5.2) proposed by Bocchiola et al. (2006), that, as E_p^* , have to be experimentally evaluated.

The proposed approach could be summarized in the following steps:

- Entrainment analysis starts from the survey sheets: data acquired during the monitoring phases allow the developing of the hydraulic model of the river, and the location of LWD in the river channel.
- From the previous information it is possible to evaluate for each discharge the undisturbed water depth, the mean velocity of the flow at the log position, and the blockage ratio provided by the log. This allows evaluating the backwater rise, according to the following procedure:
 - The Froude number of the undisturbed flow is initially compared with the critical one, enabling to evaluate if the flow in the constricted section will be choked or no.
 - If the flow is subcritical, therefore the backwater rise due to the LWD could be evaluated according to the empirical correlations due to Yarnell (1934) or El-Alfy (2006), depending on the slenderness of the log, otherwise the procedure to be used should be that proposed by Molinas (2004, 2006).
- The value of the backwater rise allows estimating the drag force, according to the formula provided by Chaberneau et al. (2001).
- Depending on the log shape and the flow conditions, the inertia and lift force could be then evaluated, according to the empirical relationships proposed.
- The calculated forces consents to estimate the entrainment parameters E_p^s , E_p^r and E_p^b : the one characterized by the lower value permits to identify the entrainment mode, while the comparison with the threshold value E_p^* allows recognizing if the entrainment condition will be achieved at the considered discharge.

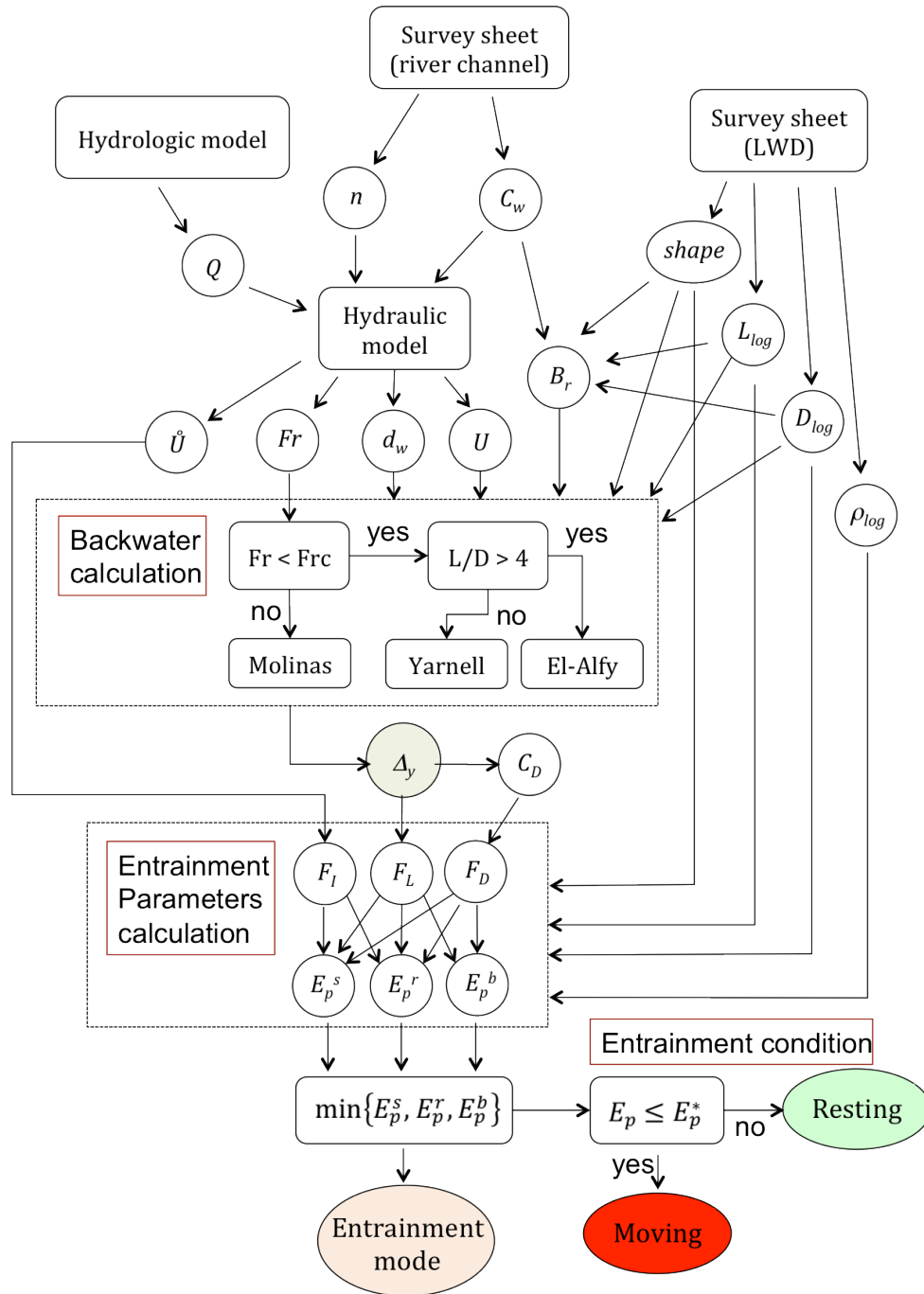


Figure 6-21: sketch of the proposed approach for LWD entrainment assessment.

Definitely a novel general approach to LWD entrainment has been developed, that takes into account most of the physical phenomena generally neglected in literature, and could be bring back to the classical approaches under simplifying hypotheses. Moreover a method to reasonably predict the drag force acting on the partially submerged log has been introduced.

In order to apply the novel approach the threshold value for the entrainment parameters have to be experimentally established. For this reason flume experiments, described in the following chapter, were carried out at the Delft University of Technology.

7 LARGE WOODY DEBRIS ENTRAINMENT: FLUME EXPERIMENTS

Wood mainly moves during large floods when direct observations of logs dynamics are inhibited by evident safety and logistic limits. Presently, well-controlled laboratory experiments or numerical simulations are the main source of information on open-channel dynamics and are used in the interpretation of river phenomena, even if laboratory open-channel studies are typically carried out under idealized conditions of uniform flow and flat beds with a fairly homogeneous bed roughness distribution rarely found in rivers. Despite these discrepancies flume experiments are invaluable instruments for the researchers, essential to confirm hypothesis and characterize unknown or lesser-known features, necessary to update models and consequently upgrade the existing knowledge.

To date, only few flume experiments have analysed wood entrainment. In all cases fixed gravel or sand bed has been considered.

Analysis of the state of the art (refer to section 5.3) has shown how the main lacks of LWD entrainment models available in literature seems to be related to a realistic evaluation of the buoyancy force: the marked changes in the velocity field across the partially submerged log, dramatically modify the pressure distribution acting on the log surface, making the Archimedes' law no more realistic. Moreover the standing wave generating on the lateral surface of the log, produces a wetted volume that could be very different from the hydrostatic case, producing great uncertainties in the buoyancy force evaluation.

In this work a novel mechanistic approach for LWD entrainment has been developed (refer to chapter 6), in which LWD entrainment has been related to the change in the buoyancy force with respect to the hydrostatic case (dimensionless parameter E_p : Eq. 6-65). According to the force balance, analyzed and discussed in chapter 6, entrainment arises when E_p becomes greater than the right hand side of the Eqs. 6-75, 6-76 and 6-77, related to the three different entrainment modes. The right hand side of the three expressions can be evaluated using appropriate correlations found in literature (and extensively described in chapter 6), which have been adapted to the case study because usually adopted in different context. The outcomes of this analysis are three entrainment parameters (Eqs. 6-82, 6-83, 6-84) that offer even the possibility to discern between different entrainment modes (sliding, rolling and buoyancy). The incipient motion of the log, in fact, arise when one of the entrainment parameters becomes lower than the dimensionless parameter E_p , and the entrainment mode is therefore the one associated to that entrainment parameter.

In order to apply the proposed approach, it is required to estimate the value that the dimensionless parameter E_p assumes at the entrainment (the threshold value E_p^*), establishing definitively an entrainment criterion (Eq. 6-81).

No experimental correlation has been found in literature, able to predict the change in the buoyancy force for a partially submerged body with respect with the hydrostatic case. For this reason, an experimental approach has been used: according to the Buckingham π theorem, all the physical variables expected to influence this parameter have been considered and a regression analysis on the available experimental data has been performed (refer to paragraph 7.3.3 of this chapter).

This chapter explains procedures for flume experiments carried out, thanks to the collaboration with the research group of A. Crosato, at the Fluid Mechanics Laboratory of Delft University of Technology, and describes the analysis of the available experimental data (taken from literature and directly measured), performed in order to define the threshold value of the proposed entrainment parameter, which can not be theoretically estimated.

7.1 PRELIMINARY CONSIDERATIONS

As stated in the previous sections it is within lowland channel types that LWD has the greatest range of functions (refer to section 3.2.2.3), so flow conditions characterizing these rivers have been considered for the experimental tests.

Lowland rivers are normally wide, with bed dominated by fine sediments and a meandering course lacking rapids. The slope of the river channel is low, typically spanning a range of gradients between about 0.1 and 3 per cent. Because of this, the water depth variation along the river length is negligible if compared to the mountain and Piedmont Rivers, and the flow is subcritical ($Fr < 1$) with smooth, undisturbed water surfaces. The Reynolds number of the flow is typically greater than 3000 denoting a turbulent motion (Braudrick, 2000).

Although the differences within watersheds all over the world, a common issue of more general importance is the risk of accumulation of smaller woody debris, such as parts of branches that can be trapped against a bridge or a culvert (Cottingham, Bunn, Price, & Lovett, 2003). This suggests focusing the entrainment investigation for the smaller LWD (characterized by a diameter between 100 mm and 200 mm), as they are the first to be mobilized during high flow conditions.

Similitude and theory of models (Allen, 1947; Henderson, 1966) indicate that for flows driven by gravity the principal dynamic criterion to be satisfied is usually the constancy of Froude number between model and prototype at geometrically similar location. To model LWD entrainment condition, it is therefore necessary to correctly scale flow velocities as well as flow depths and LWD dimensions to have a Froude similarity. Scale effects occur in all physical hydraulic models when forces usually negligible in rivers (e.g. viscous), become influential in the model (Henderson, 1966). It is necessary to take extreme care in planning and conducting physical model tests to

eliminate or minimize scale effects, since the scale effects can lead to erroneous conclusions from models. Thus, diverging similitude between model and prototype influences how proficiently model results can be applied to the prototype (Allen, 1947), particularly as model size decreases. The complex phenomena related to entrainment suggest using low scale ratio.

The literature review and the analysis of the main forces acting on the partially submerged log have shown that drag and buoyancy forces mainly influence entrainment. In particular in section 5.3 the importance of the standing wave, produced by partially submerged log, has been underlined, as it could significantly alter the buoyancy force acting on the log. The laboratory experiments carried out by Crosato et al. (2011 and 2013) indicate that standing wave generation seems to be emphasized in case of high blockage ratio.

While the drag coefficient is strongly influenced by the blockage ratio, which is the main responsible of the backwater rise, its variation instead appears to be less influenced by the slenderness ratio (L_{log}/D_{log} ; log length L_{log} and log diameter, L_{log}) of the log (Gippel et al., 1996), much more by the orientation with respect to the flow direction. Accordingly it seems not to be so important to preserve the length of the dowels, as specified by LWD definition. Moreover from risk assessment point of view it is sufficient to consider the worst conditions: LWD oriented with an angle of 0° and 90° , as these provide the greater CD values (see Figure 6-6).

For all these reasons, the experimental setup proposed by Crosato (2011 and 2013) was chosen even for the new performed tests. Actually using a straight, horizontal flume 0.40 m wide, with a blockage ratio in presence of the object ranging from 0.3 to 0.63, the upstream elevation of the water surface is marked and easily detectable, and at the same time it reproduces a quite investigated situation which is known in literature in the context of lagoon's shipping in narrow channels. These conditions allows to reduce the uncertainties related to the evaluation of the Drag and Lift force, as described in section 6.3 and 6.4. Finally it is quite normal to find isolated woody debris near channel sinuosity or large boulders (refer to chapter 2.2.2), providing a constriction for the flow around the log

Handmade cylindrical pieces of wood, with no roots or branches, were considered, and several tests performed on fixed bed, to observe the hydrodynamic conditions at incipient motion of dowels having different cross-sectional shape and orientation with respect to water flow. The investigated angles of orientation to the flow were 0° and 90° , where 0° is parallel to the flow, 90° perpendicular to the flow.

Experiments were performed considering subcritical flow conditions characterizing Lowland and Piedmont Rivers with Froude number less than one, with mean velocity ranged from 0.134 to 0.406 m/s. All the experiments were conducted within a range of Reynolds' numbers typical of turbulent flow (10^3 - 10^5).

7.1.1 Similitude between model and prototype

Experimental simulation is central in all hydraulic modelling: small-scale physical models could be proficiently used to study complex flow phenomena under controlled laboratory conditions. The relationships between quantities in the model and in the prototype have to be derived from dimensional analysis and provide a means for determining the values that should be used in a model (e.g., the velocity or flow depth) to correctly represent the corresponding quantities in the prototype. These modelling laws also provide for scaling quantities measured in a model (e.g., head loss, drag force, or water surface profile) to prototype conditions.

The forces associated with open channel flow are attributable to:

- *Fluid inertia*: important in almost all situations involving fluid movement.
- *Gravity*: of prime importance for free-surface flows in which simulation of fluid surface profile is a modelling goal.
- *Physical properties of the fluid*: forces associated with the material properties of the fluid (especially viscosity, density, surface tension, and vapour pressure) increase in importance for flow situations where flow behaviour is influenced by change in fluid properties.
- *Boundary drag and friction*: modelling of flow profile requires stricter attention to similitude of channel resistance to flow. That requirement can be relaxed when modelling local flow behaviour because the flow lengths usually are sufficiently short that differences in water surface elevation due to flow resistance are insignificant.

Failure to simulate the forces associated to fluid properties (especially viscosity and surface tension) may cause a small model to exhibit substantially different flow behaviour that occurs at full scale.

Models of open channel flows are frequently operated according to Froude model laws since gravity is usually important for these flows. This essentially requires that the ratio of inertia to gravity forces be the same in model (subscript m) and prototype (subscript p). As model is subjected to the same gravitational field that occurs at full scale, the Froude number similarity criterion prescribes:

$$(Fr)_r = \frac{(Fr)_p}{(Fr)_m} = \frac{U_r}{\sqrt{(d_w)_r}} = 1 \quad (7-1)$$

In other words by setting the ratio of Froude numbers between model and prototype equal to unity, the scale ratio for flow velocity is seen to be the square root of the scale ratio for flow depth. Considering that economic concerns suggest using water in hydraulic models to simulate the characteristic of water flow ($\rho_r = 1$), the Froude number criterion produces the following scale ratios.

Table 7-1 states that under these conditions, by setting the geometrical scale ratio to a defined value L_r , the Reynolds similitude will be not verified, being the square root of the cube of the geometric scale factor.

Table 7-1: scale relationships based on Froude number similitude, with $\rho_r=1$. From "Hydraulic modelling concept and practice" ASCE manual and reports on engineering practice n. 97 (2000).

Variable	Relationship	Scale	Scale for Vertically Distorted Model, $G = X_r / Y_r$
length	$L = \text{length}$	$L_r = X_r = Y_r$	horizontal length: $L_{rx} = X_r$ vertical length: $L_{ry} = Y_r$
slope	$S = \frac{\text{horizontal length}}{\text{vertical length}}$	$S_r = \frac{L_r}{L_r} = 1$	$S_r = \frac{Y_r}{X_r} = \frac{1}{G}$
velocity	$U = \frac{\text{length}}{\text{time}}$	$U_r = L_r^{1/2}$	$U_r = Y_r^{1/2} = \left(\frac{X_r}{G}\right)^{1/2}$
time	$t = \frac{\text{length}}{\text{velocity}}$	$t_r = \frac{L_r}{U_r} = L_r^{1/2}$	horizontal motion: $t_{xr} = \frac{X_r}{Y_r^{1/2}} = (GX_r)^{1/2}$ vertical motion: $t_{yr} = \frac{Y_r}{Y_r^{1/2}} = Y_r^{1/2}$
acceleration	$a = \frac{\text{velocity}}{\text{time}}$	$a_r = \frac{U_r}{t_r} = \frac{L_r^{1/2}}{L_r^{1/2}} = 1$	horizontal motion: $a_r = \frac{U_r}{t_{xr}} = \frac{1}{G}$ vertical motion: $a_{yr} = \frac{U_r}{t_{yr}} = 1$
discharge	$Q = \text{velocity} \times \text{area}$	$Q_r = U_r A_r = L_r^{5/2}$	horizontal component: $Q_{hr} = U_r Y_r X_r = GY_r^{5/2}$ vertical component: $Q_{vr} = U_r X_r X_r = G^2 Y_r^{5/2}$
Force	$F = \text{mass} \times \text{acceleration}$	$F_r = \rho_r L_r^2 L_r = L_r^3$	horizontal component: $F_{hr} = a_{hr} Y_r X_r^2 = Y_r^2 X_r$ vertical component: $F_{vr} = a_{vr} Y_r X_r^2 = Y_r X_r^2$
Pressure and Stress	$p = \sigma = \frac{\text{force}}{\text{area}}$	$p_r = \sigma_r = \frac{\rho_r L_r^2 L_r}{L_r L_r} = L_r$	horizontal component: $p_{hr} = \sigma_{hr} = \frac{Y_r^2 X_r}{Y_r X_r} = Y_r$ vertical component: $p_{vr} = \sigma_{vr} = \frac{Y_r X_r^2}{X_r^2} = Y_r$
Reynolds number	$Re = \frac{UL}{\nu}$	$(Re)_r = L_r^{1/2} L_r = L_r^{3/2}$	$(Re)_{ry} = Y_r^{1/2} Y_r = Y_r^{3/2} = \frac{X_r^{3/2}}{G}$

Reynolds numbers express the relative magnitude of forces attributable to fluid inertia and viscosity. If the objective is to model flow around a hydraulic structure, similitude of flow field is of great importance. For problems such as the one being addressed in this research, it is desirable to represent both gravitational and viscous effects in the model, as the distribution of flow near a solid obstacle is influenced by fluid viscosity and the roughness of the boundary. At the same time the gravitational effects are important to correctly represent the force causing the flow and the behaviour of the standing waves created by the obstacle (LWD), which include the effects that generate the backwater due to the partially submerged obstacle. Consequently as the flow field around the object may vary with Re and the relative roughness, the Reynolds similitude in conjunction with geometric similitude should be verified. In other words when both flow resistance and gravitational effects must be represented in a model, difficulties arises since it is impossible to satisfy simultaneous Reynolds and Froude criterion if the same fluid is used in both the model and the prototype.

However if fully rough flow exists at full scale and model scale, exact satisfaction of the Reynolds number criterion is not needed. It is sufficient that values of Reynolds at full scale and model scale place the flows in the same flow regime. In fact as illustrated in the Moody diagram, a change in Re does not alter boundary resistance, provided that flow in the model is fully rough as at full scale. Similarly a change in Re may not

alter significantly the pattern of flow near the structure or alter drag coefficient C_D , if the flow is fully turbulent as at full scale. Modelling difficulties may arise for models designed primarily on the basis of Froude number similitude, because the reduced value of the Reynolds number at model scale could shift the flow from the rough zone into a transition flow zone, producing a change in local flow pattern near boundaries, exaggerated emphasis in the model of viscous resistance relative to form resistance, and an overall increase in resistance coefficient. In this case, attaining adequate dynamic similitude may require a geometrically distorted model. The most common form of geometric distortion in modelling entails use of a vertical scale smaller than the horizontal scale, producing a distorted flow depth. Sometimes this approach is used to facilitate sufficiently accurate measurements of flow properties.

However, in all cases, it is necessary to use extreme care in planning and conducting physical model tests to eliminate or minimize scale effects, since the scale effects can lead to erroneous conclusions from models.

Due to the difficulties described, and considering the characteristics of LWD and Lowland River, described in the previous section, and the dimensions of the flume available at the Fluid Mechanics Laboratory of Delft University of Technology, it has been verified that it is possible to conserve a full scale during the experiments.

7.2 TEST DESCRIPTION

The main objective of these experiments was to determine the water depth and flow velocity at which logs start moving. Logs with circular and square cross section were considered for the experiments. Entrainment was tested on fixed gravel bed. The experimental runs were performed under as steady as possible flow conditions.

During each test the dowels were positioned, parallel or perpendicular to the water flow, in the centre line of the flume, at 7 m from the input gate for water, in order to minimize the boundary effects. The logs were initially resting. Then, water depth d_w was gradually increased, by augmenting the discharge through the flume circulation facility until each log started to move. Every rise of discharge was slight, producing slow depth increments (about 1 mm in 10 min). A rest period was subsequently applied to bypass the transient flow interval after each increment, reproducing a sequence of quasi-steady flow states in the flume. Checking of incipient motion was carried out visually. After that, one time for each type of test, the dowel was removed to measure with a point gauge the undisturbed water depth at the critical discharge for initiation of motion, in the spot formerly occupied by the dowel. Water depth measurements were taken also at distance from the upstream boundary of 4.0 m and 9.0 m, in order to validate the HEC-RAS one-dimensional hydrodynamic model used to calculate the undisturbed water surface profile along the flume (refer to 6.4.7). Due to time constraints, these measurements were not taken during all tests.

The water depth at entrainment was measured also 1 cm and 20 cm upstream and 1 cm and 20 cm downstream of the log, holding the log at its initial position. All depth

measures were acquired with a resolution of 0.1 mm, even if, due to the local turbulence of the flow field around the dowels, accuracy was low. A camera placed at the right side of the flume recorded the log movements.

To improve accuracy, every test was repeated three times for each shape and orientation. After each trial, the dowel was removed and the water depth lowered. Then, the procedure was repeated. The average value of flow depth and discharge was taken. The logs were weighted immediately before and after each test with a sharp balance with an accuracy of 1.0 gr.

The sequence of experiments was executed in the same gravel bed flume used in 2010 by Crosato et al., maintaining the same geometrical and physical conditions (dimension, roughness). The novelties introduced were a different test location with respect to the upstream gate of the flume and a different shape for the dowels that preserved wood type and size, but differed for the geometry of the edges that were smoothed.

7.2.1 Log settings

The preliminary considerations reported in section 7.1 suggested considering the smaller LWD to evaluate the threshold value of the proposed entrainment parameter. Large woody debris comprises trees, branches and limbs that fall into waterways, and are conventionally defined as material with a diameter greater than 0.1 metres and greater than 1 metre in length. So it was decided to use the same cylindrical shaped log used by Crosato in a previous set of experiments (Crosato et al., 2010), with a diameter of 0.15 metres. Considering the flume width, this value permits to have a blockage ratio near to 0.3, inducing upstream backwater level rise markedly. This condition allows a better estimate of the drag force acting on the log at the entrainment as illustrated in section 6.3.

The low variation of drag coefficient with the log slenderness ratio (see Figure 6-6), together with the considerations stated in the next section regarding the longitudinal flow depth profile, suggests limiting the length of the log. For these reasons the same dowels used by Crosato, with a fixed length of 25 cm were used, allowing to extend the tests even to a blockage ratio of 0.63, and to consider a log orientation orthogonal to the flow. Moreover with this choice has been possible maintaining similitude scale factors equal to one, which, as stated in section 7.1.1, is suitable in case of problems such as the one being addressed in this research, wherein it is desirable to represent both gravitational and viscous effects in the model.

Log models were prepared using birch wood, a broadleaved deciduous hardwood tree of the genus *Betula*. Generally, this type of wood is used to form Betonplex. Circular and Square shaped logs were used, considered as the two shapes defining a sort of tolerance zone for a true trunk cross-section. Moreover square shaped logs can provide a more robust estimate of the threshold value because for this shape uncertainties are smaller:

- The centre of instantaneous rotation C could be reasonably considered coincident with the downstream edge of the log (refer to Figure 6-1);
- The lift force could be reasonably neglected, being the lateral log surface vertical: the depression created by the accelerated flow in the constricted section should not realistically provide actions in the vertical direction.

In order to evaluate just the effect of different shapes on the entrainment parameter, approximately the same volume of logs was considered for circular and square logs both. Accordingly the same length was maintained.

Table 7-2: design log size

Log shape	Circular	Square
Width (cm)		13.2
Height (cm)		13.2
Diameter (cm)	15	
Length (cm)	25	25
Cross-sectional area (cm ²)	176.6	175.2
Volume (cm ³)	4415.6	4356

In Figure 7-1 the complete set of logs used in the trials.

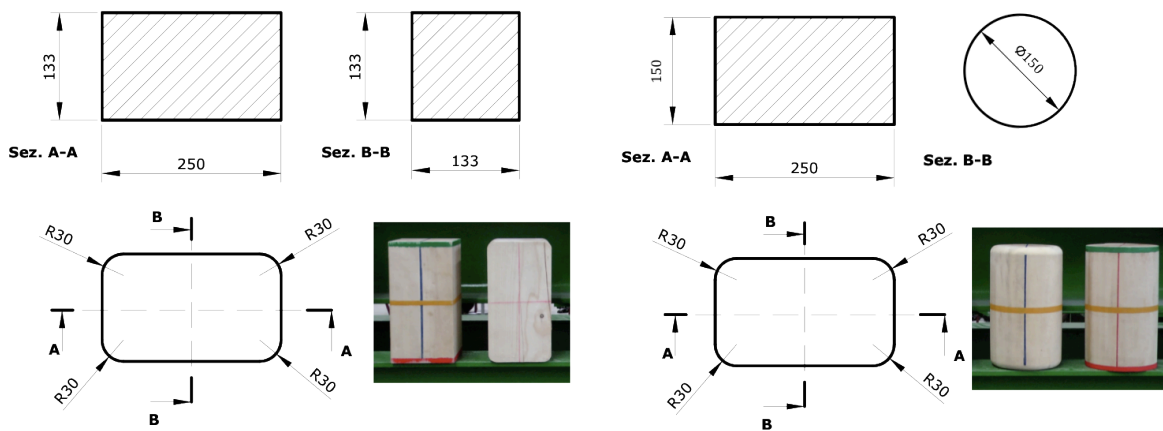


Figure 7-1: design sizes for smoothed square and circular log.

As stated in section 6.3, the drag force acting on a partially submerged obstacle can be related to the backwater rise. Literature review on this topic, particularly copious in the research field of bridge piers, has shown that the shape of the obstacle affects this phenomenon. This is more evident in case of scour: shape of the nose of a pier can have up to a 20% influence on scour depth. Streamlining the front end of a pier reduces the strength of the horseshoe vortex, thereby reducing scour depth. Streamlining the downstream end of piers reduces the strength of the wake vortices. A square-nose pier will have maximum scour depths of about 10% greater than either a round-nose pier (Arneson et al., 2012). Therefore even dowels with their sharp edges smoothed were considered as first attempt to evaluate how log shape could affect the entrainment

condition: corners were rounded with a 15 mm fillet radius. Tests with the sharp edged dowels were performed also in the new experimental condition to relate the results to the precedent experiments.

In order to take into account for the porosity of wood, the density of the logs was evaluated before and after each test, they were initially either dry or wet.

7.2.2 Flume setup

The experiments were carried in a 14 m long and 40 cm wide laboratory flume, with a wooden bed and glass sidewalls. A camera was installed laterally to the flume to record the rotation/sliding of the log at the incipient motion condition.

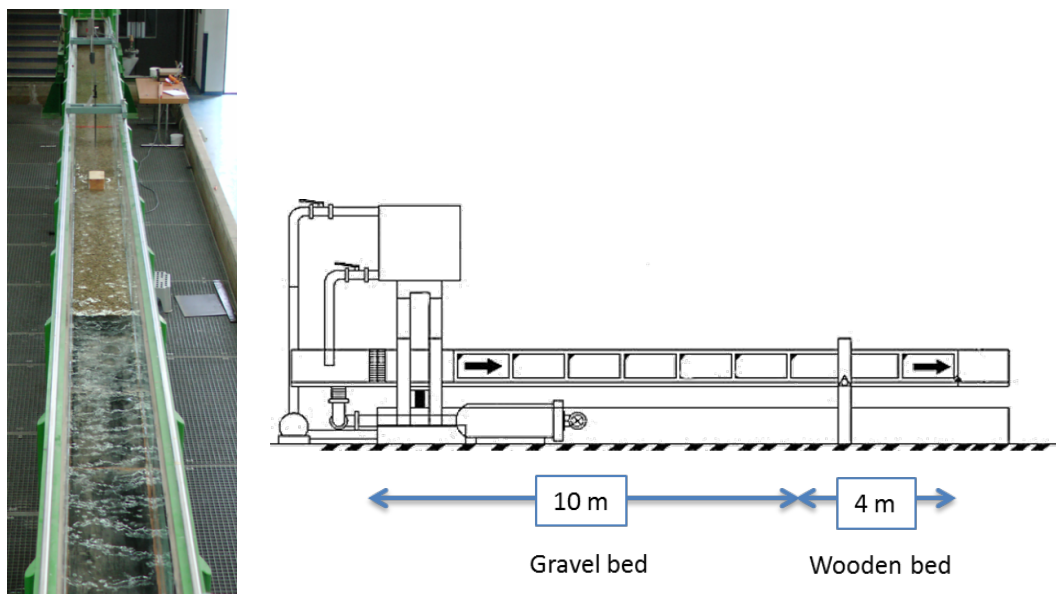


Figure 7-2: flume set up for fixed gravel bed trials.

One type of artificial roughness was investigated using bottom lining of gravel. Gravel was glued to the channel bottom, to investigate only clear water conditions. Literature suggests that for the entrainment of logs, water depth should be at least equal to half the diameter of log to entrain it. For the smallest size of LWD (13 cm), this leads to water depths of 6.0 – 7.0 cm. These values permit to get the full turbulent flow for relative large size of bed roughness. Hence even in these tests a gravel of 5-6 mm of diameter was used, corresponding to the gravel size used by Crosato in her previous experiments. The adopted grains were sharp edged and a single layer thick gravel bed was placed, covering the first 10 m of the wooden bed.

The same static friction between the wooden log and the fixed gravel bed used by Crosato was considered ($\mu_{bed} = 0.63$), obtained by pushing or pulling blocks across the test bed, in different positions, using a digital force gauge.

The bed slope gradient of the flume required for the experiments was very low, in order to reproduce the typical flow conditions of lowland river (0.1%-1%). Due to the subcritical nature of the flow the effects of any perturbation propagate back up to the channel, hence for a given discharge a really uniform steady flow was possible just at a certain distance from the end of the flume. The characteristic distance L_b upstream where the effect of a disturbance is felt, and normal depth is re-established, is known as the backwater length. A rough estimate of this distance could be established by 0.7-1.0 the ratio between the flow depth at the disturbance d_w and the down-channel slope of the river S_o (Parker, 2004).

$$L_b \sim 0.7 \div 1.0 \cdot \frac{d_w}{S_o} \quad (7-2)$$

Taking d_w to scale with the characteristic flow depth H_{bf} , some estimates of the backwater length are given below, where the subscript "bf" denotes "bank-full".

Table 7-3: typical Lowland rivers backwater lengths

River	Bed	H_{bf} (m)	S	L_b (m)
South Fork Clearwater River, Idaho, USA	Gravel	1.06	0.0055	0.2 km
Minnesota River, Wilmarth, USA	Sand	4.6	0.00019	24.2 km
Fly River, Kuambit, PNG	Sand	9.45	0.000051	185.3 km

As shown in Table 7-3, backwater lengths tend to be very long in lowland-piedmont rivers. Normal flow is an equilibrium state defined by a perfect balance between the downstream gravitational impelling force and resistive bed force, in the absence of any perturbation due to backwater. The resulting flow is constant in time and in the downstream, or x direction. The approximation of normal flow is often a very good one in mountain streams, but is not so realistic for lowland-piedmont rivers.

For flume experiments an accurate estimate of the backwater length could be obtained using the backwater formulation for steady, gradually varied flow under the constraint of constant water discharge Q and an imposed water elevation at the downstream boundary (Chanson, 1999; Chaudhry, 1993; Chow, 1959).

$$\frac{dy}{dx} = \frac{S_o - j}{1 - Fr^2} \quad (7-3)$$

in which Fr is the Froude number of the considered section, and j is the energy line slope, which could be evaluated as:

$$j = \frac{Q^2}{k_s^2 \sqrt[3]{R_H^4 A^2}} \quad (7-4)$$

where A and R_H are respectively the flow section area and the hydraulic radius of the considered section, k_s the Grauckler Strickler coefficient of the bed.

The water level profile could be obtained imposing the water depth at the end of the flume. Considering a free-fall condition this value could be taken coincident with the critical height y_c :

$$y_c = \sqrt[3]{\frac{Q^2}{gC_w^2}} \quad (7-5)$$

where C_w is the width of the flume.

Considering the maximum slope representative of Lowland rivers, and the discharge conditions at entrainment from the experiment of Crosato:

- $S_{o(\max)} = 0.002$ channel slope
- $k_s = 42.43 \text{ m}^{1/3}\text{s}^{-1}$ Gauckler-Strickler coefficient for gravel bed
- $C_w = 0.4 \text{ m}$ Flume width
- $Q = 0.0121 \text{ m}^3/\text{s}$ Discharge

The backwater length is about 70 m, as shown in Figure 7-3, obtained considering the critical depth of 0.0456 m, provided by Eq. 7-5. The dashed green line represents the normal water depth, 0.0954 m, calculated with Eq. 7-4 considering the energy line slope equal to the bed slope.

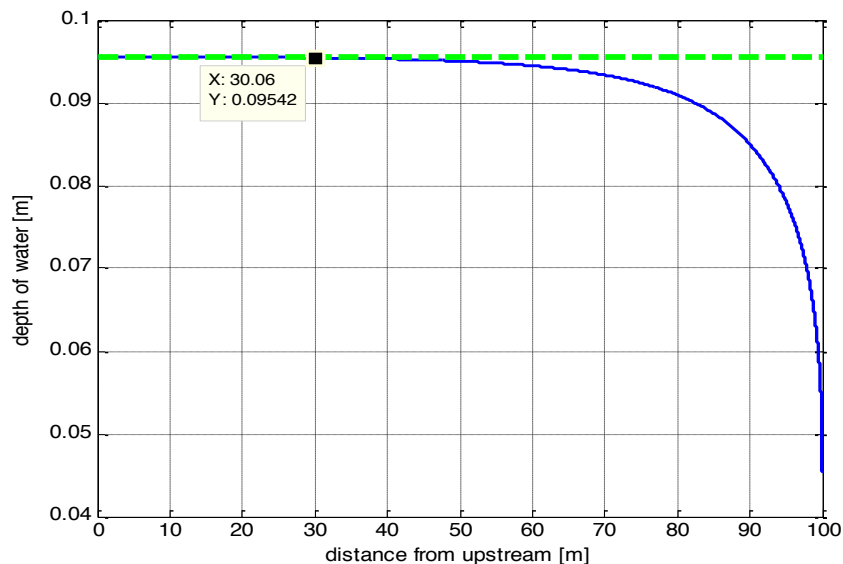


Figure 7-3: flume water surface profile for free fall condition.

The backwater length, and the corresponding normal water depths, becomes very high for smaller channel slope. In particular the depth of water characterizing normal flow is higher than the buoyancy depth, the water depth in which the dowel begin to float in still water. According to Eq. 5-1, the buoyancy depth for the dowels considered

in this work, characterized by a relative density ρ_{log}/ρ_w approaching 0.5, is about 0.075 m, half of the log diameter (see Figure 5-1).

Normally the tail water gate at the end of the flume is used to control the water level inside the channel, in order to obtain a constant water level. This approach leads to modify the tailgate for every discharge considered. In order to reduce the time required for a single measurement, the tailgate was not applied and the flume outlet was left as a free over-fall: the longitudinal water depth profiles were obtained considering Eq. 7-3 for gradually varying steady flow. In Figure 7-4 the simulations of the water level profile for some tailgate configurations are shown.

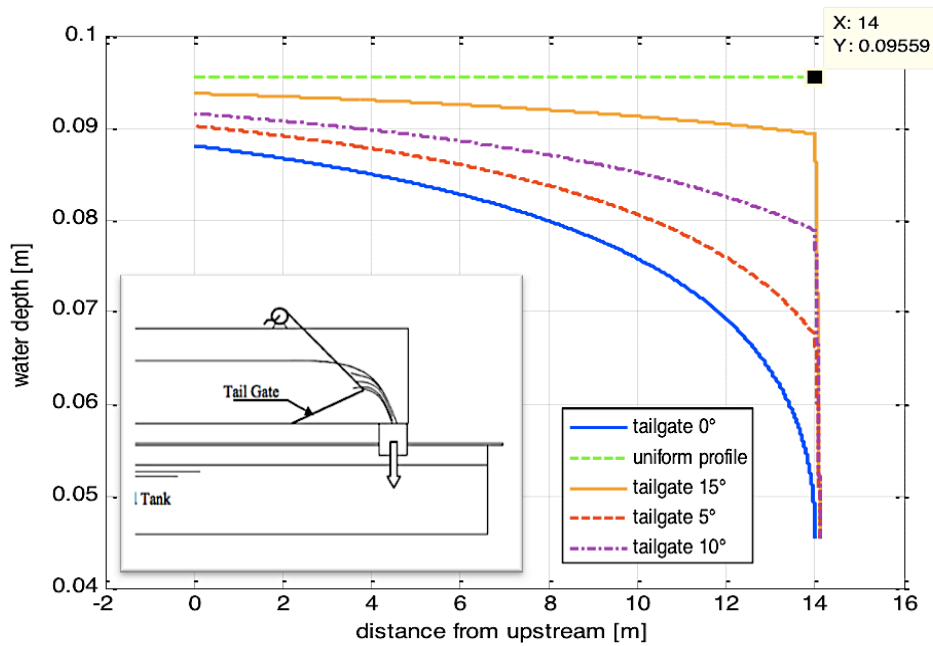


Figure 7-4: flume water level may be regulated by tail gate adjustment.

The free over-fall condition leads to a slightly accelerated flow, but if the log is not very long in the flow direction, as the cases considered in this work, the undisturbed water depth variation along the dowel is practically negligible and the undisturbed flow could be considered uniform. Furthermore, as stated by Alonso (2004) quasi constant flow accelerations of about 0.001 ms^{-2} are commonly observed in lowland rivers, making the experiment more representative of real situations, without alter significantly the drag and lift coefficients.

The water discharge was determined from the water height (H) measured over the sharp-crested weir, using the Rehbock formula:

$$Q = \frac{2}{3} \left(0.605 + 0.08 \frac{H}{Z} + \frac{0.001}{H} \right) \sqrt{2g} \cdot B \cdot H^{3/2} \quad (7-6)$$

where Z is the crest height in meters (according to Figure 7-5).

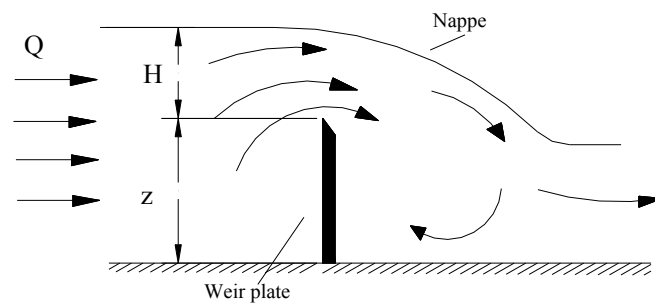


Figure 7-5: sharp crested weir geometry.

The flume was equipped with two-point gauges, with a resolution of 0.1 mm, one for measuring the water depth one for deriving the water discharge. Paper scale of 100 cm was attached to the flume wall for quick observation of longitudinal and vertical log movement as well as rough water depth measurement. A camera placed in front of one sidewall of the flume registered the trials for the entire duration.

7.3 RESULTS

For each test the water level at the log entrainment was measured near the flume position occupied by the dowel, as well the discharge, the undisturbed water level, and the weight of the log before and after the test, as shown in Table 7-4, in which a sample of the registered data during the tests performed in Delft is reported.

Table 7-4: example of the collected data for one type of test.

test No.	log shape	initial log orientation angle with flow [deg]	Entrainment discharge [l/s]	type of motion
10	smoothed square	<i>parallel to the water flow</i>	9.16	sliding
volume [cmc]		4390.52		
initial weight [g]		1936.0	density [kg/mc]	441
final weight [g]		1990.6	density [kg/mc]	453
distance from upstream boundary [m]		gauge reading at flume [cm]		remarks
		bed level	water level	
6.80		7.00	15.53	<i>20 cm upstream of log</i>
6.99		6.88	16.40	<i>1 cm upstream of log</i>
7.26		7.10	12.50	<i>1 cm downstream of log</i>
7.45		7.40	13.10	<i>20 cm downstream of log</i>
4.00		6.89	14.98	<i>undisturbed water depth</i>
7.00		7.19	13.93	
9.00		7.17	13.10	

The collected experimental data have been subsequently utilized to estimate, at the incipient motion condition, all the quantities taking part in the evaluation of the three proposed entrainment parameters (according to Eqs. 6-82, 6-83, 6-84). Actually these quantities are not directly measurable according to the experimental procedure. At the instantaneous condition of the log entrainment, the criterion expressed by Eq. 6-81 becomes an equality and the threshold value E_p^* can be therefore estimated.

In order to increase the reliability of the performed results analysis, additional experimental data, taken from literature, have been considered. In Table 7-5 are summarized the principal characteristics of the experimental settings employed to collect the examined data (for details refer to Bocchiola et al. 2006, Crosato et al. 2011, and to paragraphs 7.2.1 and 7.2.2 of this chapter). In all the mentioned experiments two different orientations of the dowels were explored, respectively parallel and perpendicular to the water flow direction.

Table 7-5: flume and dowels properties in the Bocchiola, Rulli and Rosso experiment (BRR 2006) and in the Delft experiments performed by Crosato and her group in 2010 (AC 2010) and by Vergaro in 2011 (AV 2011).

TEST	FLUME PROPERTIES					LOG PROPERTIES				
	Length [m]	Width b [m]	Slope if [m/m]	grain size Ds50 [m]	bed roughness n	cross section	log length [m]		log width [m]	edges
BRR 2006	30	1	0.006	0.002	0.016	circular	0.25	0.5	0.027÷0.099	sharp
AC 2010	14	0.4	0	0.005-0.006 wood bed	0.024 0.014	circular/square	0.25		0.13/0.15	sharp
AV 2011	14	0.4	0	0.005-0.006	0.024	circular/square	0.25		0.13/0.15	sharp/smoothed

The obtained values of the threshold value E_p^* , evaluated for different experimental conditions (referring Table 7-5), have been subsequently analysed to identify the relationship between the threshold value and the dimensionless quantities necessary to describe the physical phenomenon, according to dimensional analysis reported in section 7.3.3 and resulting in Eq. 7-10.

The following sections contain the examination of the experimental conditions observed during the Delft tests, and the regression analysis of the whole available experimental data.

7.3.1 Preliminary experimental data analysis

In order to correctly evaluate the threshold value E_p^* from the experimental data, care have to be taken in the estimation of all the derived dimensions required to calculate the proposed Entrainment parameters (Eqs. 6-82, 6-83, 6-84). In particular: a) the mean bed level, from which is possible to evaluate the water depth at the entrainment, b) the correct density of the log that could change due to the porosity of wood, c) the undisturbed velocity profile in the position of the log, in order to evaluate the lever arm of the drag force (refer to Chapter 6.3.2), d) the backwater prediction capability of

the proposed approach (refer to section 0), as it allows to consider experimental data from literature, for which the drag coefficient provided is usually roughly estimated and is affected by great uncertainties.

In the following sections these aspects have been investigated.

7.3.1.1 Water depth estimation

Water depth is normally obtained as the difference between the gauge readings at water level and bed level. Due to the presence of the gravel, the measure of the bed level was affected by the position of the gauge: little displacement of the gauge around the measuring point produced random variation of the measured depth, naturally related to the roughness of the bed. In order to increase the accuracy of the water depth evaluation, the mean value (7.18 cm) of the bed level was considered.

Given N samples (36 for the case considered) the accuracy of the estimate of the mean of the parent population could be estimated by the standard deviation of the mean, which is related to the standard deviation of all the data:

$$\sigma_{\bar{x}} = \frac{\sigma_x}{\sqrt{N}} \quad (7-7)$$

The standard deviation of the measured data is 0.222 cm. Thus the accuracy of the mean bed depth could be stated to be ± 0.04 cm.

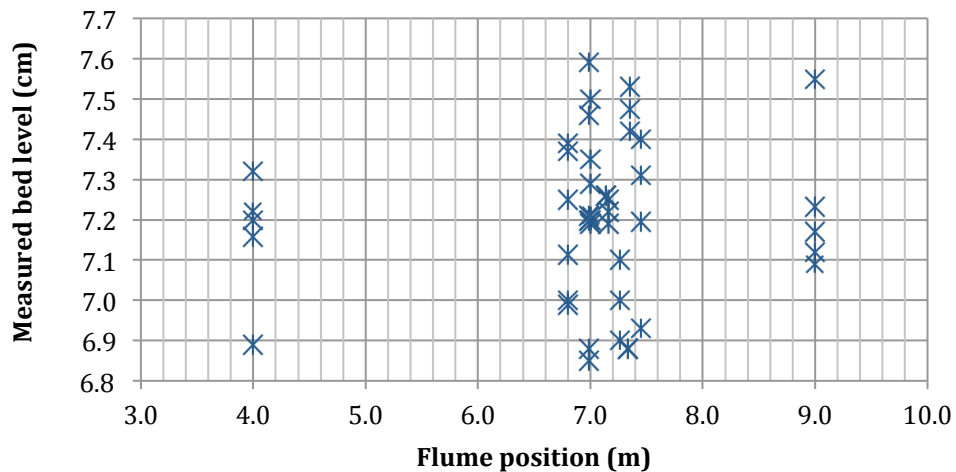


Figure 7-6: measured flume bed level at different locations.

7.3.1.2 Log density variation

The first data to be analysed is the density of the log at the entrainment. Density in fact is strongly related to the main force acting in the vertical direction, the weight

force, which affects buoyancy. Density has been calculated from the weight, considering the volume of the log. Due to the porosity of wood, density could change significantly during the test. An example of the variation of the density for different tests is reported in Figure 7-7.

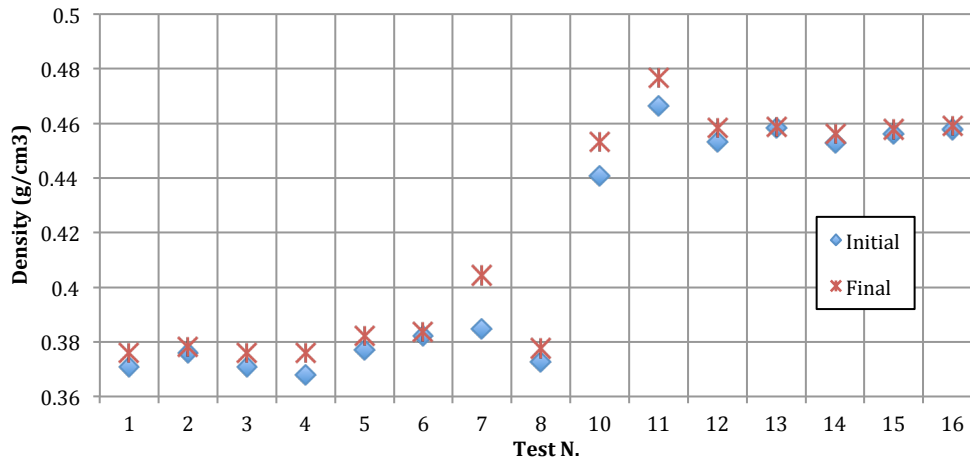


Figure 7-7: density variation during different tests.

As shown the final density of dowels is always greater than the initial one, even if this variation is very low due to the type of wood considered, and the short time of resting. Clearly the final density has to be considered for the correct evaluation of the entrainment condition. This could lead evident difficulties for the application of the proposed approach, as this value is difficult to obtain from the field survey. Moreover it could change with time depending from natural deterioration of wood due to climatic, mechanical and biologic factors (alternation of wet and dry conditions, impacts, parasites). Despite these difficulties, as stated in section 6.2, it is possible to predict the final density of the log starting from the moisture content and the contact period with water, evaluable by the water level increment (0.1 mm/min), and the differences between the measured final and initial water depth. For the wood considered (an hard, waterproof wood) it is reasonable to assume an absorption coefficient A_w of $6.0 \text{ g m}^{-2} \text{ s}^{-1/2}$. The initial water content of the wood could be established considering the mass of the dry dowel, and the equilibrium moisture content M_{eq} at the relative humidity h and temperature of the surround air. The mean error provided was about of 1%, adequately accurate for risk assessment analysis.

7.3.1.3 Flume characterization: undisturbed velocity profiles

In order to apply the proposed approach, the undisturbed flow conditions have to be known at the position of the log. Discharge and water depth at the entrainment were directly measured, while the unknown parameters were obtained by numerical simulations of the flow field, solving the one-dimensional steady flow Eq. 7-3: if we

consider a gradually varying flow with $dy/dx \ll 1$ it is reasonable to impose the one-dimensional velocity assumption. In particular discharges and undisturbed water depths were used to define the manning coefficient for both gravel and wood bed.

Experimental data from Crosato (2011) were also considered, in order to increase the accuracy of the flume characterization.

In Figure 7-8 is reported an example of the water profile provided by the simulation for a discharge of 0.012 mc/s, in which is possible to note the change in the free surface in correspondence of the end of the gravel bed at 10 m from the upstream flume inlet, due to the change of the manning coefficient.

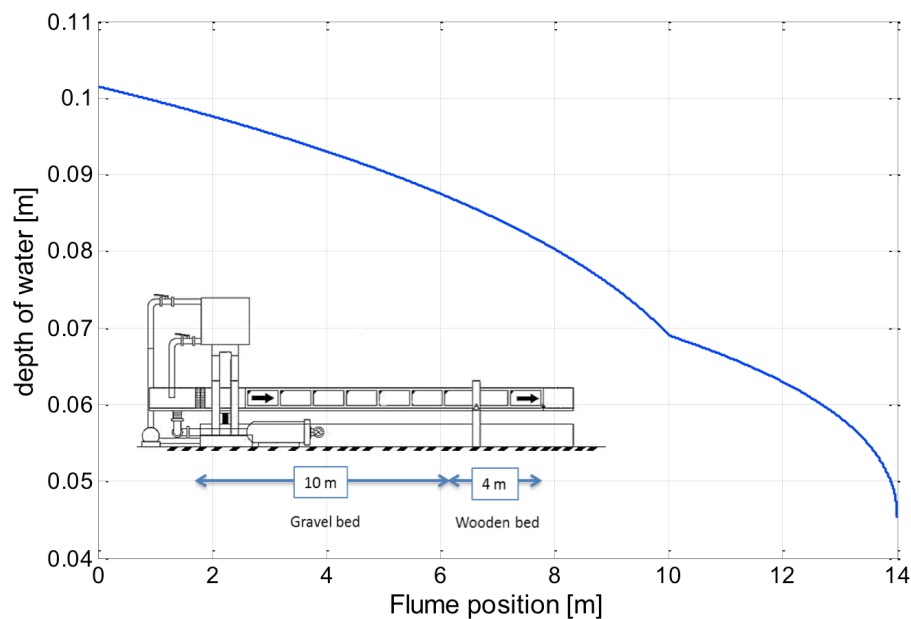


Figure 7-8: water surface profile obtained the one-dimensional steady flow equation.

The manning coefficients were then estimated by a simple model updating technique, based on least square method, applied to the measured flow chart of the flume: the following manning's roughness, analogous with the values found in literature, were provided:

- Wood bed: $n=0.014$
- Gravel bed: $n=0.024$

In Figure 7-9 and Figure 7-10 the measured water surface elevations for a given discharge (highlighted with the diamond symbols) have been compared with the discharge curve provided by the numerical simulation, showing an excellent correlation with a max error of 5.6 % for low discharges: the first refers to the section at 5.5 m from the inlet for the wooden bed flume, the latter to the section at 7 m from the inlet for the gravel bed flume.

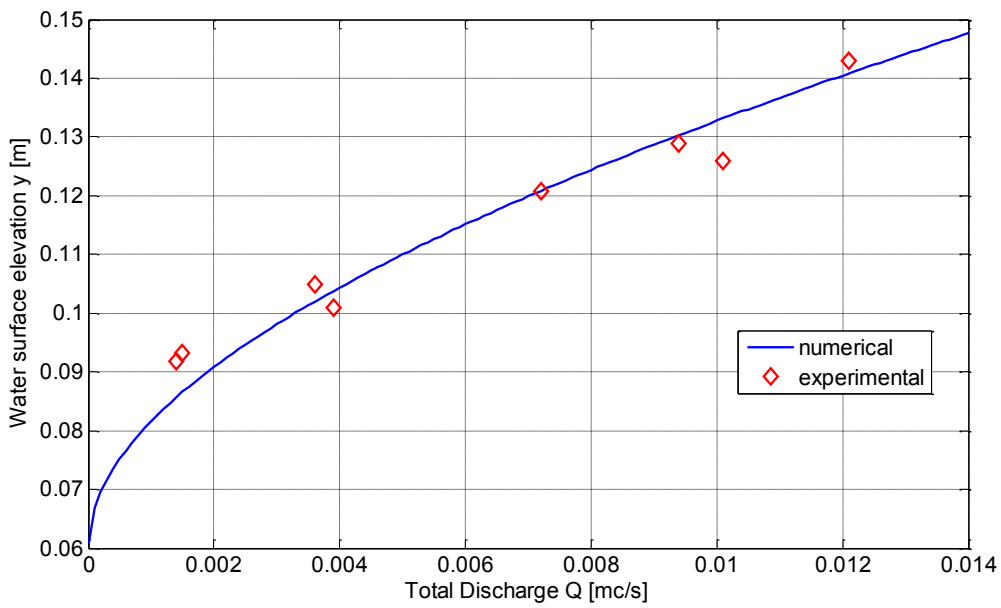


Figure 7-9: comparison between measured and modelled water depth for different water discharge at 5.5 m from the inlet. Referring to the wooden bed flume.

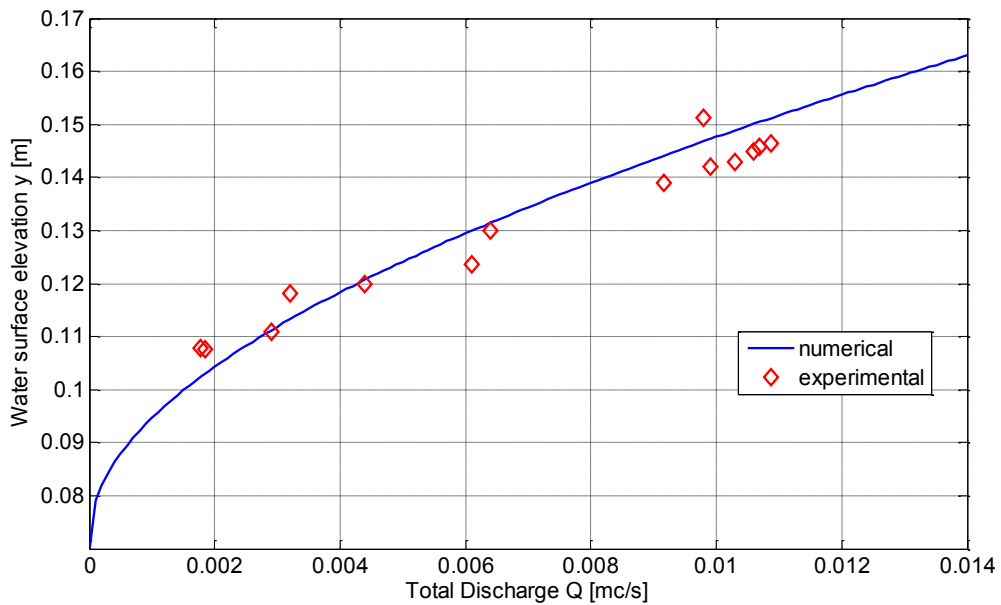


Figure 7-10: comparison between measured and modelled water depth for different water discharge at 7.0 m from the inlet. Referring to the gravel bed flume.

Results have been also compared with those provided by HEC-RAS in order to verify the algorithm implemented for the water depth profile along the flume, exhibiting a reliable agreement.

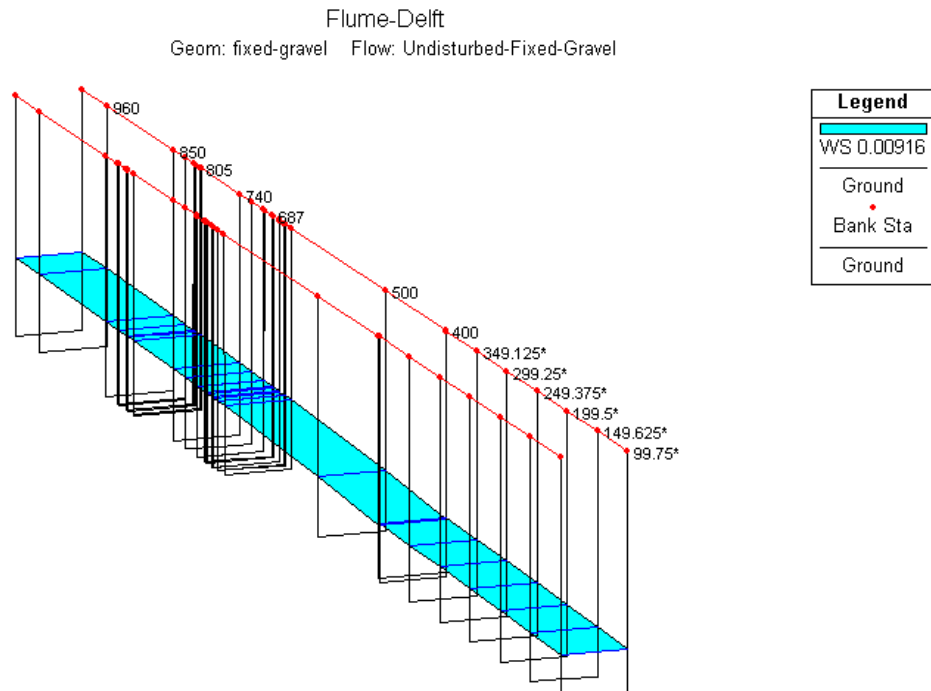


Figure 7-11: flume modelled with HEC-RAS.

The results of the simulation run in HEC-RAS (Figure 7-11) could be summarized in the following Figure 7-12, showing the water depth as a function of the main channel distance, for different value of the discharge.

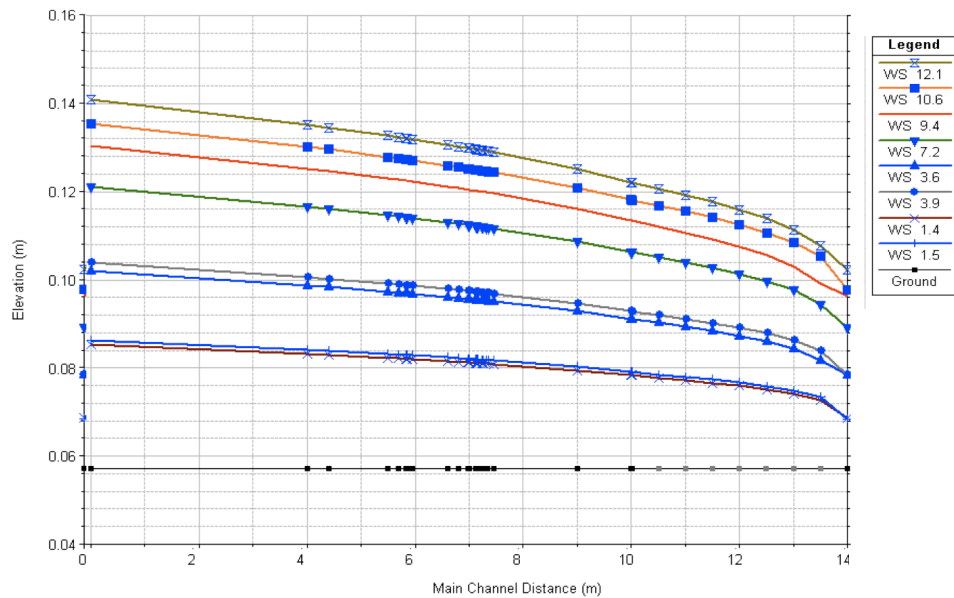


Figure 7-12: water profile modelled with HEC-RAS for different discharges.

Due to the non-uniform condition of the stream in the flume, the flow acceleration was calculated in order to verify if it was slight enough to be considered negligible, or otherwise compatible with that referred by Alonso as typical of Lowland rivers, and small enough to not alter significantly the drag and lift coefficient.

In the worst case, considering the higher discharge registered at the entrainment, the flow acceleration in the test location was 0.0055 m/s^2 , as shown in Figure 7-13, which is of the same order of the value provided by Alonso: 0.001 m/s^2 , providing inertia forces that are 1 or 2 order lesser of the drag forces.

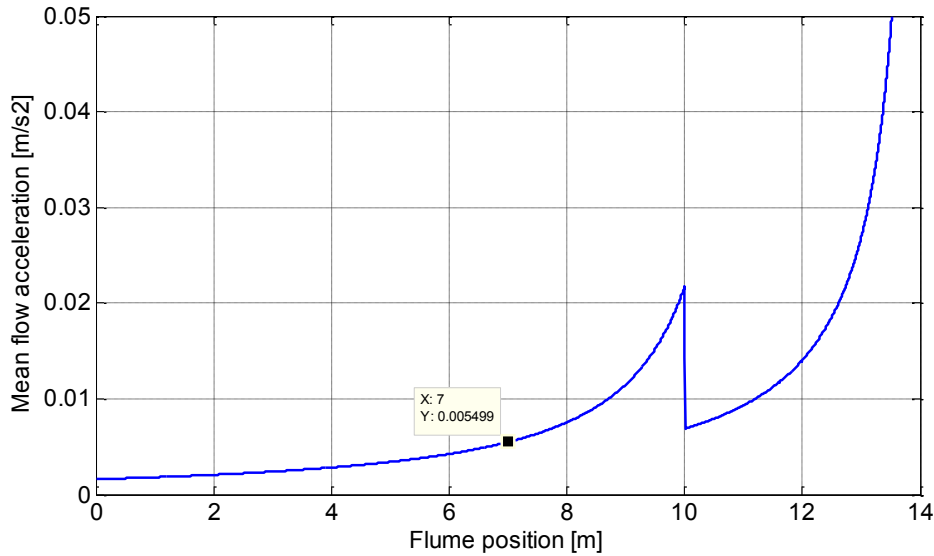


Figure 7-13: acceleration of the flow provided by the simulation.

The use of the simulation has allowed using the experimental results produced by Crosato in a previous research, taking into account the different log positions shown in Figure 7-14.

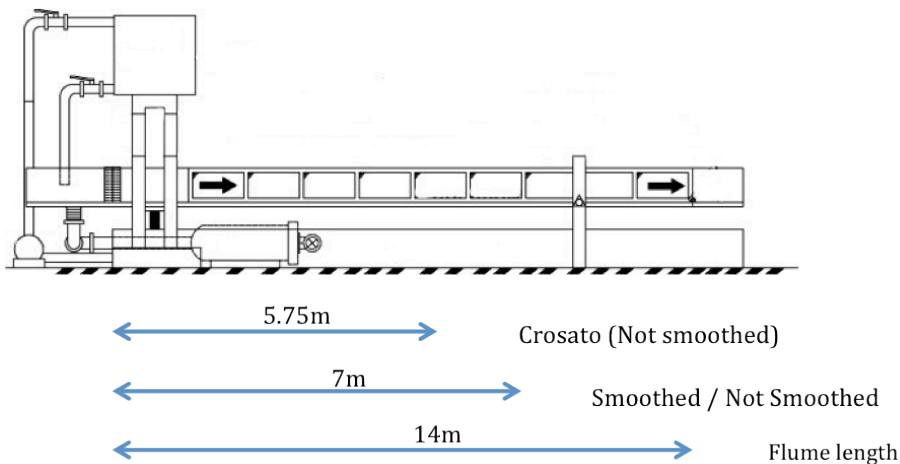


Figure 7-14: experimental location for different tests.

As the flow is not uniform in the stream-wise direction, different sections along the flume show different flow characteristics at the same discharge. In Figure 7-15 the measured undisturbed water depths for fixed gravel bed are summarized, for different discharge: the solid red line and the dashed blue line represent the position of the logs, respectively for Vergaro and Crosato tests.

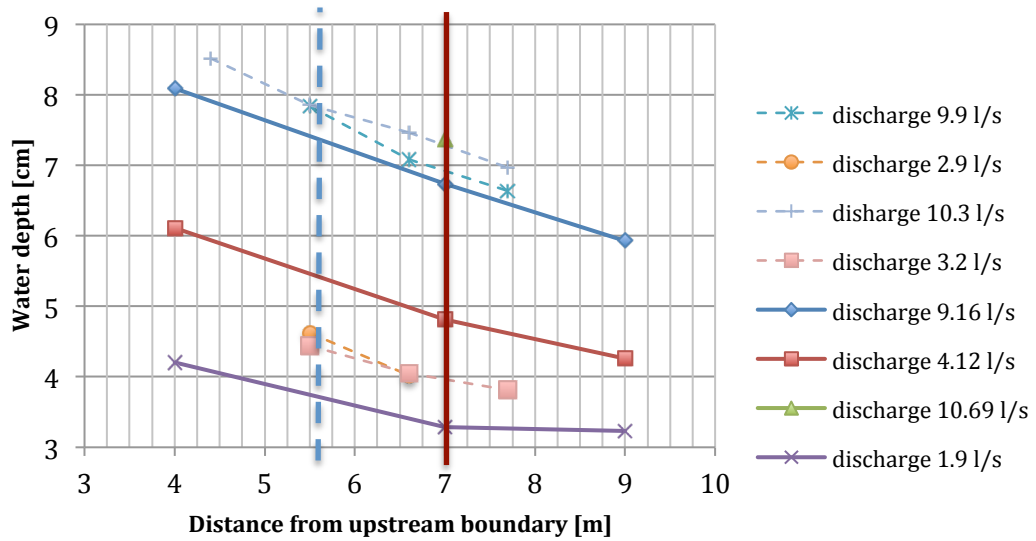


Figure 7-15: measured water depth at different discharges and undisturbed conditions; different locations for experimental tests are marked.

For a given discharge it is possible to obtain the velocity profile, which is necessary for the rough estimate of the lever arm of the drag force (refer to section 6.3.2). An example of the calculated profiles is represented in the following figures (Figure 7-16 and Figure 7-17) for the same dowel at the entrainment. In particular the blue and the red lines represent the undisturbed velocity profile at the entrainment for two tests performed in the same cross section but with different bed roughness, while the green line refers to an experiment performed in a different cross section with the same roughness of the blue test. Even in this case it is possible to verify that the flow condition at the entrainment could be different for the same dowel (identical shape and orientation) depending on the Froude number and the bed roughness.

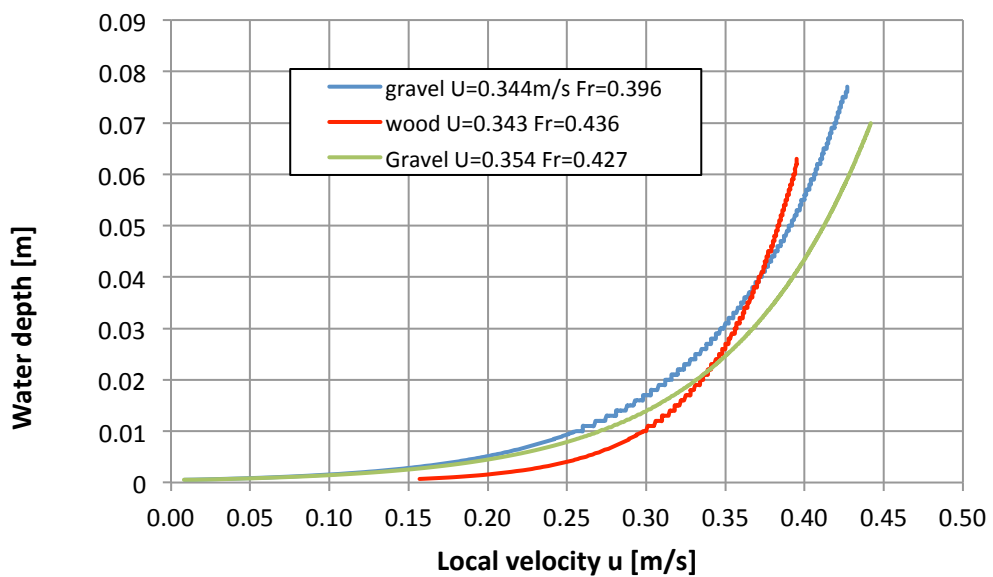


Figure 7-16: velocity profile at the entrainment for equivalent dowels shape and orientation but different bed roughness or experimental location.

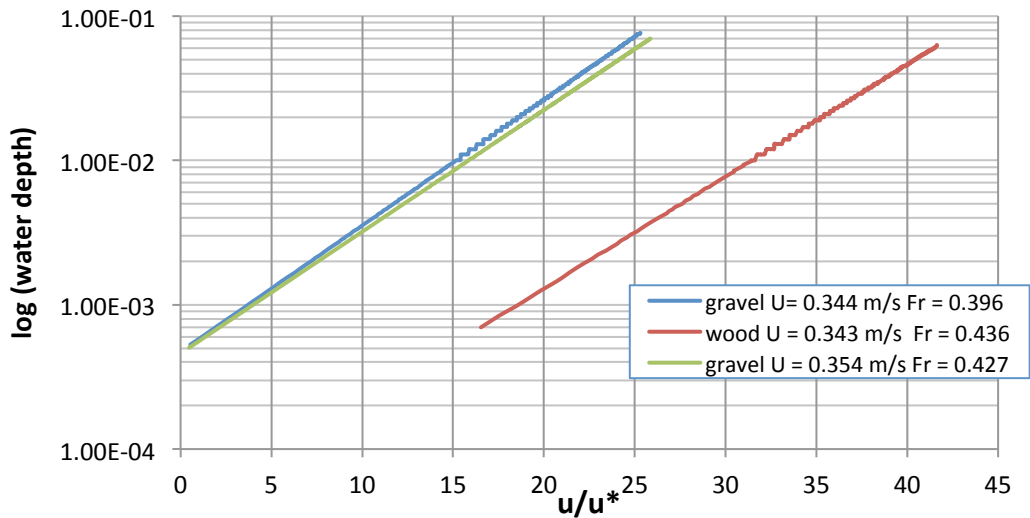


Figure 7-17: velocity profile at the entrainment for equivalent dowels shape and orientation but different bed roughness or experimental location (u^* is the friction velocity).

Comparison between the mean velocity, obtained by the measured discharge, and the value obtained integrating the velocity profile, shows that the log-shaped velocity profile is the correct one for most of the cases considered. When the water depth is small compared with the roughness of the bed this is not true, as is the case of some tests carried out by Bocchiola et al. (2006), which therefore have not been considered for the subsequent analysis (section 7.3.2 and 7.3.3).

7.3.1.4 Backwater prediction

As stated in chapter 6.3, one of the main novelties of the proposed approach is to relate the drag force acting to the log to the backwater upstream of the obstacle. This consents to have a better estimate of the effective drag force, which is difficult to experimentally evaluate. In Figure 7-18 is shown the typical backwater rise experienced during the tests.



Figure 7-18: backwater rise induced by the presence of a dowel perpendicular to the streamwise direction, corresponding to a blockage ratio of 0.63.

Relating the drag force to the backwater rise allows using the relationships found in literature (refer to section 6.3), reducing the uncertainties in the evaluation of the drag coefficient, due the complex phenomena related to the standing surface wave generating along the partially submerged log surface in the stream-wise direction.

The first step is therefore verifying the capability of these relationships to predict suitable values for the backwater rise in presence of the log (Figure 7-18). In Figure 7-19 a comparison between the numerical (refer to paragraph 6.3.1) and measured water depth upstream of the log is reported. The experimental water depth is that measured 20 cm upstream of the log, which could be reasonably considered representative of the backwater rise.

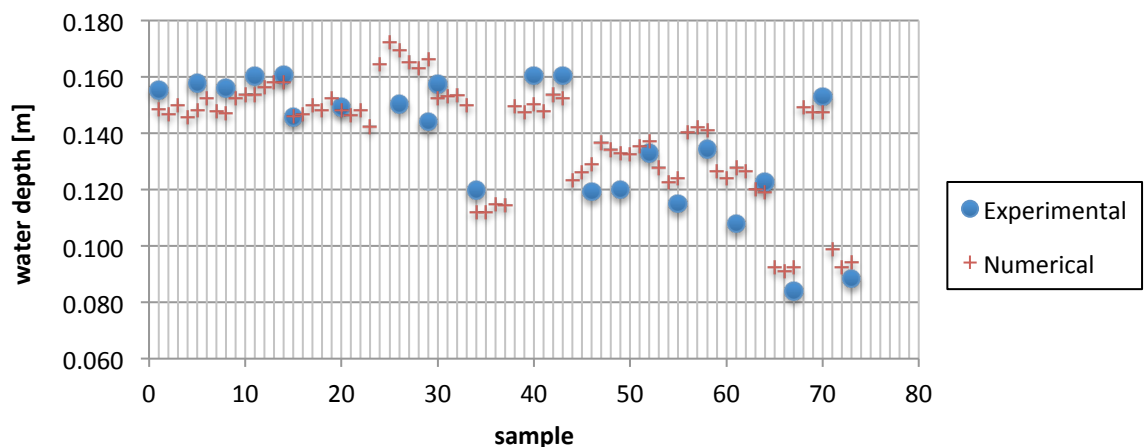


Figure 7-19: experimental and numerical water depth due to backwater for different tests.

The relationships found are able to predict with a reasonable precision the backwater rise due to the partially submerged body. This allows taking into account even experimental data from literature, for which the drag coefficient provided is usually roughly estimated or taken from literature.

7.3.2 Analysis of the incipient motion condition during tests

The entrainment modes detected during the tests have been exclusively sliding and rolling modes, according to what expected observing the tendency revealed in Figure 6-20: simple buoyancy may occur only if there are impediments to the other motion modes (e.g. bed sediments).

The explored range of Froude and Reynolds numbers, at the Delft flume, was respectively from 0.28 to 0.47, and from 2.3×10^3 and 2.8×10^4 , as shown in Figure 7-20 and Figure 7-21, consistent with representative values of flow depths and velocities occurring in natural streams for low flow condition, i.e. when logs in touch with bed can move (Braudrick and Grant, 2000).

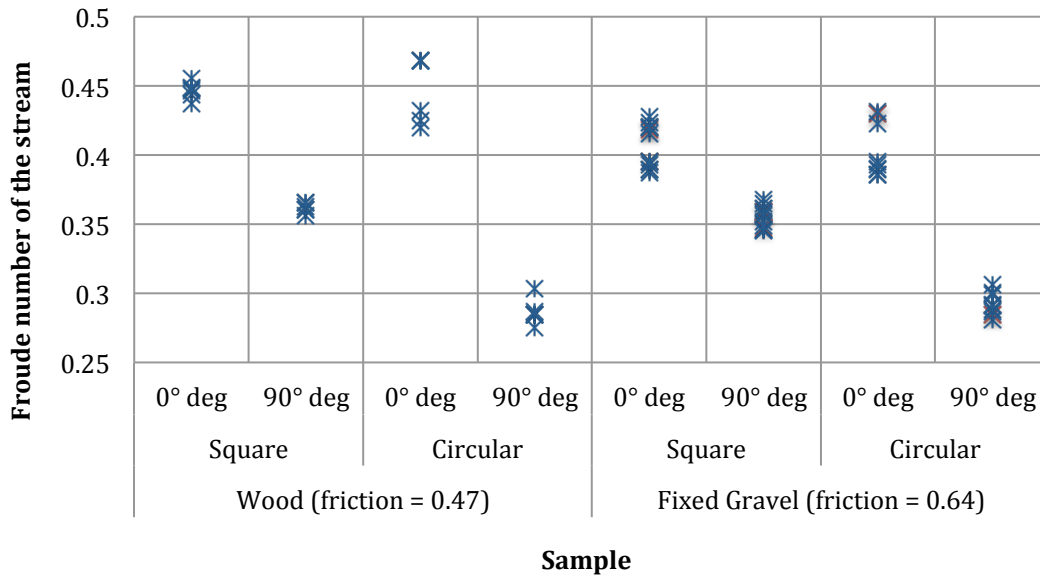


Figure 7-20: Froude number at the entrainment for different tests.

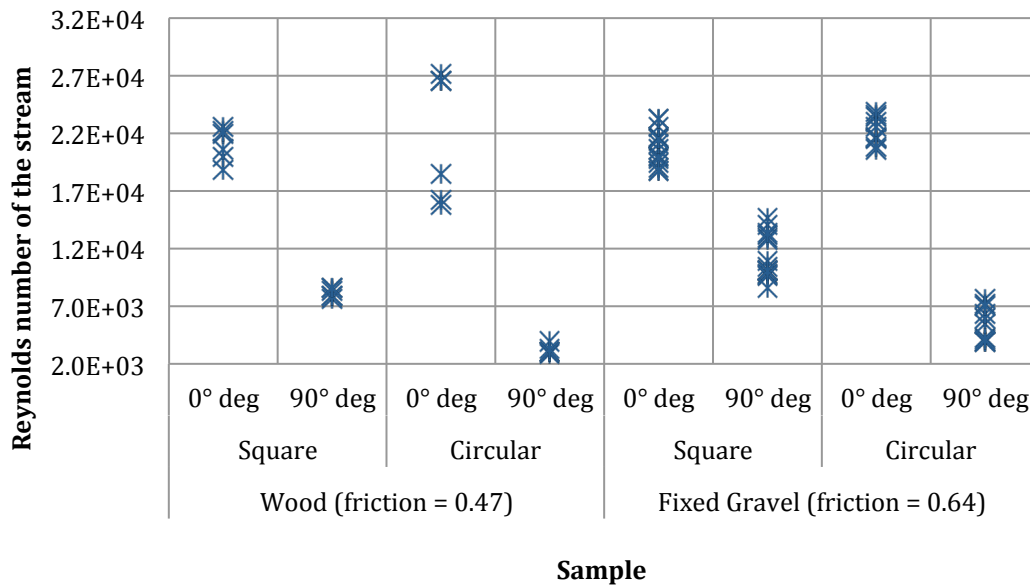


Figure 7-21: Reynolds number at the entrainment for different tests.

A summarizing picture of the Froude numbers of the experimental tests is shown in Figure 7-22. Examining this picture some observation may be done: comparing the behaviour of the smoothed dowels in box A with the sharp ones in box B, no evident influence of the shape of edge is detectable. Differences become more evident with higher Froude numbers, as can be observed comparing the sample in box C with the ones in box D, where the reported results refer to dowels parallel to the flow. Differentiations may be ascribed to the turbulence induced by the sharp edge, which produce a more fluctuating wave profile on the lateral surface of the log, even if the main shape of the wave seems to be not affected by it (Figure 7-23), in which are compared the surface water profile for sharp and smoothed edge dowels.

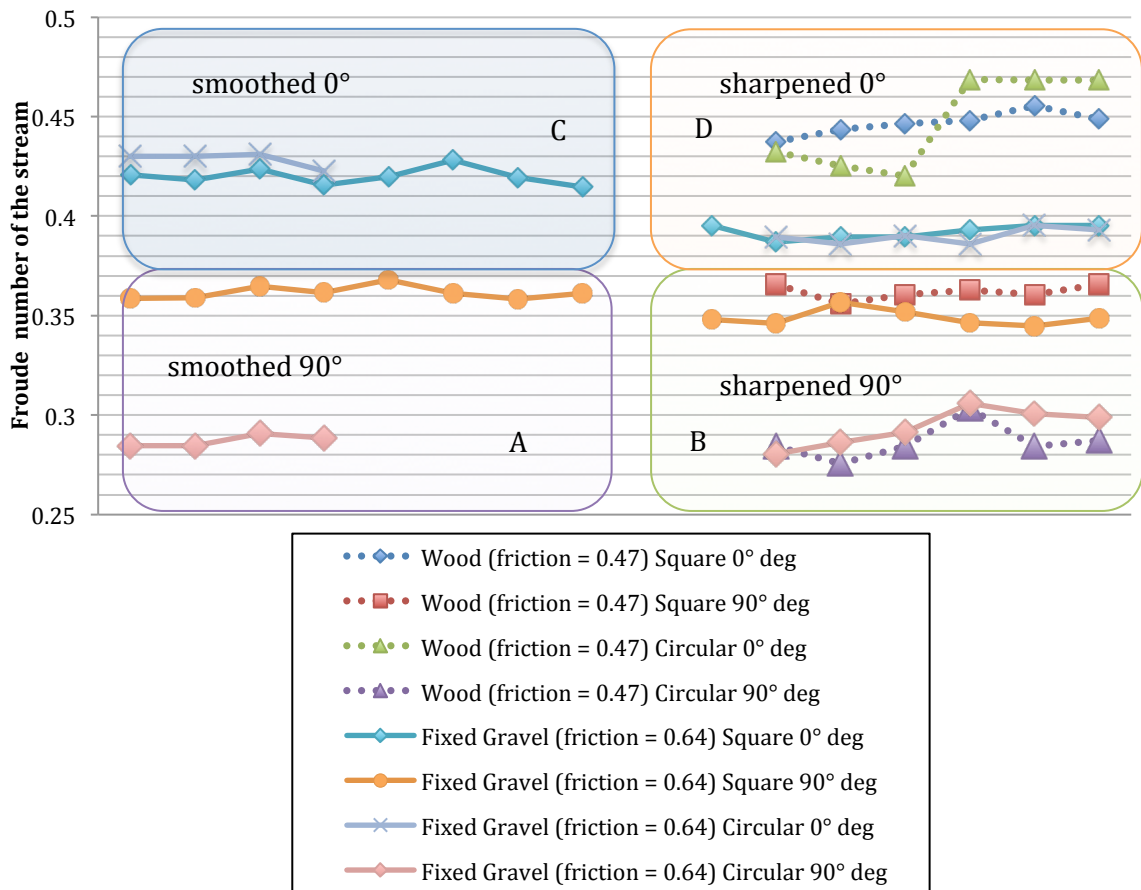


Figure 7-22: comparison of Froude numbers at the entrainment for different experimental conditions.

Comparing the sample in box D identically shaped dowels show different performance in conjunction with different roughness of the flume bed, suggesting the significance of the velocity profile developing along the water depth, which is certainly affected by flume bed roughness.

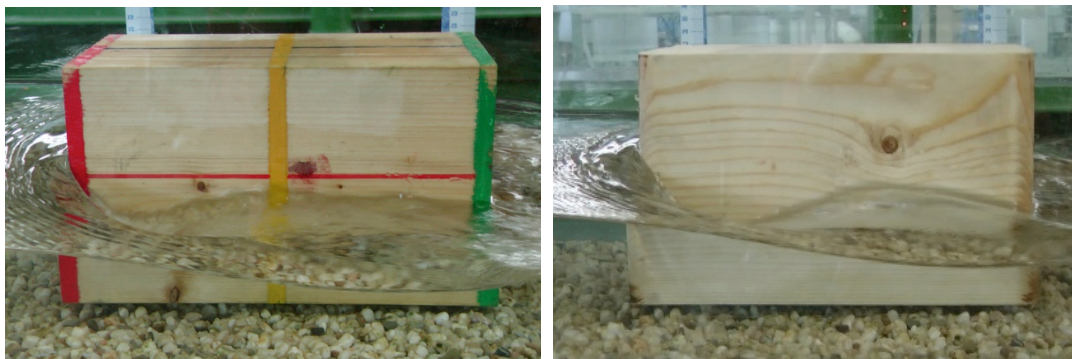


Figure 7-23: different surface water profile for sharp edged dowels and for smoothed edges dowels.

Blockage ratio, which surely greatly alters the flow field around the log, seems to not have a great influence on the shape of the standing wave, as shown in Figure 7-24, in which can be notice the same pattern of wave and wake for two different blockage ratio: the left picture refers to a value of the Br of 0.66, the right to 0.33.

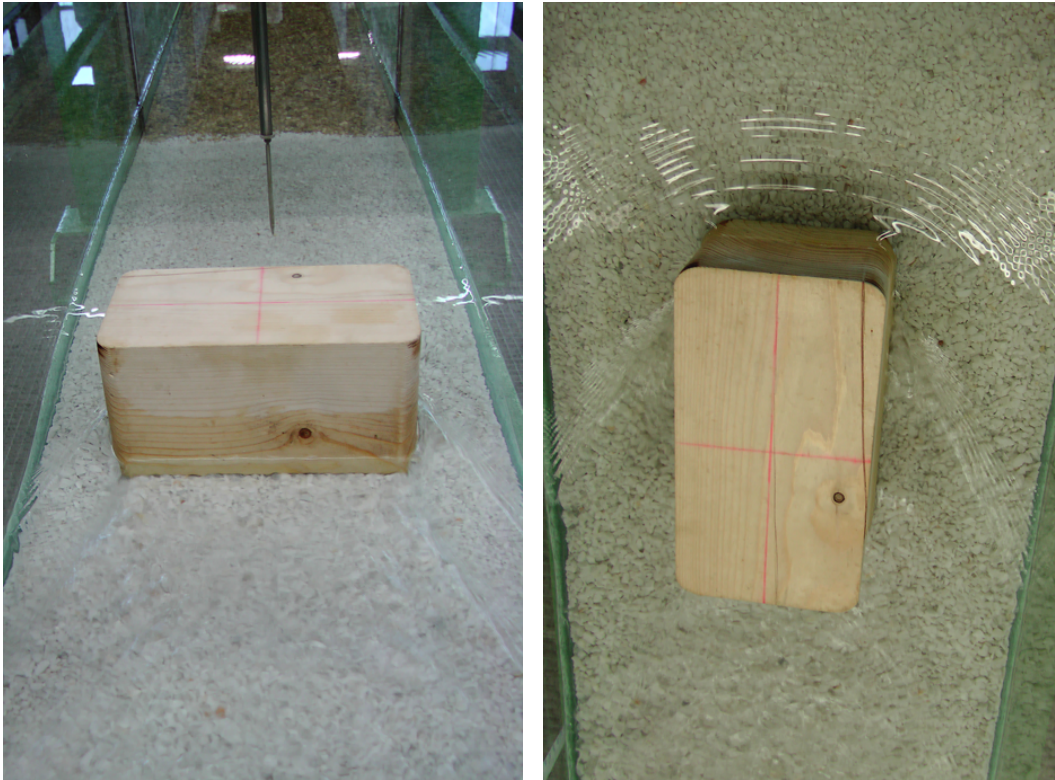


Figure 7-24: logs positioned in the two experimental orientations: perpendicular to the stream-wise direction (90°) on the left, parallel to the stream-wise direction (0°) on the right.

The slight influence of Blockage ratio on the wave shape is more evident considering the water profile along the stream-wise surface of the log in two really different conditions, as shown in Figure 7-25: the left picture refers to a value of the Br of 0.33, the right to 0.04 (data taken by the work of Bocchiola et al, 2006). The length of the log is the same (0.25 m).

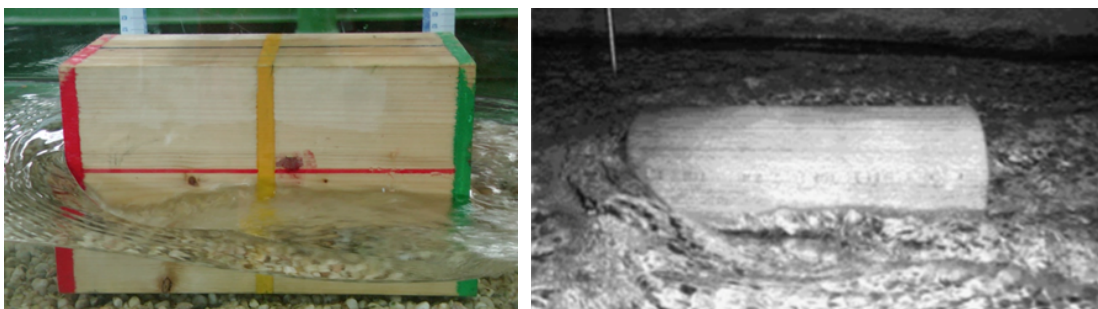


Figure 7-25: Water surface around dowels oriented parallel to the flow corresponding to different blockage ratio, 0.33 for the left picture, 0.04 for the right picture from Bocchiola et al, 2006.

Because buoyancy is strictly related to the wetted volume of the log, it seems reasonable to conclude that turbulence, and the macro eddies at the edge of the log, which surely have a great influence on the flow field and the drag force, do not affect significantly the threshold value E_p^* , being just related to buoyancy.

To investigate possible experimental correlations, the variation of E_p^* as a function of the main dimensionless parameters used in the context of LWD entrainment is

plotted in the following figures. In order to make easier to recognize the differences between the plotted data, different colours and marker have been used, accordingly to the following abbreviations:

- *AV-gravel*: indicates data from the flume tests performed within the present research work (filled symbols) using square and circular cylinders on fixed gravel bed, with the orientation parallel to water flow (0°), or perpendicular to water flow (90°);
- *AC*: denotes data from the flume tests performed by Alessandra Crosato and her collaborators using square and circular cylinders on fixed gravel bed (AC-gravel) or fixed wood bed (AC-wood), with the orientation parallel to the streamwise direction (0°), or perpendicular to the streamwise direction (90°);
- *BRR-sand*: indicates data from the flume tests performed by Bocchiola, Rulli and Rosso on fixed sand bed, with circular cylinders oriented parallel to water flow.

In Figure 7-26 the measured threshold value E_p^* versus Reynolds number Re of the flow is presented.

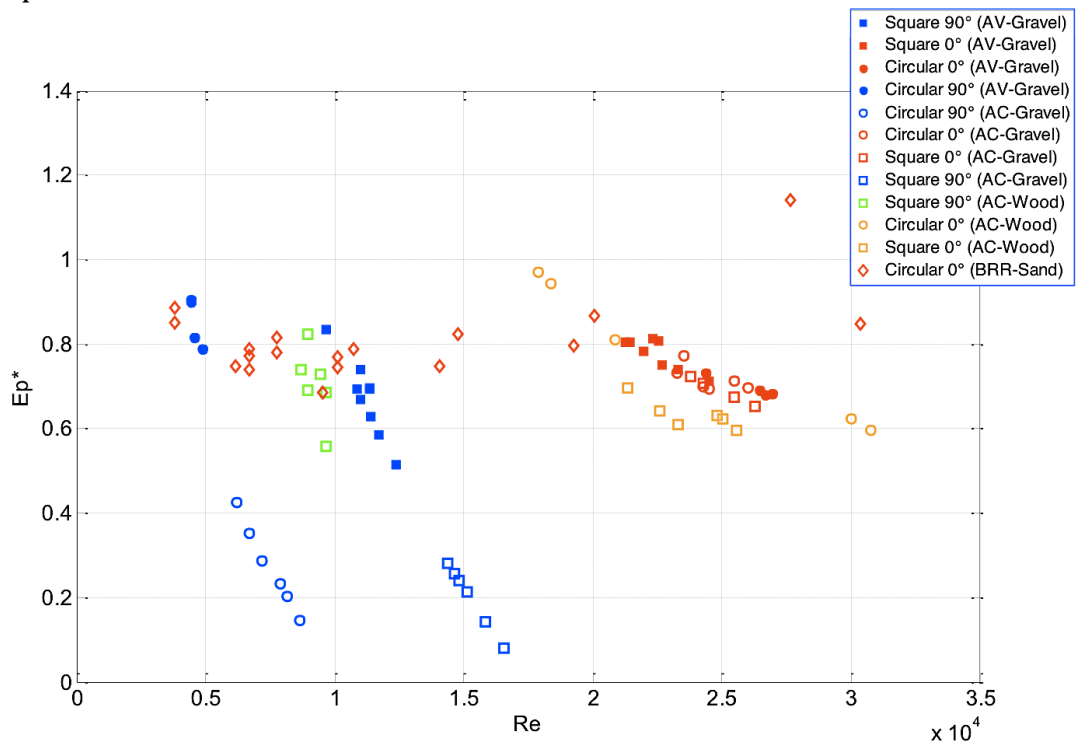


Figure 7-26: measured threshold values E_p^* of the entrainments parameters vs. the Reynolds number Re .

Differently from what expected, a correlation between E_p^* and the Reynolds number could be noticed, even if different relationships seems to exist for different dowel shapes (square and circular cross-sections) and different log orientations. Surely different entrainment modes play an essential role in this relationship, even if it is not possible to separate sliding mode, occurred for the entire dowel aligned to the

flow (0°) and rolling mode, the prevalent, but not the exclusive entrainment behaviour for log oriented normal to the stream-wise direction (90°).

Despite the flow around the log could be considered completely turbulent, the correlation with Re confirms the need to use a full-scale ratio between model and prototype in order to correctly represent both gravitational and viscous effects in the model (refer to section 7.1.1).

It is interesting to observe that for a given shape and orientation of the log, the threshold value E_p^* decrease as Re increase. According to the definition of the parameter E_p , which represents a measure of the effects of the standing wave on the buoyancy force, this result is analogue to what happens for a vessel increasing its speed: a sort of “wake displacement effect”, most clearly presents at the stern, usually reducing the stern wave height (refer to section 0).

A similar behaviour could be noticed for the Froude number, as shown in Figure 7-27.

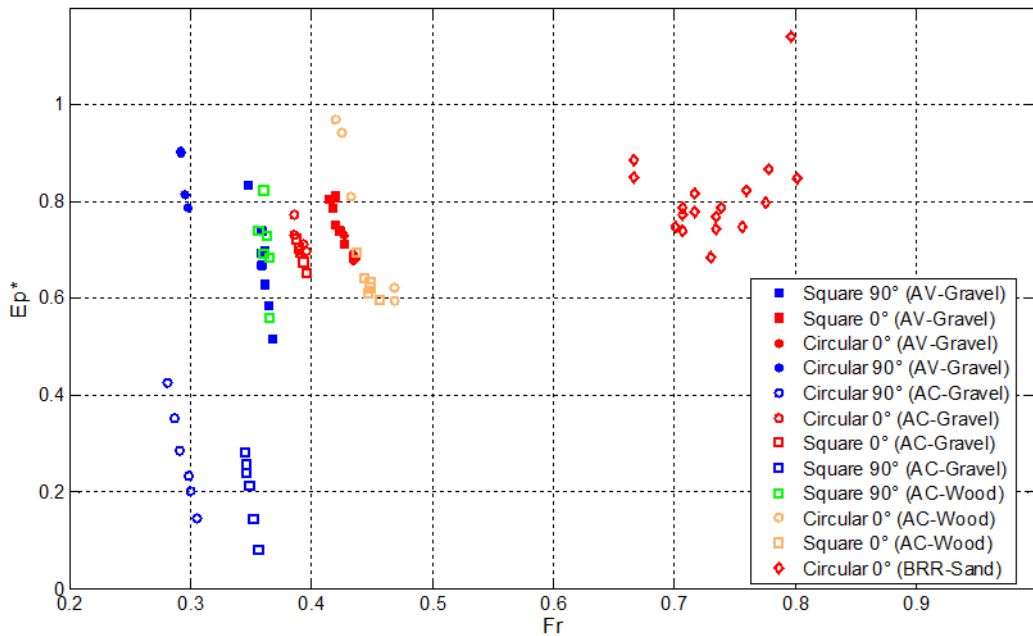


Figure 7-27: measured threshold values E_p^* of the entrainments parameters vs. the Froude number Fr .

Plotting E_p^* versus the blockage ratio it is noticeable that in correspondence of the investigated Br values, E_p^* assumes different values (see Figure 7-28). In particular in correspondence of $Br = 0.63$, E_p^* shows a relatively large variability. This behaviour may be explained with what observed during the experimental tests: $Br = 0.63$ relates to logs with an orientation of 90° with respect to the stream-wise direction, in this condition two possible entrainment modes were experimentally observed: rolling or sliding; mainly related to the dowels cross section. This does not happen for logs parallel to the flow direction, which during the tests move exclusively according the sliding mode.

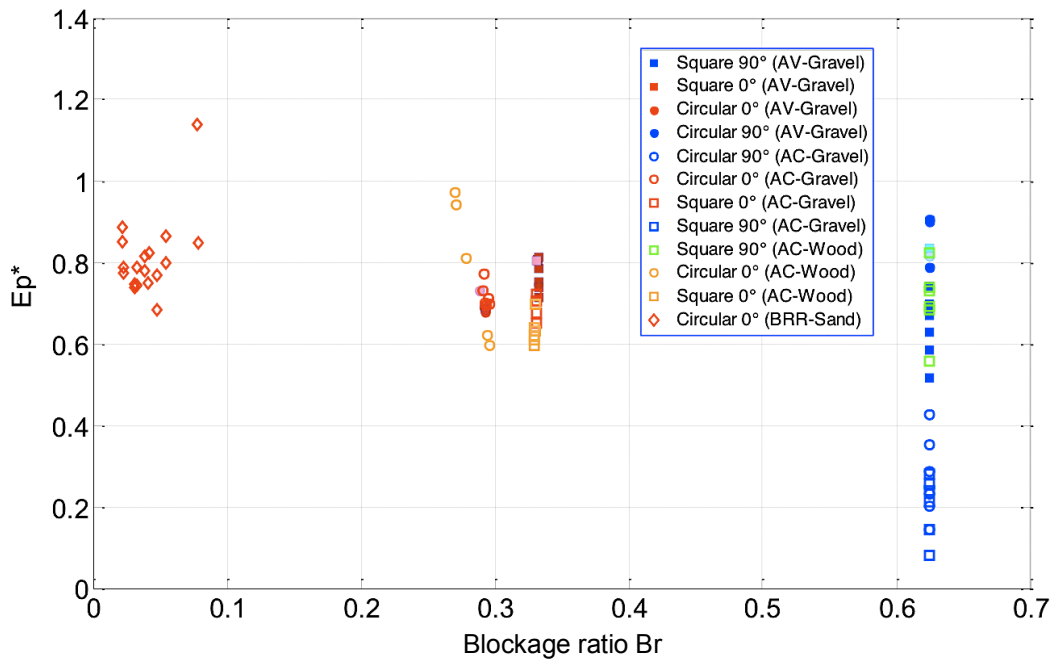


Figure 7-28: measured threshold values E_p^* of the entrainments parameters vs. the blockage ratio Br .

A different behaviour is observed considering the dimensionless parameter related to the shape, and density of the log, even if it is not so easy to recognize a well-defined trend of data.

A marked scattered dependence with the relative submergence could be notice in Figure 7-29.

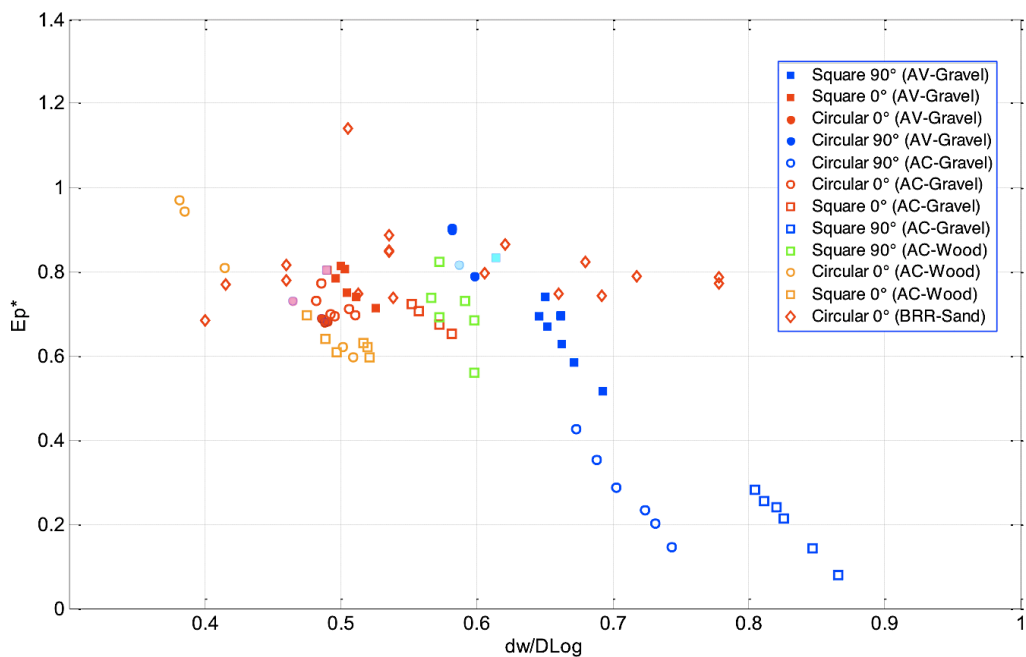


Figure 7-29: measured threshold values E_p^* of the entrainments parameters vs. relative submergence d_w/D_{log} .

The influence of the relative density ratio is shown in Figure 7-30. Scatter of data shows a random distribution, without a defined pattern.

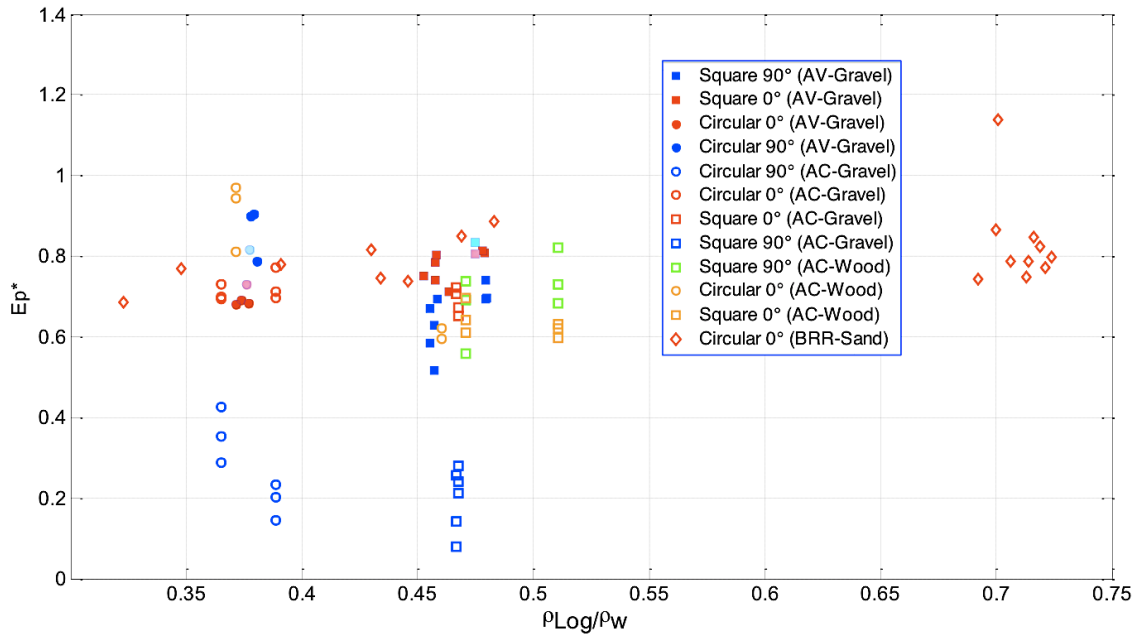


Figure 7-30: measured threshold values E_p^* of the entrainments parameters vs. the relative density ratio ρ_{log}/ρ_w .

7.3.3 Evaluation of the entrainment threshold: regression analysis

The entrainment condition $\min\{E_p^s, E_p^r, E_p^b\} \leq E_p^*$ states that log will be destabilized by the flow when the ratio between the buoyancy force and the reference one (the force acting according to the Archimedes' law in case of still water at the undisturbed water depth) reaches a threshold level, depending on the flow conditions, the shape and the main dimension of the log and the provided blockage ratio. At the incipient motion this threshold value can be evaluated, as it matches the minimum value of the proposed entrainment parameters, which can be evaluated according to the developed novel approach. The main objective of this experimental data analysis was then to identify an empirical relation for the entrainment threshold value E_p^* .

Because the confidence level of a parameter is strictly related to the number of samples, to increase the reliability of the threshold value proposed, data from literature were taken into account. In particular, data from the experiments of Crosato (2011), and Bocchiola (2006) were considered. The proposed approach was applied considering the entrainment conditions provided by the authors.

From dimensional analysis, analogously to that provided for the drag coefficient, the entrainment threshold E_p^* of a partially submerged obstacle can be expressed in terms of a functional equation. Entrainment is traditionally expressed (i.e. Bocchiola et al., 2006) in terms of some of the following dimensionless parameters: Reynolds (Re) and Froude number (Fr) of the flow, the blockage ratio of the dowel (Br), its

slenderness (L_{log}/D_{log}), the submergence ratio (d_w/D_{log}), the density ratio (ρ_{log}/ρ_w), the shape factor of the log K_s , and the angle between the log and the flow direction (θ).

Most of the above parameters are indeed included in the expressions used for the calculus of the entrainment parameters (Eqs. 6-82, 6-83, 6.84). For example the shape factor K_s and the blockage ratio are explicitly considered in the expression of the backwater rise, equally θ included in the equation for the evaluation of the blockage ratio, in case of angled log. Nevertheless any parameter suited to express the relationship between the variation of the buoyancy force and the wave produced by the flow around the partially submerged body has been considered in literature. The standing wave produced by log is expected to have a great influence on the threshold value as it modify the wetted volume of the log, which has been identified as the main lack of traditional approach to entrainment (refer to Chapter 5).

As it has been stated, entrainment is due to the balance between the driving forces (mainly the drag force, which for free surface flow is essentially related to the Froude number of the flow Fr_w) and the resting ones (the friction between log and the flow bed). Friction forces are related to the buoyancy forces, which, are strongly affected by the wave profile around the log in the streamline direction (refer to section 6.5).

In ship's hydrodynamic the main parameter affecting the ship's drag, including the wave making resistance, is the Froude number Fr_L , defined considering as characteristic dimension the length of the waterline L_w (coincident with the length of the log in the stream-wise direction in our case).

Based on these considerations it is expected to find a strong relationship between E_p^* and a further dimensionless parameter given by the ratio between the undisturbed water depth d_w and the length of the log in the stream-wise direction L_{eq} , defined by the following equation, for a general orientation (see Fig. 6-1):

$$L_{eq} = L_{log} \cdot \cos \theta + c(d_w, D_{log}) \cdot \sin \theta \quad (7-8)$$

in which $c(d_w, D_{log})$ is a trigonometric function (Eq. 6-51) that permits to evaluate the undisturbed wetted profile of the cross section of the log.

In case of log oriented parallel to the flow L_{eq} coincide with L_{log} , while in case of log oriented perpendicular to the flow the value of L_{eq} depends on the shape of the log. In particular, for the square dowel it coincide with its width, as the water depth does not affect the waterline near the log, while for circular dowels it is a function of water depth and log diameter.

It is possible to verify that the dimensionless parameter d_w/L_{eq} represents the ratio between the aforementioned Froude numbers:

$$\frac{d_w}{L_{eq}} = \frac{U^2}{gL_{eq}} \cdot \frac{gd_w}{U^2} = \left(\frac{\frac{U}{\sqrt{gL_{eq}}}}{\frac{U}{\sqrt{gd_w}}} \right)^2 = \left(\frac{Fr_L}{Fr_w} \right)^2 \quad (7-9)$$

Moreover, considering that the Froude number based on water depth (that is the main parameter affecting free surface flow) plays also part in the formation of the waves generated in shallow water, it was reasonable to aspect that d_w/L_{eq} (which is related to both Froude numbers) would be a good predictor, able to take into account a great percentage of the variation of E_p^* . Consequently the following dimensionless expression has been considered for the regression analysis:

$$E_p^* = f \left(Re, Fr, Br, \frac{L_{log}}{D_{log}}, \frac{d_w}{D_{log}}, \frac{\rho_{log}}{\rho_w}, \frac{d_w}{L_{eq}} \right) \quad (7-10)$$

It has to be underlined that the new parameter d_w/L_{eq} is a combination of the traditional explanatory variables, as can be demonstrate:

$$\frac{d_w}{L_{eq}} = \frac{U}{\sqrt{gL_{eq}}} \cdot \frac{\sqrt{gd_w}}{U} = \frac{U}{\sqrt{gL_{eq}}} \cdot \sqrt{\frac{d_w}{L_{eq}}} = \frac{Fr_L}{Fr_w} \cdot \sqrt{\frac{d_w}{D_{log}} \cdot \frac{D_{log}}{L_{eq}}} \quad (7-11)$$

in which compare the slenderness and the relative submergence ratio of the log.

To produce an estimate of the relationship between the dimensionless parameters provided by dimensional analysis (Eq. 7-10) and the proposed entrainment threshold E_p^* , a multiple linear regression has been performed. The resulting regression equation is:

$$E_p^* = 2.344 + 1.081 \cdot 10^{-5} Re - 1.600 Fr - 0.01287 Br - 0.01657 \frac{L_{log}}{D_{log}} - 1.100 \frac{d_w}{D_{log}} + 1.063 \frac{\rho_{log}}{\rho_w} - 3.894 \frac{d_w}{L_{eq}} \quad (7-12)$$

The results of the performed analysis are summarized in the following table in which are reported the T statistic for each coefficient and the corresponding p-value, by which the significance level of each coefficient can be evaluated.

Table 7-6: coefficients (Coef) and corresponding standard error (SE Coef), T statistic (T) and p-value (P) for each parameter used in the linear regression, Eq. 7-11.

Predictor	Coef	SE Coef	T	P
Constant	2.34350	0.174964	13.3942	0.000
Re	0.00001	0.000002	4.9199	0.000
Fr	-1.59947	0.229703	-6.9632	0.000
Br	-0.01287	0.238928	-0.0539	0.957
Llog/Dlog	-0.01657	0.006135	-2.7011	0.008
dw/Dlog	-1.10011	0.229607	-4.7913	0.000
plog/pw	1.06293	0.182790	5.8150	0.000
dw/Leq	-3.89427	0.305944	-12.7287	0.000

Analyzing the significance level of each coefficient the Blockage ratio Br resulted the poorest predictor (with a P-value = 0.957), as shown in Table 7-6. This result suggested to drop this variable from the regression: subset models may actually estimate the regression coefficients and predict future responses with smaller variance than the full model using all predictors.

In order to identify the subset models that produce the highest R values from full set of the predictor variables, several regression have been performed: all possible subsets of the predictors have been considered, beginning with all models containing one predictor, and then all models containing two predictors, and so on. The two best models for each number of predictors are reported in Table 7-7.

Table 7-7: results of different linear regressions using different subsets of predictors.

R-Sq	R-Sq(adj)	Cp	S	Re	Fr	Br	Llog/Dlog	dw/Dlog	ρlog/ρw	dw/Leq
44.5	43.9	192.6	0.15166							X
26.8	25.9	280.1	0.17422			X				
58.8	57.8	124.1	0.13145				X			X
58.0	56.9	128.4	0.13282		X					X
70.9	69.8	66.5	0.11117		X		X			X
69.2	68.0	75.2	0.11449			X	X			X
75.9	74.7	44.0	0.10185		X		X		X	X
74.1	72.9	52.5	0.10546		X	X	X			X
82.9	81.8	11.6	0.08644	X	X			X	X	X
79.5	78.2	28.4	0.09462		X		X	X	X	X
84.4	83.2	6.0	0.08299	X	X		X	X	X	X
82.9	81.6	13.3	0.08683	X	X	X		X	X	X
84.4	83.0	8.0	0.08352	X	X	X	X	X	X	X

As ansues from this analysis the new parameter d_w/L_{eq} by itself is able to take into account about a large percentage of the variation in E_p^* (about the 44%), and the best subset of predictors could be obtained simply dropping the Blockage Ratio Br from the regression. The resulting regression equation shows practically the same level of significance, with a slightly better adjusted R-square value of 83.2%, and the p-values of all the coefficients below the 0.01% (Table 7-8):

$$E_p^* = 2.337 + 1.082 \cdot 10^{-5} Re - 1.591 Fr - 0.016663 \frac{L_{log}}{D_{log}} - 1.092 \frac{d_w}{D_{log}} + 1.057 \frac{\rho_{log}}{\rho_w} - 3.905 \frac{d_w}{L_{eq}} \tag{7-13}$$

Moreover the residual plots show a good random distribution as shown in Figure 7-31.

Table 7-8: analysis of variance of the multiple linear regression, Eq. 7-13, considering six independent variables (Re , Fr , L_{log}/D_{log} , d_w/D_{log} , ρ_{log}/ρ_w , d_w/L_{eq}).

Source	Degree of freedom	SS variance	MS Mean square	F	P
Regression	6	2.90466	0.48411	70.293	0.000
Residual Error	78	0.53719	0.00689		
Total	84	3.44185			

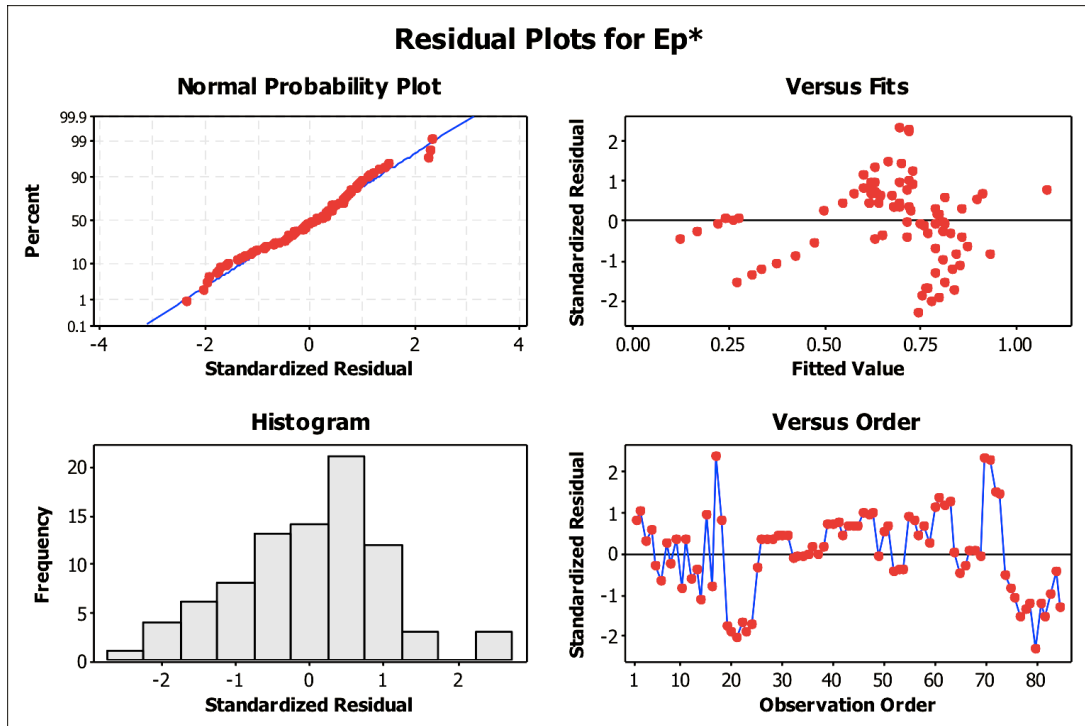


Figure 7-31: residual plots of the observed data according to the multiple linear regression, Eq. 7-13, with the six parameters: Re , Fr , L_{log}/D_{log} , d_w/D_{log} , ρ_{log}/ρ_w , d_w/L_{eq} .

Despite the importance attributed to the blockage ratio planning the experimental setting, this variable resulted to be the poorest predictor for the proposed parameter E_p . This result confirms the preliminary considerations done during the pre-analysis of experimental data (section 7.3.1). It has to be underlined that it does not mean that Br is not a relevant factor in the physics of LWD entrainment. The blockage ratio undoubtedly affects the flow field surrounding the partially submerged log, but it seems to have negligible influence on the wetted volume that is the essential quantity for the definition of E_p . Actually the wave shape around the object seems to be not so affected by the blockage ratio. See for example the flow around the log in two different conditions (Figure 7-25).

Due to the relevant influence of the new parameter d_w/L_{eq} showed in Table 7-7, it has been considered suitable to evaluate a general non-linear regression based just on this predictor. This choice was suggested observing the plot of the variation of E_p^* with respect to the dimensionless parameter d_w/L_{eq} , in which it is possible to recognize a well-defined non-linear trend, as shown in Figure 7-32.

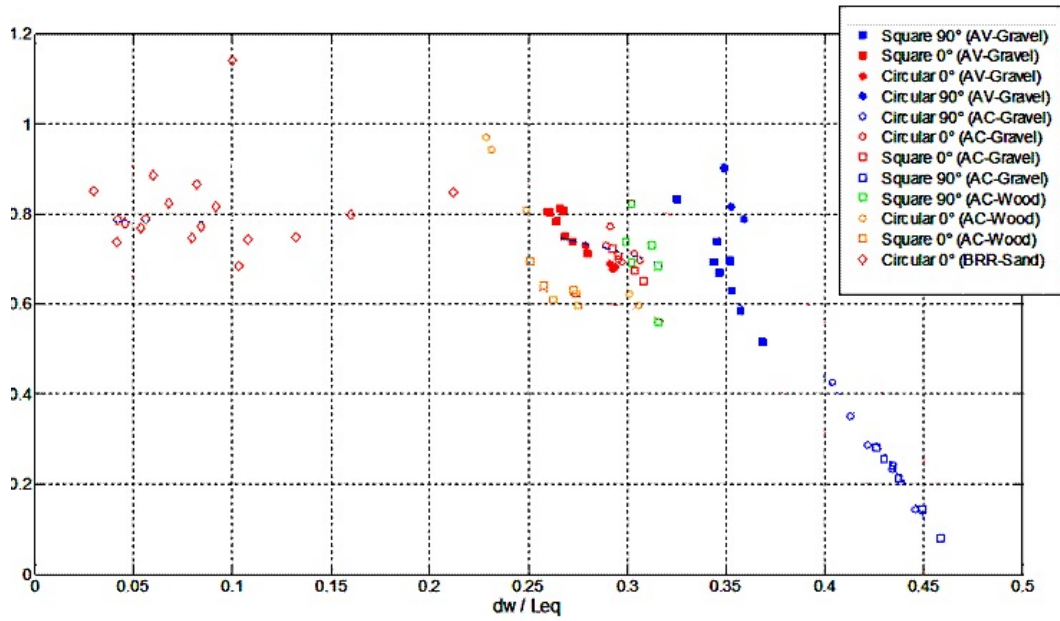


Figure 7-32: measured threshold values E_p^* of the entrainment parameters vs. the ratio d_w/L_{eq} .

The best model (goodness of fit: R-square: 0.875) was the power law shown in Figure 7-33 with the blue continuous line.

$$E_p^* = -51.19 \left(\frac{d_w}{L_{eq}} \right)^{5.454} + 0.7831 \quad (7-14)$$

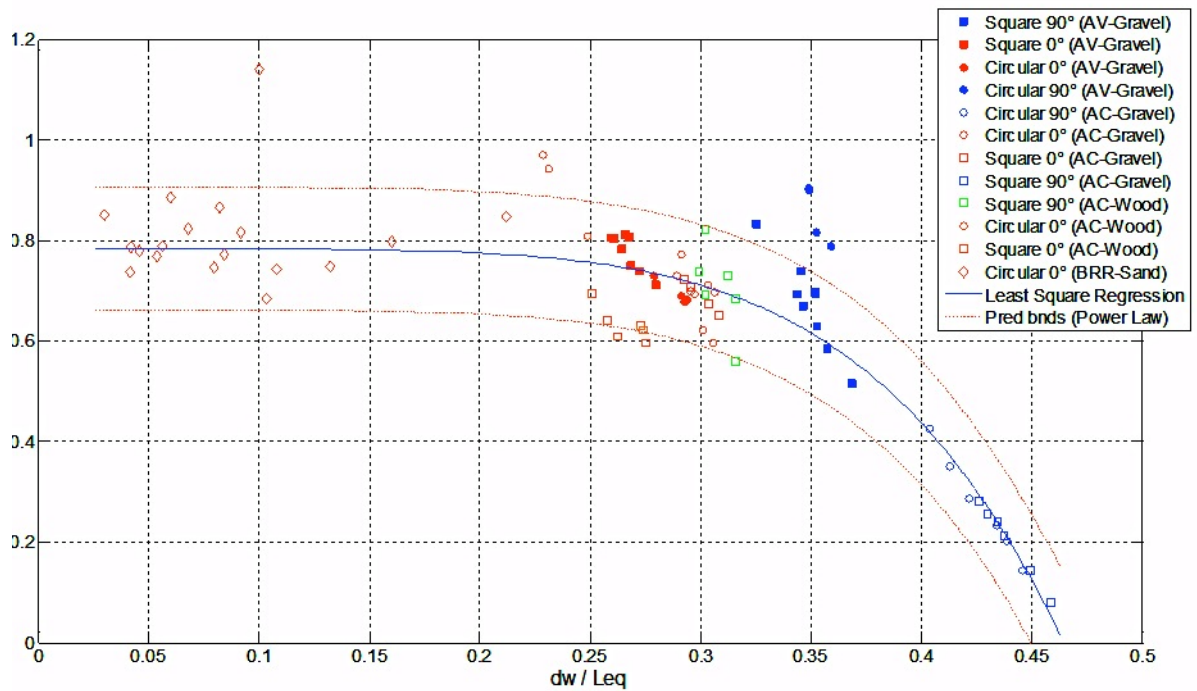


Figure 7-33: measured threshold values E_p^* of the entrainment parameters vs. the ratio d_w/L_{eq} .

This model is able to take into account about the same percentage of variation of the entrainment parameter of the multiple linear regression model (Eq. 7-13) with a pretty good dispersion of the residuals, which show an approximately normal distribution, even if the residuals on fitted values plot indicate a slight uneven variability (Figure 7-34).

According to Eqs. 7-8 and 7-11 it is possible to rewrite the experimental correlation for E_p^* (Eq. 7-14), in a more complex way, as:

$$E_p^* = -51.19 \cdot \left\{ \frac{\frac{Fr_L}{Fr} \cdot \sqrt{\frac{d_w}{D_{log}}}}{\sqrt{\frac{L_{log}}{D_{log}} \cos \theta + c \left(\frac{d_w}{D_{log}}\right) \sin \theta}} \right\}^{5.454} + 0.7831 \quad (7-18)$$

in which many dimensionless parameters of Eq. 7-10 come out.

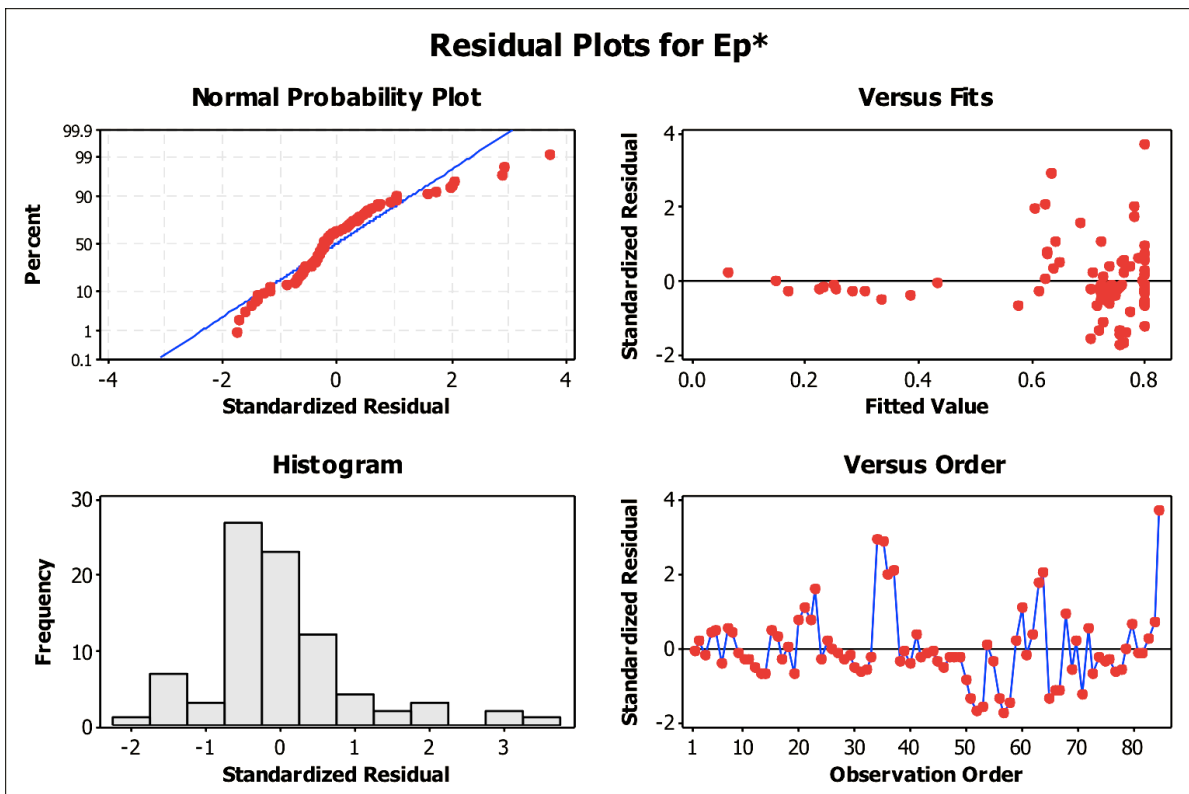


Figure 7-34: residual plots of the observed data according to the non-linear regression, Eq. 7-14.

Beside these analyses, the main advantage of the regression model provided by Eq. 7-14 is that it allows a clearer visualization of the range of the threshold value reached by the introduced parameter at the incipient motion condition and an advantageous facilitation in the application of this tool.

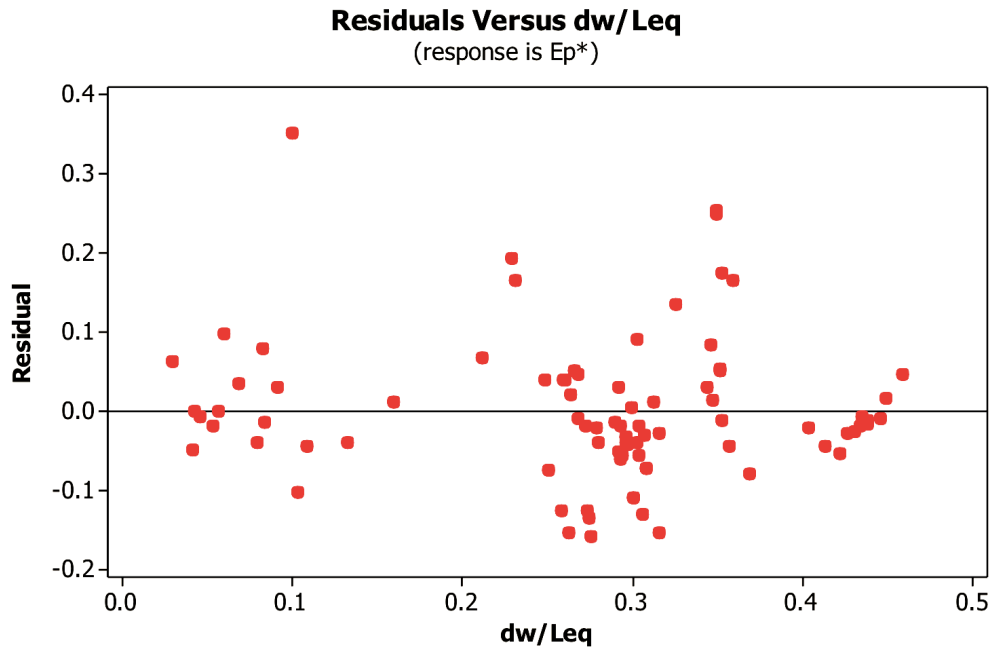


Figure 7-35: residual plot versus d_w/L_{eq} according to the non-linear regression, Eq. 7-14.

In order to investigate the capability of the proposed approach to discern between the different possible entrainment modes (sliding, rolling, and buoyancy) it could be useful to analyse the experimental data related to the square log oriented at 90° with respect to the stream-wise direction. As shown in Table 7-9 for some logs (test n. 14 and 15) the incipient motion was different at the same flow condition.

Table 7-9: measured data at the entrainment related to square shaped log, oriented at 90° with respect to the flow, on gravel bed.

Test no.		16	14		15		22	21	23	17
type of motion		sliding	sliding few cm	rolling	sliding few cm	rolling	sliding	sliding	sliding	rolling
discharge	[m3/s]	0.00439	0.00445	0.00473	0.00460	0.00500	0.00458	0.00443	0.00458	0.00390
shape		0	square	square	square	square	square	square	square	square
angle	[deg]	90	90	90	90	90	90	90	90	90
Width/Diameter	[m]	0.133	0.133	0.133	0.133	0.133	0.133	0.133	0.133	0.1325
Length	[m]	0.25	0.25	0.25	0.25	0.25	0.25	0.25	0.25	0.25
Final Density	[kg/m3]	458.54	455.58	455.58	457.17	457.17	479.42	479.23	480.08	475.03
Mean velocity	[m/s]	0.2402	0.241	0.249	0.245	0.255	0.245	0.241	0.245	0.226
water depth	[m]	0.074	0.046	0.048	0.047	0.049	0.047	0.046	0.047	0.043
Froude	[1]	0.359	0.359	0.365	0.361	0.368	0.361	0.358	0.361	0.348
Reynolds	[1]	1.76E+04	1.10E+04	1.17E+04	1.14E+04	1.24E+04	1.14E+04	1.10E+04	1.14E+04	9.67E+03
dw/Leq	[1]	0.56	0.35	0.36	0.35	0.37	0.35	0.35	0.35	0.33

It is remarkable that for the test n. 14 and n. 15, for which the entrainment was characterized by a first sliding destabilization and subsequent rolling motion, the values of the entrainment parameters related to both sliding and rolling, approach to the very similar values, as shown in Figure 7-36, suggesting that the two modes are both feasible.

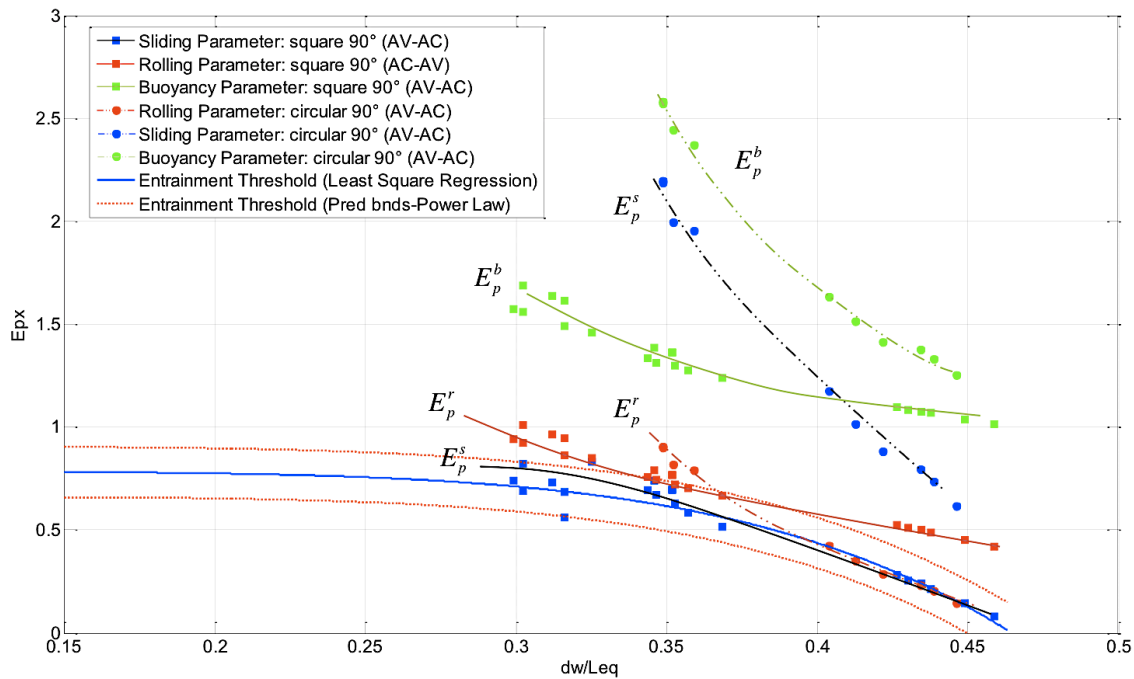


Figure 7-36: values of the entrainment parameters E_p^s , E_p^r , E_p^b vs. the ratio d_w/L_{eq} for square and circular logs oriented at 90° with respect to the stream flow direction.

For the cylindrical shaped logs instead the sliding entrainment parameter is always significantly greater than the rolling one, indicating that for cylindrical logs oriented to 90° with respect of the flow, the only entrainment mode possible is rolling.

This result confirms the capability of the proposed approach to discern between different entrainment modes.

The analysis performed on the collected data has shown that, although just two orientation have been considered, the main influence of this variable on the threshold value is on the entrainment mode: all the logs oriented to 90° with respect of the flow are characterized by a high value of the ratio d_w/L_{eq} , and very low E_p^* , meaning an high tendency to be destabilized by the flow, and a propensity to reach a more stable condition with the log oriented parallel to the flow. So it is possible to discern two different zones for the experimental correlation (Figure 7-37), related to the entrainment mode: a) rolling zone, characterized by high values of the d_w/L_{eq} parameter (above about 0.35) and a very low dispersion with respect to the proposed experimental correlation; b) a sliding zone characterized by low values of the independent parameter (below about 0.25) and an approximating constant value of the entrainment threshold of 0.8, with a more evident dispersion of data.

Between these two zones a transition zone exist (for d_w/L_{eq} values between 0.25 and 0.35) in which both entrainment modes could take place, depending on the shape and orientation of the log.

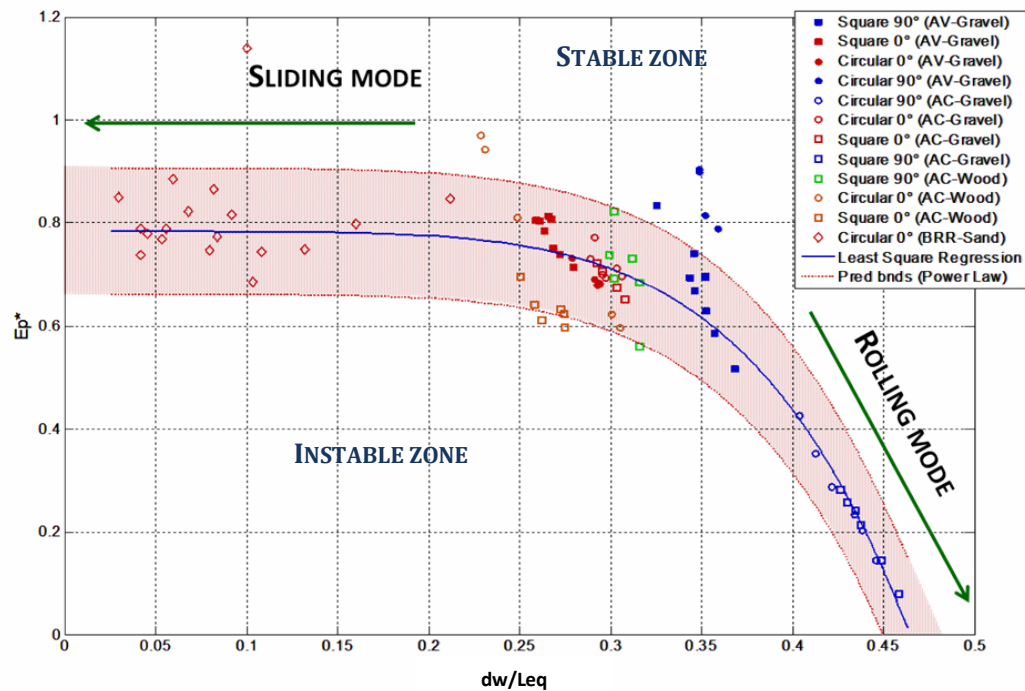


Figure 7-37: stability diagram for the experimental conditions.

It is interesting to observe that the analysis of experimental data have shown that for all the cases considered in this work, the entrainment threshold value is below the unit. Taking in mind the physical meaning of the entrainment parameter, defined as the ratio between the buoyancy force acting on the log (depending on the flow condition around the log), and the force due to the Archimedes' law in case of still water, it seems that the presence of flow has the effect to stabilize the log.

To conclude it is useful to remind that for its nature regression is just a mathematical approach based on statistics, which have no claim to interpret the physics of the considered process, even if it is able to suggest which variables can be used as predictors, and which seem to do not affect the process, or to influence it very low. For this reason all the consideration exposed in this chapter are made just on the basis of the statistical evidence proved by the regression, without any claim to use it to describe the physic of the process. Despite this, the result of this analysis is the product of physical reasoning: in fact all physical processes supposed to be influent on log entrainment have been taken into account in the experimental correlations (described in chapter 6), used to determine the right hand side of Eqs. 6-75, 6-76, 6-77 (the entrainment parameters), which have to be evaluated in order to obtain the threshold value E_p^* .

Furthermore even if the correlation procedure cannot represent a physical interpretation of the process its results are in good agreement with the main considerations made in Chapter 5 and 6.

7.4 CONCLUSIONS

A generalized framework has been proposed to model entrainment of single LWD. The model incorporates all the hydrodynamic forces known to act on submerged bodies, and it is able to discern between the different entrainment modes, allowing predicting also the type of incipient motion.

The provided modelling approach have to be implemented in conjunction with computational stream evolution models, in order to provide the undisturbed flow conditions necessary to establish the entrainment condition. Moreover the model developed can be used also in unsteady streams, naturally more appropriate for a risk assessment, because hydrodynamic coefficients obtained for steady flows, experience short-lived fluctuation as the stream velocity varies, even if the inertia of single logs is not a significant factor (Alonso, 2004).

The degree to which a model of this type will agree with field tests depends on accurate characterization of all the hydrodynamic forces. A brief review of these forces and the available experimental data needed for their characterization has been presented. Moreover some simplifications have been proposed in order to simplify the applicability of the algorithm, which has been implemented in Matlab.

Some issues related to the characterization of hydrodynamic forces acting on logs in a fluvial environment still require attention. Among these are the effect of log roughness, the appropriate evaluation of the friction between log and riverbed, the presence of rootwads and branches, which surely modify the flow profile along the log, and interact with bed sediments, even if the least condition is less for a risk assessment, due to the stabilizing effects of rootwads and branches.

Finally it has to be mentioned that during the experimental tests the final density of dowels was always greater than the initial one, due the porosity of wood, even if this variation was very low due to the type of wood considered, and the short time of resting. Clearly the final density has to be considered for the correct evaluation of the entrainment condition. This could lead evident difficulties, as this value it is not easy to obtain from the field survey. Moreover it could change with time, depending on natural deterioration of wood due to climatic, mechanical and biologic factors (alternation of wet and dry conditions, impacts, parasites).

8 SYNOPSIS

The research work is directed to the improvement of management skills for the assessment of the hydrologic risk associated to the presence of large woody debris (LWD) in rivers.

The abundance of wood in wild and urban rivers reaches (due to recent forestry management strategy and to socio-economic changes), the dichotomy in wood actions in rivers: essential ecologic role, stabilizing effects on the river corridor, improvement to the destructive power of a flood event (as recent catastrophic events have shown everywhere); lead to the necessity of management practices for LWD in rivers.

Despite that, at present, a method for the systematic implementation of wood within the process of elaboration of hazard maps is still lacking, with a consequent underestimation of hazard impacts (Mazzorana and Fuchs, 2009).

Considering the dynamical processes of wood in river reaches:

- Production and recruitment;
- Entrainment and transport;
- Halt and deposition;
- Exit (burial, deterioration, leaving);

given that several aspects in large woody debris dynamics are not yet well known, and that the physical phenomenon is characterized by the superposition of several natural processes (hydrogeological, forestry and climatic), the research work has been dedicated to an in depth analysis of some aspects of wood behaviour and to the development of effective tools to perform hazard analysis in the perspective of a comprehensive approach to the hydraulic risk assessment.

In particular, after a general analysis on LWD damaging potential based on literature material and direct observations in different river reaches, the activity tasks have been:

- The development of survey methods for mapping and monitoring the in-channel wooden material;
- The achievement of an entrainment condition for LWD.

8.1 SURVEY METHODS

Monitoring is a primary tool in environmental management: it allows to establish the existing condition necessary for planning management intervention, and to check

over the time the system variability and response in absence or presence of interventions.

Within the research activity two survey methods have been considered: direct and remote.

For the direct collection of information a survey sheets form has been implemented and tested in field in two Italian rivers.

The sheets represent an investigation instrument for wood and river reach monitoring which answer to several information requests involved in different step of the risk assessment procedure (risk identification, hazard analysis, evaluation of the system vulnerability). They permit to collect information on the reach morphology and on the wooden material: distribution, size, physical condition, interactions with water flow and bed sediments, and the collected data allow to produce statistics on species, age, dimension, decay, etc., and to produce a GIS representation of wood distribution and critical river sections (Figure 8-1).

SAMPLES	DIMENSION		GPS POSITION		ORIENTATION °N	ROOTWAD		SPECIES	TYPE	SPROUTS age	BARK COVER %	DECAY	VITALITY
	L	D	N	E		L	D						
T11	13.5	0.15	4905952	574833	170	1.4	1.3	P	log	/	90	solid	dead
T12	17.5	0.16	4905924	574941	160	1	1.3	P	log	/	20	solid	dead
T13	8.2	0.18	4905921	574939	330	0.8	1	P	cut	/	30	porous	dead
T16	7.9	0.13	4905925	574936	140	0.7	1.6	S	log	/	10	solid	dead
T17	2	0.2	4905914	574940	290	0.45	1.2	P	log	/	100	porous	dead
T14	14.5	0.2	4905952	574922	30	/	/	P	cut	/	10	solid	dead
T15	1.6	0.26	"	"	"	/	/	NC	cut	/	40	solid	dead
W1	4.4	0.18	4890201	571611	270	/	/	P	log	/	<5	solid/porous	dead
W2	11	0.15	4906256	575090	175	0.6	/	P	log	/	70	solid/porous	dead
W3	5.7	0.15	"	"	205	2.1	0.5	P	log	/	10	porous	dead
W4	2.7	0.21	4906273	575080	50	/	/	P	log	/	15	decayed	dead
W5	17	0.22	"	"	200	1	1.2	P	log	/	10	solid	dead
W6	11.8	0.13	4906302	575085	200	1.05	0.8	A	log	/	20	solid	dead
W7	13.3	0.15	"	"	22	1.3	0.8	P	log	/	50	solid	dead

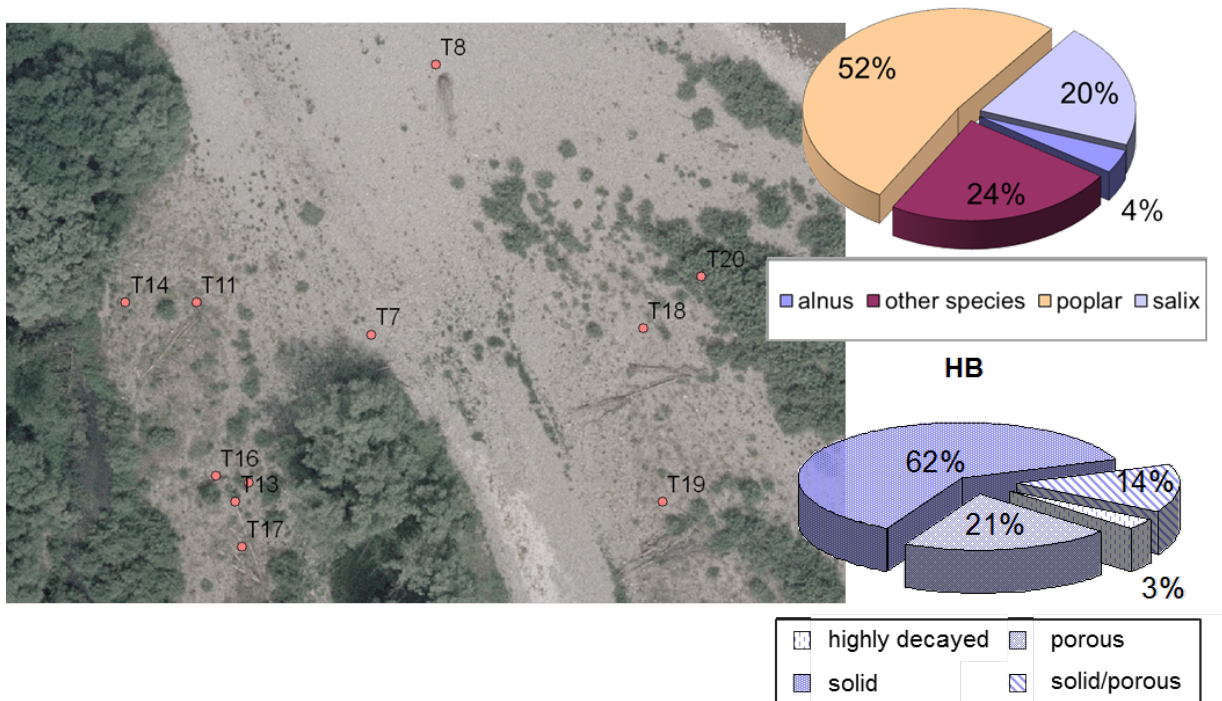


Figure 8-1: an example of the collected data and their elaboration.

Although principally intended for the collection of quantitative and qualitative data for the application of a predicting model, they are generally conceived to collect useful information for a wider analysis of the behaviour of wood in rivers, thus they are adaptable for quick or detailed surveys according to the monitoring purposes. Furthermore when reduced to essential information and evaluations (i.e. size and position, fresh or dated material, etc.) which do not require particular technical experience, the sheets are approachable, after a quick training, even by unprofessional users with basic instruments; that means that all the stakeholders in the river and riverine settlements protection (i.e. fisheries associations, ecologist associations, civil protection volunteers, etc.) may be involved in monitoring operations.

The form adapted from the structure of the survey sheet form for geomorphological characterization of river channels proposed by Thorne (1998) represents an original instrument for LWD survey.

Actually it is focused on the river morphology characterization and the in-channel wooden material evaluation but its modular structure is suitable for integrations: extending, for example, the survey to the hill slopes or the standing vegetation state.

Direct surveys have been compared with remote investigations performed using geo-referred high-resolution aerial imagery. While this method present indubitable advantages to monitoring wide areas or very large channels, nevertheless it present evident limits related principally to the photograms resolution, to the standing vegetation hiding, and to the debris inclination respect to the terrain surface. In a rational management strategy both methods may be used agreeing the survey purposes.

8.2 ENTRAINMENT CRITERION

Among whole dynamical processes involving LWD in rivers, entrainment has been considered a crucial one for risk management. First of all because stable debris do not produce significant effect on water level till their cross-sectional area is lesser than the 10% of the whole channel (Rutherford et al., 2002), while moving debris may hit hydraulic infrastructures, may convey to narrow sections and obstruct them causing backwater flooding or increasing pressure on structures, etc. Before to understand where wood can be delivered by the flow it is important to establish how many and which debris may be mobilized with high probability during a flood event.

The entrainment condition is traditionally physically based on the stationary equilibrium of gravity, buoyancy, friction and hydrodynamic forces acting on the body partially submerged in a flow field.

In this work no any force has been neglected a priori and an original interpretation of some aspects of the problem has been adduced taking cues from different disciplines.

Considering that in literature (Braudrick and Grant 2000; Bocchiola et al., 2006; Crosato et al., 2011) deterministic models were derived under simplified and limitative

assumptions, and tested with a limited set of experimental data, in this research work a correlation (Figure 8-2) between known characteristic dimensions:

- Re Reynolds number;
- Fr Froude number;
- Br Blockage ratio;
- L/D_{log} slenderness (L = length of the log);
- d_w/L where d_w is the undisturbed water depth;
- ρ_{log}/ρ_w density ratio;
- d_w/D_{log} submergence ratio;
- θ log orientation respect to the water flow;
- d_w/L_{eq} standing wave parameter

and a properly defined parameter E_p , is derived for the incipient condition, from experimental data available from literature and from designed further experiments performed for the purpose. The non-dimensional parameter E_p represent a measure of the variation of the real buoyancy force B due to the modified profile of the water in presence of the object, which represent the main source of uncertainties for LWD entrainment assessment. Flow conditions typical of low land rivers have been taken into account for the experimental setting, being within these channel types that LWDs have the greatest range of functions (Lisle and Kelsey, 1982; Keller et al., 1985; Montgomery et al., 1995).

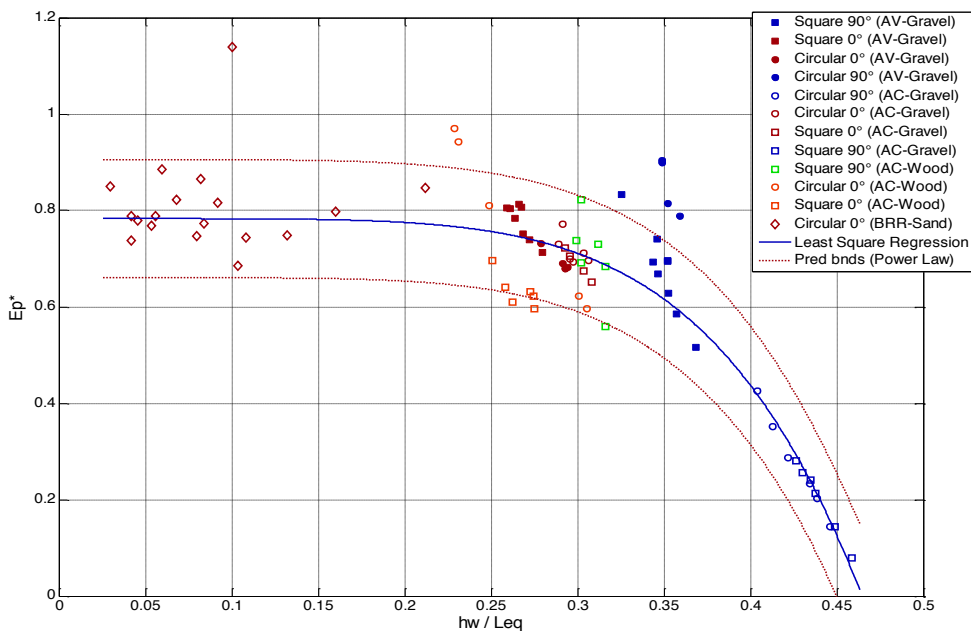


Figure 8-2: Measured threshold values of the parameter E_p^* vs. the ratio h_w/L_{eq} .

The provided correlation establish, for each particular configuration of the debris (shape and orientation,) the threshold value for the proposed entrainment criterion that allows determining, for a discharge with a certain recurrence interval, the probability of motion and the relative entrainment mode.

8.3 CONCLUSIONS

Keeping in mind the early phases in the risk management process, the research activity has been generally directed to a better comprehension of the risk sources and the catchment vulnerability, this knowledge transferred on the territory consent to an effortless recognition of the critical sections along the river channel. The monitoring sheet form – appositely developed in this work - permit to identify the catchment exposure detecting critical sections and wood availability, and to collect the necessary information for mapping woody debris distribution along the river channel.

It has to be considered that the superposition of several natural processes in LWD's dynamics results in significant uncertainties on cause-effect relationships and on widespread system loadings and system response. Considering the complexity of the whole phenomenon, the possibility to apply the current methods of risk analyses for natural hazards, usually based on quantitative methods of impact assessment to a given environmental setting, results in simplifications that may be not able to effectively define the hazard scenarios.

Nevertheless a hydrodynamic model, able to predict water depth and mean velocity at the location of any debris, associated to an entrainment threshold condition, as the one originally achieved within the research activity, may lead to the estimation of the volume of wood that will start to move with high probability during a designed event, which is an essential starting point for the construction of hazard scenarios and at first stage may represent a basic approach to risk assessment.

Taking into account that correlations coming from different research fields have been proposed for the estimation of some of the unknown quantities of the problem, (i.e. backwater rise, buoyancy centre position), a suitable reliability to the case study have to be addressed with proper investigations.

Considering that a complex natural subject has been modelled with a very simplified geometry, in a simplified environment, further researches are needed: particularly to address LWD interaction with bed sediments using mobile bed experimental conditions. This setting introduces a significant time dependence in the entrainment model as the modified flow field near the log influences the sediment transport for every water discharge, even the ones insufficient to mobilize the wooden debris, modifying bed configuration and then log stability. This interaction is exacerbated by the complex shape of natural large woody debris, which are usually characterized by tree's features (like rootwad and branches) that increase stability. Even maintaining simple log geometry, different shapes and orientations of dowels and mutual interaction needs to be investigated too.

9 BIBLIOGRAPHY

- Abbe, T., & Montgomery, D. (2003). Patterns and processes of wood debris accumulation in the Queets river basin, Washington. , *Geomorphology Volume 51, Issues 1-3* , 81–107.
- Abbe, T., & Montgomery, D. (2006). Influence of logjam-formed hard points on the formation of valley-bottom landforms in an old-growth forest valley, Queets River, Washington, USA . *Quaternary Research* 65 , 147 – 155.
- Abbe, T., & Montgomery, D. (1996). Large woody debris jams, channel hydraulics, and habitat formation in large rivers. . *Regulated rivers: research and management* 12 , 201-221.
- Abbe, T., Montgomery, D., Petroff, C., & Pess, G. (1997). *Technical summary: North Fork Stillaguamish River habitat enhancement and bank protection* . Washington.
- Allen, J. (1947). *Scale Models in Hydraulic Engineering*. London, England: Longmans, Green & Co.
- Alonso, C. (2004). Transport mechanics of stream-borne logs. *Riparian vegetation and Fluvial Geomorphology* , 8, 59-69.
- Archimedes of Syracuse. (around 250 BCE). *On floating bodies*.
- Arneson, L., Zevenbergen, L., Lagasse, P., & Clopper, P. (2012). *Evaluating scour at bridge*. Report No. FHWA-HIF-12-003.
- Baiamonte, G., Giordano, G., & Ferro, V. (1995). *Advances on velocity profile and flow resistance law in gravel bed rivers*. Excerpta.
- Barrass, C. B. (1979). The phenomenon of ship squat. *International Shipbuilding Progress*, 26, pp. 44-47.
- Batchelor, G. (1967). *An Introduction to Fluid Dynamics*. New York: Cambridge Univ. Press.
- Betti, M., Ginanni, F., Becchi, I., & Rinaldi, M. (2006). Dinamica di accumulo dei detriti arborei in alvei fluviali. *Atti del XXX Convegno di Idraulica e Costruzioni Idrauliche, IDRA 2006, Roma, 10–15 Settembre 2006*.
- Bilby, R. E. (1984). Removal of woody debris may affect stream channel stability. *Journal of Forestry*, v. 82 , 609-613.
- Bisson, P. A., Wondzell, S. M., Reeve, G. H., & Gregory, S. V. (2003). Trends in Using Wood to Restore Aquatic Habitats and Fish Communities in Western North American Rivers. *American Fisheries Society Symposium* 37, (pp. 391-406).

- Bocchiola, D., Catalano, F., Menduni, G., & Passoni, G. (2002). An analytical–numerical approach to the hydraulics of floating debris in river channels. *Journal of Hydrology* 269 , 65–78.
- Bocchiola, D., Rulli, M., & Rosso, R. (2006). Flume experiments on wood entrainment in rivers. *Advances in Water Resources* , 29 (1), 182-1195.
- Booth, D., Montgomery, D., & Bethel, J. (1997). Large woody debris in urban streams of the Pacific Northwest. *Effects of watershed development and management on aquatic ecosystems: Engineering Foundation Conference, Proceedings, Snowbird, Utah, August 4-9, 1996* (pp. 178-197). Roesner, L.A.
- Bradley, J., Richards, D., & Bahner, C. (2005). *Debris Control Structures: Evaluation and Countermeasures, Third Edition*. U.S. Department of Transportation Federal Highway Administration.
- Braudrick, C. A. (1998). *Entrainment, Transport, and Deposition of Large Woody Debris in Streams: Results from a Series of Flume Experiments*. Master of Science Thesis, Oregon State University.
- Braudrick, C., & Grant, G. (2001). Transport and deposition of large woody debris in streams: a flume experiment. *Geomorphology, Volume 41, Issue 4* , 263-283.
- Braudrick, C., & Grant, G. (2000). When do logs move in rivers? *Water Resources* , 36 (2), 571–83.
- Brighenti, A., Di Bussolo, R., Fiorin, F., Pavon, M., & Sebastiani, G. (2003). *Manuale di Navigazione Lagunare – Guida per l'operatore professionale ed il diportista*. Provincia di Venezia, Settore Mobilità e Trasporti, Venezia.
- Brooks, A., & al., e. (2006). *Design guideline for the reintroduction of wood into Australian streams*. Canberra: Land & Water Australia.
- Brooks, A., Brierley, G., & Millar, R. (2003). The long-term control of vegetation and woody debris on channel and floodplain evolution: insights from a paired catchment study between a pristine and a disturbed lowland alluvial river in southeastern Australia. *Geomorphology* 51 , 7-29.
- Brownlie, W. R. (1981). Re-examination of Nikuradse roughness data. *Journal of hydraulics division* , 89 (5), 327-333.
- Brunner, G. (2010). *HEC-RAS, River Analysis System Hydraulic Reference Manual*. CPD-69, U.S. Army Corps of Engineers, Hydrologic Engineering Center.
- Buffin-Bélanger, T., & Roy, A. (1998). Effects of a pebble cluster on the turbulent structure of a depth-limited flow in a gravel-bed river. *Geomorphology* , 25 (3-4), 249-267.
- Candanedo, L., & Derome, D. (2005). NUMERICAL SIMULATION OF WATER ABSORPTION IN SOFTWOOD. *Ninth International IBPSA Conference*, (pp. 123-130). Montréal, Canada.

- Carling, P., Hoffmann, M., Blatter, A., & Dittrich, A. (2002). Drag of emergent and submerged rectangular obstacles in turbulent flow above bedrock surface. *Internation workshop on rock scour due to high-velocity jets*. Lausanne, Switzerland.
- Chanson, H. (1999). *The Hydraulics of Open Channel Flow*. John Wiley and Sons, Inc. .
- Charbeneau, R., & Holley, E. (2001). *Backwater effect on bridge piers in subcritical flow*. Research Report Number 0-1805-1, Texas Department of Transportation, TX, USA.
- Chaudhry, M. (1993). *Open Channel flow*. Prentice-Hall, Inc.
- Chow, V. T. (1959). *Open-channel hydraulics*. New York, N.Y.: McGraw-Hill Book Co.
- Cottingham, P., Bunn, S., Price, P., & Lovett, S. (2003). *Managing wood in streams*. Canberra: Land & Water Australia.
- Crosato, A., Rajbhandari, N., Comiti, F., & Uijttewaal, W. (2011). Experimental study on entrainment of large wood in lowland rivers. *EUROMECH Colloquium 523 Ecohydraulics: linkages between hydraulics, morphodynamics and ecological processes in rivers*. Clermont-Ferrand, France.
- Crosato, A., Rajbhandari, N., Comiti, F., Cherradi, X., & Uijttewaal, W. (2013). Flume experiments on entrainment of large wood in low-land rivers. *J. of Hydraulic Research* , 51 (5), 581-588.
- Crowe, C., Roberson, J., & Elger, D. (2001). *Engineering fluid mechanics*. John Wiley and Sons.
- Delhommeau, G., Noblesse, F., & Guilbaud, M. (2007). Simple analytical approximation to a ship bow wave. *22nd IWWWFB*, (pp. 59-52). Plitvice, Croatia.
- El Alfy, K. S. (2009). Backwater rise due to flow constriction by bridge piers. *Thirteenth International Water Technology Conference, IWTC 13*, (pp. 1295-1313). Hurghada, Egypt.
- Eryuzlu, N. E., & Hausser, R. (1978). Experimental investigation into some aspects of large vessel navigation in restricted waterway. *Proceedings of the Symposium of Aspects of Navigability of Constraint Waterways Including Harbor Entrances, 2*, pp. 1-15.
- European, C., & Directorate, G. E. *Directive 2007/60/EC of the European Parliament and of the Council of 23 October 2007 on the assessment and management of flood risks. OJ L 288, 6.11.2007, P.27.*
- Fenton, J. (2003). The effects of obstacles on surface levels and boundary resistance in open channels. *Proc. 30th IAHR Congress. (2)*, pp. 9-16. Thessaloniki, Greece: J. Ganoulis and P. Prinos.
- Fenton, J., & McKee, W. (1990). On calculating the lengths of water waves. *Coastal engineering* , 14, 499-513.
- Flammer, G., Tullis, J., & Mason, E. (1970). Free surface, velocity gradient flow past hemispheres. *Journal of Hydraulics Division* , 96, 1485-1502.

- Forest Service Department of Agriculture. (n.d.). From http://lterdev.fsl.orst.edu/lter/pubs/webdocs/reports/detritus/GTR_estimates_site/Templates/tables.shtml
- Gippel, C. (1995). Environmental hydraulics of large woody debris in streams and rivers. *Journal of Environmental Engineering* 121 , 388– 395.
- Gippel, C. J., Finlayson, B., & O'Neill, I. (1991). The hydraulic basis of snag management. *n International Hydrology and Water Resources Symposium, 2*, pp. 610-611. Perth.
- Gippel, C., Finlayson, B., & Oneill, I. (1996). Distribution and hydraulic significance of large woody debris in a lowland Australian river. *Hydrobiologia* 318 (3) , 179–194.
- Gurnell, A. M., Petts, G., Hannah, D., Smith, B., Edwards, P., Kollmann, J., et al. (2000). Wood storage within the active zone of a large European gravel-bed river. *Geomorphology* 34 , 55-72.
- Gurnell, A., Piégay, H., Swanson, F., & Gregory, S. (2002). Large wood and fluvial processes. *Freshwater Biology* 47 , 601–619.
- Haga, H., Kumagai, T., Otsuki, K., & Ogawa, S. (2002). Transport and retention of coarse woody debris in mountain streams: An in situ field experiment of log transport and a field survey of coarse woody debris distribution. *Water Resources Research* , 38 (1), 1-16.
- Harmon, M., Woodall, C., Fasth, B., & Sexton, J. (2008). *Woody detritus density and density reduction factors for tree species in the United States: a synthesis*. Gen. Tech. Rep. NRS-29, U.S. Department of Agriculture, Forest Service, Northern Research Station, Newtown Square, PA.
- Hartley, C. (1958). *Evaluation of Wood Decay in Experimental Work*. Report No. 2119, USDA Forest Service, Forest Products Laboratory, Madison, Wisconsin.
- Hassan, I. (2004). Identification of pressure and velocity coefficients along block-stones ramp. *Eighth-th International Water Technology Conference, IWTC8 2004*, (pp. 615-626). Alexandria, Egypt.
- Havelock, T. H. (1908). The Propagation of Groups of Wave in Dispersive Media, with Application to Waves on Water Produced by a Travelling Disturbance. *Proc. Royal Society of London*, (pp. 398-430).
- Havelock, T. H. (1934). Wave Patterns and Wave Resistance. *Trans. Inst. of Naval Architects* , 76, 430-442.
- Havelock, T. H. (1951). Wave Resistance Theory and its Application to Ship Problems. *Trans. Society of Naval Architects and Marine Engrs.* , 59, 13-24.
- Henderson, F. M. (1966). *Open channel flow*. New York: Macmillan Publishing Co.
- Hughes, M., McDowell, P., & Marcus, W. (2006). Accuracy assessment of georectified aerial photographs: Implications for measuring lateral channel movement in a GIS. *Geomorphology* 74 , 1 –16.

- Hunt, J. H., & Brunner, G. W. (1995). *Flow Transition in Bridge Backwater Analysis*. RD-42, US Army Corps of Engineers, Institute for Water Resources Hydrologic Engineering Center.
- Hygelund, B., & Manga, M. (2003). Field measurement of drag coefficients for model large woody debris. *Geomorphology*, *51*, 175–185.
- Ishikawa, Y. (1989). *Studies on disasters caused by debris flows carrying floating logs down mountain streams*. PhD thesis, Kyoto University.
- Jackson, T. R., Haggerty, R., & Apte, S. V. (2013). A fluid-mechanics based classification scheme for surface transient storage in riverine environments: quantitatively separating surface from hyporheic transient storage. *Hydrol. Earth Syst. Sci.*, *17*, 2747–2779.
- Kail, J. (2003). Influence of large woody debris on the morphology of six central European streams. *Geomorphology* *51*, 207–223.
- Keller, E. A., MacDonald, A., Tally, T., & Merritt, N. J. (1985). *Effects of large organic debris on channel morphology and sediment storage in selected tributaries of Redwood Creek*. Geomorphic Processes and Aquatic Habitat in the Redwood Creek Drainage Basin, U. S. Geological Survey.
- Keller, E., & Swanson, F. (1979). Effects of large organic material on channel form and fluvial processes. *Earth Surface Processes* *4*, 361-380.
- Khazaei, J. (2008). Water absorption characteristics of three wood varieties. *Cercetari Agronomice in Moldova*, *XLI* (2 (134)), 5-16.
- Krus, M., & Künzel, H. (1993). *Determination of Dw from A-value*. IEA Annex XXIV.
- Kumar, A., & Flynn, P. (2006). Uptake of fluids by boreal wood chips: Implications for bioenergy. *Fuel Processing Technology*, *87*, 605 –608.
- Kumaran, M. (1999). Moisture diffusivity of building materials from water absorption measurements. *Journal of Thermal Envelope and Building Science*, *22*, 349–355.
- Labbe, T., Grotefendt, P. G., Grotefendt Photogrammetric Services, I., Carter-Mortimer, A., LLC, A. C., Jones, J. L., et al. (2005). *Dosewallips River Habitat Assessment: Coupling High-Resolution Remote Sensing and ground surveys to Prioritize Aquatic Conservation, Olympic Mountains, Washington State*. Final Report to: Watershed Restoration Coordinator USDI – Bureau of Indian Affairs Portland.
- Lagasse, P. F., Clopper, P. E., Zevenbergen, L. W., Spitz, W. J., Girard, L. G., & AYRES ASSOCIATES, I. (2010). *Effects of Debris on Bridge Pier Scour*. NCHRP REPORT 653.
- Langbein, W. (1962). *Hydraulics of River Channels as Related to Navigability*. Geological Survey, United States Department of the Interior. Washington: United States Government printing office.

- Lisle, T. E., & Kelsey, H. M. (1982). Effects of large roughness elements on the thalweg course and pool spacing. In A. G. Group, *Field Trip Guidebook* (pp. 134-135). Pinedale, Wyoming, Conference : Leopold, L. B., ed.
- Lyn, D. A. (1991). Resistance in flat-bed sediment-laden flows. *Journal of hydraulic engineering* , 117 (1), 94-115.
- Lyn, D. A., Cooper, T., Yi, Y.-K., Sinha, R., & Rao, A. R. (2003). *Debris Accumulation at Bridge Crossings: Laboratory and Field Studies*. Purdue University, School of Civil Engineering. Joint Transportation Research Program.
- Mäkinen, H., Hynynen, J., Siitonen, J., & Sievänen, R. (2006). Predicting the decomposition of Scots pine, Norway spruce and birch stems in Finland. *Ecological Applications* , 16, 1865–1879.
- Mäkipää, R., & Linkosalo, T. (2011). A non-destructive field method for measuring wood density of decaying logs. *Silva Fennica* 45(5) , 1135–1142.
- Marchand, J., Jarret, R., & Jones, L. (1984). *Velocity profile, surface slope, and bed material size for selected streams in Colorado*. U.S. Geol. Surv.
- Marcus, W. A., Marston, R., Colvard, C. J., & Gray, R. (2002). Mapping the spatial and temporal distributions of woody debris in streams of the Greater Yellowstone Ecosystem, USA. *Geomorphology* 44 , 323–335.
- May, C. L., & Gresswell, R. E. (2003). Large wood recruitment and redistribution in headwater streams in the southern Oregon. Coast Range, USA. *Can. J. For. Res.* 33(6) , 1352–1362.
- Maynard, S. T. (1991). Flow resistance of rip-rap. *Journal of hydraulic engineering* , 117 (6), 687-696.
- Mazzorana, B., & Fucks, S. (2010). Fuzzy Formative Scenario Analysis for woody material transport related risks in mountain torrents. *Enviromental Modelling & Software* , 25, 1208-1224.
- Mazzorana, B., & Fucks, S. (2009). Improving risk assessment by defining consistent and reliable scenarios. *Natural Hazards and Earth System Science* , 9, 145-159.
- Mazzorana, B., Hübl, J., Zischg, A., & Largiader, A. (2011). Modelling woody material transport and deposition in alpine rivers . *Nat Hazards* 56 , 425-449.
- Mazzorana, B., Zischg, A., Largiader, A., & Hübl, J. (2009). Hazard index maps for woody material recruitment and transport in alpine catchments. *Natural Hazards and Earth System Sciences* 9 , 197-209.
- Miles, P., & Smith, W. (2009). *Specific gravity and other properties of wood and bark for 156 tree species found in North America*. Res. Note. NRS-38, U.S. Department of Agriculture, Forest Service, Northern Research Station.
- Molinas, A., & Wu, B. (2001). Choked flows through short contractions. *Journal of hydraulic engineering* , 657-662.

- Molinas, A., & Wu, B. (2005). Energy losses and threshold conditions for choking in channel contractions. *Journal of Hydraulic Research* , 43 (2), 139-148.
- Monin, A., & Yaglom, A. (1971). *Statistical Fluid Mechanics: Mechanics of Turbulence. 1.*
- Montgomery, D. R., & Buffington, J. M. (1993). *Channel classification, prediction of channel response, and assessment of channel condition: Washington State Department of Natural Resources* . Report TFW-SH10-93-002, 84 p.
- Montgomery, D. R., Abbe, T. B., Buffington, J. M., Peterson, N. P., Schmidt, K. M., & Stock, J. D. (1996). Distribution of bedrock and alluvial channels in forested mountain drainage basin. *Nature* 381 , 587-589.
- Montgomery, D., Collins, B., Buffington, J., & Abbe, T. (2003). Geomorphic effects of wood in rivers. . *American Fisheries Society Symposium*.
- Mutz, M. (2003). Hydraulic effects of wood in streams and rivers . *American Fisheries Society Symposium*, (pp. 93-107).
- Nakamura, F., & Swanson, F. J. (1994). Distribution of coarse woody debris in a mountain stream, western Cascade range, Oregon. *Canadian Journal of Forest Research* 24 , 2395-2403.
- Nelson, J., McLean, S., & Wolfe, S. (1993). Mean flow and turbulence fields over two-dimensional bed forms. *Water Resour. Res.* , 29 (12), 3935-3953.
- Nezu, I., & Nakagawa, H. (1993). *Turbulence in open-channel flows. IAHR*. Rotterdam, Netherlands.
- Nezu, I., & Rodi, W. (1986). Open-channel flow measurements with a laser-Doppler anemometer. *Journal of Hydraulic Engineering* , 112 (5), 335-355.
- Nikora, V., & Smart, G. (1997). turbulence characteristics of New Zealand gravel-bed rivers. *Journal of hydraulic engineering* , 123 (9), 764-773.
- Nikuradse, J. (1933). Stromungsgesetze in rauhen rohren. *Forsh. Geb. Ingenieurwes Wes.* , 4 (361).
- Northern Research Station. (n.d.). From <http://www.nrs.fs.fed.us/>
- O' Connor, D. J. (1995). Inner region of smooth pipes and open channels. *Journal of hydraulic engineering* , 121, 555-560.
- Parker, G. (2004). *1-D sediment transport morphodynamics with applications to rivers and turbidity currents*. From http://vtchl.uiuc.edu/people/parkerg/morphodynamics_e-book.htm
- Piégay, H. (2003). Dynamics of wood in Large rivers . *American Fisheries Society Symposium 2003*, (pp. 109-132).
- Pliefke, T., Sperbeck, S., Urban, M., Peil, U., & Budelmann, H. (2007). A Standardized Methodology for Managing Disaster Risk – An Attempt to Remove Ambiguity. *5th International Probabilistic Workshop, Ghent, 2007*.

- Prandtl, L., & Tietjens, O. (1934). *Applied Hydro & Aeromechanics* (Vol. II). New York: Dover.
- Rajala, T., Peltoniemi, M., Pennanen, T., & Mäkipää, R. (2010). Relationship between wood-inhabiting fungi and quality of decaying logs. *Canadian Journal of Forest Research*, *40*, 2384–2397.
- Rajbhandari, N. (2010). *Mutual interaction of large floating debris and morphodynamic processes in low-land Rivers*. MSc Thesis, UNESCO-IHE Institute for Water Education.
- Ranga Raju, K. G., Rana, O. P., Asawa, G. L., & N., P. A. (1983). Rational assessment of blockage effect in channel flow past smooth circular cylinders. *J. Hydraulic Res.*, *21*, 289-302.
- Ranga Raju, K., Rana, O., Asawa, G., & Pillai, A. (1983). Rational assesment of blockage effect in channel flow past smooth circular cylinders. *Journal of Hydraulic Research* *21*, 289– 302.
- Remich, J. (2002). *Large woody debris in streams*. Ohio Stream Management Guide No. 21.
- Robison, E., & Beschta, R. (1990). Identifying trees in riparian areas that can provide coarse woody debris to streams. *Forest Science* *36*, 790-801.
- Rouse, H. (1961). *Fluid Mechanics for Hydraulic Engineers*. New York: Engineering Societies Monograph, Dover.
- Rutherford, I., Jerie, K., & Marsh, N. (2000). *A Rehabilitation Manual for Australian Streams, Land and Water Resources*. Research and Development and Cooperative Research Centre for Catchment Hydrology, Canberra, Australia.
- Rutherford, I., Marsh, N., Price, P., & Lovett, S. (2002). *Managing woody debris in rivers*. Australian Government, Land & Water Australia.
- Saldi-Caromile, K., Bates, K., Skidmore, P., Barenti, J., & Pineo, D. (2004). *Stream Habitat Restoration Guidelines: Final Draft*. Olympia, Washington: Washington Department of Fish and Wildlife and Ecology and the U.S. Fish and Wildlife Service.
- Salo, E. O., & Cundy, T. W. (1987). *Streamside Management: Forestry and Fishery Interactions* (Vol. Contribution No. 57). Seattle: University of Washington, College of Forest Resources.
- Sarpkaya, T., & Garrison, C. (1963). Vortex formation and resistance in unsteady flow. *Journal of Applied Mechanics*, *30*, 265-285.
- Saunders, H. (1957). *Hydrodynamics in ship design* (Vol. I). Soc. Naval Architects and Marine Engineers.
- Scholz, R., & Tietje, O. (2002). *Embedded Case Study Methods*. London: Sage.
- Shields, D., & Gippel, C. (1995). Prediction of effects of woody debris removal on flow resistance. *J. Hydraul Eng.*, *121* (4), 341–54.

- Shields, F. D., & Cooper, C. M. (2000). Woody vegetation and debris for in-channel sediment control. *International Journal of Sediment Research*, Vol. 15, No. 1 , 83-92.
- Shields, F., & Gippel, C. (1995). Prediction of effects of woody debris removal on flow resistance. *Journal of Hydraulic Engineering* 121 , 341– 354.
- Shields, F., & Smith, R. (1992). Effects of large woody debris removal on physical characteristics of a sand-bed river . *Aquat. Cons. mar. freshwat. Ecosys.* (2), 145-163.
- Shields, F., Asce, M., Morin, N., & Cooper, C. (2004). Large Woody Debris Structures for Sand-Bed Channels. *Journal of hydraulic engineering* , 130 (2), 208-230.
- Simpson, W. (1973). Predicting equilibrium moisture content of wood by mathematical models. *Wood and Fiber* , 5 (1), 41–49.
- Simpson, W., & TenWolde, A. (1999). Physical Properties and Moisture Relations of Wood. In *Wood handbook—Wood as an engineering material* (Vol. Chapter 3).
- Sollins, P. (1982). Input and decay of coarse woody debris in coniferous stands in western Oregon and Washington. *Canadian Journal of Forest Research* , 12, 18-28.
- Southerland, W. B. (2010). Performance of Engineered Log Jams in Washington State- Post Project Appraisal. *Proceedings from the 2nd Joint Federal Interagency Conference*. Las Vegas.
- Surian, N., & Rinaldi, M. (2004). Channel adjustment in response to human alteration of sediments: fluxes examples from italian rivers. *Sediments transfer through the fluvial system proceeding symposium*. 288, pp. 276-282. Moscow: IAHS Publ.
- Surian, N., & Rinaldi, M. (2003). Morphological response to river engineering and management in alluvial channels in Italy. *Geomorphology* , 50, 307-326.
- Svoboda, C., Cuhaciyan, C., & Kimbrel, S. (2013). *Improving Public Safety of Large Wood Installations: Scoping Proposal Report of Findings*. U.S. Department of the Interior, Bureau of Reclamation.
- Swanson, F. J., Lienkaemper, G. W., & Sedell, J. R. (1976). *History, physical effects, and management implications of large organic debris in western Oregon streams*. Pacific Northwest Forest and Range Experimental Station. Portland, Oregon: USDA Forest Service.
- Swanson, F., & Lienkaemper, G. (1979). Interactions among fluvial processes, forest vegetation, and aquatic ecosystems, South Hoh River, Olympic National Park, Washington. *Proceedings of the Second Conference on Scientific research in the National Parks, Nov 26-30 1979, vol 7*, (pp. 23-34). San Francisco, Ca.
- Thorne, C. R. (1998). *Stream reconnaissance handbook. Geomorphological investigation and analysis of river channel*. Chichester: Wiley.
- Tsutsui, T. (2008). Fluid force acting on a cylindrical pier standing in a scour. *BBA VI International Colloquium on: Bluff Bodies Aerodynamics & Applications*. Milano, Italy.

- Tuck, E. O., & Taylor, P. J. (1970). Shallow water problems in ship hydrodynamics. *Proceedings of the 8th Symposium on Naval Hydrodynamics*. Pasadena, CA.
- Van Manen, J., & Van Oossanen, P. (1988). *Principles of Naval Architecture Resistance, Propulsion and Vibration* (Vol. II). NJ: E. V. Lewis.
- Wallerstein, N. P., & Thorne, C. R. (2004). "Influence of Large Woody Debris on Morphological Evolution of Incised, Sand-Bed Channels. *Geomorphology*, Vol. 57 , 53–73.
- Wallerstein, N., Alonso, C., Bennett, S., & Thorne, C. (2002). Surface wave forces acting on submerged logs. *J Hydraul Eng* , 128 (3), 349–53.
- Wallerstein, N., Thorne, C. R., & Doyle, M. W. (1997). Spatial Distribution and Impact of Large Woody Debris in Northern Mississippi. *Proceedings of the Conference on Management of Landscape Disturbed by Channel Incision* (pp. 145-150). Oxford, MS: Wang, S. S. Y.; Langendoen, F. D.; Shields, F. D., Jr.
- Weinblum, G., Amstberg, H., & Bock, W. (1950). *Tests on wave resistance of immersed bodies of revolution*. Transl. no. 234, The David W. Taylor Model Basin, Washington D.C.
- Wigley, W. C. (1953). Water forces on submerged bodies in motion. *Trans. Inst. Naval Arch.* , 95, 268–279.
- Woodall, C., Rondeux, J., Verkerk, P., & Ståhl, G. (2009). Estimating dead wood during national forest inventories: A review of inventory methodologies and suggestions for harmonization. *Environmental Management* , 44, 624-631.
- Woudenberg, S., Conkling, B., O'Connell, B., LaPoint, E., Turner, J., & Waddell, K. (2010). *The Forest Inventory and Analysis database: Database description and users manual version 4.0 for Phase 2*. Gen. Tech. Rep. RMRS-GTR- 245, U.S. Department of Agriculture, Forest Service, Rocky Mountain Research Station.
- Wright, J., & Yamamoto, T. (1979). Wave forces on cylinders near plane boundaries. *Journal of Waterway, Port, Coastal and Ocean Division* , 105, 1-13.
- Yarnell, D. (1934). *Bridge piers as channel obstructions*. Tech. Bull. No. 442, U. S. Department of Agriculture.
- Yen, B. C. (1991). *Channel flow resistance: centennial of mannin's formula*. Highlands Ranch, Colorado: Water resource publications.
- Young, W. (1991). Flume study of the hydraulic effects of large woody debris in lowland rivers. *Regulated Rivers: Res. Manage.* 6 , 203–211.

APPENDIX A:

A filled in example of the survey sheets form and of the recorded data is presented in the following pages.


1. REACH DESCRIPTION			
General			
Date	<u>29/05/10</u>	Operators	<u>LWDTEAM</u>
River	<u>MAGRA</u>	Reach	<u>UPPERREACH</u>
Reach code	<u>M.R1</u>		
<u>GPS position</u>			
Upstream end	N <u>4912054</u>	E	<u>1571543</u>
Downstream end	N <u>4904320</u>	E	<u>1575430</u>
General morphological characteristics			
Alluvial channel (large)	<input type="checkbox"/>	Intermediate	<input checked="" type="checkbox"/>
Channel morphology (alluvial or intermediate)	<input checked="" type="checkbox"/> W	R=straight, S=sinuuous, R-S BA=straight or sinuous with alternate bars M=meandering, W=wandering, CI=braided, A=anastomosing	
Bed configuration	<input checked="" type="checkbox"/> RP	R=cascade, SP=step pool, LP=plane bed, RP=riffle pool, DR=duneripple	
Reach sketch (length possibly of about 20 times channel width)			
			
To report: reach limits, subreaches (following sheets) limits, measured representative cross section			
Notes and comments			
Stabilized islands			

Figure A - 1:sheet 1: reach description.

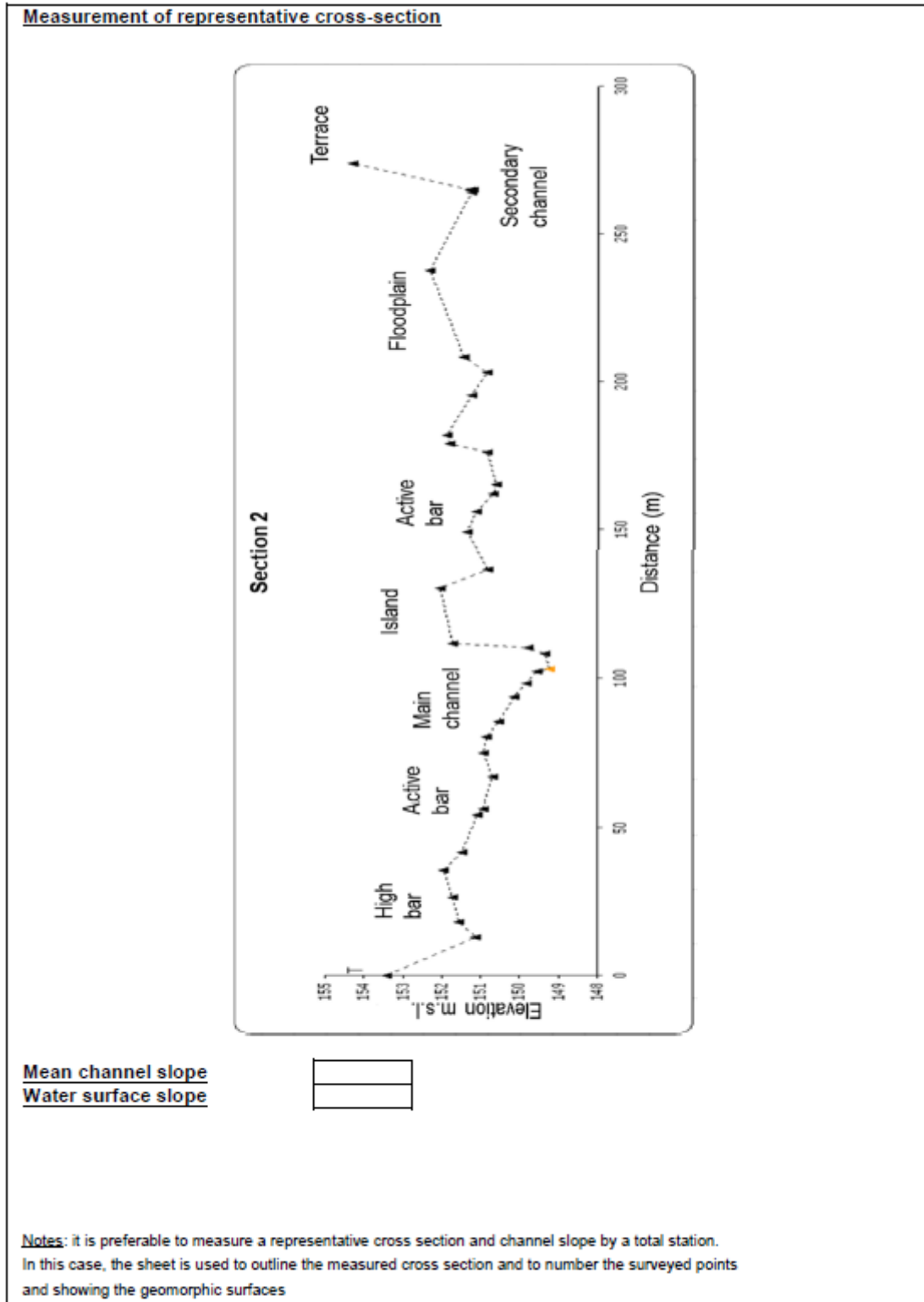


Figure A - 2: sheet 1: reach description.

2. SUB-REACH GEOMORPHOLOGICAL CHARACTERISTICS			
Identification data			
Sub-reach code	SECTION 2.1		
GPS positions			
Downstream end	N 4907936	E 1574153	
General morphological characteristics			
Bed configuration	RP R=cascade, SP=step pool, LP=plane bed, RP=riffle pool, DR=duneripple		
Bed sediments	GM A=clay, L=silt, S=sand, G=gravel, C=cobbles, M=boulders, R=bedrock		
Bars	A/L/O LA=lateral, LO=longitudinal, M=point, C=confluence, D=diagonal		
Surfaces	left	mid	right
active channel	<input type="checkbox"/>	<input type="checkbox"/>	<input checked="" type="checkbox"/>
chute channel	<input checked="" type="checkbox"/>	<input type="checkbox"/>	<input checked="" type="checkbox"/>
bar (LA, LO, M, C, D)	<input checked="" type="checkbox"/>	<input checked="" type="checkbox"/>	<input checked="" type="checkbox"/>
high bar	<input checked="" type="checkbox"/>	<input type="checkbox"/>	<input checked="" type="checkbox"/>
pioneer islands	<input type="checkbox"/>	<input type="checkbox"/>	<input type="checkbox"/>
established island	<input type="checkbox"/>	<input checked="" type="checkbox"/>	<input type="checkbox"/>
berm/bench/shelf	<input type="checkbox"/>	<input type="checkbox"/>	<input type="checkbox"/>
floodplain	<input checked="" type="checkbox"/>	<input type="checkbox"/>	<input type="checkbox"/>
sec. channel (in floodplain)	<input checked="" type="checkbox"/>	<input type="checkbox"/>	<input type="checkbox"/>
terrace	<input checked="" type="checkbox"/>	<input type="checkbox"/>	<input checked="" type="checkbox"/>
hillslope	<input type="checkbox"/>	<input type="checkbox"/>	<input type="checkbox"/>
Planform sketch (length possibly of about 1-3 times channel width)			
Symbols			
Subreach limits	Bar/island HB, AB, BLO	LWD jam (with code)	
North	Retreating bank	LWD (with code)	
Flow direction	Structures	Photo	
Notes and comments			
vegetation	shrubs if not specified		
MC main channel	CC chute channel	MC secondary channel	

Figure A - 3: sheet 2: sub-reach description.

Cross section sketch

Note: show the geomorphic surfaces and vegetation

Bankfull channel size

Width (m) Measurement method (C=field, FA=aerial photos)

Mean depth (m)

Banks

	left	right	
Type	<input type="text" value="NC"/>	<input type="text"/>	NC=non cohesive, C=cohesive, CO=composite, S=layered
Stability	<input type="text" value="S"/>	<input type="text" value="AR"/>	S=stable, AR=retreating, AV=advancing
Process	<input type="text"/>	<input type="text" value="MM"/>	E=erosion, MM=mass movement

Vegetation

A=absent, E=grass/shrubs, AL=trees

	left	mid	right	Main species
bank	<input type="text" value="AL"/>		<input type="text" value="AL"/>	<u>Robinia, Populus</u>
active bar	<input type="text" value="E"/>	<input type="text" value="E"/>	<input type="text" value="E"/>	
high bar	<input type="text" value="E"/>		<input type="text"/>	<u>Populus, Salix, Ailanthus</u>
pioneer island		<input type="text" value="AL"/>		<u>Populus, Salix</u>
established island		<input type="text" value="AL"/>		<u>Populus, Salix</u>
berm/bench/shelf	<input type="text"/>		<input type="text"/>	
floodplain	<input type="text" value="NC"/>		<input type="text"/>	<u>Robinia, Populus</u>
terrace	<input type="text" value="AL"/>		<input type="text" value="AL"/>	<u>Robinia, Populus</u>
hillslope	<input type="text"/>		<input type="text"/>	

In-channel structures

Transversal structures P=bridge, T=weir, S=sill, C=check dam

Bank protections left right M=wall, G=gabion, P=groyne, IN=bioengineering

Notes and comments

Figure A - 4: sheet 2: sub-reach description.

3. LWD JAM SHEET		
Identification data		
Jam Code <u>2. J4</u>	18 pictures	
GPS Position N <u>4908135</u>	E <u>0573569</u>	
Classification		
Components		
in-situ/autochthonous <input type="checkbox"/>	combination <input type="checkbox"/>	transport/allochthonous <input checked="" type="checkbox"/>
Type		
bank input <input type="checkbox"/>	valley jam/debris dam <input type="checkbox"/>	debris flow jam <input type="checkbox"/>
log step <input type="checkbox"/>	flow deflection jam <input type="checkbox"/>	flood jam <input type="checkbox"/>
		bench jam <input type="checkbox"/>
		bar apex jam <input type="checkbox"/>
		bar top jam <input checked="" type="checkbox"/>
		meander jam <input type="checkbox"/>
		log rafts <input type="checkbox"/>
		bank edge/top <input type="checkbox"/>
		bank revetment <input type="checkbox"/>
Position		
Section	Bank	Plan view
thalweg (A1) <input type="checkbox"/>	bank toe <input type="checkbox"/>	point bar <input type="checkbox"/>
shallow (A2) <input type="checkbox"/>	anchored bank base <input type="checkbox"/>	lateral bar <input checked="" type="checkbox"/>
chute channel (A2, B1) <input type="checkbox"/>	anchored bank <input type="checkbox"/>	longitudinal bar <input type="checkbox"/>
active bar (B1) <input checked="" type="checkbox"/>	bank top <input type="checkbox"/>	outer meander bank <input type="checkbox"/>
high bar (B2) <input type="checkbox"/>		bridge <input type="checkbox"/>
berm/bench/shelf (B2) <input type="checkbox"/>	Vegetation	Channel
secondary channel (B2, C) <input type="checkbox"/>	shrubs <input type="checkbox"/>	step <input type="checkbox"/>
pioneer island (B2, C) <input type="checkbox"/>	pioneer veget (2-5 yrs) <input type="checkbox"/>	riffle <input type="checkbox"/>
established island (B2, C) <input type="checkbox"/>	established veget (> 5 yrs) <input type="checkbox"/>	pool <input type="checkbox"/>
floodplain (C) <input type="checkbox"/>		glide <input type="checkbox"/>
terrace (D) <input type="checkbox"/>		
Sketch of jam position		
<p style="text-align: center;"><i>bankfull</i></p>	<p style="text-align: center;">Planview sketch</p>	
<p style="text-align: center;">cross section sketch</p>		

Figure A - 5: sheet 3: jam description.

Jam characteristics		
Jam size	Texture	Key elements
length (m) <input style="width: 40px;" type="text" value="23"/>	tight braided mesh <input style="width: 30px;" type="text"/>	number key elements <input style="width: 40px;" type="text" value="1"/>
width (m) <input style="width: 40px;" type="text" value="3.5"/>	loose braided mesh <input style="width: 30px;" type="text"/>	well visible <input style="width: 30px;" type="text" value="X"/>
height (m) <input style="width: 40px;" type="text" value="0.8"/>	tight parallel disposition <input style="width: 30px;" type="text"/>	partially visible <input style="width: 30px;" type="text"/>
number elements d>0.1 m <input style="width: 40px;" type="text" value="3"/>	loose parallel disposition <input style="width: 30px;" type="text"/>	presumable <input style="width: 30px;" type="text"/>
	no dominant disposition <input style="width: 30px;" type="text"/>	
	abundant fine debris <input style="width: 30px;" type="text"/>	

Jam sketch	
Point out key element(s), raked and relative identification code (LWDRn / LWDRn)	
<p style="text-align: center;">planview</p>	<p style="text-align: center;">cross section</p>
Notes and comments	

Figure A - 6: sheet 3: jam description.

4. LARGE WOODY DEBRIS SHEET										
Identification data										
Type <input checked="" type="checkbox"/> K K=key, R=racked, S=single										
Code <u>2.J4.S21</u>										
GPS Position N <u>4908124</u>					E <u>0573598</u>					
(only in case of single debris, otherwise the Jam position is considered)										
Characteristics										
Type			Branches			Roots				
tree <input type="checkbox"/>			no branches <input type="checkbox"/>			Rootwad <input checked="" type="checkbox"/> Y				
shrub <input type="checkbox"/>			only butts <input checked="" type="checkbox"/> X			Diameter (m) <u>.60</u>				
log <input checked="" type="checkbox"/> X			some broken <input type="checkbox"/>			Fine roots <input checked="" type="checkbox"/> N				
harvest residual <input type="checkbox"/>			all almost intact <input type="checkbox"/>							
Trunk decay			bark cover (%) <u>30</u>			Origin				
intact (with bark) <input type="checkbox"/>			leaves <input type="checkbox"/>			natural mortality <input type="checkbox"/>				
no bark but solid <input checked="" type="checkbox"/> X						bank erosion <input type="checkbox"/>				
porous <input type="checkbox"/>			species <u>Salix(?)</u>			landslide/debris flow <input type="checkbox"/>				
highly decayed <input type="checkbox"/>						floated <input checked="" type="checkbox"/> X				
Size		diameter (m) <u>0.18</u>	length (m) <u>2.8</u>		height (m) <input type="checkbox"/>					
tree/shrub:		width (m) <input type="checkbox"/>	length (m) <input type="checkbox"/>							
Age and conditions										
Trunk age (years) <input type="checkbox"/> (when possible)					Present vegetative activity					
					no activity <input checked="" type="checkbox"/> X					
					before deposition <input type="checkbox"/>					
Vitality					after deposition (adventitious sprouting) <input type="checkbox"/>					
strong <input type="checkbox"/>					max age adventitious sprouts <input type="checkbox"/>					
poor <input type="checkbox"/>										
dead <input type="checkbox"/>										
Position										
Section			Bank			Plan view				
thalweg (A1) <input type="checkbox"/>			bank toe <input type="checkbox"/>			point bar <input type="checkbox"/>				
shallow (A2) <input type="checkbox"/>			anchored bank base <input type="checkbox"/>			lateral bar <input checked="" type="checkbox"/> X				
chute channel (A2, B1) <input type="checkbox"/>			anchored bank <input type="checkbox"/>			longitudinal bar <input type="checkbox"/>				
active bar (B1) <input checked="" type="checkbox"/> X			bank top <input type="checkbox"/>			outer meander bank <input type="checkbox"/>				
high bar (B2) <input type="checkbox"/>						bridge <input type="checkbox"/>				
berm/bench/shelf (B2) <input type="checkbox"/>			Vegetation			Channel				
secondary channel (B2, C) <input type="checkbox"/>			shrubs <input type="checkbox"/>			step <input type="checkbox"/>				
pioneer island (B2, C) <input type="checkbox"/>			pioneer veget (2-5 yrs) <input type="checkbox"/>			riffle <input type="checkbox"/>				
established island (B2, C) <input type="checkbox"/>			established veget (> 5yrs) <input type="checkbox"/>			pool <input type="checkbox"/>				
floodplain (C) <input type="checkbox"/>						glide <input type="checkbox"/>				
Sketch of element position										
sx		bankfull						dx		
D										
C		referto sheet 3								
B2										
B										
B1										
A2										
A										
A1										
	X1	X2	X3	X4	X5	X6	X7	X8	X9	X10

Figure A - 7: sheet 4: key element description.

4. LARGE WOODY DEBRIS SHEET										
Identification data										
Type	<input checked="" type="checkbox"/> R K=key, R=racked, S=single									
Code	2.J4.S19									
GPS Position	N _____				E _____					
(only in case of single debris, otherwise the Jam position is considered)										
Characteristics										
Type	<input type="checkbox"/> tree		<input type="checkbox"/> shrub		<input checked="" type="checkbox"/> log		<input type="checkbox"/> harvest residual			
Trunk decay	<input checked="" type="checkbox"/> intact (with bark)		<input type="checkbox"/> no bark but solid		<input type="checkbox"/> porous		<input type="checkbox"/> highly decayed			
Branches	<input type="checkbox"/> no branches		<input checked="" type="checkbox"/> only butts		<input type="checkbox"/> some broken		<input type="checkbox"/> all almost intact			
Roots	<input checked="" type="checkbox"/> Rootwad		Diameter (m) 0.7		<input checked="" type="checkbox"/> Fine roots					
Origin	<input type="checkbox"/> natural mortality		<input type="checkbox"/> bank erosion		<input type="checkbox"/> landslide/debris flow		<input checked="" type="checkbox"/> floated			
Size	diameter (m)	0.17		length (m)	21.3		height (m)			
tree/shrub:	width (m)			length (m)			height (m)			
Age and conditions										
Trunk age (years) <input type="checkbox"/> (when possible)					Present vegetative activity					
Vitality					no activity <input type="checkbox"/>					
strong <input type="checkbox"/>					before deposition <input type="checkbox"/>					
poor <input type="checkbox"/>					after deposition (adventitious sprouting) <input checked="" type="checkbox"/>					
dead <input checked="" type="checkbox"/>					max age adventitious sprouts 1 yr					
Position										
Section			Bank				Plan view			
thalweg (A1) <input type="checkbox"/>			bank toe <input type="checkbox"/>				point bar <input type="checkbox"/>			
shallow (A2) <input type="checkbox"/>			anchored bank base <input type="checkbox"/>				lateral bar <input checked="" type="checkbox"/>			
chute channel (A2, B1) <input type="checkbox"/>			anchored bank <input type="checkbox"/>				longitudinal bar <input type="checkbox"/>			
active bar (B1) <input checked="" type="checkbox"/>			bank top <input type="checkbox"/>				outer meander bank <input type="checkbox"/>			
high bar (B2) <input type="checkbox"/>			Vegetation				Channel			
berm/bench/shelf (B2) <input type="checkbox"/>			shrubs <input type="checkbox"/>				step <input type="checkbox"/>			
secondary channel (B2, C) <input type="checkbox"/>			pioneer veget (2-5 yrs) <input type="checkbox"/>				riffle <input type="checkbox"/>			
pioneer island (B2, C) <input type="checkbox"/>			established veget (> 5yrs) <input type="checkbox"/>				pool <input type="checkbox"/>			
established island (B2, C) <input type="checkbox"/>							glide <input type="checkbox"/>			
floodplain (C) <input type="checkbox"/>										
Sketch of element position										
sx			bankfull				dx			
D										
C		refer to sheet 3								
B2										
B	B1									
A	A2									
	A1									
		X1	X2	X3	X4	X5	X6	X7	X8	
									X9	
									X10	

Figure A - 8: sheet 4: racked element description.

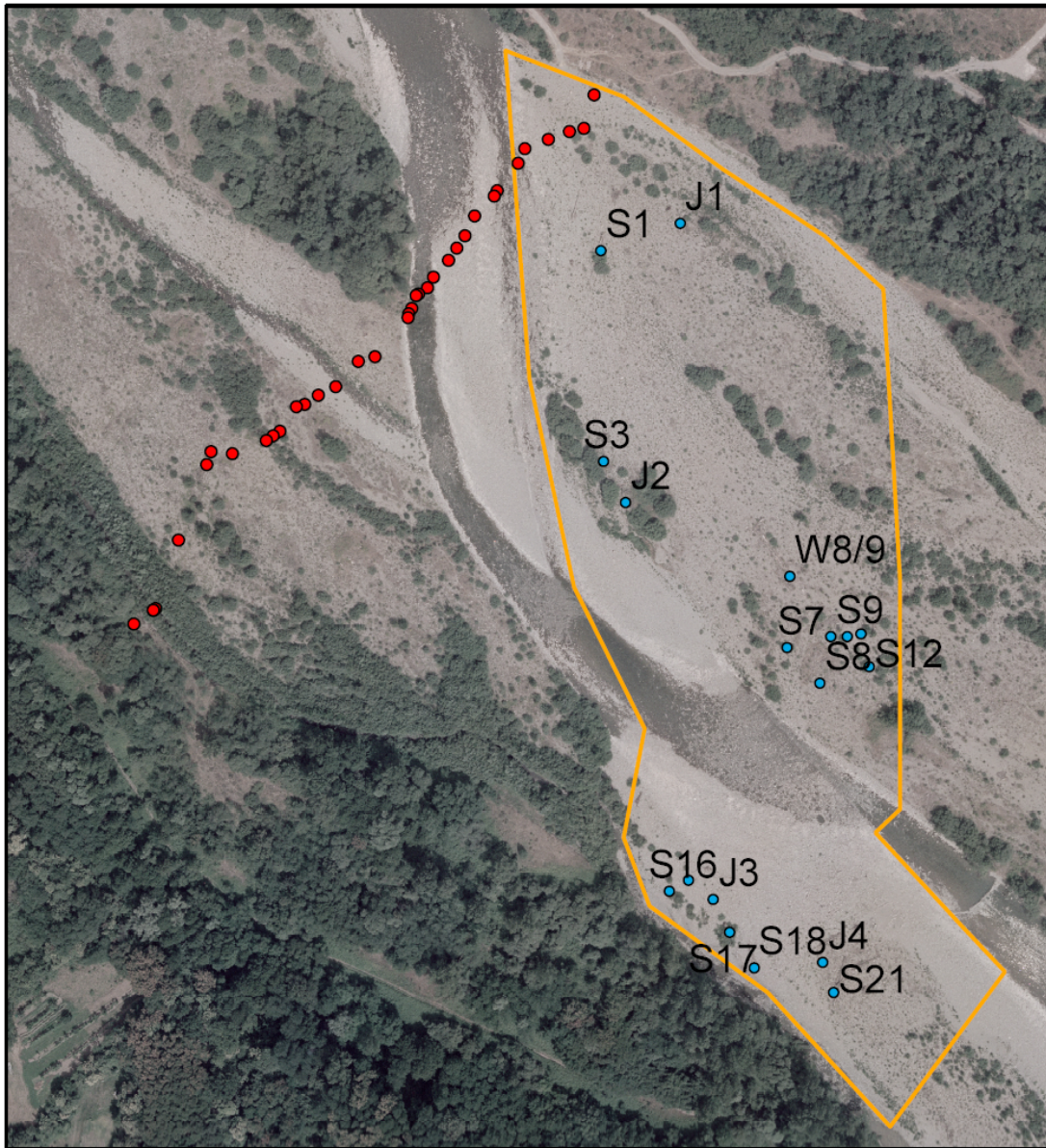
4. LARGE WOODY DEBRIS SHEET																			
Identification data																			
Type <input checked="" type="checkbox"/> R K=key, R=racked, S=single																			
Code <u>2.J4.S20</u>																			
GPS Position N _____ E _____																			
(only in case of single debris, otherwise the Jam position is considered)																			
Characteristics																			
Type			Branches			Roots													
tree <input type="checkbox"/>			no branches <input type="checkbox"/>			Rootwad <input checked="" type="checkbox"/> Y													
shrub <input type="checkbox"/>			only butts <input checked="" type="checkbox"/> X			Diameter (m) <u>0.65</u>													
log <input type="checkbox"/>			some broken <input type="checkbox"/>			Fine roots <input checked="" type="checkbox"/> N													
harvest residual <input checked="" type="checkbox"/> X			all almost intact <input type="checkbox"/>																
Trunk decay			bark cover (%) <u>5</u>			Origin													
intact (with bark) <input type="checkbox"/>			leaves <input type="checkbox"/>			natural mortality <input type="checkbox"/>													
no bark but solid <input checked="" type="checkbox"/> X						bank erosion <input type="checkbox"/>													
porous <input type="checkbox"/>			species <u>Poplar</u>			landslide/debris flow <input type="checkbox"/>													
highly decayed <input type="checkbox"/>						floated <input checked="" type="checkbox"/> X													
Size		diameter (m) <u>0.21</u>	length (m) <u>0.7</u>																
tree/shrub:		width (m) <input type="checkbox"/>	length (m) <input type="checkbox"/>		height (m) <input type="checkbox"/>														
Age and conditions																			
Trunk age (years) <input type="checkbox"/> (when possible)					Present vegetative activity														
					no activity <input checked="" type="checkbox"/> X														
Vitality					before deposition <input type="checkbox"/>														
strong <input type="checkbox"/>					after deposition (adventitious sprouting) <input type="checkbox"/>														
poor <input type="checkbox"/>					max age adventitious sprouts <input type="checkbox"/>														
dead <input type="checkbox"/>																			
Position																			
Section			Bank			Plan view													
thalweg (A1) <input type="checkbox"/>			bank toe <input type="checkbox"/>			point bar <input type="checkbox"/>													
shallow (A2) <input type="checkbox"/>			anchored bank base <input type="checkbox"/>			lateral bar <input checked="" type="checkbox"/> X													
chute channel (A2, B1) <input type="checkbox"/>			anchored bank <input type="checkbox"/>			longitudinal bar <input type="checkbox"/>													
active bar (B1) <input checked="" type="checkbox"/> X			bank top <input type="checkbox"/>			outer meander bank <input type="checkbox"/>													
high bar (B2) <input type="checkbox"/>						bridge <input type="checkbox"/>													
berm/bench/shelf (B2) <input type="checkbox"/>			Vegetation			Channel													
secondary channel (B2, C) <input type="checkbox"/>			shrubs <input type="checkbox"/>			step <input type="checkbox"/>													
pioneer island (B2, C) <input type="checkbox"/>			pioneer veget (2-5 yrs) <input type="checkbox"/>			riffle <input type="checkbox"/>													
established island (B2, C) <input type="checkbox"/>			established veget (> 5yrs) <input type="checkbox"/>			pool <input type="checkbox"/>													
floodplain (C) <input type="checkbox"/>						glide <input type="checkbox"/>													
Sketch of element position																			
S X		<i>bankfull</i>						dx											
D																			
C																			
referto sheet 3																			
B2																			
B																			
B1																			
A2																			
A																			
A1																			
X1		X2		X3		X4		X5		X6		X7		X8		X9		X10	

Figure A - 9: sheet 4: racked element description.

5. INTERACTION LWD, HYDRODYNAMICS AND SEDIMENTS			
Location within the river corridor			
Left, right, mid <input type="text" value="L"/>	Jam orientation to the north (°) <input type="text" value="237"/>	Rootwad orientation upstream <input type="text" value="S21"/>	Element orientation to the north (°) <input type="text" value="166"/>
	to low flow direction (°) <input type="text"/>	downstream <input type="text"/>	to low flow direction (°) <input type="text"/>
	to flood direction (°) <input type="text"/>	lateral (L/R) <input type="text" value="S20/S19"/>	to flood direction (°) <input type="text"/>
	inclination to horizontal (°) <input type="text"/>		inclination to horizontal (°) <input type="text"/>
Causes of deposition (for floated elements only)			
Captured	Stranded		
protruding clasts <input type="text" value="S20/S19*"/>	widenning <input type="text" value="S21"/>	abrupt curvature <input type="text"/>	shallowing <input type="text"/>
banks <input type="text"/>		wreckage <input type="text"/>	
vegetation <input type="text"/>			
anthropic structures <input type="text"/>			
obstacle-surrounding <input type="text"/>			
vortex <input type="text"/>		Other <input type="text" value="*and from KEY element"/>	
Flow - LWD interaction			
completely submerged <input type="text"/>	Sketch		
partially submerged <input type="text"/>			
submersion head (cm) <input type="text"/>			
submersion toe (cm) <input type="text"/>			
underflow <input type="text"/>			
underflow depth (cm) <input type="text"/>			
flow deflection <input type="text"/>			
contraction % <input type="text"/>			
plunging jet <input type="text"/>			
drop height (m) <input type="text"/>			
Interaction LWD - sediments			
Local processes			
upstream	on the jam/element	downstream	
fill <input checked="" type="checkbox"/>	partially buried by sediment <input type="checkbox"/>	fill <input type="checkbox"/>	
scour <input type="checkbox"/>	totally buried by sediment <input type="checkbox"/>	scour <input checked="" type="checkbox"/>	
lateral deposition (L/R) <input type="text"/>		lateral deposition (L/R) <input type="text"/>	
lateral scour (L/R) <input type="text"/>		lateral scour (L/R) <input type="text"/>	
length (m) <input type="text"/>		length (m) <input type="text"/>	
width (m) <input type="text"/>		width (m) <input type="text"/>	
depth/height (m) <input type="text"/>		depth/height (m) <input type="text"/>	
Sediments			
upstream	on the key/jam	downstream	
clay <input type="checkbox"/>	clay <input type="checkbox"/>	clay <input type="checkbox"/>	
silt <input type="checkbox"/>	silt <input type="checkbox"/>	silt <input type="checkbox"/>	
sand <input type="checkbox"/>	sand <input type="checkbox"/>	sand <input type="checkbox"/>	
gravel <input checked="" type="checkbox"/>	gravel <input type="checkbox"/>	gravel <input checked="" type="checkbox"/>	
cobble <input type="checkbox"/>	cobble <input type="checkbox"/>	cobble <input type="checkbox"/>	
boulder <input checked="" type="checkbox"/>	boulder <input type="checkbox"/>	boulder <input checked="" type="checkbox"/>	
Notes and comments			

Figure A - 10: sheet 5: LWD and sediments interaction.

SECTION 2 UPPER REACH



LEGEND

- Cross_sectionR1_pts
- Inspected debris
- ▭ Surveyed region boundary

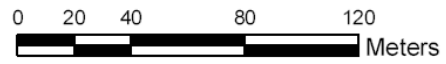
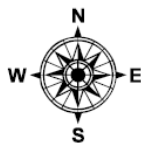


Figure A - 11: surveyed region in proximity of section 2 of the upper reach.

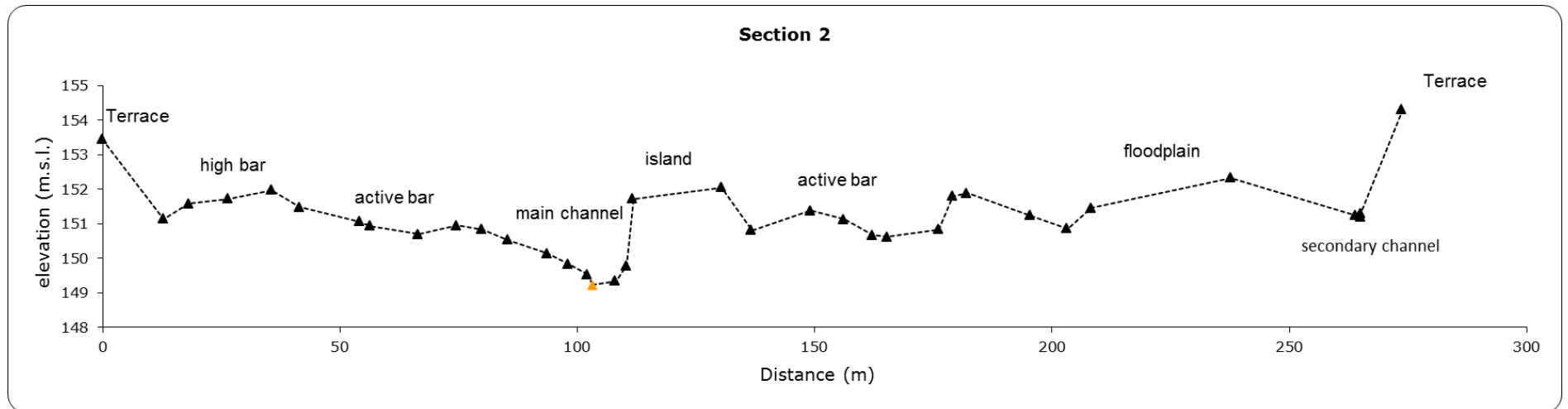


Figure A - 12: topographic survey of section 2.

Table A - 1 : collected data in proximity of section 2.

ACTIVE BAR

SAMPLES	DIMENSION		GPS POSITION		ORIENTATION °N	ROOTWAD		SPECIES	TYPE	SPROUTS age	BARK COVER %	DECAY	VITALITY	LEAVES	FINE ROOTS
	L	D	N	E		L	D								
S1	21.2	0.29	4908395	573513	205	1.4	1.1	P	log	1yr	90	intact	strong	Y	Y
S1	22.5	0.28	"	"	"	"	"	"	"	"	"	"	"	"	"
S13	12.1	0.12	4909158	573554	295	0.8	1.2	P	log	/	100	intact	poor	Y	Y
S14	10.6	0.15	"	"	"	0.6	0.3	P	log	/	100	intact	poor	N	Y
S15	2.6	0.12	4908165	573545	20	/	/	NC	log	/	0	porous	dead	N	N
S16	6.3	0.11	4908161	573538	180	0.3	0.6	NC	log	<1yr	100	intact	strong	Y	NC
S17	19.7	0.17	4908146	573560	165	1.5	1.85	NC	log	<1yr	100	intact	strong	Y	Y
S17	"	"	"	"	"	"	"	"	"	"	"	"	"	"	"
S18	9.5	0.11	4908133	573569	140	1.5	0.9	S	log	/	100	intact	dead	N	N
S19	21.3	0.17	4908135	573594	237	1.4	0.7	P	log	1yr	100	intact	poor	N	Y
S20	10.7	0.21	"	"	"	1.2	0.65	P	cut	/	5	solid	dead	N	N
S21	12.8	0.18	4908124	573598	166	0.5	1.6	S(?)	log	/	30	solid	dead	N	N

APPENDIX A

Table A - 2: collected data in proximity of section 2.

HIGH BAR

SAMPLES	DIMENSION		GPS POSITION		ORIENTATION °N	ROOTWAD		SPECIES	TYPE	SPROUTS age	BARK COVER %	DECAY	VITALITY	LEAVES	FINE ROOTS
	L	D	N	E		L	D								
S3	19.5	0.4	4908318	573514	160	1.5	3.8	P	tree	/	60	solid	dead	N	Y
S4	16	0.14	4908303	573522	250	1.1	0.35	NC	log	/	40	solid	dead	N	Y
S5	8.4	0.18	"	"	180	/	/	NC	log	/	0	solid	dead	N	N
S6	11.8	0.19	"	"	184	0.9	0.45	S(?)	log	/	50	solid	dead	N	N
S7	18.7	0.25	4908250	573581	170	1.5	1.2	P	log	/	40	solid	dead	N	Y
S8	4.4	0.15	4908237	573593	55	/	/	NC	cut	/	0	porous	dead	N	N
S9	1.4	0.13	4908254	573597	190	0.4	0.5	NC	log	/	0	porous	dead	N	N
S10	2.5	0.13	4908254	573603	220	/	/	A	log	/	10	solid	dead	N	N
S11	3.2	0.17	4908255	573608	NC	/	/	P	cut	/	50	solid	dead	N	N
S12	1.8	0.23	4908243	573611	70	/	/	NC	log	/	0	porous	dead	N	N
K1	5.1	0.31	4908292	573542	190	0.5	0.85	P(?)	cut	/	50	solid	dead	N	Y
K1	3.5	0.21	"	"	"	"	"	"	"	/	"	"	"	"	"
R1	7.2	0.2	"	"	"	1.7	0.5	P	log	/	50	solid	dead	N	Y
W8	16.7	0.15	4908276	570582	330	1.8	1.6	P	log	/	90	solid/porous	dead	N	Y
W9	14.2	0.16	"	"	NC	0.9	0.8	P	log	/	0	solid/porous	dead	N	Y



Debris in jam

Blue: debris with more than one trunk

SPECIES: P = POPULUS; S = SALIX; A = ALNUS

NC stays for NOT CLASSIFIED or NOT MEASURED

NV stays for NOT VISIBLE

VEGETATION SURVEY

		I PLOT	II PLOT
GPS	N	4908425	4908275
	E	0373545	0573586
POPULUS		3	44
SALIX		14	28
AILANTHUS		1	8
ROBINIA		0	1
TOTAL		18	81
Hm		0.5	1

Table A - 3: pioneer standing vegetation survey in the high bar.

APPENDIX B:

Here are reported whole steps performed in order to establish if the entrainment condition is satisfied for a given LWD. To evaluate the entrainment parameters the following quantities have to be known:

Flume characteristics:

- Flume slope $S_o = 0$
- Flume width $C_w = 0.4 \text{ m}$
- Mean bed level $y_b = 0.0718 \text{ m}$ (refer to Figure 7-6)
- Friction coefficient $\mu_{bed} = 0.64$ (referring section 7.2.2)
- Strickler Glaucher coefficient $K_{SG} = 41.67 \text{ m}^{1/3} \text{ s}^{-1}$

For the measured data proposed in this example, the Strickler Glaucher coefficient was obtained by numerical simulations in HEC RAS, using a regression analysis of the experimental undisturbed water depth measured at different locations of the flume, according to the Least Square Method.

Dowel characteristics:

- Shape smoothed square
- Log orientation $\theta = 0^\circ$ (log parallel to the flow)
- Log diameter $D_{log} = 13.3 \text{ cm}$
- Log length $L_{log} = 25 \text{ cm}$
- Log density $\rho_{log} = 452.85 \text{ kg/m}^3$
- Encroachment Coefficient $K_s = 0.8$

In this case the value of the encroachment coefficient is chosen considering the presence of a small fillet radius.

Constants:

- Acceleration due to gravity $g = 9.8125 \text{ m/s}^2$
- Water density $\rho_w = 1000 \text{ kg/m}^3$
- Kinematic viscosity $\nu_w = 1.008 \text{ E-6 m}^2/\text{s}$

Measured quantities at the incipient motion:

- Undisturbed water level $y_w = 0.139 \text{ m}$
- Volumetric discharge $Q = 0.00916 \text{ [m}^3/\text{s]}$

The procedure first evaluates the water depth:

$$d_w = y_w - y_b = (0.139 - 0.0718) \text{ m} = 0.0671 \text{ m}$$

The mean velocity could be calculated according to the following equation:

$$U = \frac{Q}{C_w \cdot d_w} = 0.365 \text{ m/s}$$

If a bed slope is present ($So > 0$) then the Darcy-Weisbach friction coefficient is calculated according to Eq. 6-60. Otherwise if the bed slope is 0, as in this case, the roughness height k_s is calculated considering the Manning's coefficient as the reciprocal of the Strickler Glaucher coefficient:

$$k_s = \left(\frac{6.51 \cdot \sqrt{g}}{K_{SG}} \right)^6 = 0.0137$$

Calculated the hydraulic radius ($R_h = 0.0502 \text{ m}$) it is possible to obtain the Colebrook friction coefficient $f = 0.0844$ resolving the following equation:

$$\frac{1}{\sqrt{f}} = -2 \log_{10} \left(k_s (4R_h)^{-\frac{1}{3.7}} + \frac{2.51}{R_e \cdot \sqrt{f}} \right)$$

in which has been considered the Reynolds number based on the hydraulic radius:

$$R_e = \frac{U \cdot R_H}{\nu_w} = 0.0137$$

It is possible now to calculate the boundary shear stress, the friction velocity u^* and the Roughness Reynolds number Re^* :

$$\tau_b = \frac{f}{8} \rho_w U^2 = 1.2262 \text{ N/m}^2$$

$$u^* = \sqrt{\frac{\tau_b}{\rho_w}} = 0.035 \text{ m/s}$$

$$Re^* = \frac{u^* \cdot k_s}{\nu_w} = 476.5$$

This allows evaluating the logarithmic velocity profile, considering that for $Re^* > 70$ the flow is hydraulically rough and:

$$y_o = k_s/30 = 0.000458 \text{ m}$$

according to the following formula, in which κ is the von Karman's constant (approximately 0.41 for clear water):

$$\frac{u}{u^*} = \frac{1}{\kappa} \cdot \ln \left(\frac{y}{y_o} \right)$$

This profile is then numerically integrated (using the simple trapezoidal rule) starting from the roughness parameter y_o , in order to obtain the depth averaged velocity \bar{U} :

$$\bar{U} = \frac{1}{d_w} \int_{y_o}^{d_w} u(y) \cdot dy = 0.358 \text{ m}$$

This value is then compared with the previous one, obtained by the measured quantities, in order to verify the hypothesis of a log shaped velocity profile, providing a relative error less than 2%, that could be considered satisfactory for the hypothesis of a log-shaped velocity profile. If the relative error is too high, the procedure is then repeated according to the formulas proposed by Maynard (1991) that could be used for most riprap problems.

The nominal submerged frontal area of the dowel, the blockage, and open ratio are then calculated:

$$A_{sub} = \left(\cos^{-1} \left(1 - \frac{2 \cdot d_w}{D_{log}} \right) - \sin \left(\cos^{-1} \left(1 - \frac{2 \cdot d_w}{D_{log}} \right) \right) \right) \cdot \frac{D_{log}^2}{8} = 0.0089 \text{ m}^2$$

$$L_{eq} = \frac{A_{sub}}{d_w} \cdot \sin(\theta) + L_{log} \cdot \cos(\theta) = 0.250 \text{ m}$$

$$L_{obs} = \frac{(A_{sub} \cos \theta + d_w L_{log} \sin \theta)}{d_w} = 0.133 \text{ m}$$

$$Br = \frac{(A_{sub} \cos \theta + d_w L_{log} \sin \theta)}{d_w C_w} = 0.3325$$

$$Or = 1 - Br = 0.6675$$

The stream Froude number downstream of the dowel (Fr_3) is obtained considering the undisturbed water depth.

$$Fr_3 = \frac{U}{\sqrt{gd_w}} = 0.42$$

from which it is possible to evaluate the contraction and expansion length (considering for simplicity $Fr_2 = 1$, the max value that could assume the Froude number in the constricted section):

$$CR = 2 \cdot \frac{L_c}{L_{obs}} = 2.07 - 0.33 \cdot \left(\frac{Fr_2}{Fr_3} \right) = 1.285$$

$$ER = 2 \cdot \frac{L_e}{L_{obs}} = 0.489 + 0.608 \cdot \left(\frac{Fr_2}{Fr_3} \right) = 1.936$$

obtaining:

$$L_c = CR \cdot \frac{L_{obs}}{2} = 0.085 \text{ m}$$

$$L_e = ER \cdot \frac{L_{obs}}{2} = 0.129 \text{ m}$$

and the computational length L1 and L2:

$$L_1 = L_c + 0.5 \cdot L_{eq} = 0.21 \text{ m}$$

$$L_2 = L_e + 0.5 \cdot L_{eq} = 0.254 \text{ m}$$

The algorithm then verify if there is a critical flow condition in the contracted section, according to the procedure proposed by Molinas:

1. K_L , K_{et} , K_φ are then evaluated according the provided equations

$$K_L = 0.625 \cdot (1 - e^{-L^*}) = 0.2905$$

$$K_\varphi = (\varphi^*)^{0.87} = 1$$

$$k_{eT} = 0.432(K_L + K_\varphi) \cdot K_S \cdot (1 + O_r)^{0.25} \cdot \exp\left(\frac{0.18}{O_r}\right) = 0.4435$$

2. The threshold condition for choking is evaluated resolving the following equation with respect to Fr_{1c}

$$O_r = \left(\frac{3 + k_{eT}}{C_c^{\frac{2}{3}}} \right)^{\frac{3}{2}} \frac{Fr_{1c}}{(2 + Fr_{1c}^2)^{\frac{3}{2}}}$$

Obtaining the Froude number at the section 1 providing the choking condition in section 2: $Fr_{1c} = 0.318$

3. A first value of the backwater rise upstream of the dowel is obtained according to Yarnell or El-Alfy equation, depending on the slender ratio of the dowel, assuming a subcritical flow in the constricted section (section 2). In this case the slenderness ratio is 1.88, so the Yarnell relationship is the more appropriate:

$$\frac{\Delta y}{y_3} = K_S \cdot (K_S + 5 \cdot Fr_3^2 - 0.6) \cdot (B_r + 15 \cdot B_r^4) \cdot Fr_3^2$$

providing a backwater rise $\Delta y = 0.0117 \text{ m}$. The upstream water depth will be then:

$$y_1 = d_w + \Delta y = 0.0788 \text{ m}$$

4. The upstream Froude number Fr_1 is then evaluated resolving:

$$y_1 = \sqrt[3]{\frac{Q^2}{g \cdot C_w^2 \cdot Fr_1^2}}$$

obtaining in this case $Fr_1 = 0.33$

Because $Fr_1 > Fr_{1c}$ the flow is choked in section 2, and the water depth upstream of contraction is then evaluated according the correlation due to Molinas, which is valid for choked flows:

$$C_d^* = \frac{C_c}{(3 + k_{eT})^{\frac{3}{2}}} = 0.1672$$

$$Fr_1^* = C_d^* O_r = 0.1116$$

$$Fr_1^* = \frac{Fr_1}{(2 + Fr_1^2)^{\frac{3}{2}}} = 0.344$$

producing a $\Delta y = 0.0096 \text{ m}$, at which correspond a water level:

$$w_1 = d_w + \Delta y + y_b = 0.149 \text{ m}$$

that could be compared with the experimental water level measured at 20 cm upstream of the dowel (0.155 m) producing a relative error around the 4%, that could be considered accurate for the scope of this work. The experimental water depths were measured at 20 cm upstream of the log, because the contraction reach length is smaller than the obstacle width.

It is now possible to evaluate all the forces acting on the partially submerged log:

- The drag coefficient is evaluated according the procedure proposed by Chaberneau, being all the quantities known:

$$C_D = \frac{1}{O_r F_{r3}^2} \left[2 \frac{\Delta y}{y_3} + \left(\frac{\Delta y}{y_3} \right)^2 \right] - \frac{f}{16} \frac{L}{y_3} \frac{\Phi_\tau}{O_r} + \frac{2}{O_r F_{r3}^2} \frac{L}{y_3} S_b \left[\left(1 + \frac{\Delta y}{y_3} \right) \frac{L_1}{L} + \frac{L_3}{L} \right] - \frac{2}{O_r} \left(\frac{\frac{\Delta y}{y_3}}{1 + \frac{\Delta y}{y_3}} \right) = 3.96$$

providing a Drag force:

$$F_D = \frac{U^2}{2} \rho_w C_D \cdot (A_{sub} \cos \theta + d_w L_{log} \sin \theta) = 2.054 \text{ N}$$

- Known the upstream water depth, it is possible to calculate the log shaped velocity profile upstream of the log in the same manner of the previous one. This allow to estimate the Dynamic force acting on the frontal area of the log and its lever arm:

$$y_D = \frac{1}{F_D} \int_0^{d_{up}} \left[\gamma_w (d_{up} - z) + \rho_w \frac{u(y)^2}{2} \right] c(y) \cdot y \cdot dy - \frac{1}{F_D} \int_0^{d_{down}} \gamma_w (d_{down} - y) \cdot c(y) \cdot y \cdot dy = 0.04 \text{ m}$$

- For a log aligned with the flow, the center of instantaneous rotation could be considered coincident with a edge of the log:

$$\begin{aligned}x_C &= L_{eq} \\y_C &= 0 \\x_{CG} &= \frac{L_{eq}}{2} \\y_{CG} &= \frac{D_{log}}{2}\end{aligned}$$

- In order to evaluate the center of buoyancy a sinusoidal wave according to those proposed by Delhommeau it is considered. The height of the bow wave, y_{bw} , above the mean free surface, is given by (considering a waterline entrance angle of 45°):

$$y_{bw} = \frac{2.2 U^2}{1 + Fr} \cdot \frac{\tan(\alpha_E)}{g \cos(\alpha_E)} = 0.005 \text{ m}$$

this lead to consider a water level near the log :

$$w_l = d_w + \Delta y + y_b + y_{bw} = 0.154 \text{ m}$$

that is not so much different from the experimental water level measured at 1 cm upstream of the log (0.164 m).

It is possible therefore evaluate the wave profile according:

$$y(x) = d_w + \Delta y - \frac{\Delta y}{L_{eq}} x + y_{bw} \cos\left(\frac{2\pi}{\lambda} x\right)$$

considering a wavelength $\lambda = 2\pi \sqrt{\frac{U^2 d_w}{6g(1-Fr)}} = 0.238 \text{ m}$. This allows a very rough estimate of the center of buoyancy:

$$x_{CB} = 0.066 \text{ m}$$

$$y_{CB} = 0.058 \text{ m}$$

The entrainment parameters are then evaluated according the following equations, considering zero the inertia and lift forces:

$$E_p^s = \frac{\rho_{Log} A_{Log}}{\rho_w A_{sub}} \left(\cos \alpha - \frac{\sin \alpha}{\mu_{bed}} \right) - \frac{F_D + F_I + \mu_{bed} F_L}{\mu_{bed} g \rho_w A_{sub} L_{log}} = 0.749$$

$$E_p^r = \frac{\rho_{Log} A_{Log}}{\rho_w A_{sub}} \cdot \left[\frac{(x_C - x_{CG}) \cdot \cos \alpha - (y_{CG} - y_C) \cdot \sin \alpha}{(x_C - x_{CB})} \right] - \frac{1}{g \rho_w A_{sub} L_{log}} \left[F_D \frac{(y_D - y_C)}{(x_C - x_{CB})} + F_I \frac{(y_{CB} - y_C)}{(x_C - x_{CB})} + F_L \frac{(x_C - x_L)}{(x_C - x_{CB})} \right] = 0.849$$

$$E_p^b = \frac{\rho_{Log} A_{Log}}{\rho_w A_{sub}} - \frac{F_L}{g \rho_w A_{sub} L_{log}} = 0.898$$

According to the proposed approach the entrainment mode will be established by the lesser entrainment parameter:

$$\min\{E_p^s, E_p^r, E_p^b\} \leq E_p^*$$

For the case considered then the entrainment mode will be sliding E_p^s

This parameter has to be compared to the threshold value evaluated according to the proposed empirical correlation, in order to verify if the log will be displaced or not by the flow:

$$E_p^* = -51.19 \cdot \left(\frac{d_w}{L_{eq}} \right)^{5.454} + 0.7831 = 0.7439$$

In this case the log is close to be entrained.